STUDIES ON THE PATHOPHYSIOLOGY OF CANCER-INDUCED BONE PAIN

STUDIES ON THE PATHOPHYSIOLOGY OF CANCER-INDUCED BONE PAIN

By

ROBERT G. UNGARD, M.Sc., B.A.S. (HONOURS)

A Thesis

Submitted to the School of Graduate Studies

In Partial Fulfilment of the Requirements

for the Degree

Doctor of Philosophy

McMaster University

DOCTOR OF PHILOSOPHY (2020) McMaster University

(Medical Sciences) Hamilton, Ontario, Canada

TITLE: Studies on the pathophysiology of cancer-induced bone pain

AUTHOR: Robert Gavin Ungard, M.Sc. (McMaster University), B.A.S. (Honours) (University of Guelph)

SUPERVISOR: Professor Gurmit Singh, Ph.D.

NUMBER OF PAGES: xvi, 234

Lay Abstract

The tools we have right now to manage severe and chronic pain are insufficient. Patients with advanced cancers including bone cancer can suffer from very severe pain. This pain is generated in a number of ways including by the tumour itself releasing chemicals that activate pain-sensing nerves, by the destruction of the bone in and around the tumour, and by the sensitization of the nervous system, which can make pain worse and longer lasting. We have taken three approaches to researching cancer pain and to investigating new treatments. We have found that by reducing the amount of glutamate that cancer cells can release into their environment, we can reduce cancer pain in mice. We also found that treating rats with pregabalin and progesterone can change nerve signaling and reduce neuropathic pain, but that this effect is most pronounced in male rats with neuopathic pain and smaller in female rats with neuropathic pain, and even smaller in rats with cancer pain. We also analyzed expression of all the protein-coding genes in dorsal root ganglia from rats with cancer pain and found that there are many differences from rats without pain. Some of these differences may be promising new research targets. Going forward this research has provided important evidence necessary for next steps to develop new therapies and research strategies for cancer pain.

Abstract

Metastatic bone cancers cause severe symptoms including pain that compromises patient functional status, quality of life, and survival. Current treatment strategies have limited efficacy and dose-limiting side effects. Cancer-induced bone pain (CIBP) is a unique pain state that shares features with but is distinct from the pathology of neuropathic and inflammatory pain. This dissertation investigates how CIBP is generated and maintained by the direct effects of cancer cells on their metastatic microenvironment and the peripheral nervous system, including unique signaling properties and gene expression changes. In particular, we found that genetic knockdown of the functional subunit xCT of the system xC- cystine/glutamate antiporter can reduce CIBP, further elucidating this as a therapeutic of interest. We found that the neuroprotective voltage-gated calcium channel inhibitors progesterone and pregabalin markedly reduce mechanical hypersensitivity and excitability in sensory neurons of the dorsal root ganglion (DRG) in male rat models of neuropathic pain, but that these effects and less pronounced in females. In cancer pain, these sex differences are reversed, with females but not males demonstrating a delay in time-to-onset of mechanical hypersensitivity. We also analyzed gene expression at the DRG by RNA-Sequencing of rat models of CIBP. Our findings uncovered differential gene expression between CIBP and sham controls and between ipsilateral and contralateral DRGs in CIBP model rats. These studies have identified several promising avenues for therapeutic research for CIBP.

Preface

This doctoral dissertation is presented as a sandwich thesis that includes four manuscripts prepared for publication during the author's Ph.D. tenure and on which the author of this dissertation is also the primary author of the manuscript. Three manuscripts have been published and indexed (Chapters 1, 2, and 3), and one manuscript is prepared for publication and pending submission (Chapter 4). Each manuscript is presented as a separate chapter and includes a preface detailing each author's contributions, and a description of the manuscript in the context of this thesis. The first manuscript presented in Chapter 1 is a review-style book chapter published in *Oncodynamics: Effects of Cancer Cells on the Body*. This manuscript provides a conceptual overview and comprehensive background information on the context and pathophysiology of cancer pain and cancer-induced bone pain in particular. Subsequent chapters (Chapters 2, 3, and 4) are primary research manuscripts describing experiments that were performed during the author's Ph.D. tenure. A concluding chapter (Chapter 5) summarizes and concludes this dissertation and discusses promising future directions to follow-up on the findings presented here

Literature cited within each manuscript are independent and consistent with the requirements of their corresponding journal. Literature cited elsewhere uses the *Council of Science Editors Name-Year* style and is included in a separate References section following the Conclusions in Chapter 5. Three Appendices are included describing unpublished methodology and results and two copyright licences.

Acknowledgements

I am deeply grateful for the love, support, and patience that I have been shown throughout this Ph.D., and I am very fortunate to have been given the opportunity to pursue this degree at McMaster University.

Thank you to my supervisor Dr. Gurmit Singh for your generosity of time, enthusiasm, understanding, and unparalleled curiosity. Thank you also to my supervisory committee Dr. Mark Inman and Dr. Norm Buckley for your interest, support and critical analysis. Thank you also to all the students and researchers who I have been so fortunate to know and work alongside: Yong Fang, Natalie, Katja, Tanya, Jenn, Mina, Manu, Natalka, Jesse, Kimberly, Sarah, Adam, Ayesha, Wendy, Celene, Guru, Jianhan, Javy, Gurleen, Hanxin, Jianping, Daria, Heidi, Anita, Andy, Silvia, Monica, Franziska, Elena, Hannah, Peter, Gireesh, Alan, Priya, Emily W, Danny, Matt, Mohini, Eric H, Eric S, Eric D, Mike, Kevin, Julian, Ksenia, Pedrum, Chitman, Gaby, Cindy, Ali, Anthony, Marlie, Ahmed, Emily B, Élora, Rebecca, Amber, Sharon, Ayesha, Michael, Brittany, Julija, Lisa, Daphne, and more - I never cease to be impressed by how smart, diligent, and kind you all are, thank you.

Most importantly, thank you to my family for your love and support. Thank you Sasha, I love you and appreciate you - you make me a better person every day.

Table of Contents

List of Figures and Tables

List of Abbreviations

AHTM	Aβ-type high-threshold mechanosensitive fibre
ALTM	Aβ-type low-threshold mechanosensitive fibre
ASIC	Acid-sensing ion channel
ATP	Adenosine triphosphate
CIBP	Cancer-induced bone pain
CIPN	Chemotherapy-induced peripheral neuropathy
CNS	Central nervous system
CSF1	Colony-stimulating factor 1
CUT	Cutaneous neurons
CHTM	C-type high-threshold mechanosensitive fibre
DAVID	Database for Annotation, Visualization and Integrated Discovery
DEG	Differentially expressed gene
DMEM	Dulbecco's Modified Eagle Medium
DNA	Deoxyribonucleic acid
DPA	Dynamic Plantar Aesthesiometer
DRG	Dorsal root ganglion
DWB	Dynamic Weight Bearing
EASE	Expression Analysis Systematic Explorer
ET-1	Endothelin-1
ETAR	Endothelin-A receptor
ETBR	Endothelin-B receptor
FBS	Fetal bovine serum
FDR	False discovery rate
FPKM	Fragments per kilobase of transcript per million mapped reads

GFAP	Glial fibrillary acidic protein
GO:BP	Gene Ontology Biological Processes
H&E	Hematoxylin and eosin
HBSS	Hank's Balanced Salt Solution
IL	Interleukin
KD	Knockdown
KEGG	Kyoto Encyclopedia of Genes and Genomes
M-CSF	Macrophage colony-stimulating factor
MMP	Matrix metalloproteinase
MRMT-1	Mammary rat metastasis tumour
MS	Muscle spindle neuron
NEP	Neuropathic pain
NGF	Nerve growth factor
NSAID	Non-steroidal anti-inflammatory drug
OPG	Osteoprotegerin
PBS	Phosphate-buffered saline
PRE	Pregabalin
PRO	Progesterone
PTH	Parathyroid hormone
PTHrP	Parathyroid hormone related peptide
RANK	Receptor activator of nuclear factor-κB
RANKL	Receptor activator of nuclear factor-κB ligand
ROS	Reactive oxygen species
RNA	Ribonucleic acid
RPII	RNA polymerase II
SD	Sprague-Dawley

SEM	Standard error of the mean
TGF-β	Transforming growth factor-β
TNF- α	Tumour necrosis factor-α
TrkA	Tropomyosin receptor kinase A
TRPV1	Transient receptor potential channel-vanilloid subfamily member 1
VGCC	Voltage-gated calcium channel
WHO	World Health Organization

Declaration of Academic Achievement

This dissertation is presented as a combination of four manuscripts – three published papers and one completed manuscript, as follows:

Ungard R, Buckley N, Singh G. (2016). In G. Singh (Ed.), Oncodynamics: Effects of Cancer Cells on the Body (pp. 129-145). Cham: Springer International Publishing, Switzerland.

Ungard R, Linher-Melville K, Nashed M, Sharma M, Wu, JP, Singh G. (2019). xCT knockdown in human breast cancer cells delays onset of cancer-induced bone pain. Molecular Pain. 15:1-14.

Ungard R, Zhu YF, Yang S, Nakhla P, Parzei N, Zhu KL, Singh G. (2020). Response to pregabalin and progesterone differs in male and female rat models of neuropathic and cancer pain. Can J Pain. 2020:24740527.2020.1724776.

Ungard R, Shahid A, Fazzari J, Singh G. RNA-sequencing of lumbar dorsal root ganglia in a rat model of cancer-induced bone pain. (2020). Manuscript prepared for submission to: Molecular Pain.

In addition, I co-authored the following publications during my Ph.D. candidacy:

Zhu YF, Linher-Melville K, Wu J, **Ungard R**, Fazzari J, Zhu KL, Miladinovic T, Singh G. (2020). Bone cancer-induced pain is associated with glutamate signaling in peripheral sensory neurons. (Manuscript under review: Molecular Pain).

Miladinovic T, Sharma M, Phan A, Geres H, **Ungard R**, Linher-Melville K, Singh G. (2019). Activation of hippocampal microglia in a murine model of cancer-induced pain. Journal of Pain Research. 12:1003–1016.

Linher-Melville K, Sharma M, Nakhla P, Kum E, **Ungard R**, Park J, Rosa D, Gunning P, Singh G. (2019). Inhibiting STAT3 in a Murine Model of Human Breast Cancer-Induced Bone Pain Delays the Onset of Nociception. Molecular Pain. 15:1744806918823477.

Zhu YF, Kwiecien JM, Dabrowski W, **Ungard R**, Zhu KL, Huizinga J, Henry JL, Singh G. (2018). Cancer pain and neuropathic pain are associated with Aβ sensory neuronal plasticity in dorsal root ganglia and abnormal sprouting in lumbar spinal cord. Molecular Pain. 14:1-15.

Miladinovic T, **Ungard R**, Linher-Melville K, Popovic S, Singh G. (2018). Functional effects of TrkA inhibition on system xC- mediated glutamate release and cancer-induced bone pain. Molecular Pain. 14:1-15

Yazdani A, Janzen N, Czorny S, **Ungard R**, Miladinovic T, Singh G, Valliant J. (2017). Preparation of Tetrazine-Derived [2 + 1] Complexes of 99mTc and in vivo Targeting using Bioorthogonal Inverse Electron Demand Diels-Alder Chemistry. Dalton Transactions. DOI: 10.1039/c7dt01497j.

Zhu YF, **Ungard R**, Zacal N, Huizinga J, Henry JL, Singh G. (2017). Rat model of cancer-induced bone pain: changes in nonnociceptive sensory neurons in vivo. PAIN Reports. 2(2017) e603

Nashed M, **Ungard R**, Young K, Zacal N, Seidlitz E, Frey B, Singh G. (2017). Behavioral effects of using sulfasalazine to inhibit glutamate released by cancer cells: A novel target for Cancer-Induced Depression. Scientific Reports. 7:41382.

Linher-Melville K, Nashed M, **Ungard R**, Gunning P, Singh G. (2016). Chronic inhibition of STAT3/STAT5 activation in two representative human breast cancer cell lines: convergence on the ROS/SUMO pathway and its effects on system xC-. PLoS One. 11(8).

CHAPTER 1: Cancer-Induced Pain

Robert G Ungard, Norman Buckley, Gurmit Singh In G. Singh (Ed.), Oncodynamics: Effects of Cancer Cells on the Body (pp. 129-145). Cham: Springer International Publishing, Switzerland.

Preface

In this chapter, an author-generated version of the manuscript titled "Cancer-Induced Pain", published in 2016 as a book chapter in G. Singh (Ed.), *Oncodynamics: Effects of Cancer Cells on the Body* (pp. 129-145). Cham: Springer International Publishing, Switzerland, is presented. This chapter is reprinted with permission from Springer Publishing (see **Appendix 1** for License Agreement).

For this manuscript, I performed the literature review, wrote the manuscript, designed and produced the figure. Dr. Buckley and Dr. Singh provided conceptual input and reviewed the content and structure of the chapter.

Context and Background Information

This chapter provides a thorough review of the pathophysiology of cancer-induced pain, with background information included on prevalence and other pain states to contextualize cancer pain in the broader landscape of pain research. This chapter is included in a textbook which introduces the concept of oncodynamics as "the impact of abnormal cues generated by tumors on the physiological functioning of the body". This chapter specifically focuses on cancer pain as an oncodynamic effect.

This chapter includes an introduction describing background information on pain including detail on nociceptive pathways and neuropathic and inflammatory pain states. The concept of cancer pain as a distinct pain state is introduced and essential definitions, epidemiology and initiating factors are included.

This chapter goes on to describe the pathophysiology of cancer pain in detail, providing mechanistic and clinical findings that are essential to the conceptualization behind the work presented in this dissertation. This introductory chapter describes how factors secreted from tumours and tumour-associated cells can directly provoke pain and expands on some of the most well-known secreted factors and some of the most promising,

including glutamate. The effects of tumours on their host tissue is described, including a detailed review of the literature on cancer-induced bone pain (CIBP) and the multiple factors that contribute to the initial generation and long-term maintenance of this pain, including bone remodelling and pathological signalling and molecular changes in the peripheral and central nervous systems. This chapter also includes a review of therapeutic practices and promising therapeutic candidates for pain with a focus on those that have evidence for use in treating cancer pain.

This manuscript does not include the hypothesis and objectives of this dissertation; therefore, the hypothesis is included here:

> *Cancer-induced bone pain is a unique pain state that shares features with but is distinct from neuropathic and inflammatory pain states, and that is generated and maintained by the direct effects of cancer cells on their metastatic microenvironment, including unique signalling properties and gene expression changes in sensory neurons and associated cells.*

This hypothesis was investigated through three distinct objectives, discussed in the context of the papers presented in Chapters 2, 3, and 4.

Objective 1: *Establish and investigate the impact of genetic knock-down of xCT in human cancer cells on cancer-induced bone pain.*

Objective 2: *Investigate the impact of the neuroprotective treatments progesterone and pregabalin on neuropathic pain and cancer-induced bone pain.*

Objective 3: *Investigate gene expression by mRNA selective RNA-Sequencing of dorsal root ganglia isolated from a model of cancer-induced bone pain.*

Cancer-induced pain

Robert G. Ungard, Norman Buckley and Gurmit Singh

Content

Introduction

The ability to sense physiological pain is an essential self-preservational quality of an organism that allows the avoidance of tissue damage and the recognition of damaging pathological states. However, the physiological systems that allow us to perceive pain in a useful manner can also become pathological themselves, either seemingly independently as is the case with some chronic pain conditions, or as the result of an unrelated disease state, such as cancer. The pain produced by cancer can range from mild discomfort to severe, intractable, and self-propagating states of chronic pain.

Some type of cancer-induced pain is estimated to be experienced by 30–50% of all cancer patients, and by 75–90% of those with late stage metastatic cancer (1). Metastatic cancer-induced bone pain is the most common source of cancer pain reported by patients (2), and has also been the most well-studied. Cancer pain can be debilitating and intractable and is a major impediment to the maintenance of quality of life and functional status in cancer patients (3,4). And yet, many barriers to the effective management of cancer pain still remain. These include significant sociological and regulatory barriers, but also a deficit of knowledge regarding the mechanisms and control of chronic pain itself, and of cancer pain in particular. It has been recently determined by systematic review that approximately 1/3 of patients undergoing treatment for cancer pain are undertreated, although this number is highly variable globally (5). This chapter will summarize the molecular mechanisms of cancer-induced pain as an oncodynamic effect of great importance to people living with cancer.

Pain

Pain is defined by the International Association for the Study of Pain as an unpleasant sensory and emotional experience associated with actual or potential tissue damage, or described in terms of such damage (6). The human experience of pain is multifaceted and subjective and difficult to quantitatively study. Mechanistically, pain is subcategorized into three physiological sources; nociceptive, inflammatory, and neuropathic pain. In many painful conditions, including many conditions of cancer pain, all three of these pain types will play a contributory role in the overall mechanisms and quality of the experience of pain.

Acute nociceptive pain arises from the stimulation of specialized sensory nerve fibres called nociceptors. This includes the myelinated and rapidly-conducting Aβ- and Aδ-fibres, and the unmyelinated, slow-conducting C-fibres. Nociceptors innervate most somatic tissues at differing densities, and exhibit receptors that allow sensitivity to a range of inputs including noxious thermal, mechanical, and chemical stimuli. Most nociceptors in the body remain constitutively inactive until activated with unusual stimuli,

as is the case when the distortion of a broken bone stimulates dormant mechanically-sensitive nociceptors. The cell bodies of nociceptors that innervate the body lie in the dorsal root ganglia (DRG), lateral to the spinal cord at the vertebral column, or in the trigeminal ganglion for facial nociceptive innervation. The central terminals of nociceptors synapse with second-order neurons in the central nervous system (CNS), usually at the dorsal horn of the spinal cord. Here, these connections are subject to inhibitory, facilitory and other modulatory influence by central descending neurons and by glial cells (7). Ascending neurons generally pass along the spinothalamic or spinoreticulothalamic tracts to the thalamus and brainstem, and further to the cortex (8). Multiple brain regions are involved in the perception and processing of pain signalling, including primarily the primary and secondary somatosensory cortex, as well as the insular cortex, anterior cingulate cortex and prefrontal cortex (9). Nociceptors are widely variable in their structures and functions, including their activating stimuli and thresholds, the extent of their receptive fields, and their speed and frequency of signalling. This heterogeneity allows the sensation of a wide variety and quality of painful sensations at the CNS (10).

Inflammatory pain is pain produced by nociceptors activated by the mediators and molecular products of inflammation. Nociceptors express many receptors for individual products of inflammation, including but not limited to substance P, bradykinin, prostaglandins, adenosine triphosphate (ATP), nerve growth factor (NGF), tumour necrosis factor-α (TNF-α), and protons. These are secreted by the peripheral terminals of nociceptors, and by cells associated with inflammatory states including mast cells, macrophages, and fibroblasts, to the extracellular “inflammatory soup” of pro-inflammatory and algesic signaling molecules that is characteristic of inflammatory sites (11).

Neuropathic pain is pain that arises as a direct consequence of damage or disease affecting the somatosensory system (6). This can arise from a number of conditions including surgical or traumatic damage, chronic inflammation, and invasive cancer.

There is increasing evidence that despite the phenotypic similarities of many conditions of pain, the mechanisms that contribute to the production and maintenance of pain can be significantly divergent. There are peripheral and central mechanistic differences between painful conditions, and between sexes experiencing the same condition that are relevant to treatment (12).

Despite their etiological differences, all pain regardless of the source or any modulation must be transmitted by neuronal cells to the brain in order for perception to occur. This is as true for cancer pain as it is for the pain of any other condition. Also at play, regardless of the source of the pain, is that chronic nociceptive signalling and pathological conditions can produce dramatic reorganization of the structures that transmit and regulate pain signalling. This reorganization includes physiological changes in neurons and glial cells that are associated not only as indicators of a state of chronic pain, but as factors implicit in the maintenance of that pain. Ultimately these pain pathways can transition from acute activation to chronic ongoing activation through the processes of peripheral and central sensitization. Sensitization results in the conditions of hyperalgesia and allodynia, whereby a lower stimulus threshold triggers a nociceptive response, and a normally non-nociceptive stimulus becomes painful, respectively. These processes are essential to the physiology of chronic pain conditions, including cancer pain.

Cancer Pain

As befitting such a diverse pathological condition as cancer, pain resulting from cancer can arise from many physical, chemical, and thermal stimuli. Cancer pain can be nociceptive, inflammatory and neuropathic, and is commonly a result of situations such as physical pressure from the tumour itself, damage to or remodelling of tissues in close proximity to the tumour, and peritumoural inflammation. Central and peripheral sensitization render cancer pain into a chronic condition that can become constant and intractable. Treatments of cancer also often cause pain as a side-effect, most notably, chemotherapy-induced peripheral neuropathy (CIPN), and opioid-induced hyperalgesia,

however these conditions are not directly oncodynamic, and as such, will not be addressed in this review.

Conditions of cancer pain are defined by the source tissue of the primary cancer, and the host tissue from which the pain emanates. A list of common clinical cancer-associated pain syndromes and their treatment can be found in this review by Portenoy (13). The quality and intensity of these pain conditions are widely variable, for example the pain emanating from a primary tumour in the breast, if any, presents very differently than the pain of a metastatic breast cancer growing in the spine. One of the challenges of cancer pain management, however is the inconsistency of the influence of location or tumour type in the generation of pain. One patient's tumour may not cause pain until late stages, whereas a similar tumour in another patient may generate severe pain before the lesion is detectable by other means (14). This is due to widely differing primary cancers, but also the structures and functions of host tissues in the body, which play a defining role not only in the progression of the invading cancer, but also in the nature and extent of the oncodynamic consequences of that invasion. Despite this, regardless of the host tissue, cancers can cause pain by similar mechanisms. Many cancers secrete a host of algesic chemicals capable of stimulating and sensitizing nociceptors. In innervated tissue, these chemicals would be expected to be independently capable of nociceptive stimulation, as has been shown to be the case with endothelin-1 (ET-1) which can cause pain following secretion from several different types of cancer cells in multiple tissues (15–18).

Breakthrough cancer pain is a separate condition that is defined by its relationship to pain treatment. It is a transitory exacerbation of pain in excess of the otherwise effective analgesic regimen of the patient (19). This pain can arise spontaneously or as a result of an action or movement committed by the patient in which case it is labelled as incident pain. The rapid onset and occasional unpredictability of breakthrough pain makes it particularly difficult to control and burdensome for the patient.

Secreted Factors

Many algogenic factors that contribute to cancer pain are secreted from cancer cells and associated stromal cells. Several of these are also mediators of inflammation and inflammatory pain secreted from immune cells recruited to the tumour site. Other classes of secreted factors include neurotrophins, neurotransmitters and cell-signalling molecules including hormones and cytokines. There have been several lines of research focussed on pursuing the importance of particular secreted factors to cancer pain, some of which have have shown more potential for treatment that others. It is appearing more evident that targeting a single factor is unlikely to emerge as a valid treatment of cancer pain in isolation. Many secreted factors play complex and intertwined roles in inducing and maintaining cancer pain, and determining their physiological roles and respective importance to cancer pain is an important pursuit.

Nerve Growth Factor

Nerve growth factor (NGF) has recently been found to be an important compound in the development and treatment of multiple pain states including cancer pain, and particularly cancer-induced bone pain. Targeting NGF in cancer pain has accumulated much primary basic and clinical evidence of efficacy, and is emerging as a promising therapeutic avenue. NGF can directly activate nociceptors that bear either the tropomyosin receptor kinase-A (TrkA) receptor or the low-affinity neurotrophin receptor p75. NGF is known to be upregulated in inflammatory pain states, and NGF-TrkA signalling is a mediator of sensitization through action at the spinal cord and DRG (20). In mouse models of osteosarcoma, NGF promotes the rapid neurogenesis of TrkA positive sensory and sympathetic fibres that eventually reach a pathologic density in the periosteum of tumour-bearing bone (21). Antibody sequestration of tumour-generated NGF reduces pain and pathological neurogenesis in animal models of osteosarcoma, prostate cancer, and breast cancer in bone (21–23). NGF also promotes the development of sensitization through transcriptional upregulation of neuropeptides and ion channels at the DRG in nociceptors, including substance P, calcitonin gene-related peptide (CGRP), and brain-derived

neurotrophic factor (BDNF) (21). BDNF is a neurotrophin that binds the TrkB receptor, and, like NGF, also to p75. The overexpression of BDNF at the spinal cord is likewise involved in the generation of central sensitization in both inflammatory and neuropathic pain states (24). Microglial production of BDNF is also involved in the development of central sensitization in an animal model of metastatic breast cancer-induced bone pain. Treatment of these animals with a tetracycline inhibitor of microglial activation, minocycline, reduced BDNF at the dorsal horn simultaneously with behavioural evidence of pain (25).

Endothelin-1

Endothelins are vasoactive and nociceptive peptides usually secreted from endothelial cells but also important in the regulation of angiogenesis, bone turnover, and tumour growth. Endothelin-1 (ET-1) can directly stimulate and sensitize nociceptors, and has been found to be secreted by breast and prostate cancer cells (26), fibrosarcoma (15,16) and oral squamous cell carcinoma (17). Much research has been focussed on the role of endothelins in cancer pain and they continue to pose a promising, if complex, target for treatment. Inhibition of the endothelin-A receptor (ETAR) which is expressed by sensory neurons and sensitive to ET-1, has successfully reduced cancer pain in multiple animal models (15–17), however these findings have not yet been validated at clinical trial (27). Interestingly, inhibition of the endothelin-B receptor (ETBR) can have the opposing effect of increasing cancer pain in animal models (28).

Acidic environment

Acidic microenvironments are characteristic of tumours and can directly stimulate nociceptors and induce downstream mediators of pain through several signalling cascades. Acid is a well-characterized mediator of pain. In cancer pain, particularly cancer-induced bone pain, it has been proposed that this acidic microenvironment in bone following tumour growth and osteoclast upregulation may produce sufficient acid to activate the low pH receptors acid-sensing ion channel (ASIC) and transient receptor

potential channel-vanilloid subfamily member 1/capsaicin receptors (TRPV1) that are present on nociceptors (29). In addition, expression of both of these receptors at the DRG is elevated in animal models of cancer-induced bone pain (30,31), and TRPV1 inhibition has reliably decreased cancer pain in animal models (32).

Glutamate

Many cancer cells secrete the neurotransmitter and cell-signalling amino acid glutamate, including breast, prostate, melanoma and glioma cells. In these cell types, the mechanism of glutamate secretion has been found to be the cystine/glutamate antiporter system xC- (33,34). Depending on the host tissue or metastatic site, this glutamate release can be a severely a disruptive influence on normal host tissue cell signaling, and can directly activate and sensitize primary afferent nociceptors (35). In glioma in the CNS, this glutamate release provides a functional advantage to the tumour, promoting malignancy, causing the excitotoxic cell death of neurons, and inducing detrimental oncodynamic side-effects including seizures, and possibly headache (33,36,37). In peripheral tissues, glutamate secretion and pain have been investigated in the context of cancer-induced bone pain. Reducing glutamate release from cancer cells by inhibiting the system xC- transporter can reduce cancer pain in animal models of breast cancer metastasized to the bone (38). This outcome may be due to the direct effects of secreted glutamate on the glutamate-sensitive nociceptors in the bone and peritumoural space, or due to differential changes in bone physiology that are susceptible to glutamatergic interference.

There are many other relevant secreted factors to cancer pain. These include but are not limited to: proteases, prostaglandins, bradykinin, TNF-α, interleukins-1 and 6, epidermal growth factor, transforming growth factor-β (TGF-β), and platelet-derived growth factor. These many factors have been detailed in a number of comprehensive reviews (14,39,40).

Physical Factors

Visceral pain syndromes often result from physical interference with one or more visceral organs by a tumour mass. Commonly this pain results from obstructions or distension of the visceral organs due to tumour growth or associated edema, including hepatic distension and intestinal obstructions (13). The bulk of a growing tumour also poses a risk of physically encountering a sensory neuron that varies with the characteristics and innervation of the host tissue. Physical contact between a tumour and neuron can cause nerve entrapment and injury and induce neuropathic pain states including plexopathies and radiculopathies. In animal models, the leading edge of tumours in bone were found to come into contact, injure and then destroy the distal processes of sensory fibres in conjunction with the development of neuropathic cancer pain states (41). In addition to stimulating and sensitizing sensory neurons, some of the secreted factors described above, including proteases, can also directly damage neurons, given certain conditions.

Sensitization

Cancer pain, like other enduring pain states, eventually becomes a state of chronic pain through the development of peripheral and central sensitization. Evidence of physiological changes indicative of sensitization in animal models of cancer pain are plentiful, including central sensitization at the dorsal horn (42–45), peripheral sensitization of local primary afferent C nociceptors (15,46–48), and cellular and neurochemical changes in the dorsal root ganglia (DRG) neurons and dorsal horn of the spinal cord (41,45,49).

Cancer-Induced Bone Pain

Bone pain from cancer is the most common type of cancer pain and despite the transition of several mechanistically targeted therapies into clinical practice, cancer-induced bone pain has remained extremely difficult to manage.

Cancer in bone can be a result of primary cancers of bone tissues and of metastases from distant sites. Bone metastases are extremely disruptive to normal bone cell metabolism, often resulting in the development of lesions featuring the dysregulated destruction and formation of mineralized bone tissue and the release of pro-inflammatory and algogenic substances into the bone microenvironment. This disruption is responsible for a host of intertwined pathologic consequences including bone fractures and microfractures, spinal cord compression, hypercalcaemia, and severe pain. Cancers of the lung, prostate, kidney, thyroid and breast are the most likely to produce a bone metastasis, with lung, prostate and breast cancer accounting for the vast majority of these cases (50).

Pain in metastatic cancer afflicted bone can arise from a number of stimuli and from any location within the bone. Bones are densely but unevenly innervated with sympathetic and sensory nerve fibres. Aβ-, Aδ- and C-fibres have been identified in the periosteum, as well as throughout mineralized bone and the bone marrow (51,52). The densely innervated periosteum is highly sensitive to disruption, however many painful lesions have been found to entirely lack periosteal involvement (1).

Animal models have revealed that cancer-induced bone pain is a unique pain state exhibiting distinct neurochemical and cellular features in the spinal cord and DRG that are not shared with other inflammatory or neuropathic pain states. In particular, changes in the expression of both substance P and CGRP were observed in the dorsal horn of the spinal cord in both inflammatory and neuropathic animal models, but neither neuropeptide was altered in models of bone cancer pain. In addition, bone cancer pain resulted in a much greater increase in glial fibrillary acidic protein (GFAP), a marker of astrocyte proliferation and hypertrophy than other modelled pain states (53).

As discussed above, a number of factors involved in tumour metastasis, growth and lesion formation have the potential to cause pain both directly and indirectly. The confluence of multiple contributing algogenic substances and extensive physical disruption at the tumour site indicate that the mechanisms responsible for cancer-induced bone pain are heterogeneous and complex.

The growing tumour itself contributes to pain generation through pressure on the periosteum or sensory nerves in bone, and through the destruction of sensory neurons. Both osteolytic (net bone resorbing) and osteoblastic (net bone forming) lesions are characterized by weaker bone that is more prone to fracture, compression, and collapse (54). Microfractures of the bone trabeculae and fractures of the whole bone compress sensory neurons and distort the periosteum, contributing significantly to pain (2).

The mechanisms of pathological bone cell turnover itself have also been linked to cancer-induced bone pain. Osteoblastic lesions commonly arise from prostate cancers and from ~25% of breast cancers (55). Their promotion of bone formation in the lesions associated with the metastatic tumour has been associated with the production by the tumour cells of a number of factors that are secreted into the bone microenvironment. The most well-characterized of these many associated factors is the aforementioned ET-1 which is released by typically osteoblastic prostate and breast cancer cell lines, and has been shown to act at ETAR on osteoblast cells (56). A number of other tumour associated factors are involved in the promotion of bone volume including osteoprogenetrin (OPG), TGF-β, urokinase, fibroblast growth factors, and possibly also prostate-specific antigen, all of which are associated with osteoblast cell proliferation (55). Pathological osteoblast activity associated with bone metastases is not just the overactive production of normal mineralized woven bone or osteons; rather cancerous osteoblastic lesions are typically dysregulated and osteosclerotic tissue that is of poor functional quality and conducive to pain (57).

Many cancers including multiple myeloma and most breast cancer metastases produce primarily osteolytic lesions which extensively degrade mineralized bone and are frequently severely painful. Other conditions including postmenopausal osteoporosis and hormone-ablative therapies in cancer treatment, are also associated with pathological osteolysis (58). Most of the osteolytic degradation associated with metastatic cancer is a result of the pathological activation of osteoclasts by the tumour; however, it has also been demonstrated that tumour cells can directly resorb bone even in the absence of osteoclast cells. Like osteoblastic metastases, osteoclastic bone resorption is stimulated by

the tumour through the release of a number of stimulatory factors that upregulate osteoclast proliferation and activity. One released factor, parathyroid hormone related peptide (PTHrP) shares many structural and functional similarities with parathyroid hormone (PTH). At the bone, PTHrP stimulates osteoclast proliferation through osteoblastic production of the receptor activator of nuclear factor-κB ligand(RANKL) (59). Treatment of animal models of metastatic bone cancer with neutralizing antibodies to PTHrP significantly reduces bone metastasis and resorption (60). However, PTHrP may have a dual role in bone remodelling, as its expression by prostate cancer cells has conversely been associated with the extent of osteoblastic lesions (61). Other osteolysis-inducing factors either released directly or induced to be released by tumour cells include macrophage colony-stimulating factor (M-CSF), TGF-β, TNF-α and β, interleukin-1, 6, and 11 (62), and Jagged1 of the Notch signalling pathway (63).

One of the roles of mineralized bone matrix is to act as a reservoir of minerals and growth factors that can be re- released into circulation by osteoclastic bone-resorption. Bone resorption in the event of a lytic metastasis results in the pathologic release of these same reserved substances. Ca^{2+} release in this manner is partially responsible for the hypercalcaemia that is characteristic of bone metastases (64), and the release of both mineral and growth factor has been implicated in a positive-feedback cycle of tumour growth and bone destruction commonly referred to as the vicious cycle hypothesis. The vicious cycle consists of the release of osteoclast stimulating factors including PTHrP from the metastatic tumour cells which promote osteoclast cells to increase bone resorption, resulting in the release of tumour cell-stimulating cytokines and growth factors from the bone matrix reserves, that further stimulate tumour growth and perpetuate the “vicious” cycle. Factors released in this manner from mineralized bone that stimulate tumour cell growth include TGF-β, insulin-like growth factor 1, and Ca^{2+} itself (55).

Bone resorption can also occur independently of osteoclasts through the direct action of cancer cells. This ability has been demonstrated in vitro in several cancer types including breast (65), prostate (66), murine melanoma (67), and giant cell tumour of bone (68).

MMPs secreted from these cancer cells are thought to play a significant role in this process, particularly MMP-2 and 9 (69), and MMP-13 (68). Inhibition of MMPs reduced the ability of in vivo human breast cancer cells to degrade bone (69).

Inhibitors of osteoclast activity have reliably been demonstrated to limit bone pain, and the enhancement of resorption has conversely been demonstrated to increase pain, but this could be due to a number of factors (70). Osteoclastic bone resorption is initiated through the acidification of the resorption compartment of the osteoclast cell at the mineralized bone surface by vacuolar-ATPase H+ transporters. Due to this process and to the induction of an acidic microenvironment by cancer cells themselves, the extracellular environment of various human tumours becomes progressively acidic as tumours develop (71). This acidic microenvironment in bone following tumour growth and osteoclast upregulation may produce sufficient acid to activate the ASIC and TRPV1 low-pH receptors that are present on nociceptors in bone (29).

Cancer-Induced Bone Pain Treatment

An impediment to the effective treatment of cancer-induced bone pain is that current standard treatments are largely based on principles developed from studies of non-cancer pain (1). Standard treatment for progressive ongoing pain involves adherence to the WHO analgesic ladder following progression from non-opioid analgesics for mild pain through strong opioids in conjunction with non-opioids and adjuvant treatment for moderate to severe pain. Adjuvant treatments in this case are non-analgesics that modify analgesic outcomes. The use of adjuvant treatments in the management of pain is quite common, and standard treatments can include the use of antidepressants or anticonvulsants. In the treatment of cancer-induced bone pain the use of drugs that prevent osteoclastic bone resorption are widely used as adjuvants. Bisphosphonates are a class of antiresorptive compounds with a high affinity to bind Ca^{2+} and therefore to become sequestered in the Ca^{2+} rich bone matrix. When released and absorbed by osteoclasts, bisphosphonates inhibit the enzyme farnesyl diphosphate synthase which then limits the downstream ability of the cell to produce several essential GTP-binding proteins, inducing apoptotic

cell death (72). This limits the extent of osteoclastic resorption in the bone and therefore limits pain from mechanical stress and osteoclast-associated algogenic factors. Bisphosphonate treatment has also been tentatively shown to reduce metastasis to bone and increase survival in breast cancer patients without current bone metastases (73). These results have fuelled the search for drugs that, like bisphosphonates, inhibit osteoclastic bone resorption. Treatments with OPG, the decoy receptor for RANKL has successfully limited bone pain and tumour growth in animal models (74). A fully human monoclonal antibody to RANKL, denosumab, has also been developed as a more specific inhibitor of osteoclast activity than bisphosphonates. In multiple phase III clinical trials denosumab was superior to several bisphosphonates in the prevention of skeletal related events including pain in both prostate and breast cancer patients (53). The inhibition of osteoclasts appears to have several serious side effects that has limited treatment with these drugs. Bisphosphonates are associated with occasional atrial fibrillation, osteomyelitis, and more commonly, osteonecrosis of the jaw of which bisphosphonate treatment is involved in over 90% of all cases (75). Standard treatments for cancer in bone can also have an impact on pain including radiotherapy and surgery. Both are applied palliatively with pain control as the primary intention (76). Recently, a fully humanized monoclonal antibody to NGF, tanezumab has demonstrated clinical efficacy in the treatment of cancer-induced bone pain (77).

Currently, μ-agonist opioids remain the gold standard for the treatment of moderate to severe cancer pain in adherence to the WHO pain ladder. Their efficacy is limited by the occurrence of severe side-effects at the doses necessary for adequate analgesia and patient quality of life suffers as a result. Adjuvant treatments are successfully utilized in cancer-induced bone pain management, but reliable pain relief in a manner not independently detrimental to patient quality of life remains elusive.

Current treatment

The effective management of cancer pain is largely performed in accordance with the principles of the World Health Organization (WHO) guidelines for cancer pain relief.

The core of the guidelines is based upon adherence to the WHO Analgesic Ladder which stipulates a treatment progression from non-opioid analgesics through weak opioids to strong opioids as is necessary to treat progressively worsening pain. Adjuvant drug supplementation and other supplementary interventions including radiotherapy and alternative treatments are applicable throughout as necessary. Adherence to this treatment paradigm has been validated as effective for good or satisfactory pain relief in the majority of cancer patients; however, 24% of treated patients do not experience complete pain control, with 12% reporting inadequate pain control (78,79). It has also been reported that approximately two-thirds of patients undergoing treatment with opioids experience episodes of breakthrough pain (19). Episodes of breakthrough pain are treated usually with a "rescue dose" of the patient's current analgesic, or with a different fast-acting transmucosal μ-opioid agonist (80).

Current analgesic treatment practices are often effective at their priority of reducing the experience of pain for the cancer patient, but that pain relief often comes at the cost of otherwise impairing the patient's quality of life through treatment side effects. Opioids in particular induce a number of serious dose-limiting side effects including nausea, constipation, vomiting, respiratory depression, sedation, somnolence, and cognitive impairment, and prolonged use can induce the development of physical dependence, tolerance and addiction (81,82). Non-steroidal anti-inflammatory drugs (NSAIDs) are most often the first analgesic treatment for cancer pain, and they too are associated with dose-dependent adverse effects, most predominantly, gastrointestinal and renal side-effects (83,84). Patient or caregiver concern about treatment-associated side effects or of the consequences of dependence on pain treatment with analgesics can often result in the insufficient control of otherwise manageable pain, as can layers of regulation governing access to controlled pain medications (85,86). For these patients who cannot or do not access adequate pain relief, in addition to those patients whose pain cannot be fully controlled with available analgesics, inadequate cancer pain management yet remains a global public health concern.

Conclusion

In conclusion, the oncodynamic effect of cancer pain is a common and severely detrimental consequence for patients living with cancer. As cancer treatments continue to improve, and cancer patients live longer with their disease, strategies of pain control that maintain patient quality of life become ever more valuable, and the understanding and high-quality management of chronic cancer pain becomes a more pressing priority.

References

1. Sabino MAC, Mantyh PW. Pathophysiology of bone cancer pain. J Support Oncol. 2005 Jan;3(1):15–24.

2. Mercadante S. Malignant bone pain: pathophysiology and treatment. Pain. 1997 Jan;69(1-2):1–18.

3. Valeberg BT, Rustøen T, Bjordal K, Hanestad BR, Paul S, Miaskowski C. Self-reported prevalence, etiology, and characteristics of pain in oncology outpatients. Eur J Pain. 2008 Jul;12(5):582–90.

4. Cleeland CS. The impact of pain on the patient with cancer. Cancer. 1984 Dec 1;54(11 Suppl):2635–41.

5. Greco MT, Roberto A, Corli O, Deandrea S, Bandieri E, Cavuto S, et al. Quality of cancer pain management: an update of a systematic review of undertreatment of patients with cancer. J Clin Oncol. 2014 Dec 20;32(36):4149–54.

6. Loeser JD, Treede R-D. The Kyoto protocol of IASP Basic Pain Terminology. Pain. 2008 Jul 31;137(3):473–7.

7. Todd AJ. Anatomy of primary afferents and projection neurones in the rat spinal dorsal horn with particular emphasis on substance P and the neurokinin 1 receptor. Exp Physiol. 2002 Mar;87(2):245–9.

8. Basbaum AI, Bautista DM, Scherrer G, Julius D. Cellular and molecular mechanisms of pain. Cell. 2009 Oct 16;139(2):267–84.

9. Borsook D. Neurological diseases and pain. Brain. 2012 Feb;135(Pt 2):320–44.

10. Voscopoulos C, Lema M. When does acute pain become chronic? Br J Anaesth. 2010 Dec 10;105(Supplement 1):i69–85.

11. Gold MS, Gebhart GF. Nociceptor sensitization in pain pathogenesis. Nat Med. 2010 Nov;16(11):1248–57.

12. Sorge RE, Mapplebeck JCS, Rosen S, Beggs S, Taves S, Alexander JK, et al. Different immune cells mediate mechanical pain hypersensitivity in male and female mice. Nat Neurosci. 2015 Jun 29;18(8):1081–3.

13. Portenoy RK. Treatment of cancer pain. Lancet (London, England). 2011 Jun 25;377(9784):2236–47.

14. Mantyh PW, Clohisy DR, Koltzenburg M, Hunt SP. Molecular mechanisms of cancer pain. Nat Rev Cancer. 2002 Mar;2(3):201–9.

15. Cain DM, Wacnik PW, Turner M, Wendelschafer-Crabb G, Kennedy WR, Wilcox GL, et al. Functional interactions between tumor and peripheral nerve: changes in excitability and morphology of primary afferent fibers in a murine model of cancer pain. J Neurosci. 2001 Dec 1;21(23):9367–76.

16. Wacnik PW, Eikmeier LJ, Ruggles TR, Ramnaraine ML, Walcheck BK, Beitz AJ, et al. Functional interactions between tumor and peripheral nerve: morphology, algogen identification, and behavioral characterization of a new murine model of cancer pain. J Neurosci. 2001 Dec 1;21(23):9355–66.

17. Schmidt BL, Pickering V, Liu S, Quang P, Dolan J, Connelly ST, et al. Peripheral endothelin A receptor antagonism attenuates carcinoma-induced pain. Eur J Pain. 2007 May;11(4):406–14.

18. Yuyama H, Koakutsu A, Fujiyasu N, Fujimori A, Sato S, Shibasaki K, et al. Inhibitory effects of a selective endothelin-A receptor antagonist YM598 on endothelin-1-induced potentiation of nociception in formalin-induced and prostate cancer-induced pain models in mice. J Cardiovasc Pharmacol. 2004 Nov;44 Suppl 1:S479–82.

19. Caraceni A, Portenoy RK. An international survey of cancer pain characteristics and syndromes. IASP Task Force on Cancer Pain. International Association for the Study of Pain. Pain. 1999 Sep;82(3):263–74.

20. Mantyh PW, Koltzenburg M, Mendell LM, Tive L, Shelton DL. Antagonism of nerve growth factor-TrkA signaling and the relief of pain. Anesthesiology. 2011 Jul;115(1):189–204.

21. Mantyh WG, Jimenez-Andrade JM, Stake JI, Bloom AP, Kaczmarska MJ, Taylor RN, et al. Blockade of nerve sprouting and neuroma formation markedly attenuates the development of late stage cancer pain. Neuroscience. 2010 Dec 1;171(2):588–98.

22. Bloom AP, Jimenez-Andrade JM, Taylor RN, Castañeda-Corral G, Kaczmarska MJ, Freeman KT, et al. Breast cancer-induced bone remodeling, skeletal pain, and sprouting of sensory nerve fibers. J Pain. 2011 Jun;12(6):698–711.

23. Jimenez-Andrade JM, Ghilardi JR, Castañeda-Corral G, Kuskowski MA, Mantyh PW. Preventive or late administration of anti-NGF therapy attenuates tumor-induced nerve sprouting, neuroma formation, and cancer pain. Pain. 2011 Nov;152(11):2564–74.

24. Merighi A, Salio C, Ghirri A, Lossi L, Ferrini F, Betelli C, et al. BDNF as a pain modulator. Prog Neurobiol. 2008 Jul;85(3):297–317.

25. Wang L-N, Yang J-P, Zhan Y, Ji F-H, Wang X-Y, Zuo J-L, et al. Minocycline-induced reduction of brain-derived neurotrophic factor expression in relation to cancer-induced bone pain in rats. J Neurosci Res. 2012 Mar;90(3):672–81.

26. Nelson JB, Hedican SP, George DJ, Reddi AH, Piantadosi S, Eisenberger MA, et al. Identification of endothelin-1 in the pathophysiology of metastatic adenocarcinoma of the prostate. Nat Med. 1995 Sep;1(9):944–9.

27. Nelson JB, Love W, Chin JL, Saad F, Schulman CC, Sleep DJ, et al. Phase 3, randomized, controlled trial of atrasentan in patients with nonmetastatic, hormone-refractory prostate cancer. Cancer. 2008 Nov 1;113(9):2478–87.

28. Quang PN, Schmidt BL. Peripheral endothelin B receptor agonist-induced antinociception involves endogenous opioids in mice. Pain. 2010 May;149(2):254–62.

29. Yoneda T, Hata K, Nakanishi M, Nagae M, Nagayama T, Wakabayashi H, et al. Involvement of acidic microenvironment in the pathophysiology of cancer-associated bone pain. Bone. 2011 Jan;48(1):100–5.

30. Pan H-L, Zhang Y-Q, Zhao Z-Q. Involvement of lysophosphatidic acid in bone cancer pain by potentiation of TRPV1 via PKCε pathway in dorsal root ganglion neurons. Mol Pain. 2010 Jan;6:85.

31. Qiu F, Wei X, Zhang S, Yuan W, Mi W. Increased expression of acid-sensing ion channel 3 within dorsal root ganglia in a rat model of bone cancer pain. Neuroreport. 2014 Aug 20;25(12):887–93.

32. Ghilardi JR, Röhrich H, Lindsay TH, Sevcik MA, Schwei MJ, Kubota K, et al. Selective blockade of the capsaicin receptor TRPV1 attenuates bone cancer pain. J Neurosci. 2005 Mar 23;25(12):3126–31.

33. Chung WJ, Lyons SA, Nelson GM, Hamza H, Gladson CL, Gillespie GY, et al. Inhibition of cystine uptake disrupts the growth of primary brain tumors. J Neurosci. 2005 Aug 3;25(31):7101–10.

34. Sharma MK, Seidlitz EP, Singh G. Cancer cells release glutamate via the cystine/glutamate antiporter. Biochem Biophys Res Commun. 2010 Jan 1;391(1):91–5.

35. Cairns BE, Gambarota G, Svensson P, Arendt-Nielsen L, Berde CB. Glutamate-induced sensitization of rat masseter muscle fibers. Neuroscience. 2002 Jan;109(2):389–99.

36. Buckingham SC, Campbell SL, Haas BR, Montana V, Robel S, Ogunrinu T, et al. Glutamate release by primary brain tumors induces epileptic activity. Nat Med. 2011 Oct;17(10):1269–74.

37. Robert SM, Buckingham SC, Campbell SL, Robel S, Holt KT, Ogunrinu-Babarinde T, et al. SLC7A11 expression is associated with seizures and predicts poor survival in patients with malignant glioma. Sci Transl Med. 2015 May 27;7(289):289ra86.

38. Ungard RG, Seidlitz EP, Singh G. Inhibition of breast cancer-cell glutamate release with sulfasalazine limits cancer-induced bone pain. Pain. 2014 Jan;155(1):28–36.

39. Jimenez-Andrade JM, Mantyh WG, Bloom AP, Ferng AS, Geffre CP, Mantyh PW. Bone cancer pain. Ann N Y Acad Sci. 2010 Jun;1198:173–81.

40. Slosky LM, Largent-Milnes TM, Vanderah TW. Use of Animal Models in Understanding Cancer-induced Bone Pain. Cancer Growth Metastasis. 2015 Jan;8(Suppl 1):47–62.

41. Peters CM, Ghilardi JR, Keyser CP, Kubota K, Lindsay TH, Luger NM, et al. Tumor-induced injury of primary afferent sensory nerve fibers in bone cancer pain. Exp Neurol. 2005 May;193(1):85–100.

42. Khasabov SG, Hamamoto DT, Harding-Rose C, Simone DA. Tumor-evoked hyperalgesia and sensitization of nociceptive dorsal horn neurons in a murine model of cancer pain. Brain Res. 2007 Nov 14;1180:7–19.

43. Urch CE, Donovan-Rodriguez T, Dickenson AH. Alterations in dorsal horn neurones in a rat model of cancer-induced bone pain. Pain. 2003 Dec;106(3):347–56.

44. Yanagisawa Y, Furue H, Kawamata T, Uta D, Yamamoto J, Furuse S, et al. Bone cancer induces a unique central sensitization through synaptic changes in a wide area of the spinal cord. Mol Pain. 2010 Jan;6:38.

45. Donovan-Rodriguez T, Dickenson AH, Urch CE. Superficial dorsal horn neuronal responses and the emergence of behavioural hyperalgesia in a rat model of cancer-induced bone pain. Neurosci Lett. 2004 Apr 22;360(1-2):29–32.

46. Zhao J, Pan H-L, Li T-T, Zhang Y-Q, Wei J-Y, Zhao Z-Q. The sensitization of peripheral C-fibers to lysophosphatidic acid in bone cancer pain. Life Sci. 2010 Jul 17;87(3-4):120–5.

47. Zheng Q, Fang D, Cai J, Wan Y, Han J-S, Xing G-G. Enhanced excitability of small dorsal root ganglion neurons in rats with bone cancer pain. Mol Pain. 2012 Jan;8:24.

48. Hamamoto DT, Khasabov SG, Cain DM, Simone DA. Tumor-evoked sensitization of C nociceptors: a role for endothelin. J Neurophysiol. 2008 Oct;100(4):2300–11.

49. Schwei MJ, Honore P, Rogers SD, Salak-Johnson JL, Finke MP, Ramnaraine ML, et al. Neurochemical and cellular reorganization of the spinal cord in a murine model of bone cancer pain. J Neurosci. 1999 Dec 15;19(24):10886–97.

50. Coleman RE. Clinical features of metastatic bone disease and risk of skeletal morbidity. Clin Cancer Res. 2006 Oct 15;12(20 Pt 2):6243s – 6249s.

51. Mach DB, Rogers SD, Sabino MC, Luger NM, Schwei MJ, Pomonis JD, et al. Origins of skeletal pain: sensory and sympathetic innervation of the mouse femur. Neuroscience. 2002 Jan;113(1):155–66.

52. Jimenez-Andrade JM, Mantyh WG, Bloom AP, Xu H, Ferng AS, Dussor G, et al. A phenotypically restricted set of primary afferent nerve fibers innervate the bone versus skin: therapeutic opportunity for treating skeletal pain. Bone. 2010 Feb;46(2):306–13.

53. Honore P, Rogers SD, Schwei MJ, Salak-Johnson JL, Luger NM, Sabino MC, et al. Murine models of inflammatory, neuropathic and cancer pain each generates a unique set of neurochemical changes in the spinal cord and sensory neurons. Neuroscience. 2000 Jan;98(3):585–98.

54. Halvorson KG, Sevcik MA, Ghilardi JR, Rosol TJ, Mantyh PW. Similarities and differences in tumor growth, skeletal remodeling and pain in an osteolytic and osteoblastic model of bone cancer. Clin J Pain. 2006 Sep;22(7):587–600.

55. Mundy GR. Metastasis to bone: causes, consequences and therapeutic opportunities. Nat Rev Cancer. 2002 Aug;2(8):584–93.

56. Yin JJ, Mohammad KS, Käkönen SM, Harris S, Wu-Wong JR, Wessale JL, et al. A causal role for endothelin-1 in the pathogenesis of osteoblastic bone metastases. Proc Natl Acad Sci U S A. 2003 Sep 16;100(19):10954–9.

57. Roudier MP, Vesselle H, True LD, Higano CS, Ott SM, King SH, et al. Bone histology at autopsy and matched bone scintigraphy findings in patients with hormone refractory prostate cancer: the effect of bisphosphonate therapy on bone scintigraphy results. Clin Exp Metastasis. 2003 Jan;20(2):171–80.

58. Coleman RE. Skeletal complications of malignancy. Cancer. 1997 Oct 15;80(8 Suppl):1588–94.

59. Thomas RJ, Guise TA, Yin JJ, Elliott J, Horwood NJ, Martin TJ, et al. Breast cancer cells interact with osteoblasts to support osteoclast formation. Endocrinology. 1999 Oct;140(10):4451–8.

60. Guise TA, Yin JJ, Taylor SD, Kumagai Y, Dallas M, Boyce BF, et al. Evidence for a causal role of parathyroid hormone-related protein in the pathogenesis of human breast cancer-mediated osteolysis. J Clin Invest. 1996 Oct 1;98(7):1544–9.

61. Liao J, Li X, Koh AJ, Berry JE, Thudi N, Rosol TJ, et al. Tumor expressed PTHrP facilitates prostate cancer-induced osteoblastic lesions. Int J Cancer. 2008 Nov 15;123(10):2267–78.

62. Orr FW, Lee J, Duivenvoorden WC, Singh G. Pathophysiologic interactions in skeletal metastasis. Cancer. 2000 Jun 15;88(12 Suppl):2912–8.

63. Sethi N, Dai X, Winter CG, Kang Y. Tumor-derived JAGGED1 promotes osteolytic bone metastasis of breast cancer by engaging notch signaling in bone cells. Cancer Cell. 2011 Feb 15;19(2):192–205.

64. Yates AJ, Gutierrez GE, Smolens P, Travis PS, Katz MS, Aufdemorte TB, et al. Effects of a synthetic peptide of a parathyroid hormone-related protein on calcium homeostasis, renal tubular calcium reabsorption, and bone metabolism in vivo and in vitro in rodents. J Clin Invest. 1988 Mar;81(3):932–8.

65. Eilon G, Mundy GR. Direct resorption of bone by human breast cancer cells in vitro. Nature. 1978 Dec 14;276(5689):726–8.

66. Sanchez-Sweatman OH, Orr FW, Singh G. Human metastatic prostate PC3 cell lines degrade bone using matrix metalloproteinases. Invasion Metastasis. Jan;18(5-6):297–305.

67. Sanchez-Sweatman OH, Lee J, Orr FW, Singh G. Direct osteolysis induced by metastatic murine melanoma cells: role of matrix metalloproteinases. Eur J Cancer. 1997 May;33(6):918–25.

68. Mak IWY, Seidlitz EP, Cowan RW, Turcotte RE, Popovic S, Wu WCH, et al. Evidence for the role of matrix metalloproteinase-13 in bone resorption by giant cell tumor of bone. Hum Pathol. 2010 Sep;41(9):1320–9.

69. Lee J, Weber M, Mejia S, Bone E, Watson P, Orr W. A matrix metalloproteinase inhibitor, batimastat, retards the development of osteolytic bone metastases by MDA-

MB-231 human breast cancer cells in Balb C nu/nu mice. Eur J Cancer. 2001 Jan;37(1):106–13.

70. Nagae M, Hiraga T, Wakabayashi H, Wang L, Iwata K, Yoneda T. Osteoclasts play a part in pain due to the inflammation adjacent to bone. Bone. 2006 Nov;39(5):1107–15.

71. Gatenby RA. Acid-Mediated Tumor Invasion: a Multidisciplinary Study. Cancer Res. 2006 May 15;66(10):5216–23.

72. Rodan GA, Martin TJ. Therapeutic approaches to bone diseases. Science. 2000 Sep 1;289(5484):1508–14.

73. Powles T, Paterson A, McCloskey E, Schein P, Scheffler B, Tidy A, et al. Reduction in bone relapse and improved survival with oral clodronate for adjuvant treatment of operable breast cancer [ISRCTN83688026]. Breast Cancer Res. 2006 Jan;8(2):R13.

74. Honore P, Luger NM, Sabino MA, Schwei MJ, Rogers SD, Mach DB, et al. Osteoprotegerin blocks bone cancer-induced skeletal destruction, skeletal pain and pain-related neurochemical reorganization of the spinal cord. Nat Med. 2000 May;6(5):521–8.

75. Drake MT, Clarke BL, Khosla S. Bisphosphonates: mechanism of action and role in clinical practice. Mayo Clin Proc. 2008 Sep;83(9):1032–45.

76. Clines GA, Guise TA. Molecular mechanisms and treatment of bone metastasis. Expert Rev Mol Med. 2008 Jan;10:e7.

77. Sopata M, Katz N, Carey W, Smith MD, Keller D, Verburg KM, et al. Efficacy and safety of tanezumab in the treatment of pain from bone metastases. Pain. 2015 Sep;156(9):1703–13.

78. Zech DF, Grond S, Lynch J, Hertel D, Lehmann KA. Validation of World Health Organization Guidelines for cancer pain relief: a 10-year prospective study. Pain. 1995 Oct;63(1):65–76.

79. Mercadante S. Pain treatment and outcomes for patients with advanced cancer who receive follow-up care at home. Cancer. 1999 Apr 15;85(8):1849–58.

80. Casuccio A, Mercadante S, Fulfaro F. Treatment strategies for cancer patients with breakthrough pain. Expert Opin Pharmacother. 2009 Apr;10(6):947–53.

81. Benyamin R, Trescot AM, Datta S, Buenaventura R, Adlaka R, Sehgal N, et al. Opioid complications and side effects. Pain Physician. 2008 Mar;11(2 Suppl):S105–20.

82. Meuser T, Pietruck C, Radbruch L, Stute P, Lehmann KA, Grond S. Symptoms during cancer pain treatment following WHO-guidelines: a longitudinal follow-up study of symptom prevalence, severity and etiology. Pain. 2001 Sep;93(3):247–57.

83. Brater DC. Effects of nonsteroidal anti-inflammatory drugs on renal function: focus on cyclooxygenase-2-selective inhibition. Am J Med. 1999 Dec 13;107(6A):65S – 70S; discussion 70S – 71S.

84. Wolfe MM, Lichtenstein DR, Singh G. Gastrointestinal toxicity of nonsteroidal antiinflammatory drugs. N Engl J Med. 1999 Jun 17;340(24):1888–99.

85. Cleeland CS, Gonin R, Baez L, Loehrer P, Pandya KJ. Pain and treatment of pain in minority patients with cancer. The Eastern Cooperative Oncology Group Minority Outpatient Pain Study. Ann Intern Med. 1997 Nov 1;127(9):813–6.

86. Pargeon KL, Hailey BJ. Barriers to effective cancer pain management: a review of the literature. J Pain Symptom Manage. 1999 Nov;18(5):358–68.

Figures

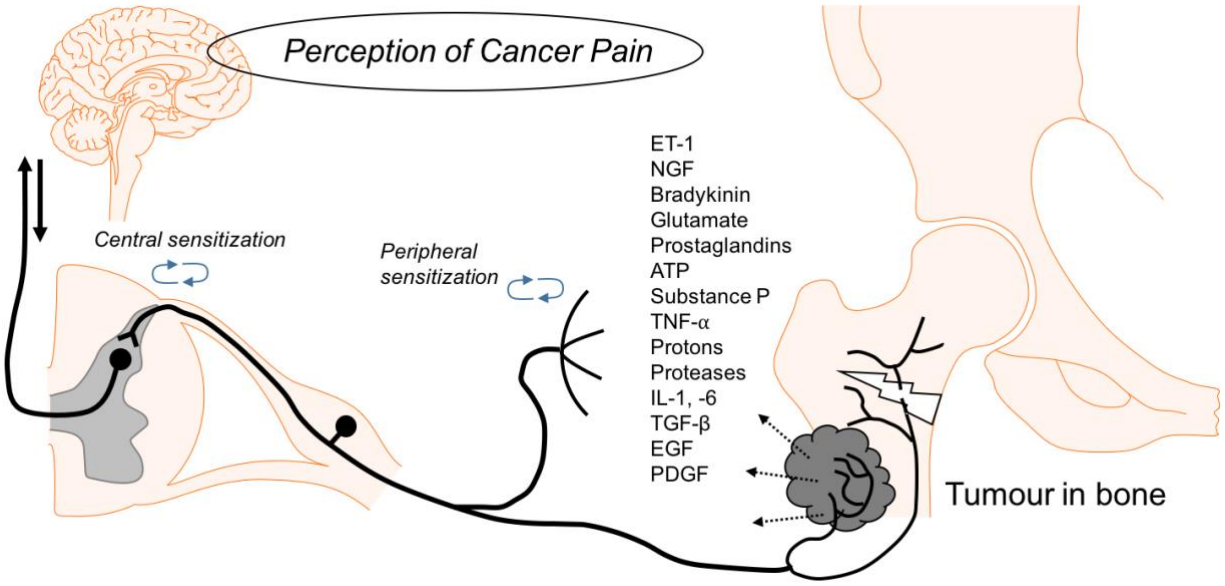

Figure 1.

Pain is perceived by transmission through sensory neurons to the central nervous system. Cancer pain is initially stimulated through many mechanisms. This figure illustrates several mechanisms of cancer-induced bone pain, including bone fracture due to weak or degraded bone structures proximal to the tumour, and multiple secreted factors from tumour cells and other cells including immune cells recruited to the tumour site. These secreted factors can modify the tumour itself, the host tissue environment, and can directly stimulate nociceptors. Pain signalling is initiated by sensory neurons in and around in the bone and tumour, and transmitted through the dorsal horn and spinothalamic or spinoreticulothalamic tracts of the spinal cord to the brain. Descending controls from the brain and spinal cord can alter pain signalling and initiate features of central and peripheral sensitization which serve to maintain and amplify pain, leading to intractable chronic cancer pain.

CHAPTER 2: xCT knockdown in human breast cancer cells delays onset of cancer-induced bone pain

Robert G Ungard, Katja Linher-Melville, Mina Nashed, Manu Sharma, Jianping Wen, Gurmit Singh. Mol Pain. 2019;15.

Preface

In this chapter, an author-generated version of the manuscript titled "xCT knockdown in human breast cancer cells delays onset of cancer-induced bone pain", published in Molecular Pain in 2019, is presented. The article is reproduced with permission from SAGE Publishing, as licensed under the terms of Creative Commons Attribution-Non Commercial 4.0 License which permits non-commercial use, reproduction and distribution of the work without further permission provided the original work is attributed as specified on the SAGE and Open Access pages. The copyright agreement is included in **Appendix 2**.

Robert Ungard and Katja Linher-Melville are co-first authors on this research report as they contributed equally to the work.

For this manuscript I cultured cancer cells for in vivo studies, induced all in vivo models of CIBP, performed behavioural tests and data analysis, and drafted and revised the manuscript. Katja Linher-Melville performed qPCR, Western Blotting and cystine uptake assays for in vitro and in vivo studies, prepared cells for RNA-Seq and contributed to writing and editing the manuscript. Manu Sharma assisted with all aspects of the in vivo studies. Jianping Wen generated and performed in vitro work to screen clones. Mina Nashed analyzed RNA-Seq data. All authors contributed to successive drafts of the manuscript. Gurmit Singh supervised the overall project, edited the manuscript, and provided funding for the study. All authors read and approved the final manuscript.

American English spelling is used throughout the manuscript, as required by the journal.

Context and Background Information

This chapter describes the current state of the hypothesis that targeting the system xC- cystine/glutamate antiporter, and in particular its glutamate release function is a

promising target in cancer pain research. This work built on the findings from our lab and others that pharmacological inhibition of system xC- induces a reduction and delay to onset of cancer pain-related behaviour (Ungard et al. 2014; Slosky et al. 2016; Fazzari et al. 2017). The rationale of this approach includes that targeting pain-inducing features of the cancer cell may spare the broad side effects of centrally-acting analgesics and have the added benefit of potentially compromising cancer cell growth. In addition, cancer cell-derived glutamate has been demonstrated to directly activate and sensitize primary afferent nociceptors in musculoskeletal tissues (Cairns et al. 2002).

To date, pharmacological approaches to researching the impact of system xC- cystine/glutamate transport on cancer pain have been limited by inconsistent specificity, off-target action, and dose-limiting side effects (Ungard et al. 2014; Robert et al. 2015).

The model of xCT knockdown cancer cells presented here allows this potential therapeutic target to be evaluated for CIBP with greater specificity than previous pharmacological approaches. This manuscript describes the development of a stable shRNA-induced knockdown of xCT, (SLC7A11) in the human breast cancer cell line MDA-MB-231. xCT knockdown was confirmed at the transcript, protein, and functional levels. To investigate possible associated differential gene expression in response to xCT knockdown in these stable clones, RNA-Sequencing was performed, identifying multiple differentially expressed genes relevant to cancer pain including nerve growth factor, interleukin-1, and colony-stimulating factor-1.

Knockdown cells were implanted in a mouse model of CIBP and evaluated for tumour growth and pain-related behaviour. We found no changes in tumour growth between groups, but observed a delay in the time to onset of pain-related behaviour in mice implanted with the xCT knockdown cell line as opposed to vector-control mice.

These results add specificity to the body of evidence suggesting that a reduction in glutamate release from cancers in bone by inhibition of the system xC- transporter may decrease the severe and intractable pain associated with bone metastases.

In addition, we developed an IPTG-inducible (shRNA) xCT knockdown clone in the same cell line with respective negative controls. These clones were validated for sustained and inducible knockdown in vitro at the transcript, protein, and functional levels, and tumour growth was confirmed and measured subcutaneously in vivo. Similarly to the work presented in this chapter with the stable xCT knockdown cell line, these IPTG-inducible xCT knockdown clones were also implanted and tested in the same intrafemoral mouse model of CIBP for pain-related behaviour relative to an uninduced control group, however insufficient numbers of mice successfully grew and retained tumours to draw conclusions from our data. The methodology and results of this investigation are presented in **Appendix 3**.

xCT knockdown in human breast cancer cells delays onset of cancer-induced bone pain

Robert G Ungard* 1,2, Katja Linher-Melville* 1,2, Mina Nashed 1,2, Manu Sharma 1,2, Jianping Wen 2, Gurmit Singh 1,2

1 Michael G. DeGroote Institute for Pain Research and Care, Medicine, McMaster University, 1280 Main St. West, Hamilton, ON L8S 4M1, Canada

2 Department of Pathology and Molecular Medicine, McMaster University, 1280 Main St. West, Hamilton, ON L8N 3Z5, Canada

*These authors contributed equally to this work

All authors declare no conflict of interest

Number of tables: 1

Number of figures: 5

Number of words: 8684

Number of supplementary tables: 1

Corresponding Author: Dr. Gurmit Singh

Department of Pathology & Molecular Medicine, McMaster University, 1280 Main Street West, Hamilton, ON L8N 3Z5, Canada

Tel.: +1 905 525 9140 x28144

E-mail address: singhg@mcmaster.ca (G. Singh)

ABSTRACT

Cancers in the bone produce a number of severe symptoms including pain that compromises patient functional status, quality of life, and survival. The source of this pain is multifaceted, and includes factors secreted from tumor cells. Malignant cells release the neurotransmitter and cell-signaling molecule glutamate via the oxidative stress-related cystine/glutamate antiporter, system xC-, which reciprocally imports cystine for synthesis of glutathione and the cystine/cysteine redox cycle. Pharmacological inhibition of system xC- has shown success in reducing and delaying the onset of cancer pain-related behavior in mouse models. This investigation describes the development of a stable shRNA-induced knockdown of the functional trans-membrane system xC- subunit xCT, (SLC7A11) in the human breast cancer cell line MDA-MB-231. Clones were verified for xCT knockdown at the transcript, protein, and functional levels. RNAseq was performed on a representative clone to comprehensively examine the transcriptional cellular signature in response to xCT knockdown, identifying multiple differentially-regulated factors relevant to cancer pain including nerve growth factor, interleukin-1, and colony-stimulating factor-1. Mice were inoculated intrafemorally and recordings of pain-related behaviors including weight bearing, mechanical withdrawal, and limb use were performed. Animals implanted with xCT knockdown cancer cells displayed a delay until the onset of nociceptive behaviors relative to control cells. These results add to the body of evidence suggesting that a reduction in glutamate release from cancers in bone by inhibition of the system xC- transporter may decrease the severe and intractable pain associated with bone metastases.

KEYWORDS

Pain; Cancer-Induced Bone Pain; Nociception; Breast Cancer; System xC-; SLC7A11; Glutamate; Bone Metastasis

INTRODUCTION

Bone is the most common site of distant breast cancer metastases [1], with an overall incidence of approximately 22 % at or following diagnosis [2]. These metastases produce symptoms including severe and often untreatable pain that compromise patient functional status, quality of life, and survival [3], and can develop into a chronic pain condition [4–6]. Current management strategies of cancer-induced bone pain (CIBP) focus on radiotherapy and analgesic drugs including strong NSAIDs and opioids that induce severe dose-limiting side-effects that are independently deleterious to treatment outcomes and patient quality of life. As the number of cancer patients living with bone metastases increases, there is a growing need for interventions that focus on the preservation of quality of life.

Using animal models, cancer pain has been revealed to be a complex state with peripheral [7,8] and central [9–11] features of neuropathic and inflammatory pain. There are multiple potential mechanisms underlying the development and maintenance of CIBP, including direct effects of tumor and stromal cells, as well as disrupted host bone cell processes. CIBP in animal models has been ameliorated by a number of promising approaches such as targeting inflammation [12], acidosis [13], and neurotrophin-induced neurogenesis [7,14,15].

We previously demonstrated that human cancer cells with the capacity to metastasize to bone release glutamate through the cystine/glutamate antiporter system xC- [16,17]. System xC- exchanges glutamate for cystine, ameliorating oxidative/nitrosative stress arising from the accumulation of intracellular reactive species, which occurs due to altered metabolism of aggressive cancer cells. This cancer cell-derived glutamate accumulates in the bone where it can disrupt host tissues and activate and sensitize the Aβ-, Aδ-, and C-fibers sensitive to noxious mechanical, thermal and chemical stimuli, all of which show changes in excitability in animal models of CIBP [18]. CIBP animal models demonstrate either a reduction or delay in the onset of nociceptive behaviors when treated with system xC--inhibitors sulfasalazine [19,20] and capsazepine [21]; and

when indirectly downregulated with peroxynitrate scavengers [20] and TrkA-inhibiting AG879 [22]. This reduction in nocifensive behavior has been associated with extracellular glutamate levels in bone [20].

We have developed a human MDA-MB-231 breast cancer cell line with a stable shRNA-induced knockdown of SLC7A11, the gene encoding the xCT transmembrane antiporter component of system xC-. This report describes the molecular and functional validation of this cell line in addition to RNAseq analysis to determine the transcriptomic consequences of xCT manipulation including changes in the expression of other pain-related factors. We also investigated the consequences of intrafemoral implantation of knockdown cells in a mouse model of CIBP to directly evaluate system xC- as a potential therapeutic target in bone tumors. Rather than targeting the nervous system, this approach exploits a feature of the cancer cell itself to decrease nociception. This proof-of-principle study follows directly from previous work by our lab and others investigating pharmacological inhibition of system xC- [20–23], and supports augmenting clinical pain management regimens with relevant system xC- blockers. This approach may reduce the requirement for increasing doses of centrally-acting analgesics, such as opioids, that are currently prescribed to patients experiencing intractable CIBP, thereby improving quality of life.

MATERIALS AND METHODS

Cell Culture

The human breast adenocarcinoma MDA-MB-231 cell line was used in all in vitro and in vivo work. Testing for mycoplasma contamination was performed throughout this study and cells were verified to be mycoplasma-free prior to surgical implantation. All cells were maintained at sub-confluent densities in a humidified incubator with 5 % CO2 in room air at 37 °C using DMEM supplemented with 10 % fetal bovine serum (FBS) and 1

% antibiotic/antimycotic. Cell numbers were quantified in multiwell plates using crystal violet staining, measuring absorbance at λ= 570 nm with an optical plate reader (BioTek, Winooski VT). Cell harvesting for in vivo implantation was performed on sub-confluent cultures and adherent cells were suspended and kept lightly agitated in sterile PBS on ice.

Knockdown Cell Generation

Stable system xC- knockdown breast cancer cells were generated using a shRNA approach with a puromycin-selectable mammalian expression vector carrying either a shRNA cassette specifically targeting the human xCT gene (SLC7A11) or an empty vector control.

MDA-MB-231 cells were transfected with 4 shRNA vectors: V2LHS-G1, V2LHS-C6, V3LHS-A12, V3LHS-F12 (Open Biosystems, Thermo Fisher Scientific, Waltham, MA), as well as a pLKO-1 empty vector control (Millipore-Sigma, Oakville, Canada), using Lipofectamine 2000 (Thermo Fisher Scientific) (2 µg shRNA + 10 µl lipofectamine 2000 /well of 6 well plate). Puromycin (5 µg/ml) (Millipore-Sigma) was added to growth media for selection after 48-hour transfection, and media was refreshed every 2-3 days until cell colonies were formed 3-4 weeks later. All cell colonies for each shRNA vector were pooled and proliferated sufficiently for further analysis. These stable knockdown cell lines were named G1, C6, A12 and F12, respectively and are maintained were normal culture conditions with 1 µg/ml puromycin.

Quantitative Real-Time PCR (qPCR)

cDNA was prepared using Superscript III (Thermo Fisher Scientific) and oligo dTs using total RNA extracted from cultured cell pellets or subcutaneous tumor tissue with the Qiagen RNeasy mini kit (Qiagen, Hilden, Germany) treated with DNase (Thermo Fisher Scientific). qPCR was carried out on a BioRad CFX Connect Real-Time System with SsoAdvanced Universal SYBR Green Supermix (Bio-Rad Laboratories, Hercules, CA). Primers specific to the human xCT gene, as well as relevant housekeeping gene primers

to amplify either β-actin or RNA polymerase II (RPII), have been described previously (Table 1). The 2-[Δ][Δ]Ct method was employed to calculate relative mRNA levels [24] and results are presented as fold changes of the control.

Western Blotting

25–50 μg of total cell lysates were loaded onto 10 % polyacrylamide gels for SDS-PAGE electrophoresis followed by immunoblotting using an anti-xCT (Novus Biologicals, Littleton, CO) antibody which detects both human and mouse xCT, and chemiluminescent signal detection. Stripped PVDF membranes were re-probed with either anti-β-actin (13E5, #4970S; Cell Signaling Technology, Danvers, MA) or anti-calnexin (H-70, sc-11397; Santa Cruz Biotechnology, Dallas, TX) antibodies. IgG horseradish peroxidase secondary antibodies (Cell Signaling Technology) were used.

Radiolabeled 14C-Cystine Uptake

Uptake of 14C-cystine (0.5 μCi/mL; Perkin Elmer, Waltham, MA) was determined using a Beckman LS6000 liquid scintillation counter as described previously [21]. Each lysate from cells plated 24 hours prior to performing the assay was run in duplicate for at least 3 independent experiments. Scintillation counts per minute were normalized to total protein, which was determined using the Bradford assay.

Glutamate Assay

The level of glutamate released into the culture media by cells plated 24 hours prior to collection was determined using a modification of the Amplex Red Glutamic Acid/Glutamate Oxidase Assay Kit (Thermo Fisher Scientific) and read on a CytoFluor Series 4000 Fluorescence Multi-Well Plate Reader (PerSeptive Biosystems, Thermo Fisher Scientific) as described previously [16]. Data from at least 3 independent experiments was normalized to total protein or cell number.

Animal Models

4-6 week-old female Balb/c nu/nu immunocompromised mice (Jackson Laboratories) were used for all xenograft experiments. Mice were sterile housed and maintained at 24 °C with a 12-hour light/dark cycle and access to autoclaved food and water ad libitum. All procedures were conducted according to the guidelines of the Committee for Research and Ethical Issues of the International Association for the Study of Pain [25] and guidelines established by the Canadian Council on Animal Care with ethical approval from the McMaster University Animal Research Ethics Board. Three days prior to cell implantation surgeries, mice were anaesthetized by isoflurane inhalation and 21 day-release pellets containing 0.25 mg of 17β-estradiol (Innovative Research of America, Sarasota, FL) were implanted subcutaneously. Although MDA-MB-231 are estrogen receptor negative, estrogen receptors are found throughout bone and play a role in the regulation of bone remodeling. In previous experiments, 17β-estradiol delivered prior to cancer cell inoculation improved the consistency of tumor establishment subcutaneously and in bone [23].

Subcutaneous Tumor Models

Mice for subcutaneous tumor models were injected at the rear right flank with $4 \times 10_6$ cancer cells suspended in 100 μL sterile PBS. Animals were randomly assigned to receive implantation of either C6 xCT knockdown cells (n = 3), A12 xCT knockdown cells (n = 3), or vector-only negative control cells (n = 3). Subcutaneous tumor growth was monitored by measuring tumor dimensions with digital calipers and calculated according to the hemi-ellipsoid equation: Volume (mm_3) = $LWH(\pi/6)$. Tumor size was evaluated 3× /week, and animals were sacrificed on day 36 post-injection prior to ethical endpoint for tumor size. Tumor tissues were collected post-sacrifice, snap-frozen in liquid nitrogen, and stored at -80 °C.

CIBP Models

Intrafemoral CIBP mouse model-induction procedures were performed as previously described [19]. Briefly, 25 μL of sterile PBS containing $4 \times 10_6$ cancer cells was percutaneously implanted into the distal epiphysis of the right femur of anaesthetized mice. Animals were randomly assigned by a random number generator to receive implantation of either C6 xCT knockdown cells (n = 9), or vector-only negative control cells (n = 9) on experimental day 0. Tumors successfully developed in n = 5 C6 xCT knockdown cell bearing mice, and n = 7 control cell bearing mice; data from all other mice was excluded from the final results. All animals were sacrificed on Day 30 post-injection prior to ethical behavioral endpoints.

Behavioral Analysis

Mice were exposed to handling and behavioral testing equipment daily for a 1 week acclimation period, and assigned individual identification prior to model induction. All behavioral testing was performed by the same observers who were blinded to group assignment throughout the duration of the study. Behavioral testing was performed 3 times prior to model induction to obtain baseline data, and 2-3 days a week beginning on day 1 following model induction and continuing until endpoint. The tests performed include two tests for spontaneous pain behaviors: the Dynamic Weight Bearing system (DWB) (BioSeb, Vitrolles, France), and open field limb use scale; and one test for elicited mechanical allodynia and hyperalgesia, the Dynamic Plantar Aesthesiometer (DPA) (Ugo Basile, Comerio, Italy). Open field observational limb use scale is an operator-derived numerical representation of the use of the animals ipsilateral limb 5 minute period of free ambulation (0: No use, 1: severe limp, 2: moderate limp, 3: slight limp, 4: Normal use) [22].The DWB apparatus allows the recording of weight and time distribution between all points of pressure of freely moving animals and is described in more detail in previous reports [19]. The movement of each animal was recorded in the DWB apparatus for 5 minutes/test and recordings were manually validated with DWB software version 1.4.2.92 (BioSeb). Results were exported as a mean weight for each

point of pressure across the validated experiment time. Postural disequilibrium of the animal could indicate an allodynic response to normal ambulation, and so a reduction in weight borne by the tumor-afflicted limb of the animal was accepted as evidence of an inability or aversion to utilize that limb, providing indirect evidence of nociception. The DPA apparatus measures the threshold force and time to paw withdrawal from a mechanical stimulus to the plantar surface of the animal paw, and is described in more detail in previous reports [19]. DPA testing was performed four times at each of the hind paws of all animals on each testing day. Animals were first given a minimum of five minutes to acclimate to the testing chambers prior to any stimulation. Mechanical withdrawal threshold is expressed as the mean force of four measurements acquired on each testing day. A reduction in force withstood by the tumor-afflicted limb was accepted as evidence of increased sensitivity, both allodynic and hyperalgesic in that particular limb, manifested as a reflexive or desired withdrawal from stimulus, and therefore as indirect evidence of nociception. DPA data is presented for the tumor-bearing ipsilateral hindlimb only.

Radiograph Lesion Scoring

High-resolution radiographic scans of all mice were taken at endpoint with a Faxitron MX-20 X-ray system (Faxitron X-ray Co., Wheeling, IL) on Kodak MIN-R 2000 Mammography film (Eastman Kodak, Rochester, NY). The extent of osteolytic lesions in the ipsilateral femurs imaged as a loss of bone density by post-mortem radiograph was scored using a custom four point (0-3) scale of bone destruction described in detail previously [19]. The scale designations are as follows: (0) normal bone, no visible lesion; (1) minor loss of bone density, minimal lesion; (2) moderate to substantial loss of bone density, lesion limited to bone trabecula and cortex; (3) substantial loss of bone density, lesion includes clear periosteal involvement or fracture.

RNA-Sequencing

20 µl of RNA at 100 ng/µl from 3 independent biological replicate RNA samples was isolated from separate passages of MDA-MB-231 vector-only negative control and C6 xCT knockdown cells for RNAseq. RNA quality was measured using the RNA 6000 Nano kit and a 2100 Bioanalyzer (Agilent Technologies, Santa Clara, CA). Library preparation was performed using the NEBNext Ultra Directional RNA Library Prep Kit for Illumina, with the Next Poly(A) mRNA Magnetic Isolation Module (New England Biolabs, Ipswich, MA) to enrich poly-A mRNA. Samples were sequenced on the Illumina HiSeq 1500 platform (Illumina, San Diego, CA) via HiSeq Rapid V2 chemistry with onboard cluster generation and 70 bp single-end reads at the Farncombe Metagenomics Facility, McMaster University. Details of the sample preparation were conducted as previously reported [26,27].

Each biological replicate was split between two lanes to mitigate lane effects, with reads being subsequently combined during analysis using the Tuxedo protocol [28]. Analysis was carried out using a web-based platform, the Galaxy Project, as previously described [26,27]. Briefly, the FastQC tool, Tophat, Cufflinks, and Cuffmerge were applied to evaluate the quality of sequencing, align reads to the human GRCh38/hg38 assembly, create assembled transcripts, and create a transcriptome assembly, respectively. Cuffdiff was then used to assess transcript abundance in fragments per kilobase of transcript per million mapped reads (FPKM) and to identify differentially expressed genes (DEG) by merging the transcriptome assembly with individual aligned reads created by Tophat. The false discovery rate-adjusted p-value (q-value) was set to > 0.05. The Bioconductor package CummeRbund for RStudio (version 0.99.467 44–46) was used to graphically visualize group and pairwise comparisons of Cuffdiff output files, including a scatter plot, volcano plot, expression level plot, and heatmap. The Lander/Waterman equation (C = LN/G) was applied to calculate mean genome coverage: C denotes coverage, G corresponds to genome/transcriptome length (for RNA-sequencing), L denotes average

read length, and N stands for the average number of reads [29]. The base coverage tool in Galaxy (https://toolshed.g2.bx.psu.edu/view/devteam/ basecoverage/b8a9e718caa3) was used to derive the total length of annotated transcripts executed on the most recent human genome assembly (GRCh38), which was applied to calculate coverage. DAVID, a web-based bioinformatics tool, was applied to perform ontological and KEGG pathway enrichment analyses to functionally interpret gene sets [30,31]. The list of DEGs for each pairwise comparison obtained from RNA-sequencing was imported into the "functional annotation" tool, with homo sapiens as the reference species. Enriched KEGG pathways and Gene Ontology Biological Processes (GO:BP) terms were identified with the Expression Analysis Systematic Explorer (EASE) threshold (maximum EASE score/p-value) set to a default of 0.1, which is used by DAVID to identify significant gene enrichment. Fold-enrichment representing the ratio of the proportion of input genes relative to the number of genes represented by a particular term or pathway within the reference human genome was also reported. qPCR was performed to validate RNA-sequencing results (see Materials and Methods section on qPCR above). For each of the 15 target genes selected for validation, pairwise comparisons were based on fold changes calculated for the C6 clone relative to control. To determine the experimental asymmetrically distributed standard error of the mean (SEM) for each mean, which is required to linearly represent data derived from an exponential analysis, SEMs derived from each ΔCT value were used to calculate upper and lower $2^{-\Delta\Delta CT}$ values [32]. Linear regression was used to test the overall correlation between RNAseq and qPCR results, with α set to 0.05 [33]. See Table 1 for a list of validated human primers and their corresponding housekeeping genes, all with melting temperatures of approximately 60 °C. Those not described previously [27,34–36] were selected based on PrimerBank (www.pga.mgh.harvard.edu/primerbank) [37].

Statistical Analyses

Results represent the mean ± the SEM of at least three independent replicates for each experiment. Statistical differences between relevant groups were established by either t-

test (denoted by stars) or one-way ANOVA coupled with a Tukey's post-test (denoted by different letters). Results were considered significant at $P < 0.05$. Immunoblots depict a representative image of three independent experiments. All behavioral data were analyzed across treatment groups with multiple unpaired t-tests and presented as mean ± SEM. Osteolytic lesion scores were compared by Kruskal-Wallis test. A power analysis was performed prior to in vivo experimentation based on DPA results as primary measurement with a type II error ($\beta = 20$ %), and a type I error ($\alpha = 5$ %). All analyses and charts were generated using GraphPad Prism 7 software (GraphPad Software, La Jolla, CA).

RESULTS

C6 and A12 MDA-MB-231 cell clones express reduced xCT mRNA and protein, and reduced membrane transport of glutamate and cystine by system xC- relative to negative control cells

Following selection by puromycin, G1, C6, A12 and F12 xCT shRNA vector-transfected cells were screened for knockdown of xCT and reduction of functional system xC- activity. G1 and F12 clones were removed from further screening for failing to show reduction in glutamate release at a preliminary stage. xCT mRNA levels, as measured by qPCR were, significantly down-regulated in both C6 and A12 xCT knockdown cell clones relative to vector-only negative control MDA-MB-231 cells (Fig. 1A). Western blotting revealed that xCT protein levels at 35 kDa were reduced in both C6 and A12 clones relative to the vector-only negative control (Fig. 1B). To confirm that this downregulation had functional consequences in the activity of the system xC- transporter that could translate to an impact on the extracellular environment, glutamate release into the culture media and cellular cystine uptake from the extracellular environment (both mediated in cancer cells by system xC-) were measured in vitro. Uptake of 14C-radiolabelled cystine, important in maintaining cancer cell redox balance, was reduced in

both C6 and A12 knockdown clones relative to the negative control (Fig. 1C). Glutamate released into the culture media over 24 hours, which is the corresponding membrane transport action of system xC-, was also reduced to approximately 0.5 fold of negative control, as measured by AMPLEX red (Fig. 1D). This confirmed the validity of the C6 and A12 clones as a model of SLC7A11/xCT knockdown in MDA-MB-231 human cancer cells.

C6 cell clones retain xCT transcript and protein reduction in subcutaneous tumor tissue from mice 36 days following implantation

Prior to implantation in a mouse model of CIBP, it was necessary to determine if these xCT knockdown cell lines could successfully induce a xenograft tumor in vivo in Balb/c nu/nu immunocompromised mice, and to determine if xCT downregulation was retained in tumor tissue following a period of in vivo growth without puromycin. C6 and A12 xCT knockdown cells, and vector-only negative control MDA-MB-231 cells ($4 \times 10_6$ cells / mouse) were implanted subcutaneously in mice (n = 3 / group). Subcutaneous tumor tissues were removed at sacrifice after 36 days of in vivo growth and examined by by qPCR for xCT mRNA and Western blotting for protein (n = 3 / group). xCT mRNA was significantly down-regulated in subcutaneous tumor tissue from the C6 and A12 xCT knockdown cell clones relative to negative control MDA-MB-231 cells (Fig. 2A). Consistent with in vitro transcript results, xCT mRNA remained significantly lower in C6 clones than in A12 xCT knockdown tumor tissue. Western blotting for xCT protein at 35 kDa revealed that while xCT was significantly lower in tumor tissue from C6 clones, there were no differences between A12 clones and control cells, as quantified by densitometry (Fig. 2B). Based on these results showing a robust and retained significant knockdown of xCT both in vitro and following in vivo growth in the C6 clone, further investigation including RNAseq and models of CIBP focused on this stable cell line. Tumor growth was measured throughout the duration of the experiment by calipers and reported as hemiellipsoid (mm3), and while tumors exhibited variability, at no point did tumor size significantly differ between groups (Fig. 2C).

RNAseq Revealed Differentially Expressed Genes in C6 xCT knockdown cell clones relative to vector-only negative control MDA-MB-231 cells

Gene expression from 3 biological replicates of C6 xCT knockdown cell clones and vector-only negative control MDA-MB-231 cells was compared by RNAseq. Differentially expressed genes (DEG) are highlighted in Figure 3, and the full list of DEGs is provided in Supplemental Table 1. Overall gene expression similarities and differences between C6 xCT knockdown cell and negative control cells is indicated by scatter plot (Fig. 3A). Volcano plotting highlights genes that were differentially expressed between C6 xCT knockdown cell and control cells by plotting−log10(P-value) against log2(fold-change) of individual genes (Fig. 3B). A density plot illustrates expression level distribution, with non-overlapping segments representing differential gene expression between C6 xCT knockdown cell and control cells (Fig. 3C). Heatmapping illustrates the level of gene expression in log10(FPKM+1) for genes that were differentially expressed between C6 xCT knockdown cell and control cells (Fig. 3D). A complete list of differentially expressed genes is shown in Supplementary Table S1. Linear regression analysis of qPCR results compared with RNAseq results including a wide range of fold-changes revealed high concordance between the two evaluations of gene expression (Fig. 3E).

15 differentially expressed genes identified by RNAseq across a range of fold changes and including cytokines, growth factors and xCT were validated by quantitative real-time RT-PCR

xCT knockdown was confirmed by RNAseq and qPCR, and other DEGs identified by RNAseq representing a range of fold changes were validated by qPCR (Fig. 4). These included SLC7A11 (xCT), which was downregulated to less than 0.5 fold at $P < 0.05$, and genes of interest related to xCT expression and CIBP in cancer cells. CCND2, CPT1A, CSF1, GSTM3, IL1A, IL1B, IL1R1, IL1R1L, NGF, and SLC1A3 were significantly up- or down-regulated to a significance level of $P < 0.01$; SENP1 was upregulated at $P <$

0.05; and MYC, NGFR, and SLC25A1 were not significantly different between C6 xCT knockdown cell clones relative to the negative control as compared by t-test.

C6 xCT knockdown cells implanted in bone produce a delayed development of pain-related behavior in mice relative to implantation of vector-only control cells

To determine if the reduction in cancer cell expression of xCT and the corresponding decrease in system xC--mediated glutamate release from these clones had an impact on behaviors indicative of nociception, C6 xCT knockdown cells and vector-only negative control MDA-MB-231 cells ($1 \times 10_6$ cells / mouse) were implanted intrafemorally in mice (n = 9 / group). Tumors developed in n = 5 C6 cell bearing mice, and n = 7 vector-only control cell bearing mice as verified by x-ray and H&E staining. Animals implanted with C6 xCT knockdown cells displayed reduced or delayed behaviors indicative of nociception relative to vector-only MDA-MB-231 controls with normal xCT expression and system xC- function. Weight borne on the rear right ipsilateral limb as measured by DWB progressively declined in both groups as tumors grew in the bone. The onset of this decline was delayed in the C6 xCT knockdown group relative to control, groups were significantly different on experimental days 19 and 22 (Fig. 5A). The decline in time of ipsilateral limb use was also delayed in the C6 clone group relative to control, with a significant difference between groups on day 19 (Fig. 5B). Other measures recorded by the DWB apparatus including paw surface area and relative weight-bearing also showed significant differences between groups at similar time points, as did reaction time as measured by DPA (data not shown). Both C6 xCT knockdown and control animal groups also demonstrate a decline in mechanical force (g) required to provoke ipsilateral paw withdrawal as measured by the DPA automated von Frey test. This decline was delayed in the C6 xCT knockdown group (Fig. 5C). Observational scoring of ipsilateral limb use (0-4 Scale) also showed a later onset of nociceptive behavior in the C6 clone group relative to control (Fig. 5D). No behavioral measures showed significant differences between groups at endpoint, indicating that this xCT-mediated decrease in nociceptive behaviors was not an overall reduction in nociception throughout the duration of the

model, but a delay in the time-to-onset of severe nociceptive behavior. Osteolytic lesion sizes in the femur at endpoint as measured by radiograph were not different between groups (Fig 5E), indicating that these behavioral differences were related to differential cancer cell phenotype rather than overall tumor size. All behavioral data was confirmed for normal distribution and analyzed across treatment groups with multiple unpaired t-tests and presented as mean ± SEM (*$P < 0.05$). Osteolytic lesion scores were compared by Kruskal-Wallis test.

DISCUSSION

Cancer pain may arise from many factors, including weak and fractured bone, inflammation, neuropathy, and disruptive signaling via molecules released by a tumor or tumor-associated cells. The findings detailed in this report follow directly from findings by our laboratory and by the Vanderah laboratory that pharmacological inhibitors of system xC- reduce or delay the onset of pain behavior in mouse models of CIBP at least in part by reducing glutamate release from the cancer cell to the bone microenvironment [20–23]. By directly targeting the expression of SLC7A11/xCT in human cancer cells without the confounding off-target factors of systemic drug treatment, we have produced a cell and in vivo mouse model that can more directly evaluate the impact of targeting xCT and therefore system xC- activity for the treatment of cancer pain.

Bone cancers are more commonly the result of metastasis than of a primary cancer of the bone, and the breast is the most common site of origin of these metastases, with the majority of late-stage breast cancers producing at least one metastatic site in the skeleton [4,38]. We chose to produce our stable xCT knockdown cell line in MDA-MB-231 triple-negative human breast adenocarcinoma which produce osteolytic lesions when implanted in bone and have been established by our lab for use in a mouse model of CIBP [19,21]. MDA-MB-231 are among many cancer cell lines from a range of tissues of origin that release glutamate via system xC-. However, this phenomenon has been most

comprehensively examined in human triple-negative breast cancer cells, where xCT was found to be highly expressed in the majority of cell lines adapted to culture, and in 40 % of a sample of patient-derived triple-negative breast tumor samples [39]. System xC- expression and activity have been implicated in cellular responses to oxidative stress, allowing enhanced cancer cell survival and acquired resistance to therapy [40,41], supporting aberrant cancer cell metabolic processes including upregulated glutaminolysis [27,42]. In the bone, glutamate is implicated in cell signaling and regulation of osteoblasts, osteoclasts, and osteocytes [43]. Bone metastases can induce dramatic disruptions in bone cell metabolism which can increase and dysregulate processes of bone resorption and apposition, producing large and painful lesions [44]. Extracellular glutamate also has the potential to activate and sensitize glutamate-receptive peripheral sensory neurons including nociceptors in and around the bone [42,45].

In vitro, two stable cell clones (C6 and A12) transfected with shRNA cassettes targeting SLC7A11/xCT, showed downregulated xCT at both the mRNA and protein levels, with significantly downregulated indicators of functional system xC-, including cystine uptake and glutamate release relative to a vector-only negative control. Following subcutaneous in vivo implantation and growth, C6 clones were selected for further investigation by RNAseq and for use in an animal model of CIBP, based on that clone's retention of approximately 50 % knockdown of xCT based on mRNA and protein levels relative to control cells. In addition, subcutaneous tumors from implanted C6 clone and negative control cells did not significantly differ in volume (mm^3) over the 30-day time period corresponding to the duration of the intrafemoral CIBP model. Although experimental interference with system xC- is often intended to reduce growth of or even kill cancer cells, this outcome could be a dramatic confound in our mechanistic investigation into the validity of xCT at a target for cancer pain. Consistency in tumor size allows a more isolated investigation of the direct impact of xCT and system xC--mediated glutamate release on CIBP.

In our CIBP model, we observed a delay between the onset of nociceptive behaviors in mice intrafemorally injected with negative control cells with normal xCT expression, and later onset in C6 clone xCT knockdown cells. In particular, we observed a reduction in behaviors indicative of mechanical allodynia in C6 clone-bearing mice, including spontaneous ipsilateral weight bearing and time-of-use with the DWB, and evoked mechanical withdrawal threshold using the DPA test, which may also be indicative of mechanical hyperalgesia. We observed a reduction in spontaneous indications of limb use limitation or avoidance with the observational 0-4 scale, possibly indicating spontaneous allodynia. Other observational measures of spontaneous nociception including guarding time and flinching were found to be inconsistent or absent in Balb/c nu/nu mice. We hypothesize that this delay in the onset of nociceptive behaviors is a result of reduced glutamate release into the extracellular environment, where elevated levels of glutamate in the femur are associated with CIBP [20]. This time-frame in a mouse model could represent a clinically relevant delay in potential targeting of xCT for CIBP in cancer patients, allowing not only a lesser overall experience of pain, but also a delay until the need for stronger analgesic intervention. By endpoint there were no behavioral differences between groups, and animals were sacrificed prior to reaching behavioral ethical endpoints, consistent with previous findings of pain amelioration by targeting system xC- [19–22]. This is indicative of the complexity of CIBP, a pain state that involves many initiating and maintaining factors apart from cancer cell-derived glutamate, including other secreted factors, mechanical distortion, and direct neuronal damage or pathology – processes that could induce pain independently of system xC- and glutamate [46,47].

In rat models of intrafemoral tumors, we have observed plasticity in the intracellular electrophysiological characteristics of cutaneous and muscle spindle peripheral sensory neurons, including nociceptive C- and Aδ-fibers, as well as normally non-nociceptive Aβ-fiber low threshold mechanoreceptors [18]. These rat models demonstrated behavioral results similar to the current mouse models, including reductions in mechanical withdrawal threshold, and measures of ipsilateral limb use [18]. It is possibly the case that

these same intrinsic membrane properties, including neuronal excitability, are altered in our mouse models of CIBP, with potentially relevant changes in particular fiber types resulting from system xC- inhibition, although in vivo intracellular recordings have yet to be performed in mice.

Changes in gene expression between C6 xCT knockdown cell clones and vector-only negative control cells as compared by RNAseq confirmed that SLC7A11 mRNA levels were significantly down-regulated in C6 cells. In addition, transcripts of other factors implicated in feedback with system xC- and pain, including NGF, which has a well-established relationship with cancer and skeletal pain [7,22], as well as interleukin 1 beta (IL1β), which has been implicated in both xCT regulation [48,49], and cancer pain [50,51] were also downregulated in C6 cells. In addition, the transcript encoding colony-stimulating factor 1 (CSF1), which modulates innate immunity, inflammation and cancer, as well as macrophage activation and the support of microglia [52,53], was also significantly down-regulated, along with its receptor CSF1R (to 0.4-fold via RNAseq) in the C6 xCT knockdown cells relative to controls at the mRNA level. Interestingly, in a T47D human mammary carcinoma cell line that over-expresses xCT and releases significantly more glutamate than wild-type T47D control cells, CSF1 levels are significantly increased by 2.5-fold [27]. C6 xCT knockdown clones also exhibited significant downregulation of TNFRSF1A (to 0.58-fold via RNAseq relative to control), which encodes the receptor for the pro-inflammatory cytokine tumor necrosis factor alpha (TNFα), which is also associated with cancer pain [54]. Our RNAseq data suggests that the xCT status of a bone tumor may be linked with other important pro-nociceptive players, and its downregulation may be beneficial not only by reducing glutamate levels, but also through concomitant down-regulation of neurotrophic factors and pro-inflammatory cytokines implicated in modulating the complex state of CIBP.

Our conclusions that xCT downregulation is associated with reduced CIBP in animal models and that xCT expression in cancer cells is linked with transcriptomic changes that include several other well-known players in the generation of cancer pain add to growing body of mechanistic CIBP research. Rationale is accumulating for the therapeutic

targeting of xCT as a way to manipulate a metabolically unique feature of many cancers that may impact not only cancer cell growth and survival, but also the associated morbidities of cancer including pain, seizures [55], and depression [56]. Our findings are consistent with the role of xCT in cancer and cancer pain. We intend to further evaluate the mechanisms and consequences of xCT manipulation in cancer cells by producing an inducible xCT knockdown system to strategically silence expression of the antiporter in a temporally controlled manner, and to evaluate the contribution of blocking cancer cell-derived glutamate in vivo in conjunction with currently used analgesics including NSAIDs such as meloxicam, or clinically relevant opioids. These experiments will build on the findings of this report and others, furthering an understanding of the value of xCT as a therapeutic target for cancer pain.

ACKNOWLEDGEMENT

We would like to thank Dr. Hanxin Lin (University of Western Ontario) for technical advice. This study was supported by grants to G. Singh from the Canadian Institutes of Health Research and the Canadian Breast Cancer Foundation, and fellowships from the Canadian Institutes of Health Research and the Michael G. DeGroote Institute for Pain Research and Care to R. Ungard.

AUTHOR CONTRIBUTIONS

Robert Ungard cultured cells for in vivo studies, induced the in vivo models, performed behavioural tests and drafted the manuscript. Katja Linher-Melville performed qPCR, Western Blotting and cystine uptake assays for in vitro and in vivo studies, prepared cells for RNAseq, and contributed to writing and editing the manuscript. Manu Sharma assisted with all aspects of the in vivo studies. Jianping Wen generated and screened stable clones. Mina Nashed analyzed RNAseq data. All authors contributed to successive

drafts of the manuscript. Gurmit Singh supervised the overall project, edited the manuscript, and provided funding for the study. All authors have read and approved the final manuscript.

DECLARATION OF CONFLICTING INTERESTS

The authors declare that they have nothing to disclose.

REFERENCES

1. Kennecke H, Yerushalmi R, Woods R, Cheang MCU, Voduc D, Speers CH, et al. Metastatic Behavior of Breast Cancer Subtypes. J Clin Oncol. 2010;28:3271–7.

2. Harries M, Taylor A, Holmberg L, Agbaje O, Garmo H, Kabilan S, et al. Incidence of bone metastases and survival after a diagnosis of bone metastases in breast cancer patients. Cancer Epidemiol. 2014;38:427–34.

3. Coleman RE. Skeletal complications of malignancy. Cancer. 1997;80:1588–94.

4. Coleman RE, Rubens RD. The clinical course of bone metastases from breast cancer. Br J Cancer. 1987;55:61–6.

5. Solomayer EF, Diel IJ, Meyberg GC, Gollan C, Bastert G. Metastatic breast cancer: clinical course, prognosis and therapy related to the first site of metastasis. Breast Cancer Res Treat. 2000;59:271–8.

6. Yavas O, Hayran M, Ozisik Y. Factors affecting survival in breast cancer patients following bone metastasis. Tumori. 93:580–6.

7. Bloom AP, Jimenez-Andrade JM, Taylor RN, Castañeda-Corral G, Kaczmarska MJ, Freeman KT, et al. Breast cancer-induced bone remodeling, skeletal pain, and sprouting of sensory nerve fibers. J Pain. 2011;12:698–711.

8. Wacnik PW, Baker CM, Herron MJ, Kren BT, Blazar BR, Wilcox GL, et al. Tumor-induced mechanical hyperalgesia involves CGRP receptors and altered innervation and vascularization of DsRed2 fluorescent hindpaw tumors. Pain. 2005;115:95–106.

9. Honore P, Rogers SD, Schwei MJ, Salak-Johnson JL, Luger NM, Sabino MC, et al. Murine models of inflammatory, neuropathic and cancer pain each generates a unique set of neurochemical changes in the spinal cord and sensory neurons. Neuroscience. 2000;98:585–98.

10. Schwei MJ, Honore P, Rogers SD, Salak-Johnson JL, Finke MP, Ramnaraine ML, et al. Neurochemical and cellular reorganization of the spinal cord in a murine model of bone cancer pain. J Neurosci. 1999;19:10886–97.

11. Wang L-N, Yang J-P, Ji F, Zhan Y, Jin X, Xu Q-N, et al. Brain-derived neurotrophic factor modulates N-methyl-D-aspartate receptor activation in a rat model of cancer-induced bone pain. J Neurosci Res. 2012;90:1249–60.

12. De Ciantis PD, Yashpal K, Henry J, Singh G. Characterization of a rat model of metastatic prostate cancer bone pain. J Pain Res. 2010;3:213–21.

13. Ghilardi JR, Röhrich H, Lindsay TH, Sevcik MA, Schwei MJ, Kubota K, et al. Selective blockade of the capsaicin receptor TRPV1 attenuates bone cancer pain. J Neurosci. 2005;25:3126–31.

14. Jimenez-Andrade JM, Ghilardi JR, Castañeda-Corral G, Kuskowski MA, Mantyh PW. Preventive or late administration of anti-NGF therapy attenuates tumor-induced nerve sprouting, neuroma formation, and cancer pain. Pain. 2011;152:2564–74.

15. Mantyh WG, Jimenez-Andrade JM, Stake JI, Bloom AP, Kaczmarska MJ, Taylor RN, et al. Blockade of nerve sprouting and neuroma formation markedly attenuates the development of late stage cancer pain. Neuroscience. 2010;171:588–98.

16. Seidlitz EP, Sharma MK, Saikali Z, Ghert M, Singh G. Cancer cell lines release glutamate into the extracellular environment. Clin Exp Metastasis. 2009;26:781–7.

17. Sharma MK, Seidlitz EP, Singh G. Cancer cells release glutamate via the cystine/glutamate antiporter. Biochem Biophys Res Commun. 2010;391:91–5.

18. Zhu YF, Ungard R, Seidlitz E, Zacal N, Huizinga J, Henry JL, et al. Differences in electrophysiological properties of functionally identified nociceptive sensory neurons in an animal model of cancer-induced bone pain. Mol Pain. 2016;12.

19. Ungard RG, Seidlitz EP, Singh G. Inhibition of breast cancer-cell glutamate release with sulfasalazine limits cancer-induced bone pain. Pain. 2014;155:28–36.

20. Slosky LM, BassiriRad NM, Symons AM, Thompson M, Doyle T, Forte BL, et al. The cystine/glutamate antiporter system xc− drives breast tumor cell glutamate release and cancer-induced bone pain. Pain. 2016;157:2605–16.

21. Fazzari J, Balenko M, Zacal N, Singh G. Identification of capsazepine as a novel inhibitor of system xc− and cancer-induced bone pain. J Pain Res. 2017;Volume 10:915–25.

22. Miladinovic T, Ungard RG, Linher-Melville K, Popovic S, Singh G. Functional effects of TrkA inhibition on system x C − -mediated glutamate release and cancer-induced bone pain. Mol Pain. 2018;14:174480691877646.

23. Ungard RG, Seidlitz EP, Singh G. Inhibition of breast cancer-cell glutamate release with sulfasalazine limits cancer-induced bone pain. Pain. 2014;155.

24. Schmittgen TD, Livak KJ. Analyzing real-time PCR data by the comparative C(T) method. Nat Protoc. 2008;3:1101–8.

25. Zimmermann M. Ethical guidelines for investigations of experimental pain in conscious animals. Pain. 1983;16:109–10.

26. Nashed MG, Linher-Melville K, Frey BN, Singh G. RNA-sequencing profiles hippocampal gene expression in a validated model of cancer-induced depression. Genes, Brain Behav. 2016;15:711–21.

27. Linher-Melville K, Nashed MG, Ungard RG, Haftchenary S, Rosa DA, Gunning PT, et al. Chronic inhibition of STAT3/STAT5 in treatment-resistant human breast cancer cell subtypes: Convergence on the ROS/ SUMO pathway and its effects on xCT expression and system xc-activity. PLoS One. 2016;11.

28. Trapnell C, Roberts A, Goff L, Pertea G, Kim D, Kelley DR, et al. Differential gene and transcript expression analysis of RNA-seq experiments with TopHat and Cufflinks. Nat Protoc. 2012;7:562–78.

29. Lander ES, Waterman MS. Genomic mapping by fingerprinting random clones: a mathematical analysis. Genomics. 1988;2:231–9.

30. Huang DW, Sherman BT, Lempicki RA. Systematic and integrative analysis of large gene lists using DAVID bioinformatics resources. Nat Protoc. 2009;4:44–57.

31. Huang DW, Sherman BT, Lempicki RA. Bioinformatics enrichment tools: paths toward the comprehensive functional analysis of large gene lists. Nucleic Acids Res. 2009;37:1–13.

32. Livak KJ, Schmittgen TD. Analysis of relative gene expression data using real-time quantitative PCR and the 2(-Delta Delta C(T)) Method. Methods. 2001;25:402–8.

33. Zhen AW, Nguyen NH, Gibert Y, Motola S, Buckett P, Wessling-Resnick M, et al. The small molecule, genistein, increases hepcidin expression in human hepatocytes. Hepatology. 2013;58:1315–25.

34. Habib E, Linher-Melville K, Lin H-X, Singh G. Expression of xCT and activity of system x c − are regulated by NRF2 in human breast cancer cells in response to oxidative stress. Redox Biol. 2015;5:33–42.

35. Linher-Melville K, Zantinge S, Sanli T, Gerstein H, Tsakiridis T, Singh G. Establishing a relationship between prolactin and altered fatty acid β-Oxidation via carnitine palmitoyl transferase 1 in breast cancer cells. BMC Cancer. 2011;11:56.

36. Linher-Melville K, Haftchenary S, Gunning P, Singh G. Signal transducer and activator of transcription 3 and 5 regulate system Xc- and redox balance in human breast cancer cells. Mol Cell Biochem. 2015;405:205–21.

37. Wang X, Spandidos A, Wang H, Seed B. PrimerBank: a PCR primer database for quantitative gene expression analysis, 2012 update. Nucleic Acids Res. Oxford University Press; 2012;40:D1144-9.

38. Coleman RE. Clinical features of metastatic bone disease and risk of skeletal morbidity. Clin Cancer Res. 2006;12:6243s–6249s.

39. Timmerman LA, Holton T, Yuneva M, Louie RJ, Padró M, Daemen A, et al. Glutamine Sensitivity Analysis Identifies the xCT Antiporter as a Common Triple-Negative Breast Tumor Therapeutic Target. Cancer Cell. 2013;24:450–65.

40. Huang Y, Sadée W. Membrane transporters and channels in chemoresistance and -sensitivity of tumor cells. Cancer Lett. 2006;239:168–82.

41. Chung WJ, Lyons SA, Nelson GM, Hamza H, Gladson CL, Gillespie GY, et al. Inhibition of cystine uptake disrupts the growth of primary brain tumors. J Neurosci. 2005;25:7101–10.

42. Fazzari J, Linher-Melville K, Singh G. Tumour-Derived Glutamate: Linking Aberrant Cancer Cell Metabolism to Peripheral Sensory Pain Pathways. Curr Neuropharmacol. 2017;15:620–36.

43. Cowan RW, Seidlitz EP, Singh G. Glutamate signaling in healthy and diseased bone. Front Endocrinol (Lausanne). 2012;3:89.

44. Orr FW, Lee J, Duivenvoorden WC, Singh G. Pathophysiologic interactions in skeletal metastasis. Cancer. 2000;88:2912–8.

45. Mach DB, Rogers SD, Sabino MC, Luger NM, Schwei MJ, Pomonis JD, et al. Origins of skeletal pain: sensory and sympathetic innervation of the mouse femur. Neuroscience. 2002;113:155–66.

46. Lozano-Ondoua AN, Symons-Liguori AM, Vanderah TW. Cancer-induced bone pain: Mechanisms and models. Neurosci Lett. NIH Public Access; 2013;557 Pt A:52–9.

47. Mantyh PW, Clohisy DR, Koltzenburg M, Hunt SP. Molecular mechanisms of cancer pain. Nat Rev Cancer. 2002;2:201–9.

48. Jackman NA, Uliasz TF, Hewett JA, Hewett SJ. Regulation of system x(c)(-)activity and expression in astrocytes by interleukin-1β: implications for hypoxic neuronal injury. Glia. 2010;58:1806–15.

49. Shi J, He Y, Hewett SJ, Hewett JA. Interleukin 1β Regulation of the System xc- Substrate-specific Subunit, xCT, in Primary Mouse Astrocytes Involves the RNA-binding Protein HuR. J Biol Chem. 2016;291:1643–51.

50. Oliveira A, Dinis-Oliveira RJ, Nogueira A, Gonçalves F, Silva P, Vieira C, et al. Interleukin-1β genotype and circulating levels in cancer patients: metastatic status and pain perception. Clin Biochem. 2014;47:1209–13.

51. Reyes-Gibby CC, Swartz MD, Yu X, Wu X, Yennurajalingam S, Anderson KO, et al. Symptom clusters of pain, depressed mood, and fatigue in lung cancer: assessing the role of cytokine genes. Support Care Cancer. 2013;21:3117–25.

52. Chitu V, Stanley ER. Colony-stimulating factor-1 in immunity and inflammation. Curr Opin Immunol. 2006;18:39–48.

53. De I, Nikodemova M, Steffen MD, Sokn E, Maklakova VI, Watters JJ, et al. CSF1 overexpression has pleiotropic effects on microglia in vivo. Glia. 2014;62:1955–67.

54. Reyes-Gibby CC, Spitz MR, Yennurajalingam S, Swartz M, Gu J, Wu X, et al. Role of Inflammation Gene Polymorphisms on Pain Severity in Lung Cancer Patients. Cancer Epidemiol Biomarkers Prev. 2009;18:2636–42.

55. Robert SM, Buckingham SC, Campbell SL, Robel S, Holt KT, Ogunrinu-Babarinde T, et al. SLC7A11 expression is associated with seizures and predicts poor survival in patients with malignant glioma. Sci Transl Med. 2015;7:289ra86.

56. Nashed MG, Ungard RG, Young K, Zacal NJ, Seidlitz EP, Fazzari J, et al. Behavioural effects of using sulfasalazine to inhibit glutamate released by cancer cells: A novel target for cancer-induced depression. Sci Rep. 2017;7.

FIGURES

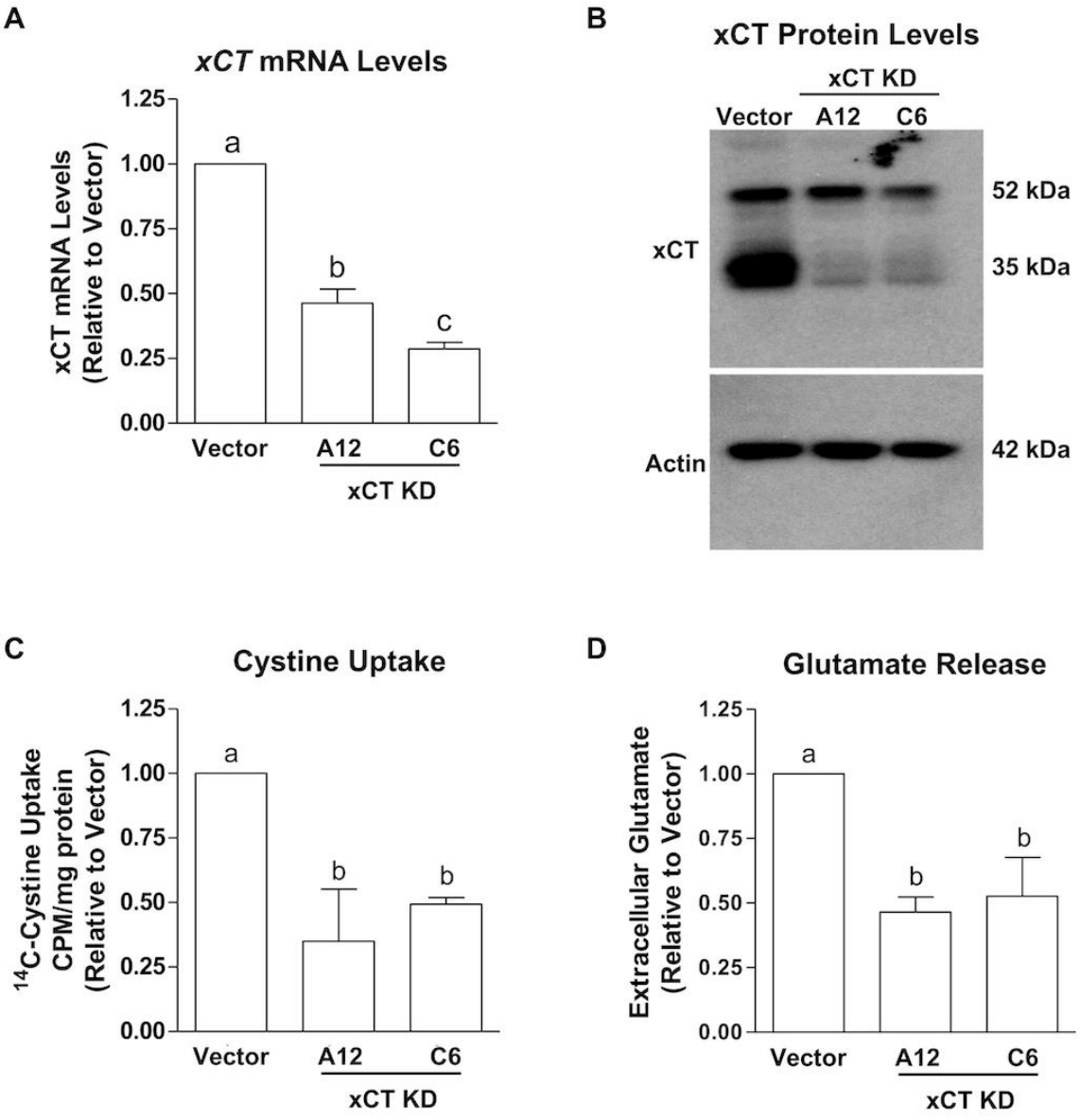

Figure 1.

xCT mRNA and protein levels, and system xC- functional cystine uptake and glutamate release are reduced in C6 and A12 xCT knockdown cell clones relative to vector-only negative control MDA-MB-231 in vitro.

(A) xCT mRNA was significantly down-regulated in both C6 and A12 xCT knockdown (KD) cell clones relative to vector-only negative control MDA-MB-231 cells (vector). xCT was also significantly lower in C6 than A12 xCT KD cells. (B) A representative Western blot image depicting that xCT protein levels at 35 kDa were lower in both C6 and A12 xCT KD cell clones relative to vector. Functional indicators of system xC- activity were reduced to approximately 0.5 fold of vector-only negative control cell activity, in concordance with xCT expression levels. These include (C) 14C-radiolabelled cystine uptake and (D) glutamate release into culture media, both from cells in culture for 24 hours. Data represent the mean of three independent experiments (±SEM) calculated relative to vector. Different letters a, b, or c in panels A, C, and D correspond to statistical differences between groups ($P < 0.05$), as determined by one-way ANOVA and post-hoc Tukey's test.

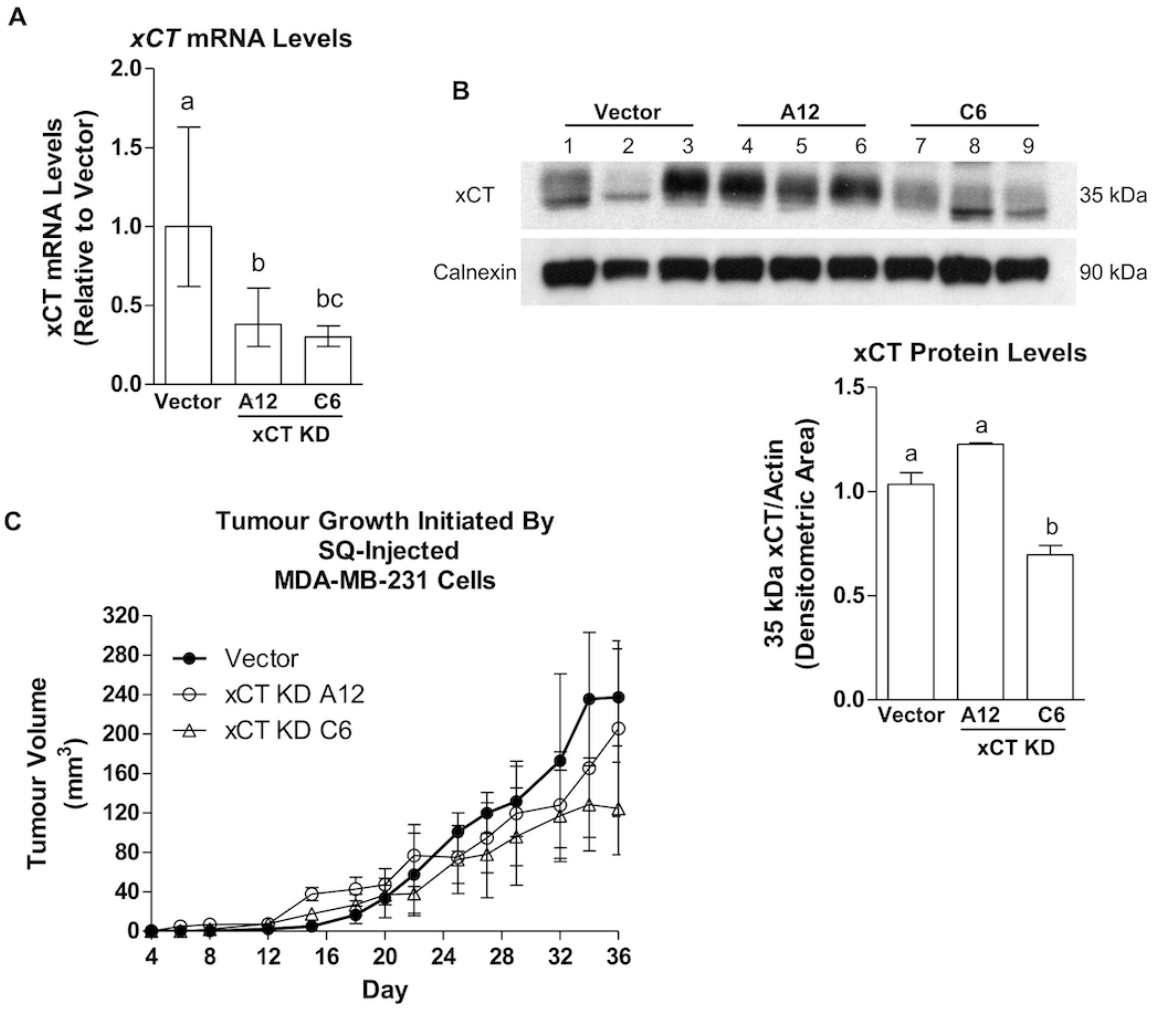

Figure 2.

xCT mRNA and protein levels remain down-regulated in subcutaneous tumor tissue from C6 xCT knockdown cells, while mRNA but not protein remains reduced in tumors from A12 xCT knockdown cell clones relative to vector-only negative controls. Subcutaneous tumors did not significantly differ in size.

$4 \times 10_6$ C6 and A12 xCT knockdown (KD) cells, and vector-only negative control MDA-MB-231 cells (vector) were implanted subcutaneously into nude mice (n = 3 / group). Tumor tissue was collected after 36 days of growth. (A) xCT mRNA levels remained significantly down-regulated in subcutaneous tumor tissue collected from both C6 and A12 xCT KD cell clones relative to vector. xCT was also lower in C6 than A12 xCT KD

cell-derived tumors. (B) xCT protein at 35 kDa was also significantly lower in C6 but not A12 xCT KD cell clones relative to vector in tumors, as quantified by densitometric analysis of xCT protein levels relative to actin measured by Western blotting. (C) Tumor growth was measured throughout the duration of the experiment; at no point did tumor size (mm3) significantly differ between groups as compared by one-way ANOVA. Data represent the mean of three independent experiments (±SEM) calculated relative to vector. Different letters a, b, or c in panels A and B correspond to statistical differences between groups ($P < 0.05$), as determined by one-way ANOVA and post-hoc Tukey's test.

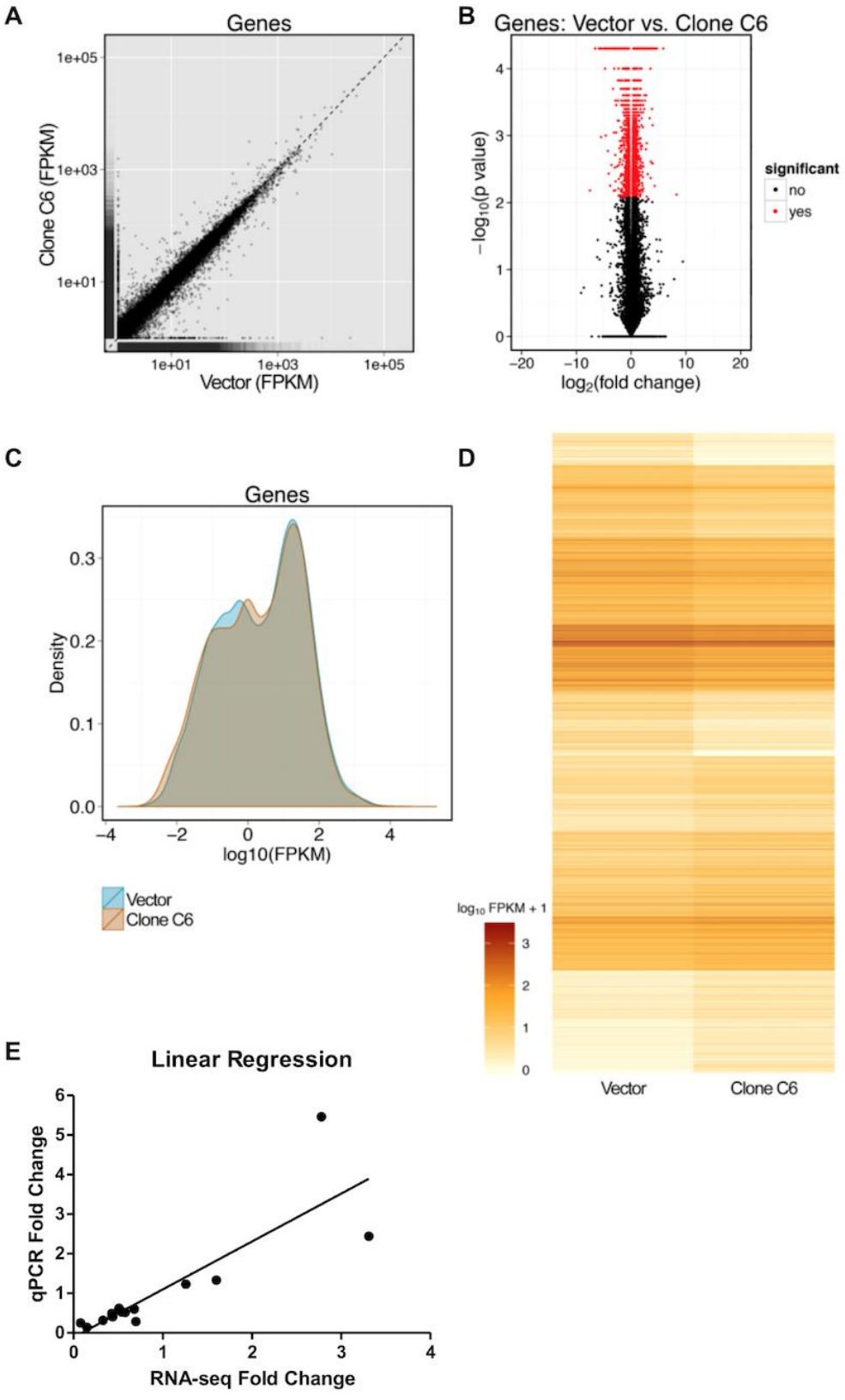
A
Genes
Clone C6 (FPKM)
Vector (FPKM)
1e+01
1e+03
1e+05
B
Genes: Vector vs. Clone C6
−log10(p value)
log2(fold change)
significant
no
yes
C
Genes
Density
log10(FPKM)
Vector
Clone C6
D
log10 FPKM + 1
Vector
Clone C6
E
Linear Regression
qPCR Fold Change
RNA-seq Fold Change

Figure 3.

A visual summary of patterns of differentially expressed genes (DEGs) derived from RNA-sequencing of C6 xCT knockdown and vector-only negative control MDA-MB-231 cells.

(A) Overall gene expression similarities and differences between C6 xCT knockdown (KD) cells and vector-only negative control cells (vector) are indicated by scatter plot. (B) Volcano plotting highlights genes that were differentially expressed between C6 xCT KD cells and vector. (C) A density plot illustrates expression level distribution, with non-overlapping segments representing differential gene expression between C6 xCT KD cells and vector. (D) Heat mapping illustrates the level of gene expression in log10(FPKM+1) for genes that are differentially expressed between C6 xCT KD cells and vector. (E) Linear regression analysis of qPCR results compared with RNAseq results revealed high concordance between the two methods.

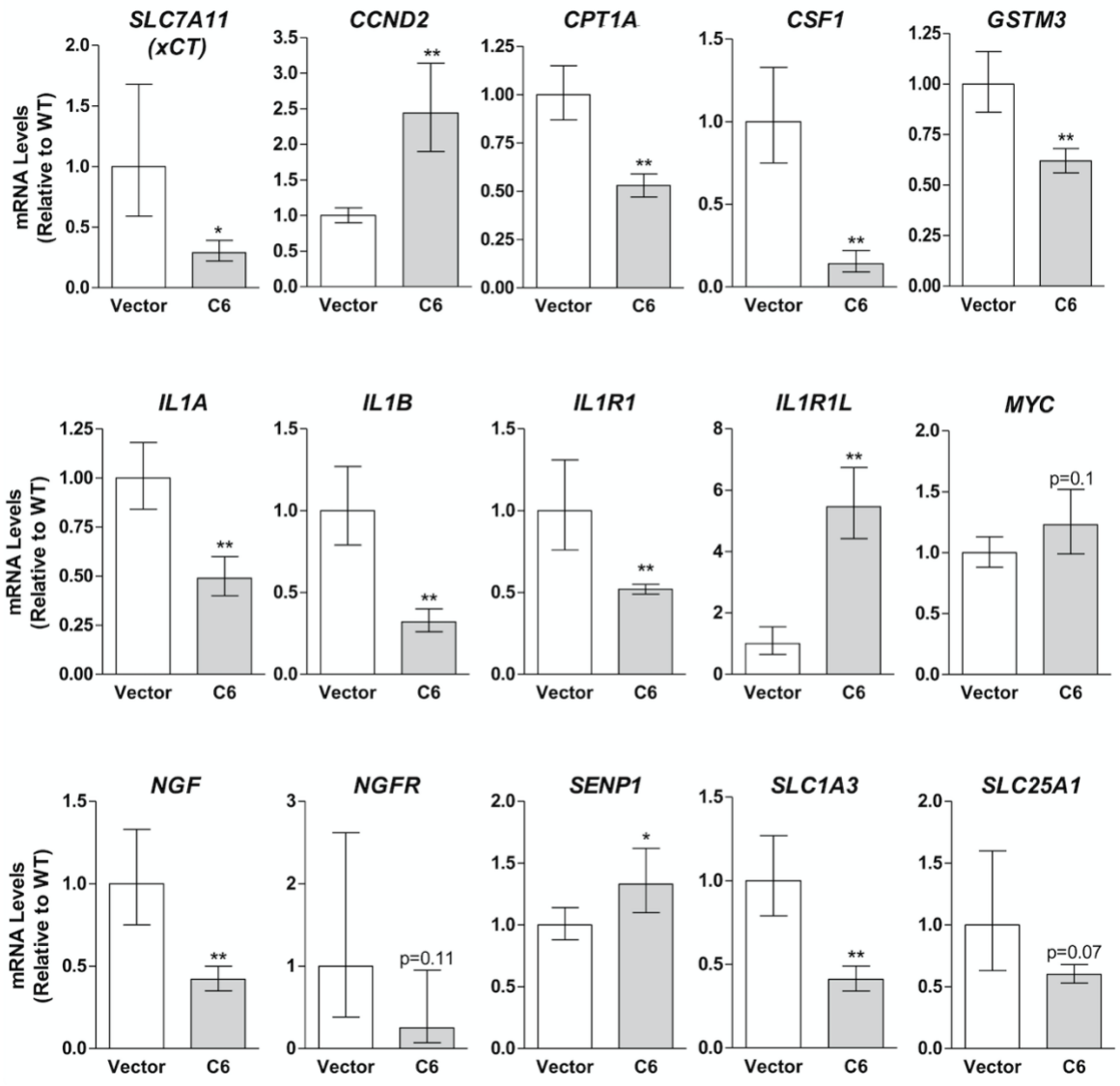

Figure 4.

15 genes selected for representation of relative qPCR fold-changes and validation of differentially expressed genes (DEGs) identified by RNA-sequencing indicate differences between gene expression in C6 xCT knockdown cell and vector-only negative control cells.

xCT knockdown was confirmed by RNAseq and qPCR, and other DEGs identified by RNAseq representing a range of fold changes were validated by qPCR. These include genes of interest related to xCT expression and CIBP in cancer cells. For each group, data represents the mean of 3 independent biological replicates, each analyzed in duplicate, with error bars indicating the SEM calculated using the 2-[Δ][Δ]Ct method. Data of the C6 xCT knockdown (KD) clone is presented relative to vector (fold-change). Means were compared using t-tests (*$P < 0.05$, **$P < 0.01$).

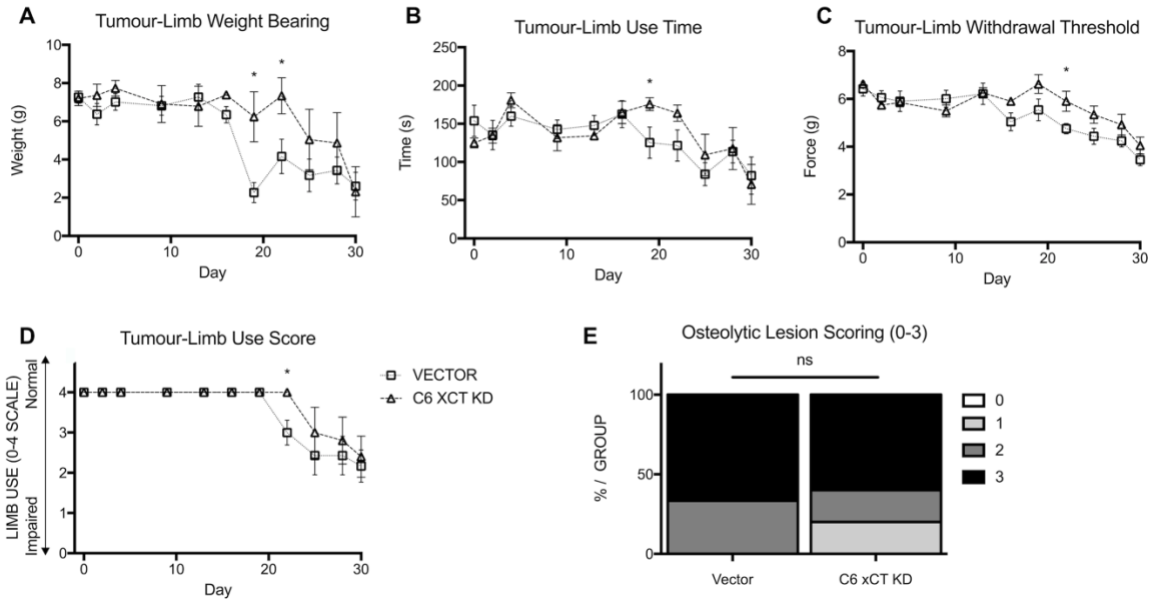

Figure 5.

xCT knockdown in implanted bone tumors delays the development of nociceptive behavior in mice including measures of limb use and mechanical withdrawal threshold.

When implanted intrafemorally to induce a mouse model of CIBP, animals with C6 xCT knockdown (KD) cells displayed reduced or delayed behaviours indicative of nociception relative to vector-only MDA-MB-231 controls (vector) with normal xCT expression and system xC- function. (A) Weight bearing on the rear right ipsilateral limb as measured by DWB progressively declines in both groups as tumors grow in the bone. The onset of this decline is delayed in the C6 xCT KD group relative to vector; groups are significantly different on experimental days 19 and 22. (B) The temporal decline of ipsilateral limb use is also delayed in the C6 clone group relative to control, with a significant difference between groups on day 19. (C) Both C6 xCT KD and vector animal groups also demonstrate a decline in mechanical force (g) required to provoke ipsilateral paw withdrawal as measured by DPA automated von Frey. This decline is delayed in the C6 xCT KD group. Groups are significantly different on experimental day 22. (D) Observational scoring of ipsilateral limb use (0-4 Scale) also shows a later onset of nociceptive behaviour in the C6 xCT KD group relative to vector, with groups

significantly differing on experimental day 22. In A-D, no measures show significant differences between groups at endpoint. (E) Osteolytic lesion size in the femur at endpoint was not different between groups. Data is reported from n = 5 C6 xCT KD cell mice and n = 7 vector cell mice; only animals with verified tumor development were included in results shown here. All behavioural data is presented as mean ± SEM analyzed across treatment groups with multiple unpaired t-tests (*$P < 0.05$). Osteolytic lesion scores were compared by Kruskal-Wallis test.

Human Gene	Ref	Primer sequence (5' to 3')	PrimerBank
***SLC7A11* (xCT)**	13,21	**FOR:** CCTCTATTCGGACCCATTTAGT	
		REV: CTGGGTTTCTTGTCCCATATAA	
CCND2	22	**FOR:** ACCTTCCGCAGTGCTCCTA	
		REV: CCCAGCCAAGAAACGGTCC	
CPT1A	23	**FOR:** CCTCCAGTTGGCTTATCGTG	
		REV: TTCTTCGTCTGGCTGGACAT	
CSF1	22	**FOR:** AGACCTCGTGCCAAATTACATT	
		REV: AGGTGTCTCATAGAAAGTTCGGA	
GSTM3	22	**FOR:** TACCTCTTATGAGGAGAAACGGT	
		REV: AGGAAAGTCCAGGTCTAGCTTG	
IL1A		**FOR:** AGATGCCTGAGATACCCAAAACC	27894329c2
		REV: CCAAGCACACCCAGTAGTCT	
IL1B		**FOR:** ATGATGGCTTATTACAGTGGCAA	27894305c1
		REV: GTCGGAGATTCGTAGCTGGA	
IL1R		**FOR:** ATGAAATTGATGTTCGTCCCTGT	27894331c1
		REV: ACCACGCAATAGTAATGTCCTG	
IL1R1L		**FOR:** ATGGGGTTTTGGATCTTAGCAAT	27894327c1
		REV: CACGGTGTAACTAGGTTTTCCTT	
MYC	22	**FOR:** GTCAAGAGGCGAACACACAAC	
		REV: TTGGACGGACAGGATGTATGC	
NGF		**FOR:** GGCAGACCCGCAACATTACT	70995318c1
		REV: CACCACCGACCTCGAAGTC	
NGFR		**FOR:** CCTACGGCTACTACCAGGATG	295842401c1
		REV: CACACGGTGTTCTGCTTGT	
SENP1		**FOR:** AGTGAACCACAACTCCGTATTC	45505133c1
		REV: AAAAGATCGGTCCAAATGTCCTT	
SLC1A3	22	**FOR:** AGCAGGGAGTCCGTAAACG	

		REV: AGCATTCCGAAACAGGTAACTTT	
SLC25A1	22	**FOR:** TTCCCCACCGAGTACGTGAA	
		REV: GTAGAGCAGGGAGCTAAGGC	
β-Actin	13	**FOR:** GATGGGCGGCGGAAAATAG	
		REV: GCGTGGATTCTGCATAATGGT	
RPII-1	23	**FOR:** GAAACGGTGGACGTGCTTAT	
		REV: TCTCCATGCCATACTTGCAC	

Table 1.

Primers used for relative qPCR to validate RNAseq results.

The sequence of validated human primers and their corresponding housekeeping genes used in this study are listed, each with a melting temperature of 60 °C. Citations are provided for previously published primers. Those not published previously were selected using PrimerBank (www.pga.mgh.harvard.edu/primerbank) [37] with the ID listed. Efficiency-tested pairing of a specific target to housekeeper gene (β-Actin orRPII-1) is indicated.

Supplementary Table S1

Supplemental material is available for this article online at:
https://journals.sagepub.com/doi/suppl/10.1177/1744806918822185

CHAPTER 3: Response to pregabalin and progesterone differs in male and female rat models of neuropathic and cancer pain

Robert G Ungard, Yong Fang Zhu, Sarah Yang, Peter Nakhla,

Natalka Parzei, Kan Lun Zhu, Gurmit Singh.

Can J Pain. 2020

Preface

In this chapter, an author-generated version of the manuscript entitled “Response to pregabalin and progesterone differs in male and female rat models of neuropathic and cancer pain”, published in the Canadian Journal of Pain in 2020, is presented. The paper is reproduced with permission from Taylor & Francis Group, LLC., as stated on the copyright agreement:

For this manuscript, I cultured and isolated cells and performed surgery to induce the in vivo CIBP models, performed behavioural tests on both neuropathic and CIBP model rats, analyzed data and drafted and revised the manuscript. Yong Fang Zhu performed surgeries to induce all rat models of neuropathic pain and conducted all electrophysiological experiments and related data analysis. Sarah Yang assisted with all aspects of the in vivo CIBP studies including drug administration and behavioural testing. Peter Nakhla assisted with all aspects of the in vivo RNU -/- studies including drug administration and behavioural testing. Natalka Parzei assisted with surgeries, behavioural testing and tissue collection from all animals. Kan Lun Zhu assisted with behavioural testing on neuropathic model animals. Gurmit Singh supervised the overall project, edited the manuscript, and provided funding for the study. All authors read and approved the final manuscript.

American English spelling is used throughout the manuscript, as required by the journal.

Context and Background Information

In **Chapter 2**, I presented evidence demonstrating the role of targeting a metabolic feature of cancer cells as a strategy to reduce pain. That hypothesis relies on evidence that extracellular glutamate is able to alter cell signalling in the immediate tumour microenvironment, particularly by action at glutamate sensitive neurons which can result in excitotoxicity (Chung et al. 2005; Buckingham et al. 2011).

Cancer pain, like other chronic pain states, can be maintained through the development of sensitization in peripheral and central sensory pathways. Evidence of physiological changes indicative of sensitization in animal models of cancer include central sensitization at the dorsal horn of the spinal cord (Urch et al. 2003; Donovan-Rodriguez et al. 2004; Khasabov et al. 2007), peripheral sensitization of local primary afferent nociceptors (Cain et al. 2001; Zhao et al. 2010; Zheng et al. 2012), and cellular and neurochemical changes in the DRG neurons and dorsal horn of the spinal cord (Donovan-Rodriguez et al. 2004; Peters et al. 2005).

One mechanism of attenuating sensitization of peripheral circuits is by eliminating the initial stimuli, as we attempted in the manuscript presented in **Chapter 2**. In the manuscript presented here in **Chapter 3** we have adopted an approach from research into traumatic brain injury and ischemia, where progesterone treatment had shown beneficial effects on verbal and motor function, and mortality (Wright et al. 2007; Xiao et al. 2007; Xiao et al. 2008), and has been demonstrated to act in a neuroprotective manner through inhibiting excitotoxic neuronal cell death by direct inhibition of L-type voltage-gated calcium channels (VGCCs) (Chen et al. 1999; Gibson and Murphy 2004; Ozacmak and Sayan 2009; Wang et al. 2010; Luoma et al. 2011 Mar).

As such, we applied progesterone and the approved analgesic pregabalin which also acts through antagonism of P/Q, N, and L-type VGCCs (Gong et al. 2001) to rat models of cancer and neuropathic pain to evaluate their effect on behaviours indicative of pain over

the course of each model, and their effects on the intrinsic membrane properties of individual DRG sensory neurons as evaluated by intracellular in vivo electrophysiology. Our results showed an unexpected divergence between both sex and model effects in the responses to treatment in both pain states. Pregabalin and progesterone induced robust recoveries in male models of neuropathic pain, while females showed a lesser response and models of CIBP largely did not demonstrate behavioural responses to treatment, despite clear electrophysiological changes in the DRG neurons of pregabilin-treated male models of CIBP. In addition, the use of an athymic RNU -/- rat model of neuropathic pain that we included to discern if the sex differences in response to treatment observed in our neuropathic model were due to T-cell dependent mechanisms did not demonstrate the hypothesized improvement in recovery, rather those animals displayed considerably more evidence of pain throughout the duration of the model.

These results show a clear rationale for further study of progesterone as a neuroprotective intervention in conditions of neuropathic pain. Pregabalin is already an approved drug for diabetic neuropathy, and our results from behavioural testing in neuropathic pain models did not show any differences between the responses to the two drugs. The rationale for continued use in CIBP is less clear, although female rats displayed a delay in the time until onset of mechanical hypersensitivity.

Response to pregabalin and progesterone differs in male and female rat models of neuropathic and cancer pain

Robert G Ungard1,2, Yong Fang Zhu1,2, Sarah Yang1,2, Peter Nakhla1,2, Natalka Parzei1,2, Kan Lun Zhu2, Gurmit Singh1,2

1 Michael G. DeGroote Institute for Pain Research and Care, Medicine, McMaster University, 1280 Main St. West, Hamilton, ON L8S 4M1, Canada

2 Department of Pathology and Molecular Medicine, McMaster University, 1280 Main St. West, Hamilton, ON L8N 3Z5, Canada

Corresponding Author: Dr. Gurmit Singh

Department of Pathology & Molecular Medicine, McMaster University, 1280 Main Street West, Hamilton, ON L8N 3Z5, Canada

Tel.: +1 905 525 9140 x28144

E-mail address: singhg@mcmaster.ca

Number of tables: 0

Number of figures: 11

Number of words: 11,321

Number of supplementary tables: 0

ABSTRACT

Background: Cancer pain involves nervous system damage and pathological neurogenesis. Neuropathic pain arises from damage to the nervous system and is driven by ectopic signaling. Both progesterone and pregabalin are neuroprotective in animal models and there is evidence that both drugs bind to and inhibit voltage-gated calcium channels.

Aims: This study was designed to characterize the effects of progesterone and pregabalin in preclinical models of cancer and neuropathic pain in both sexes.

Methods: We measured peripheral sensory signaling by intracellular in vivo electrophysiology, and behavioral indicators of pain in rat models of cancer-induced bone pain and neuropathic pain.

Results: Female but not male models of cancer pain showed a behavioral response to treatment while pregabalin reduced excitability in C and A high-threshold but not low-threshold sensory neurons of both sexes. Male models of neuropathic pain treated with pregabalin demonstrated higher signaling thresholds only in A high-threshold neurons, while behavioral data indicated a clear recovery to baseline mechanical withdrawal thresholds in all treatment groups. Female rat treatment groups did not show excitability changes in sensory neurons but all demonstrated higher mechanical withdrawal thresholds than vehicle-treated females, although not to baseline levels. Athymic female rat models of neuropathic pain showed no behavioral or electrophysiological responses to treatment.

Conclusions: Both pregabalin and progesterone showed evidence of efficacy in male models of neuropathic pain. These results add to the evidence demonstrating differential effects of treatments for pain in male and female animals, and widely differing responses in models of cancer and neuropathic pain.

KEYWORDS

Cancer pain; neuropathic pain; electrophysiology; sensory neurons; dorsal root ganglion; behavior; pregabalin; progesterone

INTRODUCTION

Neuropathic pain is a prevalent and often intractable state of pain arising from pathology of the peripheral or central nervous system, and driven by ectopic signaling from damaged or pathological neurons [1,2]. Cancer pain is also often severe and intractable and can be induced by multiple stimuli. These include nociceptive mechanical and chemical stimuli that result from the cancer growth and metastasis to the bone, as well as damage and pathology of the nervous system itself. As a result, cancer pain is described as a unique pain state that includes aspects of nociceptive, neuropathic and inflammatory pain [3,4].

In models of neuropathic pain (NEP), treatment with progesterone (PRO) has produced beneficial results, including restoring myelination of damaged neurons and ameliorating mechanical and thermal withdrawal thresholds in animal models of nerve crush [5], spinal cord injury [6], and chemotherapy-induced NEP [7]. In a rat model of sciatic cuff induced NEP, PRO treatment starting immediately after model induction and lasting for 10 days significantly limited the development of mechanical allodynia [8]. Early clinical reporting describes treatment with PRO sharply reducing or abolishing pain in patients with late-stage metastatic breast cancer including bone metastases [9]. However, PRO has yet to be investigated in animal models of cancer pain.

Calcium signaling plays a well-established role in neuronal inflammation, de-myelination, and excitotoxic cell death [10], all of which are involved in the generation and maintenance of NEP and which progesterone treatment has been experimentally demonstrated to reduce. In cultured rat striatal neurons, supraphysiological doses of PRO

have been demonstrated to inhibit excitotoxic neuronal cell death by direct inhibition of L-type voltage-gated calcium channel (VGCC) action, without effect on glutamate-mediated ion channels [11].

Pregabalin (PRE) is well-established anticonvulsant and analgesic drug approved for the management of NEP associated with diabetic peripheral neuropathy and postherpetic neuralgia. PRE also demonstrates clinical utility across many other NEP conditions including chemotherapy-induced peripheral neuropathy, trigeminal neuralgia, fibromyalgia, and post-surgical pain [12]. PRE is utilized to treat neuropathic cancer pain in the clinic. Some clinical studies demonstrate its utility in comparison to other drugs [13,14], while other studies find no beneficial effects [15]. Despite these discrepancies, PRE has not been tested in animal models of cancer pain excluding chemotherapy-induced neuropathies. Similarly to PRO, PRE has been shown to act as a VGCC antagonist by binding at the α2-δ auxiliary subunits of P/Q, N, and L-type VGCCs [16]. This VGCC inhibition and the resulting reduction of Ca^{2+}-mediated excitatory glutamate release at neuronal synapses confers a neuroprotective benefit [17], and is thought to be responsible for the effectiveness of PRE in treating NEP [12].

Due to the evidence of neuropathic involvement in cancer-induced bone pain (CIBP) and the widespread evidence of efficacy of the VGCC antagonists PRO and PRE in conditions of NEP, this investigation was designed to characterize the behavioral and electrophysiological effects of these drugs in a rat model of CIBP. Our findings are indicative of a limited and possibly sexually divergent response in CIBP and prompted further investigation in our well-established rat model of sciatic cuff induced neuropathy.

MATERIALS AND METHODS

Cell Culture

The mammary rat metastasis tumour (MRMT-1) rat mammary carcinoma cell line (provided by Dr. Philippe Sarret of the Université de Sherbrooke, Sherbrooke, QC) was used in all in vitro and in vivo work. Cells were maintained in a humidified incubator at 37 °C with 5 % CO2 in growth medium supplemented with 10 % fetal bovine serum (FBS) and antibiotics (100 U ml-1 penicillin sodium and 1 % antibiotic/antimycotic (Thermo Fisher Scientific, Inc., Waltham, MA). MRMT-1 cells were grown in RPMI 1640 (Thermo Fisher Scientific) and tested for mycoplasma contamination prior to experimental use. Cell numbers were quantified in 96-well plates using crystal violet staining, measuring absorbance at $\lambda = 570$ nm with an optical plate reader (BioTek, Winooski VT). Cells treated with PRE were plated with dialyzed FBS, and cells treated with PRO were plated with charcoal-stripped FBS (Thermo Fisher Scientific) for all measurements. All were plated at 8000 cells / well and measured 24 h post-treatment. Cell numbers are indicated relative to their respective vehicle-only control for each dose. Cell harvesting for in vivo implantation was performed on sub-confluent cultures; adherent cells were suspended and kept lightly agitated in sterile Hank's Balanced Salt Solution (HBSS) on ice.

Test Compounds

Progesterone (PRO) (4-pregnene-3,20-dione) (Sigma-Aldrich, Oakville Canada) was administered in vivo at 30 mg/kg, suspended in sesame oil. Pregabalin (PRE) was administered at 4 mg/kg dissolved in 0.9 % saline. Earlier experimentation has demonstrated the doses included here to be relevant in animal models of pain and within published safe dosing ranges [8,12]. Vehicle-treated controls (0.9 % saline) were tested in parallel with experimental animals. Drug solutions were freshly prepared and administered by daily intraperitoneal injection.

Animal Models

All procedures were conducted according to the guidelines of the Committee for Research and Ethical Issues of the International Association for the Study of Pain [18] and guidelines established by the Canadian Council on Animal Care with ethical approval from the McMaster University Animal Research Ethics Board. All experimental animals were housed in pairs with access to food and water ad libitum in a temperature-controlled room under a 12-hour light/dark cycle.

Cancer Pain Models

Male and female Sprague-Dawley (SD) rats (Charles River Inc. St. Constant, QC) weighing 170-200 g were utilized for all cancer models. Rats were randomly assigned to cancer or sham surgery groups. 3.0×104 MRMT-1 cells resuspended in 20 μL HBSS were implanted in the distal femur of each cancer pain model rat. Cells for sham surgical controls were suspended at the same concentration and inactivated by three heat/freeze cycles prior to implantation.

Rats were anaesthetized with inhaled isoflurane (3-5 % in O2) and oriented in a supine position with their right hind limb fixed to a stationary convex support to maintain the limb in a flexed position. A small incision was made on the medial side to expose the quadriceps femoris and the vests lateralis was incised to expose the medial epicondyle of the femur. A small cavity was drilled between the medial epicondyle and the adductor tubercle with a 0.8 A stereotaxic drill equipped with a 1.75 mm burr. A 25 Ga needle was inserted into this cavity to penetrate the intramedullary canal. The needle was removed and replaced with a blunted 25 Ga needle attached to a Hamilton syringe containing the live MRMT-1 or heat/freeze-inactivated MRMT-1 (sham) cell suspension. The suspension was dispensed slowly into the canal and the syringe was left in place for 1 minute to prevent leakage. The cavity was then sealed with dental amalgam and fixed using a curing light. The wound was flushed with sterile deionized water, and muscle,

fascia, and skin were sutured. Cancer cell implantation to the distal femur was performed as described in detail in previously published methods [19,20].

Neuropathic Pain Models

Male and female SD rats and female RNU -/- immunocompromised rats weighing 170-200 g were used for all neuropathic pain (NEP) models. A peripheral neuropathy was induced by the "sciatic cuff model" according to methods first described by Mosconi and Kruger [21] and described in detail in previously published work [22]. Animals were anesthetized with a mixture of ketamine (Narketan; 5 mg/100 g; Vetoquinol N.-A. Inc.; Lavaltrie, QC), xylazine (Rompun; 0.5 mg/100 g; Bayer Inc., Toronto, ON), and acepromazine (Atravet; 0.1 mg/100 g; Ayerst Veterinary Laboratories, Guelph, ON) given intraperitoneally, and the right sciatic nerve was exposed at the mid-thigh level. One cuff of 0.5 mm polyethylene (PE-90) tubing (Intramedic PE-90, Fisher Scientific Ltd., Whitby, ON) was slit longitudinally and fitted around the exposed nerve. The muscle and skin of the wound were then sutured separately.

Behavioral Analyses

Rats were exposed to handling and behavioral testing equipment for a 1-2 week acclimation period and assigned individual identification prior to model induction. All behavioral testing was repeatedly performed by the same operators, who were blinded to group assignment throughout the duration of the study. Behavioral testing was performed prior to model induction to obtain baseline data, and weekly beginning on day 7 following model induction, continuing until endpoints, which were week 3 post-model induction for all CIBP models and week 6 post-model induction for all NEP models. With the exception of week 1 acute testing, all behavior measurements were performed prior to daily drug administration.

Dynamic Weight Bearing

Weight, area, and time distribution between all points of pressure of freely moving animals were recorded with the Dynamic Weight Bearing test 2.0 (DWB) (BioSeb, Vitrolles, France). Each animal was recorded in the DWB apparatus for 5 minutes/test and recordings were manually validated with DWB software version 2.0.59 (BioSeb). Results were exported as mean weight and time for each point of pressure across the validated experiment time. DWB has been validated as a useful test for animal models of CIBP [20,23]. Postural disequilibrium of the animal could indicate an allodynic response to normal ambulation, and so a reduction in weight borne by the tumor-afflicted limb of the animal was accepted as evidence of an inability or aversion to utilize that limb, providing indirect evidence of nociception.

Limb Use Scale

The open field observational limb use scale is an operator-derived numerical representation of the use of the animal's ipsilateral limb, scored over a 5 minute period of free ambulation.

(0: no use, 1: severe limp, 2: moderate limp, 3: slight limp, 4: normal use). This scale has been validated in mouse models of cancer-induced bone pain [24,25].

Von Frey Mechanical Withdrawal

To quantify mechanical sensitivity, brisk foot withdrawal in response to normally innocuous mechanical stimuli with von Frey filaments was measured. Rats are placed in a 30 × 30 × 30 cm Plexiglas box designed for von Frey testing with a clear floor containing 0.5 cm diameter holes spaced 1.5 cm apart for access to the paws [26]. Rats habituate to the box for 15 minutes minimum until cage exploration and major grooming activities cease, prior to any stimulation. Von Frey filaments (Stoelting Co., Wood Dale, IL) were applied to the plantar surface of the ipsilateral hind paw to determine mechanical withdrawal thresholds using the up-down method of Dixon [27] as applied to rodents by Chaplan et al.

[28]. A von Frey filament was applied a maximum of 5 times for 3-4 sec each, at 3 sec intervals, to different spots on the plantar surface of the ipsilateral hind paw in ascending order of force until a clear withdrawal response was observed, starting with the 2 g filament. When a withdrawal occurred, the next lightest filament was re-applied, and the process continued until a 50 % withdrawal response threshold was derived. Brisk foot withdrawal in response to the mechanical stimulus was interpreted as a valid response. A reduction in 50 % mechanical withdrawal threshold by the tumour or cuff-afflicted limb was indicative of allodynia.

Intracellular in vivo electrophysiology

Details of intracellular electrophysiological recording techniques have been reported previously in animal models of NEP [2,22,29] and cancer pain [30,31]. Briefly, action potentials evoked by stimulation of the dorsal root and measured at the L4 DRG soma are used to compare the configuration parameters and conduction velocity of each neuron. Recorded neurons were classified as C-type high-threshold mechanosensitive fibres (CHTM), Aβ-type high-threshold mechanosensitive fibres (AHTM), or Aβ-low-threshold mechanosensitive fibres (ALTM) based on their action potential configuration, conduction velocity, and their receptive field properties as determined by utilizing hand-held mechanical stimulators [22,32,33]. Other major factors, including the rate of adaptation and the tissue location of the receptive field, were used to further classify ALTM neurons as either (CUT) or muscle spindle neurons (MS). MS neurons were classified as slowly adapting neurons with deep subcutaneous receptive fields activated by deep tissue manipulation of the muscle belly but not by cutaneous stimulation.

Soma excitability thresholds were measured by evoking action potentials in the somata of DRG neurons by direct injection of depolarizing current. To quantify soma excitability, current injections of 100 ms each were injected into the soma, at amplitudes between 0.5 to 4 nA in increments of 0.5 nA. The thresholds of depolarizing current pulses were

determined with the "Protocol Editor" function in the pClamp 9.2 software program (Molecular Devices). All animals were tested at model endpoint. CIBP model rats were recorded following week 3 behavioral testing and all NEP model rats were recorded following week 6 behavioral testing.

Statistical Analyses

In vitro data represent the mean of n = 3 biological replicates ± SEM. Data are expressed as fold-change relative to dose-matched vehicle controls. Differences within treatment groups are compared to untreated control (0 μM) by one-way ANOVA with post hoc Dunnett's multiple comparisons test. In vivo behavioral data represent the mean ± SEM from male SD CIBP rats: PRE n = 6, PRO n = 5, VEH n = 5, SHAM n = 5; and female SD CIBP rats: PRE n = 6, PRO n = 4, VEH n = 6, SHAM n = 7. Only animals with verified tumour development are included in results for CIBP-model animals. Data are collected from male SD NEP rats: PRE n = 4, PRO n = 4, PRE+PRO n = 4, VEH n = 4; female SD NEP rats: PRE n = 6, PRO n = 6, PRE+PRO n = 4, VEH n = 4 rats; female RNU -/- NEP rats: PRE n = 5, PRO n = 5, VEH n = 4, Naïve n = 3. All behavioral results are compared between and within groups across the duration of the experiment, and groups are compared independently at endpoint. Differences between treatment groups over time are compared to VEH control by RM two-way ANOVA with post hoc Dunnett's multiple comparisons test. Differences within treatment groups relative to respective baseline measurements are compared by RM two-way ANOVA with post hoc Dunnett's multiple comparisons test. Differences between treatment groups at endpoint are compared by one-way ANOVA with post hoc Tukey's multiple comparisons test or Kruskal-Wallis test with post hoc Dunn's multiple comparisons test for non-parametric limb use scale data. Acute response differences within treatment groups are compared by multiple t-tests. Electrophysiological data represent the mean ± SEM from independently recorded neurons from $n \geq 3$ rats of each group. Differences between treatment groups are compared by Kruskal-Wallis test with post hoc Dunn's multiple comparison test. All

results were considered significant at $P < 0.05$. Analyses and charts were generated using GraphPad Prism 7 software (GraphPad Software, La Jolla, CA).

RESULTS

Pregabalin and progesterone treatment delays the onset of mechanical hypersensitivity relative to vehicle-treatment in female rat models of cancer-induced bone pain but have no effects in males.

Prior to use in animal models, the growth of MRMT-1 cancer cells treated with PRE and PRO was investigated in vitro to determine if administration of these test compounds could affect cell growth and therefore tumour size and nociceptive outcomes in in vivo animal models. Cell number was measured in vitro in the presence of a range of PRE and PRO doses between 1 nM and 50 µM. Crystal violet staining showed no differences between vehicle treated MRMT-1 cells and PRE and PRO treated cells at any doses (Fig. 1). Due to these findings, no differences were expected to occur in bone tumour size between treated and untreated rats due to direct effects of treatment compounds on cancer cells.

Male CIBP-model rats do not show sustained differences indicative of reduced nociception by any behavioral measures in PRE or PRO-treated groups when compared to vehicle. There are no differences in 50 % mechanical paw withdrawal threshold in the ipsilateral limb between PRO, PRE, and vehicle treatment groups of male CIBP-model rats at any timepoint post-model induction as measured by testing with von Frey filaments (Fig. 2a). All male model groups show reduced thresholds relative to sham-surgical control animals in weeks 2 and 3. Likewise, no treatment groups of male rats including vehicle-treatment show a sustained delay past week 1 until mechanical withdrawal threshold is reduced relative to the baseline measurements for each group respectively (Fig. 2b). At endpoint (Fig. 2c), all treatment groups including vehicle are

not different from each other and all show significantly decreased paw withdrawal thresholds relative to baseline and to sham-control thresholds.

Female CIBP-model rats show evidence of a delay of onset of a reduced mechanical withdrawal threshold in both PRO and PRE treated groups relative to vehicle (Fig. 2d), where PRE-treated animals are significantly different from vehicle at week 2, and PRO-treated animals show higher thresholds on both weeks 1 and 2. No groups are different at week 3. Consistently, PRE-treated animals do not respond at lower mechanical force from baseline measurements at week 2 (Fig. 2e), and PRO-treated animals do not react to lower stimuli from their respective baseline until week 3. Vehicle-treated animals react to less force than baseline on each week following tumour implantation, and sham animals do not differ from baseline measurements at any timepoint. At endpoint (Fig. 2f) there are no differences between treatment groups and all show significantly decreased paw withdrawal thresholds relative to baseline and to Sham control.

There are no differences in ipsilateral limb use scoring (0-4 scale) as measured by observational scoring over a 5-minute period of free ambulation between PRO, PRE, and vehicle treatment groups of (Fig. 3a) male and (Fig. 3d) female CIBP-model rats at any timepoint post-model induction. All male and female groups show impaired limb use relative to Sham-surgical control animals by week 3. Likewise, no treatment groups including vehicle of (Fig. 3b) male and (Fig. 3e) female rats show sustained maintenance of normal limb use past week 2 relative to their respective baseline measurements. At week 3 all treatment groups of male rats show significantly decreased limb use scores relative to baseline and to Sham controls (Fig. 3c) and all treatment groups including vehicle are not different from each other. At endpoint, female PRE and vehicle-treated groups are significantly decreased from baseline and Sham, while PRO-treated rats show no differences from any groups (Mean ± SEM: PRE: 2.67 ± 0.33; VEH: 2.67 ± 0.42; PRO: 2.75 ± 0.75; SHAM: 4 ± 0) (Fig. 3f).

There are no differences in ipsilateral limb weight bearing as a percentage of animal body weight as measured by dynamic weight bearing between PRO, PRE, and vehicle

treatment groups of (Fig. 4a) male and (Fig. 4d) female CIBP-model rats at any timepoint post-model induction. No treatment groups of male rats (Fig. 4b) show sustained maintenance of normal ipsilateral weight bearing past week 2 relative to baseline measurements of each group. PRE and PRO-treated female rats also show decreased weight bearing at week 3, however vehicle-treated rats are not different from their respective baseline measurements. At week 3 endpoint all treatment groups of male rats show significantly decreased ipsilateral limb weight bearing relative to baseline and to Sham controls (Fig. 4c), and PRE-treated male rats are significantly lower than PRO-treated male rats. At endpoint, female PRE and PRO-treated groups are significantly decreased from baseline and Sham (Fig. 4f), however vehicle-treated rats are significantly decreased from grouped baseline measurements only, and not different from PRE or PRO.

High but not low-threshold mechanosensitive fibres in CIBP-model animals treated with PRE have excitability thresholds that are higher than vehicle and equivalent to sham controls.

Action potential responses to intracellular depolarizing current pulse injection were tested in vivo to determine the soma excitability thresholds in sensory neurons at the DRG of model animals. Representative recording images show the multiple injected current stimuli (Fig. 5a) of 100 ms each delivered between 500 to 4000 pA in increments of 500 pA, and the characteristic evoked action potentials in the mechanoreceptor neuron types evaluated in this study including CHTM (Fig. 5b), AHTM (Fig. 5c), and both cutaneous (CUT) and muscle spindle (MS) ALTM neurons; ALTM-CUT (Fig. 5d), and ALTM-MS (Fig. 5e). All CIBP model animals were tested following the conclusion of behavioral data collection at week 3.

Current activation thresholds measured in nA of CHTM neurons (Fig. 6a) were significantly decreased in vehicle-treated male CIBP rats relative to sham control rats. Treatment with PRE significantly increased activation thresholds of CHTM above both vehicle and sham groups, while PRO-treated animals showed no differences in CHTM

threshold from either vehicle or sham groups. Activation thresholds of AHTM neurons (Fig. 6b) were significantly decreased in vehicle-treated male CIBP rats relative to sham. Treatment with PRE significantly increased activation thresholds of AHTM above vehicle, while PRO-treated animals showed no differences from either vehicle or sham groups. There are no significant differences in activation threshold between any groups of ALTM-CUT neurons in males (Fig. 6c). The activation threshold of ALTM-MS neurons (Fig. 6d) in the vehicle-treated group was significantly decreased relative to sham, while both PRE- and PRO-treated ALTM-MS neurons were not significantly different from either vehicle-treated or sham male rats.

In female CIBP model rats, the activation thresholds of CHTM neurons (Fig. 6e) in the vehicle-treated group were significantly decreased relative to sham. Similarly to males, PRE-treated females had significantly increased activation thresholds of CHTM from vehicle, but they did not significantly differ from PRO-treated or sham females. PRO-treated female rats showed no significant differences from either vehicle or sham CHTM. The activation thresholds of AHTM neurons in female rats (Fig. 6f) were significantly decreased in vehicle-treated animals relative to sham. Activation thresholds of AHTM in PRE-treated female rats were higher than vehicle not different from sham, while PRO-treated females showed no differences in AHTM threshold from either vehicle or sham groups. The changes in AHTM neurons showed equivalent patterns in both male and female rats. There was no evidence of treatment effects on the activation threshold of ALTM-CUT neurons in female rats (Fig. 6g). Both PRE- and vehicle-treated group showed reduced thresholds relative to sham control, and PRO-treated rats were not different from any group. The activation threshold of ALTM-MS neurons (Fig. 6h) in vehicle-treated females was significantly decreased relative to sham, and similarly to males, both PRE- and PRO-treated ALTM-MS neuron thresholds were not significantly different from either vehicle-treated or sham female rats.

Two-week treatment with pregabalin, progesterone, and combination induces large and sustained recoveries to baseline in ipsilateral paw withdrawal threshold in male rat models of neuropathic pain, while treated female rat models show increases in withdrawal thresholds relative to vehicle-treated rats, but not to baseline thresholds.

All treatment groups of male NEP-model rats (Fig. 7a) show an initial decrease in 50 % mechanical paw withdrawal threshold in the ipsilateral limb after model-induction followed by a robust recovery where all treatment groups are increased from vehicle-treated rats at week 2 and all later timepoints. PRO and PRE treatment groups show sustained recoveries to withdrawal thresholds no different from their respective baseline measurements (Fig. 7b) by week 2. PRE+PRO combination-treated animals did not decline at any point to levels different from their baseline thresholds. In contrast, and characteristic of the sciatic-cuff model, withdrawal thresholds of vehicle-treated animals remain significantly decreased from baseline at every post-surgical timepoint with no evidence of recovery. At week 6 endpoint (Fig. 7c), paw withdrawal thresholds of all male treatment groups are not different from grouped baseline thresholds and all treatment groups show significantly increased thresholds relative to vehicle treatment. All groups of female NEP-model rats also show an initial decrease in 50 % mechanical paw withdrawal threshold in the ipsilateral limb after model-induction (Fig. 7d), however all treatment groups retain a consistently higher 50 % paw withdrawal threshold than vehicle-treated rats at all timepoints post-model induction. Unlike males, female treatment groups do not recover to withdrawal thresholds equivalent to their respective baseline measurements (Fig. 7e) at any point following treatment initiation. PRE and PRO-treatment groups remain lower than their respective baseline withdrawal thresholds at all post-surgical timepoints, and PRE+PRO combination treatment animals initially are no different from baseline, but become different at week 4 and later. At endpoint (Fig. 7f) there are no differences between treatment groups of female rats and all show significantly decreased paw withdrawal thresholds relative to baseline. PRE and PRE+PRO combination treated animals have higher withdrawal thresholds than vehicle, while PRO and vehicle are not different.

Treatment with PRE prevents reduction in excitability threshold in AHTM and ALTM-MS fibres in male rats, while all other types of sensory fibres tested demonstrate no changes in excitability thresholds in both sexes.

In male NEP model rats, there were no differences between any groups in the current activation thresholds of CHTM neurons (Fig.8a). Activation thresholds of AHTM neurons (Fig. 8b) were significantly decreased in vehicle-treated male NEP rats relative to both naïve and PRE-treated rats. There were also no differences in activation threshold between groups of ALTM-CUT (Fig. 8c), while the activation thresholds of ALTM-MS neurons (Fig. 8d) were significantly decreased in vehicle-treated male NEP rats relative to both naïve and PRE-treated rats, where had equivalent thresholds to each other. In female NEP model SD rats, there were no differences between any groups in the current activation thresholds of all types of neurons tested: CHTM (Fig. 8e), AHTM (Fig. 8f) ALTM-CUT (Fig. 8g), and ALTM-MS neurons (Fig. 8h).

Female immunocompromised rat models of sciatic-cuff induced neuropathic pain treated with pregabalin and progesterone do not show sustained differences in ipsilateral 50 % paw withdrawal thresholds from vehicle-treated rats or recoveries to baseline threshold levels.

There are no differences in 50 % mechanical paw withdrawal threshold in the ipsilateral limb between PRO, PRE, and vehicle-treatment groups of female RNU -/- sciatic-cuff induced neuropathic pain model rats at any timepoint post-model induction excluding week 3 as measured by testing with von Frey filaments (Fig. 9a). At week 3 PRE-treated rats show a significantly higher threshold than vehicle-treated rats, however this difference is not sustained in later weeks.

All model groups show reduced thresholds relative to Naïve control animals in all post-surgical weeks (not marked on chart). (Fig. 9b). In addition, all treatment groups

including vehicle show significantly reduced withdrawal thresholds relative to baseline measurements at all post-surgical time points. Naïve control rats are not different from baseline at any week. (Fig. 9c). At endpoint there are no differences between treatment groups and all show significantly decreased paw withdrawal thresholds relative to baseline and to Naïve control.

No thresholds in any fibre types show differences from naïve or vehicle in response to treatment with PRE.

In athymic female RNU -/- models of NEP, the current activation threshold of CHTM neurons (Fig.10a) was decreased in the vehicle-treated group relative to naïve RNU -/- female rats. There were no significant differences in thresholds of CHTM neurons between both PRE- and PRO-treated groups and either vehicle or naïve rats. Activation thresholds of AHTM (Fig. 10b) and ALTM-MS (Fig. 10d) neurons showed no significant differences between any groups. Activation thresholds of ALTM-CUT neurons (Fig. 10c) were significantly decreased from naïve in both the vehicle-treated and PRO-treated groups of female RNU NEP model rats. PRE-treated rats showed no differences in threshold from both either vehicle-treated or naïve rats.

Male but not female rat models of sciatic-cuff induced neuropathic pain show an acute increase in ipsilateral paw withdrawal thresholds 1-hour post-treatment with pregabalin, progesterone, or combination at post-surgical week 1.

All NEP model animals were measured at week 1 pre- and 1-hour post-treatments. Male SD rat models of sciatic-cuff induced neuropathic pain show an acute response to treatment with PRE, PRO, and PRE+PRO combination as an increase in 50 % mechanical paw withdrawal threshold as measured by testing with von Frey filaments. Withdrawal thresholds of vehicle-treated animals do not change following treatment. No acute responses to treatment are seen in any groups of (Fig. 11b) female immunocompetent SD rats or (Fig. 11c) immunocompromised RNU -/- neuropathic pain model animals.

DISCUSSION

This study was designed to assess the effects of PRE and PRO on the development of chronic hypersensitivity in CIBP and NEP animal models in both male and female groups. We present for the first time that these treatments, administered as repeated injections during the early phases of NEP and CIBP development, promoted the robust recovery of mechanical hypersensitivity in male NEP rats, partial recovery of female NEP and female CIBP rats, and no apparent effects on both male CIBP and female immunocompromised NEP models. These results add to the evidence indicative of differing mechanisms of pain generation in CIBP and NEP states, and to the evidence of sexual divergence in both the mechanisms of chronic pain itself, and in the response to pain therapeutics.

The behavioral results of this study suggest that PRE and PRO have efficacy in treating male and female NEP rats, and electrophysiological data support this for PRE-treated animals, showing excitation thresholds in nociceptive neurons equivalent to naïve. However, CIBP model male animals show no behavioral response to PRE or PRO, and female CIBP rats show only limited evidence of a delay in the onset of hypersensitivity with both treatments. Our previous investigation of the intracellular electrophysiological characteristics of sensory neurons in this CIBP model indicated that there are both nociceptive and neuropathic components of the cancer-induced pain state. These include reduced signaling thresholds of ALTM-MS neurons in both vehicle treated NEP and CIBP model rats relative to control, and morphological changes at the spinal cord indicative of a possible role for ALTM fibres in the generation or maintenance of the neuropathic component of CIBP [34]. In this study, both CHTM and AHTM nociceptive neurons and ALTM-CUT and ALTM-MS non-nociceptive neurons showed significant changes in CIBP models, and treatment with PRE induced the recovery of nociceptive neuron excitation thresholds to sham model levels in both sexes. There were no differences in treated ALTM neurons from vehicle control. In NEP male and female

model animals, we have observed that CHTM and ALTM-CUT neurons did not change in any groups relative to naïve, and that reductions in the thresholds of AHTM and ALTM-MS neurons were prevented or reversed by treatment with PRE in male NEP animals and were not significantly changed in any groups of female NEP animals. Taken together, these results indicate that in contrast to the strong behavioral responses to treatment in NEP-model rats which showed normally non-nociceptive ALTM thresholds equivalent to naïve, the absent and muted behavioral response to treatment in in male and female CIBP rats, respectively, may be associated with decreased signaling thresholds in ALTM-CUT and ALTM-MS neurons.

In this study, normally nociceptive CHTM and AHTM neurons in both pain models showed decreased excitability after treatment with PRE. Treatment with PRO produced partial reductions in neuronal excitability thresholds in CIBP animals, although none were significantly different from either vehicle or sham controls. There is pre-clinical and clinical evidence of the efficacy of both drugs for conditions involving neuronal damage and neuropathy, however the exact mechanisms of action are unclear. PRO has been shown to have neuroprotective properties including protection from excitotoxic cell death, de-myelination, and reduction of neuronal inflammation and edema, all of which can contribute to the generation of ectopic signaling [11,35], and has demonstrated some utility in treating chronic NEP in rat models in male rats [8]. PRE has demonstrated effectiveness for NEP in animal models and in humans, leading to its use as a first-line clinical therapy for NEP, however its effectiveness is inconsistent [12,36]. Both PRO and PRE inhibit VGCCs, and while the exact mechanisms of the PRO and L-type VGCC interaction have not yet been elucidated, PRE, like gabapentin, binds at the α2-δ subunits of P/Q, N, and L-type Ca^{2+} channels [11,16]. T- and N-type VGCCs are expressed on sensory afferent neurons [37,38], and it has been reported that the α2δ-1 subunit is upregulated in DRG neurons in several animal models of pain, and this is causally related to the onset of pain behavior [39–41]. It also has been reported that pregabalin reduces the depolarization-induced calcium influx at nerve terminals, resulting in a reduction of the presynaptic release of excitatory neurotransmitters, including glutamate, substance P and CGRP [42,43].

VGCCs are also expressed on glial cells [44], however their expression and function is less well understood.

A limitation of this study is that our animal models develop over different durations, where our endpoint electrophysiological data is recorded at week 6 in all NEP models and week 3 in all CIBP models. In addition, unlike the one-time nervous system damage of the cuff NEP model, our CIBP model reflects the progressive and often intractable nature of cancer pain in humans. CIBP is a conglomerate of multiple initiating factors, including a wide range of nociceptive and inflammatory stimuli including mechanical distortion and pressure on host tissues, secreted inflammatory and nociceptive mediators, and neuropathy from tumour-initiated destruction and damage of nervous tissue and pathological growth of new and dysregulated sensory neurons [45,46]. Electrophysiological measurements from week 3 endpoint may not reflect either a delay in the onset of this pain state, or may not have allowed for an adequate and comparable duration of recovery.

Female CIBP rats treated with PRE and PRO showed a delay to the onset of mechanical hypersensitivity as measured by von Frey fibres. This delay was not reflected by measures of either weight bearing or limb use. Male CIBP model rats did not show behavioral responses to treatment. In NEP model rats, males demonstrated a strong response to drug treatment where PRE, PRO and PRE+PRO treatment groups recovered to 50 % mechanical thresholds equivalent to their baseline measurements by week 2. Although all NEP-model female treatment groups remained at significantly higher withdrawal thresholds than vehicle-treated female controls throughout the experiment, no treatment groups recovered to baseline levels in contrast to male rats. These sexually divergent effects in response to treatment are suggestive of mechanistic differences between male and female CIBP and NEP models. Substantial evidence implicates that sex differences in the behavioral responses to peripheral neuropathy in animal models may involve distinct hormonal and immune system pathways. After peripheral nerve injury, microglial-neuronal signaling in the spinal cord appears to mediate hypersensitivity in male mice, while in females despite concurrent microglial proliferation, T cells infiltrate the spinal cord and maintain hypersensitive state [47–49]. There is evidence in cancer pain

states however, that microglia do play a role in the maintenance of pain in female rats [50]. To investigate if the sex differences observed in our NEP models involved the T cell dependent signaling systems in the spinal cord, we applied the sciatic-cuff model to female RNU -/- athymic rats. Our hypothesis was that the lack of mature T cells would result in chronic pain-state with behavioral responses similar to immunocompetent male rats, as has been shown in other animal models of pain [47]. It has also been demonstrated that T cell deficient nude rats develop significantly reduced mechanical allodynia following CCI compared with their heterozygous littermates [51]. Our findings showed a behavioral difference between PRE- and vehicle-treated rats at only one timepoint, and that difference was not sustained. Female athymic NEP model rats in fact demonstrated more severe mechanical hyperalgesia in treatment groups than immunocompetent females, counter to our expectations, although this could reflect strain differences. Correspondingly, CHTM and ALTM-CUT neurons in vehicle-treated immunocompromised female NEP models showed increased excitability relative to naïve controls and were not recovered by treatment.

Sex differences were also apparent in the acute behavioral response measurements performed at week 1 in all NEP model animals. Male NEP rats of all treatment groups responded with an increase in mechanical withdrawal threshold measured 1h after treatment. These increases were not apparent in vehicle-treated controls, and no groups were significantly different in female immunocompetent and immunocompromised animals.

These discrepancies in the response to treatment with PRE and PRO between sexes and immunocompromised animals indicate that the cellular immune response in the spinal cord of animals models of chronic pain is not a simple answer in this case. Inflammatory responses to injury also have adaptive functions enabling nerve repair involving IL-1 and TNF-α expression [52] and complete ablation of macrophages can result in severely impaired axon regeneration [53]. It is possible that a partially beneficial immune response to chronic injury and NEP, as is the case in the sciatic-cuff model could be limited by the absence of T cells, and by therapies that target them.

In conclusion, we show that the analgesic effects of PRE and PRO can promote recovery of tactile hypersensitivity in response to treatment initiated during the early phase of NEP development. These effects are sex-dependent, and strongest in male rat models of NEP. Female rat models of NEP show a limited response to PRE and PRO treatment. Female CIBP models also show a limited response to treatment, while males do not respond. These results indicate that sex may be an important consideration for the therapeutic utility of both PRE and PRO.

ACKNOWLEDGEMENTS

We would like to thank Dr. James L. Henry for conceptual advice. This study was supported by grants to G. Singh from the Canadian Breast Cancer Foundation (Ontario) and the Michael G. DeGroote Institute for Pain Research and Care, and fellowships from the Canadian Institutes of Health Research and the Michael G. DeGroote Institute for Pain Research and Care to R. Ungard.

DISCLOSURE OF INTEREST

The authors report no conflict of interest.

REFERENCES

1. Baron R. Mechanisms of Disease: neuropathic pain—a clinical perspective. Nat Clin Pract Neurol. 2006;2(2):95-106. doi:10.1038/ncpneuro0113

2. Zhu Y, Henry JL. Excitability of Aβ sensory neurons is altered in an animal model of peripheral neuropathy. BMC Neurosci. 2012;13(1):15. doi:10.1186/1471-2202-13-15

3. Jimenez-Andrade JM, Mantyh WG, Bloom AP, Ferng AS, Geffre CP, Mantyh PW. Bone cancer pain. Ann N Y Acad Sci. 2010;1198:173-181. doi:10.1111/j.1749-6632.2009.05429.x

4. Colvin L, Fallon M. Challenges in cancer pain management--bone pain. Eur J Cancer. 2008;44(8):1083-1090. doi:10.1016/j.ejca.2008.03.001

5. Roglio I, Bianchi R, Gotti S, et al. Neuroprotective effects of dihydroprogesterone and progesterone in an experimental model of nerve crush injury. Neuroscience. 2008;155(3):673-685. doi:10.1016/j.neuroscience.2008.06.034

6. Coronel MF, Labombarda F, Villar MJ, De Nicola AF, González SL. Progesterone Prevents Allodynia After Experimental Spinal Cord Injury. J Pain. 2011;12(1):71-83. doi:10.1016/j.jpain.2010.04.013

7. Meyer L, Patte-Mensah C, Taleb O, Mensah-Nyagan AG. Cellular and functional evidence for a protective action of neurosteroids against vincristine chemotherapy-induced painful neuropathy. Cell Mol Life Sci. 2010;67(17):3017-3034. doi:10.1007/s00018-010-0372-0

8. Dableh LJ, Henry JL. Progesterone prevents development of neuropathic pain in a rat model: Timing and duration of treatment are critical. J Pain Res. 2011;4:91-101. doi:10.2147/JPR.S17009

9. Landau RL, Ehrlich EN, Huggins C. Estradiol benzoate and progesterone in advanced human-breast cancer. JAMA. 1962;182(6):632-636.

10. Sribnick EA, Del Re AM, Ray SK, Woodward JJ, Banik NL. Estrogen attenuates glutamate-induced cell death by inhibiting Ca2+ influx through L-type voltage-gated Ca2+ channels. Brain Res. 2009;1276:159-170. doi:10.1016/j.brainres.2009.04.022

11. Luoma JI, Kelley BG, Mermelstein PG. Progesterone inhibition of voltage-gated calcium channels is a potential neuroprotective mechanism against excitotoxicity. Steroids. March 2011. doi:10.1016/j.steroids.2011.02.013

12. Verma V, Singh N, Singh Jaggi A. Pregabalin in neuropathic pain: evidences and possible mechanisms. Curr Neuropharmacol. 2014;12(1):44-56. doi:10.2174/1570159X1201140117162802

13. Raptis E, Vadalouca A, Stavropoulou E, Argyra E, Melemeni A, Siafaka I. Pregabalin vs. Opioids for the treatment of neuropathic cancer pain: A prospective, head-to-head, randomized, open-label study. Pain Pract. 2014;14(1):32-42. doi:10.1111/papr.12045

14. Mishra S, Bhatnagar S, Goyal GN, Rana SPS, Upadhya SP. A Comparative Efficacy of Amitriptyline, Gabapentin, and Pregabalin in Neuropathic Cancer Pain: A Prospective Randomized Double-Blind Placebo-Controlled Study. Am J Hosp Palliat Med. 2012;29(3):177-182. doi:10.1177/1049909111412539

15. Fallon M, Hoskin PJ, Colvin LA, et al. Randomized double-blind trial of pregabalin versus placebo in conjunction with palliative radiotherapy for cancer-induced bone pain. J Clin Oncol. 2016;34(6):550-556. doi:10.1200/JCO.2015.63.8221

16. Gong HC, Hang J, Kohler W, Li L, Su TZ. Tissue-specific expression and gabapentin-binding properties of calcium channel alpha2delta subunit subtypes. J Membr Biol. 2001;184(1):35-43.

17. Ha K-Y, Kim Y-H, Rhyu K-W, Kwon S-E. Pregabalin as a neuroprotector after spinal cord injury in rats. Eur Spine J. 2008;17(6):864-872. doi:10.1007/s00586-008-0653-6

18. Zimmermann M. Ethical guidelines for investigations of experimental pain in conscious animals. Pain. 1983;16(2):109-110.

19. Doré-Savard L, Otis V, Belleville K, et al. Behavioral, medical imaging and histopathological features of a new rat model of bone cancer pain. Lowenstein PR, ed. PLoS One. 2010;5(10):e13774. doi:10.1371/journal.pone.0013774

20. Tétreault P, Dansereau M-A, Doré-Savard L, Beaudet N, Sarret P. Weight bearing evaluation in inflammatory, neuropathic and cancer chronic pain in freely moving rats. Physiol Behav. 2011;104(3):495-502. doi:10.1016/j.physbeh.2011.05.015

21. Mosconi T, Kruger L. Fixed-diameter polyethylene cuffs applied to the rat sciatic nerve induce a painful neuropathy: ultrastructural morphometric analysis of axonal alterations. Pain. 1996;64(1):37-57.

22. Zhu YF, Wu Q, Henry JL. Changes in functional properties of A-type but not C-type sensory neurons in vivo in a rat model of peripheral neuropathy. J Pain Res. 2012;5:175-192. doi:10.2147/JPR.S26367

23. Ungard RG, Seidlitz EP, Singh G. Inhibition of breast cancer-cell glutamate release with sulfasalazine limits cancer-induced bone pain. Pain. 2014;155(1):28-36. doi:10.1016/j.pain.2013.08.030

24. Miladinovic T, Ungard RG, Linher-Melville K, Popovic S, Singh G. Functional effects of TrkA inhibition on system x C − -mediated glutamate release and cancer-induced bone pain. Mol Pain. 2018;14:174480691877646. doi:10.1177/1744806918776467

25. Ungard RG, Linher-Melville K, Nashed M, Sharma M, Wen J, Singh G. xCT knockdown in human breast cancer cells delays onset of cancer-induced bone pain. Mol Pain. 2019;15. doi:10.1177/1744806918822185

26. Pitcher GM, Ritchie J, Henry JL. Paw withdrawal threshold in the von Frey hair test is influenced by the surface on which the rat stands. J Neurosci Methods. 1999;87(2):185-193.

27. Dixon WJ. The Up-and-Down Method for Small Samples. J Am Stat Assoc. 1965;60(312):967. doi:10.2307/2283398

28. Chaplan SR, Bach FW, Pogrel JW, Chung JM, Yaksh TL. Quantitative assessment of tactile allodynia in the rat paw. J Neurosci Methods. 1994;53(1):55-63.

29. Wu Q, Henry JL. Delayed onset of changes in soma action potential genesis in nociceptive A-beta DRG neurons in vivo in a rat model of osteoarthritis. Mol Pain. 2009;5(1):57. doi:10.1186/1744-8069-5-57

30. Zhu YF, Ungard R, Seidlitz E, et al. Differences in electrophysiological properties of functionally identified nociceptive sensory neurons in an animal model of cancer-induced bone pain. Mol Pain. 2016;12:174480691662877. doi:10.1177/1744806916628778

31. Zhu YF, Ungard R, Zacal N, Huizinga JD, Henry JL, Singh G. Rat model of cancer-induced bone pain: changes in nonnociceptive sensory neurons in vivo. Pain reports. 2017;2(4):e603. doi:10.1097/PR9.0000000000000603

32. Djouhri L, Bleazard L, Lawson SN. Association of somatic action potential shape with sensory receptive properties in guinea-pig dorsal root ganglion neurones. J Physiol. 1998;513(3):857-872. doi:10.1111/j.1469-7793.1998.857ba.x

33. Lawson SN, Crepps BA, Perl ER. Relationship of substance P to afferent characteristics of dorsal root ganglion neurones in guinea-pig. J Physiol. November 1997:177-191.

34. Zhu YF, Kwiecien JM, Dabrowski W, et al. Cancer pain and neuropathic pain are associated with A β sensory neuronal plasticity in dorsal root ganglia and abnormal sprouting in lumbar spinal cord. Mol Pain. 2018;14. doi:10.1177/1744806918810099

35. Singh M, Su C. Progesterone and neuroprotection. Horm Behav. 2013;63(2):284-290. doi:10.1016/j.yhbeh.2012.06.003

36. Finnerup NB, Jensen TS. Clinical use of pregabalin in the management of central neuropathic pain. Neuropsychiatr Dis Treat. 2007;3(6):885-891.

37. Zamponi GW, Lewis RJ, Todorovic SM, Arneric SP, Snutch TP. Role of voltage-gated calcium channels in ascending pain pathways. Brain Res Rev. 2009;60(1):84-89. doi:10.1016/j.brainresrev.2008.12.021

38. Fuchs A, Fellow R, Rigaud M, et al. Contribution of Calcium Channel Subtypes to the Intracellular Calcium Signal in Sensory Neurons: The Effect of Injury. doi:10.1097/01.anes.0000267511.21864.93

39. Bauer CS, Nieto-Rostro M, Rahman W, et al. The increased trafficking of the calcium channel subunit α2δ-l to presynaptic terminals in neuropathic pain is inhibited by the α2δ ligand pregabalin. J Neurosci. 2009;29(13):4076-4088. doi:10.1523/JNEUROSCI.0356-09.2009

40. Wang H, Sun H, Della Penna K, et al. Chronic neuropathic pain is accompanied by global changes in gene expression and shares pathobiology with neurodegenerative diseases. Neuroscience. 2002;114(3):529-546. doi:10.1016/S0306-4522(02)00341-X

41. Newton RA, Bingham S, Case PC, Sanger GJ, Lawson SN. Dorsal root ganglion neurons show increased expression of the calcium channel alpha2delta-1 subunit following partial sciatic nerve injury. Brain Res Mol Brain Res. 2001;95(1-2):1-8. doi:10.1016/s0169-328x(01)00188-7

42. Han DW, Kweon TD, Lee JS, Lee Y-W. Antiallodynic effect of pregabalin in rat models of sympathetically maintained and sympathetic independent neuropathic pain. Yonsei Med J. 2007;48(1):41-47. doi:10.3349/ymj.2007.48.1.41

43. Fink K, Dooley DJ, Meder WP, et al. Inhibition of neuronal Ca2+ influx by gabapentin and pregabalin in the human neocortex. Neuropharmacology. 2002;42(2):229-236. doi:10.1016/S0028-3908(01)00172-1

44. Carmignoto G, Pasti L, Pozzan T. On the role of voltage-dependent calcium channels in calcium signaling of astrocytes in situ. J Neurosci. 1998;18(12):4637-4645.

45. Lozano-Ondoua AN, Symons-Liguori AM, Vanderah TW. Cancer-induced bone pain: Mechanisms and models. Neurosci Lett. 2013;557 Pt A(0 0):52-59. doi:10.1016/j.neulet.2013.08.003

46. Mantyh PW, Clohisy DR, Koltzenburg M, Hunt SP. Molecular mechanisms of cancer pain. Nat Rev Cancer. 2002;2(3):201-209. doi:10.1038/nrc747

47. Sorge RE, Mapplebeck JCS, Rosen S, et al. Different immune cells mediate mechanical pain hypersensitivity in male and female mice. Nat Neurosci. 2015;18(8):1081-1083. doi:10.1038/nn.4053

48. Gattlen C, Clarke CB, Piller N, et al. Spinal cord t-cell infiltration in the rat spared nerve injury model: A time course study. Int J Mol Sci. 2016;17(3). doi:10.3390/ijms17030352

49. Mapplebeck JCS, Dalgarno R, Tu YS, et al. Microglial P2X4R-evoked pain hypersensitivity is sexually dimorphic in rats. Pain. 2018;159(9):1752-1763. doi:10.1097/j.pain.0000000000001265

50. Yang Y, Li H, Li T-T, et al. Delayed Activation of Spinal Microglia Contributes to the Maintenance of Bone Cancer Pain in Female Wistar Rats via P2X7 Receptor and IL-18. J Neurosci. 2015;35(20):7950-7963. doi:10.1523/JNEUROSCI.5250-14.2015

51. Moalem G, Xu K, Yu L. T lymphocytes play a role in neuropathic pain following peripheral nerve injury in rats. Neuroscience. 2004;129(3):767-777. doi:10.1016/j.neuroscience.2004.08.035

52. Nadeau S, Filali M, Zhang J, et al. Functional recovery after peripheral nerve injury is dependent on the pro-inflammatory cytokines IL-1β and TNF: implications for neuropathic pain. J Neurosci. 2011;31(35):12533-12542. doi:10.1523/JNEUROSCI.2840-11.2011

53. Barrette B, Hébert MA, Filali M, et al. Requirement of myeloid cells for axon regeneration. J Neurosci. 2008;28(38):9363-9376. doi:10.1523/JNEUROSCI.1447-08.2008

FIGURES

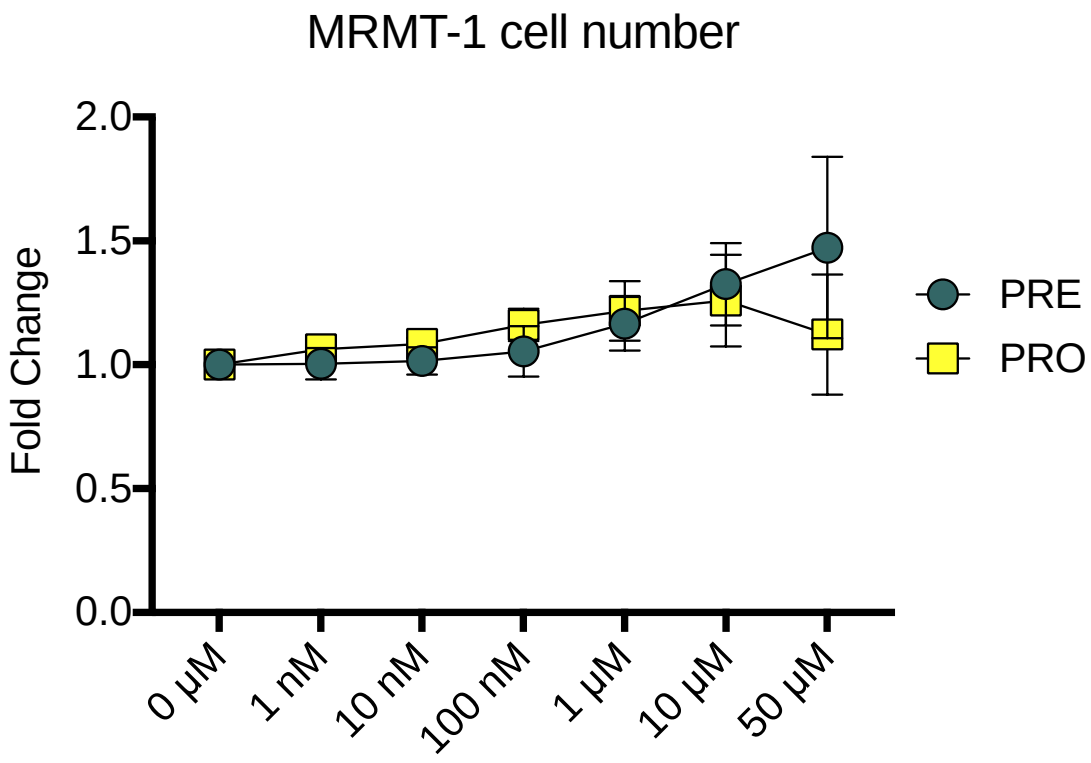

Figure 1.

MRMT-1 cell number is unaffected by treatment with pregabalin or progesterone.

Crystal violet stain for cell number showed no differences between vehicle treated MRMT-1 cells and PRE and PRO treated cells at doses ranging between 1 nM and 50 µM. This in vitro assay was to determine if the experimental drugs may affect tumour growth in our in vivo models of cancer pain. Each treatment dose is expressed as fold-change relative to the respective vehicle at that same dose, PRO was suspended in sesame oil, PRE in saline. Data represent the mean of n = 3 biological replicates ± SEM. Differences within treatment groups were compared to untreated control (0 µM) by one-way ANOVA with post hoc Dunnett's test.

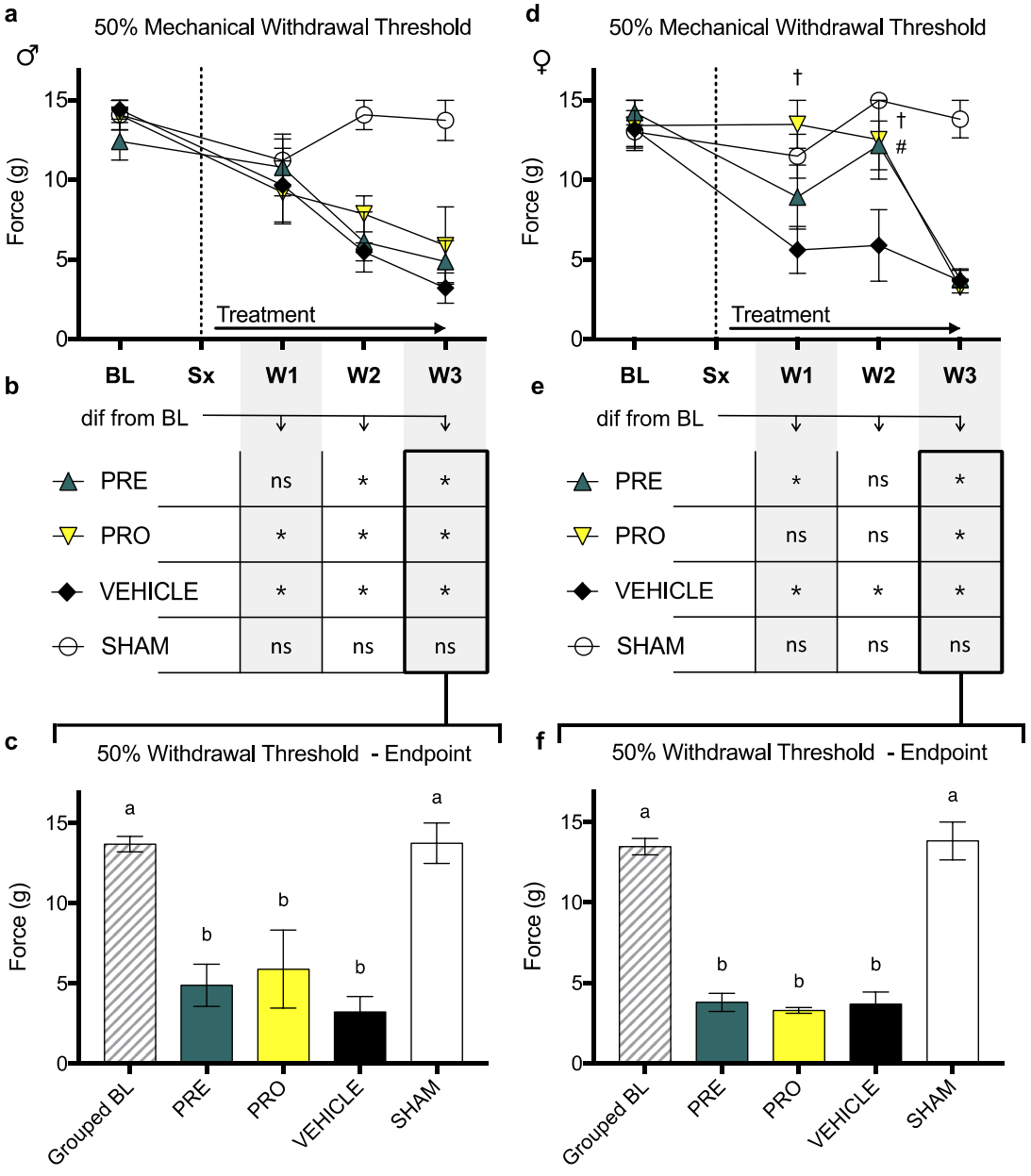
a
50% Mechanical Withdrawal Threshold
♂
Force (g)
Treatment
BL
Sx
W1
W2
W3
b
dif from BL
PRE
PRO
VEHICLE
SHAM
ns
*
c
50% Withdrawal Threshold - Endpoint
Grouped BL
d
50% Mechanical Withdrawal Threshold
♀
†
#
e
f

Figure 2.

Both pregabalin and progesterone-treated female rat models of cancer-induced bone pain show a delay until the onset of a reduced mechanical withdrawal threshold relative to vehicle-treated rats. Male rats show no differences between treatment groups.

a. There are no differences in 50% mechanical paw withdrawal threshold in the ipsilateral limb between PRO, PRE, and VEH treatment groups of male CIBP-model rats at any timepoint post-model induction as measured by testing with von Frey filaments. All male model groups show reduced thresholds relative to Sham-surgical control animals in weeks 2 and 3 (not marked on chart). **b.** Likewise, no treatment groups of male rats show a sustained delay past week 1 until withdrawal threshold is reduced relative to baseline measurements, and **c**. all treatment groups are not different from each other and all show significantly decreased paw withdrawal thresholds relative to baseline and to Sham control thresholds at endpoint. **d.** Female CIBP-model rats show evidence of a delay of onset of a reduced mechanical withdrawal threshold in both PRO and PRE treated groups relative to vehicle, where PRE-treated animals are significantly different from vehicle at week 2, and PRO-treated animals show higher thresholds on both weeks 1 and 2. No groups are different at week 3. **e.** Similarly, PRE-treated animals are not different from their respective baseline measurements at week 2, and PRO-treated animals are not different from baseline until week 3. Vehicle-treated animals are different from baseline on each week following tumour implantation, and sham animals do not differ from baseline at any timepoint. **f.** At endpoint there are no differences between treatment groups and all show significantly decreased paw withdrawal thresholds relative to baseline and to Sham control.

Data represent the mean ± SEM from male SD rats: PRE n = 6, PRO n = 5, Vehicle n = 5, SHAM n = 5; and female SD rats: PRE n = 6, PRO n = 4, Vehicle n = 6, SHAM n = 7. Only animals with verified tumour development were included in results shown. Differences between treatment groups over time (a., d.) are compared to vehicle control by RM two-way ANOVA with post hoc Dunnett's test (#$P < 0.05$, PRE vs. Vehicle), (†$P < 0.05$, PRO vs. Vehicle). Differences within treatment groups relative to baseline measurements (b., e.) are compared by RM two-way ANOVA with post hoc Dunnett's

test (*$P < 0.05$). Differences between treatment groups at endpoint (c., f.) are compared by one-way ANOVA with post hoc Tukey's test, different letters (a, b) represent differences between groups ($P < 0.05$).

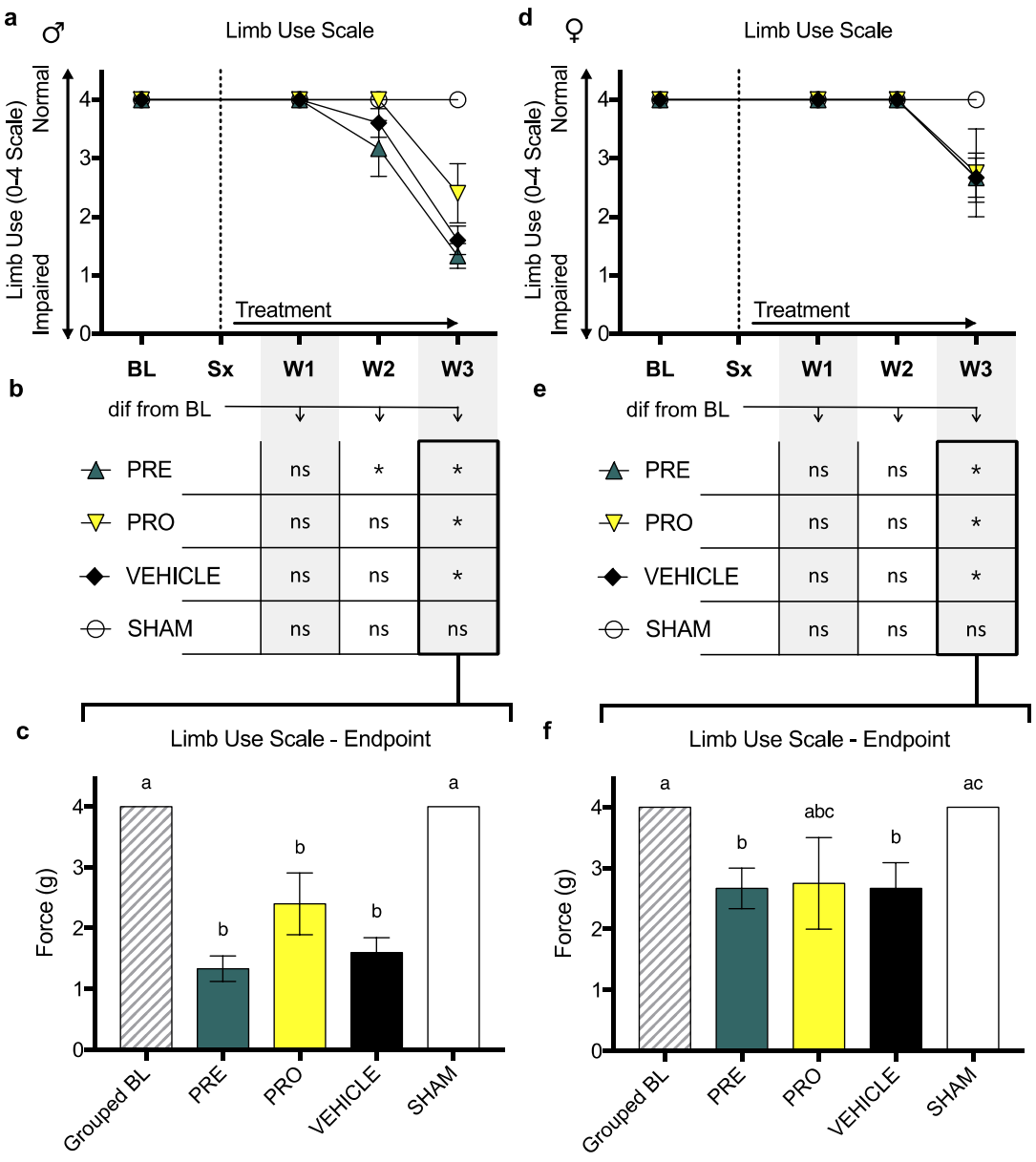

Figure 3.

No female or male rat models of cancer-induced bone pain show differences in limb use between treatment groups or vehicle-treatment as measured by observational scoring.

There are no differences in ipsilateral limb use scoring (0-4 scale) between PRO, PRE, and vehicle treatment groups of **a.** male and **d.** female CIBP-model rats at any timepoint

post-model induction as measured by observational scoring over a 5-minute period of free ambulation. All male and female groups show impaired limb use relative to Sham-surgical control animals by week 3 (not indicated on charts). Likewise, no treatment groups including vehicle of **b.** male and **e.** female rats show sustained maintenance of normal limb use past week 2 relative to baseline measurements. At week 3 endpoint all treatment groups of **c.** male rats are not different from each other and all show significantly decreased limb use scores relative to baseline and to Sham controls. At endpoint, **f.** female PRE and VEH-treated groups are significantly decreased from baseline and Sham, while PRO-treated rats show no differences from any groups.

Data represent the mean ± SEM from male SD rats: PRE n = 6, PRO n = 5, Vehicle n = 5, SHAM n = 5; and female SD rats: PRE n = 6, PRO n = 4, Vehicle n = 6, SHAM n = 7. Only animals with verified tumour development were included in results shown. Differences between treatment groups over time (a., d.) are compared to vehicle control by RM two-way ANOVA with post hoc Dunnett's test ($P < 0.05$). Differences within treatment groups relative to baseline measurements (b., e.) are compared by RM two-way ANOVA with post hoc Dunnett's test ($*P < 0.05$). Differences between treatment groups at endpoint (c., f.) are compared by Kruskal-Wallis test with post hoc Dunn's test, different letters (a, b, c) represent differences between groups ($P < 0.05$).

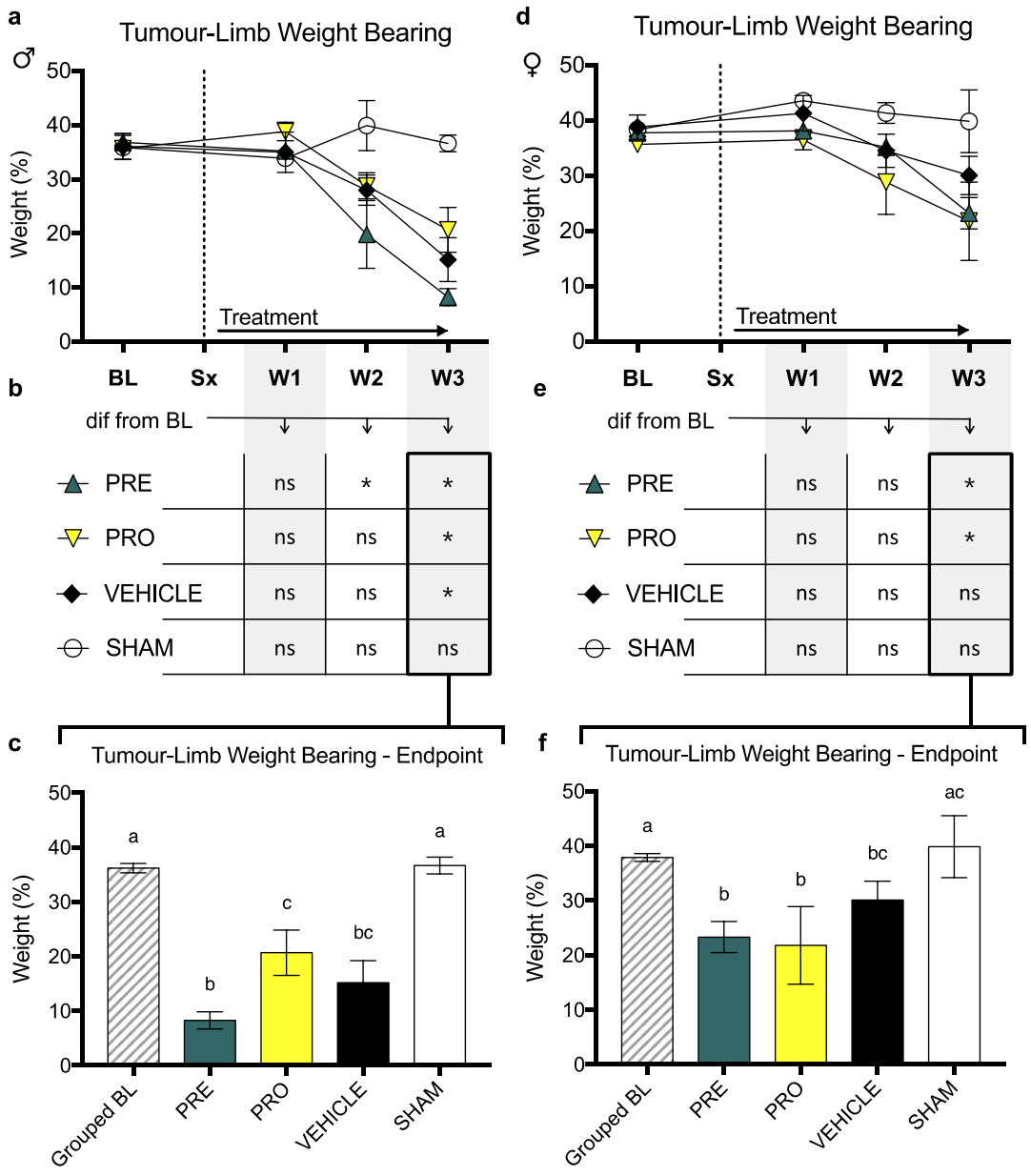

Figure 4.

No female or male rat models of cancer-induced bone pain show differences in ipsilateral limb weight bearing between treatment groups and vehicle-treatment.

There are no differences in ipsilateral limb weight bearing as a percentage of animal body weight as measured by dynamic weight bearing between PRO, PRE, and vehicle

treatment groups of **a.** male and **d.** female CIBP-model rats at any timepoint post-model induction. **b.** No treatment groups of male rats show sustained maintenance of normal weight bearing past week 2 relative to baseline measurements. **e.** PRE and PRO-treated female rats also show decreased weight bearing at week 3, however vehicle-treated rats are not different from baseline measurements.

At week 3 endpoint all treatment groups of **c.** male rats show significantly decreased ipsilateral limb weight bearing relative to baseline and to Sham controls, and PRE-treated rats are significantly lower than PRO-treated rats. At endpoint, **f.** female PRE and PRO-treated groups are significantly decreased from baseline and Sham, however vehicle-treated rats are significantly decreased from baseline measurements only.

Data represent the mean ± SEM from male SD rats: PRE n = 6, PRO n = 5, Vehicle n = 5, SHAM n = 5; and female SD rats: PRE n = 6, PRO n = 4, Vehicle n = 6, SHAM n = 7. Only animals with verified tumour development were included in results shown. Differences between treatment groups over time (a., d.) are compared to vehicle control by RM two-way ANOVA with post hoc Dunnett's test (#$P < 0.05$, PRE vs. Vehicle), (†$P < 0.05$, PRO vs. Vehicle). Differences within treatment groups relative to baseline measurements (b., e.) are compared by RM two-way ANOVA with post hoc Dunnett's test (*$P < 0.05$). Differences between treatment groups at endpoint (c., f.) are compared by one-way ANOVA with post hoc Tukey's test, different letters (a, b, c) represent differences between groups ($P < 0.05$).

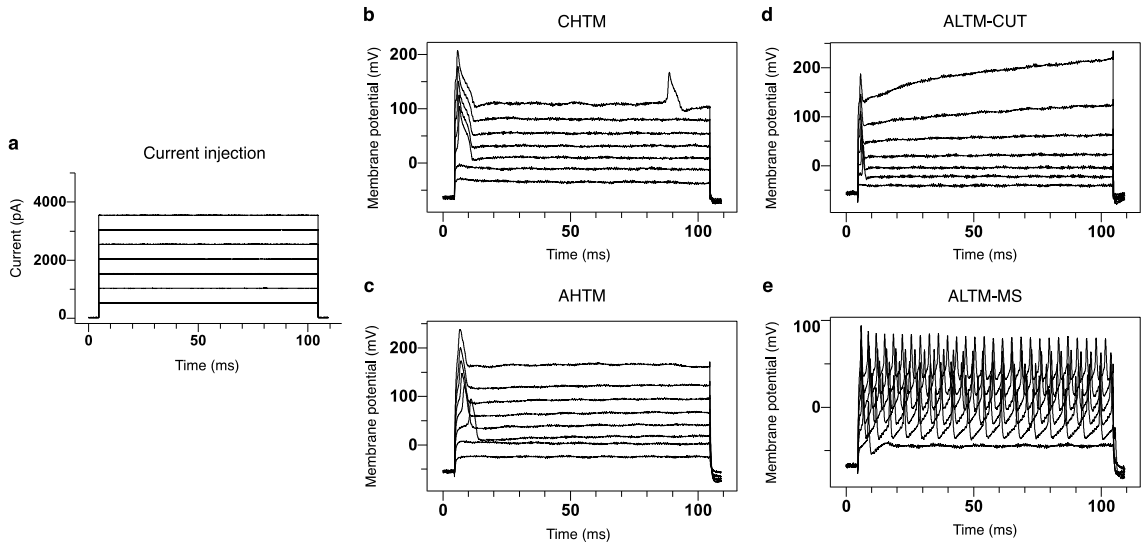

Figure 5.

Soma excitability thresholds of sensory DRG neurons were determined by evoked action potentials in the soma of sensory DRG neurons induced using stimulation by direct injection of depolarizing current. Representative recordings show the intracellular current injection pulses with threshold and repetitive charges of evoked action potentials in different types of mechanoreceptor neurons in CIBP sham male rats.

To quantify soma excitability, the threshold of depolarizing current pulses injected into the soma was determined. This was achieved by applying current injections of 100 ms each (**a.**), delivered with an amplitude of 500 to 4000 pA with increments of 500 pA [X-axis: Time (ms); Y-axis: current (pA)]. Representative raw recordings show the threshold and repetitive charges of APs evoked by intracellular current injection in the mechanoreceptor neurons evaluated in this study including (**b.**) C-type high-threshold mechanosensitive fibres (CHTM), (**c.**) Aβ-type high-threshold mechanosensitive fibres (AHTM), (**d.**) Aβ-low-threshold mechanosensitive fibres - cutaneous (ALTM- CUT), and (**e.**) Aβ-low-threshold mechanosensitive fibres – muscle spindle (ALTM-MS). Discharge was evoked by injecting a series of depolarizing current pulses into DRG soma through

the recording electrode [X-axis: Time (ms); Y-axis: Voltage (mV)]. All representative images here are from male CIBP-model sham negative control rats.

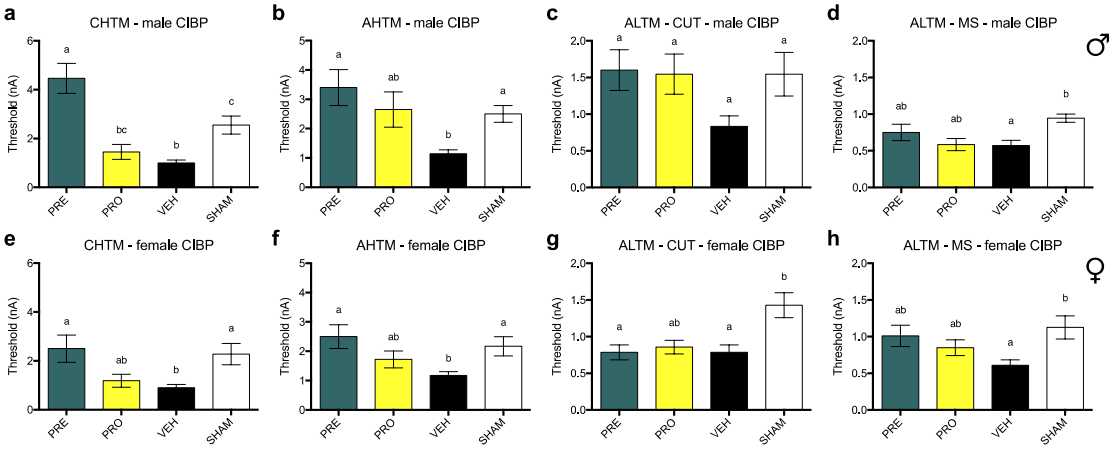

Figure 6.

All types of sensory fibres tested demonstrate reduced excitability thresholds in vehicle-treated male and female cancer models. In high-threshold mechanosensitive fibres, PRE-treated animals have excitability thresholds equivalent to sham controls. Low-threshold mechanosensitive fibres are unaffected by treatment in both sexes.

Current activation thresholds are recorded at endpoint (post-week 3) in response to intracellular current injection at the DRG soma. Activation thresholds of CHTM neurons in PRE-treated male (**a.**) and female (**e.**) rats were increased relative to vehicle. PRO-treated rats are not different from either vehicle or sham. PRE-treatment also significantly increased activation thresholds of AHTM relative to vehicle in both male (**b.**) and female (**f.**) rats. PRO-treated rats are not different from vehicle or sham. There are no significant differences in activation threshold between any groups of ALTM-CUT neurons in males (**c.**), and no effects of treatment with PRE or PRO on ALTM-CUT thresholds in female rats (**g**.). In both males (**d.**) and females (**h.**), the activation thresholds of ALTM-MS neurons in PRE- and PRO-treated rats were not significantly different from either vehicle-treated or sham groups.

Data represent the mean ± SEM from male (upper panel) SD rat DRG neurons: (CHTM: PRE n = 13, PRO n = 11, Vehicle n = 15, Sham n = 10); (AHTM: PRE n = 10, PRO n = 10, Vehicle n = 14, Sham n = 11); (ALTM-CUT: PRE n = 15, PRO n = 11, Vehicle: n =

9, Sham n = 11); (ALTM-MS: PRE n = 10, PRO n = 6, Vehicle: n = 7, Sham n = 9); and female (lower panel) SD rat DRG neurons: (CHTM: PRE n = 8, PRO n = 8, Vehicle n = 15, Sham n = 9); (AHTM: PRE n = 9, PRO n = 9, Vehicle n = 14, Sham n = 12); (ALTM-CUT: PRE n = 10, PRO n = 10, Vehicle: n = 9, Sham n = 9); (ALTM-MS: PRE n = 10, PRO n = 10, Vehicle: n = 9, Sham n = 8). Differences between treatment groups are compared by Kruskal-Wallis test with post hoc Dunn's multiple comparison test, different letters (a, b, c) represent differences between groups ($P < 0.05$). Abbreviations are as indicated in Fig. 5.

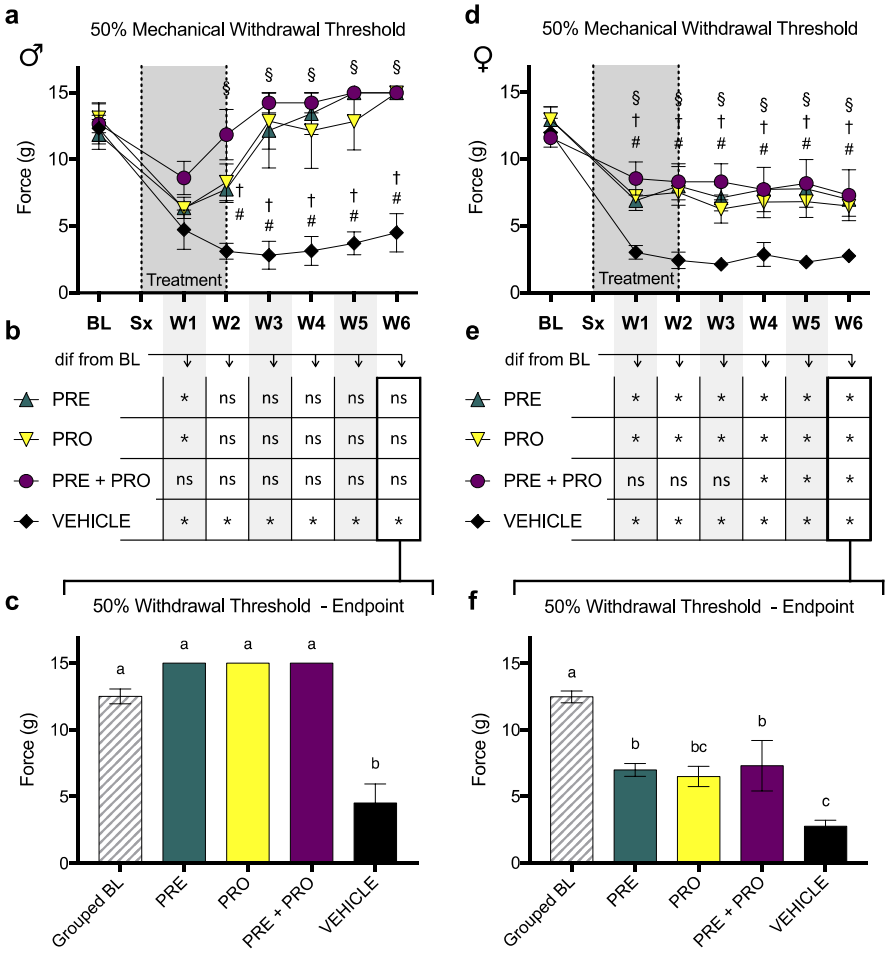

Figure 7.

Male rat models of sciatic-cuff induced neuropathic pain treated with pregabalin, progesterone, or combination show large and sustained differences from vehicle-treated rats and recoveries to baseline ipsilateral paw withdrawal thresholds. Pregabalin, progesterone, and combination treated female rat models also show differences relative to vehicle-treated rats, but do not show recoveries to baseline behavior.

Male and female models of sciatic-cuff induced NEP show increased 50 % mechanical paw withdrawal thresholds in response to treatment with pregabalin, progesterone, and combination. All treatment groups of male NEP-model rats **a.** show an initial decrease in 50 % mechanical paw withdrawal threshold in the ipsilateral limb after model-induction,

followed by a robust recovery where all treatment groups are different from vehicle by week 2. PRO and PRE treatment groups show sustained recoveries to withdrawal thresholds no different from their respective baseline measurements **b.** by week 2. PRE+PRO combination-treated animals did not decline at any point to levels different from baseline. In contrast, withdrawal thresholds of vehicle-treated animals remain significantly decreased from baseline at every post-surgical timepoint. At endpoint **c.** paw withdrawal thresholds of all male treatment groups are not different from grouped baseline and are significantly increased relative to vehicle. All groups of female NEP-model rats **d.** also show an initial decrease in withdrawal thresholds, however all treatment groups remain higher than vehicle at all timepoints post-model induction. Unlike males, female treatment groups do not recover to baseline levels **e.** at any point following treatment. PRO and PRE treatment groups remain lower than their respective baseline withdrawal thresholds at all post-surgical timepoints, and PRE+PRO combination treatment animals initially are no different from baseline, but become different at week 4 and later. **f.** At endpoint there are no differences between treatment groups and all show significantly decreased withdrawal thresholds relative to baseline. PRE and PRE+PRO combination treated animals have higher withdrawal thresholds than vehicle, while PRO and vehicle are not different.

Data represent the mean ± SEM from n = 4 male SD rats / group, and female SD rats: PRE n = 6, PRO n = 6, PRE+PRO n = 4, VEH n = 4 rats. Differences between treatment groups over time (a., d.) are compared to VEH control by RM two-way ANOVA with post hoc Dunnett's test (#$P < 0.05$, PRE vs. VEH), (†$P < 0.05$, PRO vs. VEH), (§$P < 0.05$, PRE+PRO vs. VEH). Differences within treatment groups relative to baseline measurements (b., e.) are compared by RM two-way ANOVA with post hoc Dunnett's test (*$P < 0.05$). Differences between treatment groups at endpoint (c., f.) are compared by one-way ANOVA with post hoc Tukey's test, different letters (a, b, c) represent differences between groups ($P < 0.05$).

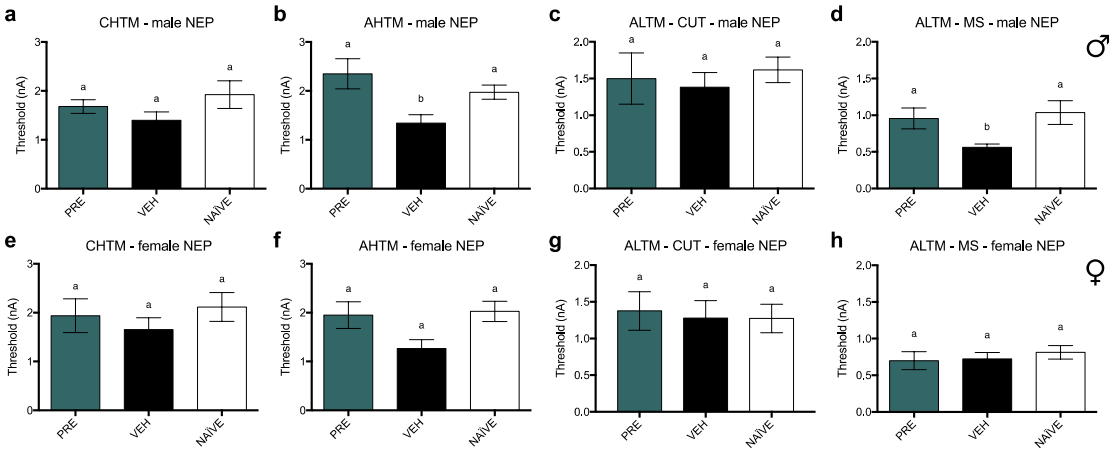

Figure 8.

PRE-treated male NEP model SD rats show current excitability thresholds in AHTM and ALTM-MS fibres that are significantly higher than vehicle-treated controls and equivalent to naïve rats. There are no differences in excitability threshold in any other fibres in males and females.

Current activation thresholds are recorded at endpoint (post-week 6) in response to intracellular current injection at the DRG soma. There are no differences between any groups in the activation thresholds of CHTM neurons in **a.** male and **e.** female NEP model SD rats. Activation thresholds of AHTM neurons in in PRE-treated male NEP rats **b.** were significantly higher that vehicle-treated neurons which were significantly decreased relative to naïve. There were no differences in activation threshold between groups in AHTM neurons of female NEP rats. There are no significant differences in activation threshold between any groups of ALTM-CUT neurons in both **c.** males and **g.** females. Activation thresholds of ALTM-MS neurons in PRE-treated **d.** male and **h.** female NEP rats are significantly increased relative to vehicle in both groups.

Data represent the mean ± SEM from male (upper panel) SD rat DRG neurons: (CHTM: PRE n = 11, Vehicle: n = 15, Naïve n = 13); (AHTM: PRE n = 10, Vehicle: n = 16, Naïve n = 20); : (ALTM-CUT: PRE n = 10, Vehicle: n = 17, Naïve n = 17); (ALTM-MS: PRE n = 11, Vehicle: n = 16, Naïve n = 14); and female (lower panel) SD rat DRG neurons:

(CHTM: PRE n = 8, Vehicle: n = 13, Naïve n = 13); (AHTM: PRE n = 10, Vehicle: n = 15, Naïve n = 19); (ALTM-CUT: PRE n = 8, Vehicle: n = 9, Naïve n = 11); (ALTM-MS: PRE n = 5, Vehicle: n = 9, Naïve n = 8). Differences between treatment groups are compared by Kruskal-Wallis test with post hoc Dunn's multiple comparison test, different letters (a, b) represent differences between groups ($P < 0.05$). Abbreviations are as indicated in Fig. 5.

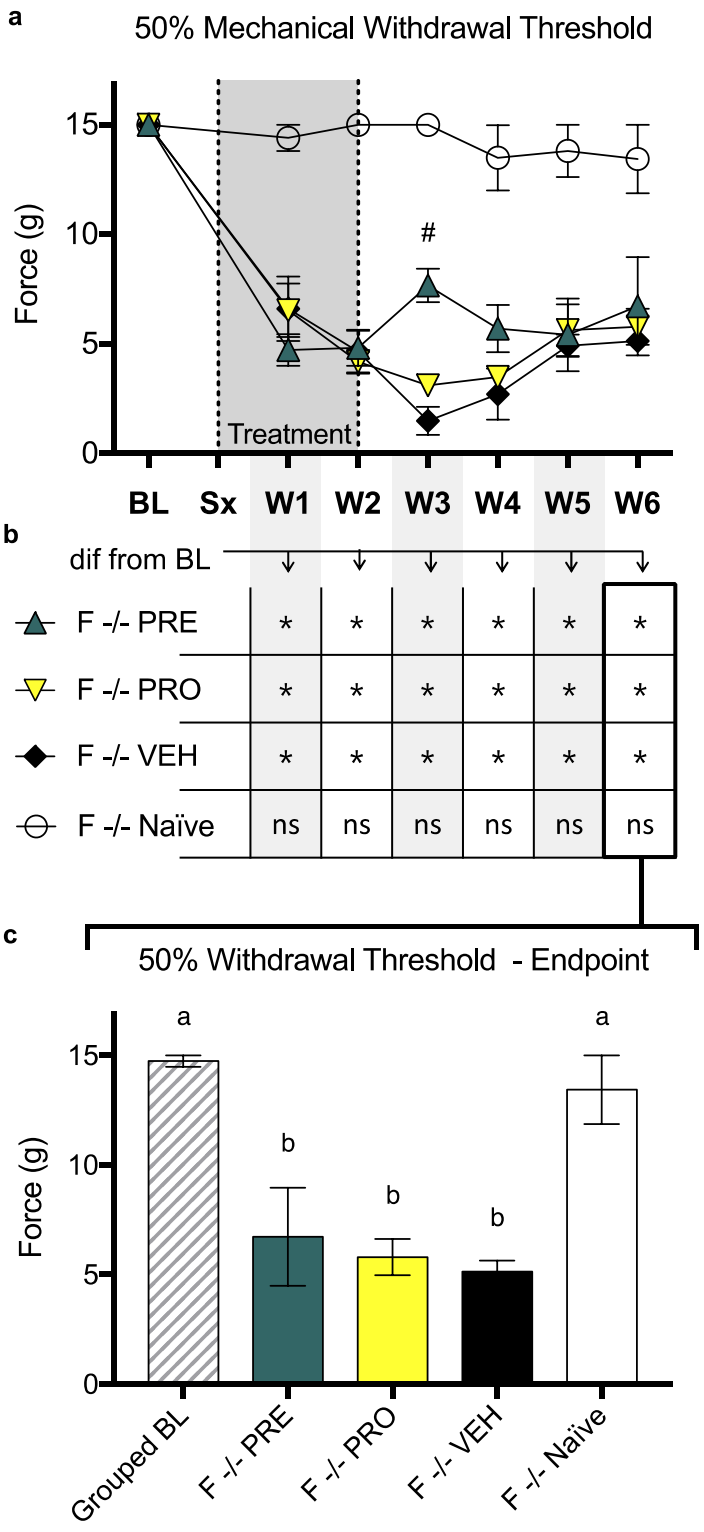
a
50% Mechanical Withdrawal Threshold
Force (g)
15
10
5
0
#
Treatment
BL
Sx
W1
W2
W3
W4
W5
W6
b
dif from BL
F -/- PRE
F -/- PRO
F -/- VEH
F -/- Naïve
*
ns
c
50% Withdrawal Threshold - Endpoint
a
b
b
b
a
Grouped BL
F -/- PRE
F -/- PRO
F -/- VEH
F -/- Naïve

Figure 9.

Female immunocompromised rat models of sciatic-cuff induced neuropathic pain treated with pregabalin and progesterone do not show sustained differences from vehicle-treated rats or recoveries to baseline ipsilateral paw withdrawal thresholds.

a. There are no differences in 50% mechanical paw withdrawal threshold in the ipsilateral limb between PRO, PRE, and VEH treatment groups of female RNU -/- sciatic-cuff induced neuropathic pain model rats at any timepoint post-model induction excluding week 3 as measured by testing with von Frey filaments. At week 3 PRE-treated rats show a significantly higher threshold than vehicle-treated rats, however this difference is not sustained in later weeks.

All model groups show reduced thresholds relative to Naïve control animals in all post-surgical weeks (not marked on chart). **b.** In addition, all treatment groups including vehicle show significantly reduced withdrawal thresholds relative to baseline measurements at all post-surgical time points. Naïve control rats are not different from baseline at any week. **c.** At endpoint there are no differences between treatment groups and all show significantly decreased paw withdrawal thresholds relative to baseline and to Naïve control.

Data represent the mean ± SEM from female RNU -/- rats: PRE n = 5, PRO n = 5, VEH n = 4, Naïve n = 3 rats. Differences between treatment groups over time (a.) are compared to VEH control by RM two-way ANOVA with post hoc Dunnett's test (#$P < 0.05$, PRE vs. VEH). Differences within treatment groups relative to baseline measurements (b.) are compared by RM two-way ANOVA with post hoc Dunnett's test (*$P < 0.05$). Differences between treatment groups at endpoint (c.) are compared by one-way ANOVA with post hoc Tukey's test, different letters (a, b) represent differences between groups ($P < 0.05$).

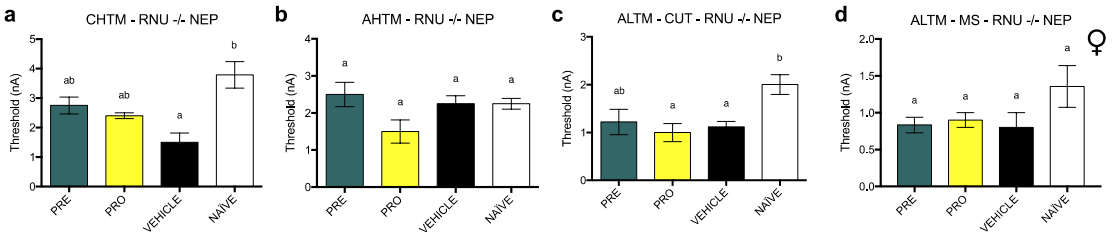

Figure 10.

Immunocompromised female rat models of NEP show decreases in the excitability thresholds of both CHTM and ALTM-CUT fibres. PRE-treatment prevents this decrease relative to naïve animals, but these thresholds are not significantly different from vehicle.

Current activation thresholds are recorded in athymic female RNU -/- models of NEP at endpoint (post-week 6) in response to intracellular current injection at the DRG soma. Activation thresholds of CHTM neurons **a.** are decreased in the vehicle-treated group relative to naïve, however there are no significant differences in the thresholds of CHTM neurons between both PRE- and PRO-treated groups and either vehicle or naïve rats. There are no significant differences in activation threshold between any groups of **b.** AHTM neurons. Activation thresholds of ALTM-CUT neurons **c.** were significantly decreased from naïve in both the vehicle-treated and PRO-treated groups. PRE-treated rats showed no differences in ALTM-CUT threshold from both vehicle-treated and naïve rats. Activation thresholds of d. ALTM-MS neurons not different between groups.

Data represent the mean ± SEM from female RNU -/- rat DRG neurons: (CHTM: PRE n = 8, PRO n = 5, Vehicle n = 6, Naïve n = 7); (AHTM: PRE n = 7, PRO n = 6, Vehicle n = 6, Naïve n = 4); (ALTM-CUT: PRE n = 9, PRO n = 7, Vehicle: n = 13, Naïve n=15); (ALTM-MS: PRE n = 6, PRO n = 5, Vehicle: n = 5, Naïve n = 7). Differences between treatment groups are compared by Kruskal-Wallis test with post hoc Dunn's multiple comparison test, different letters (a, b) represent differences between groups ($P < 0.05$). Abbreviations are as indicated in Fig. 5.

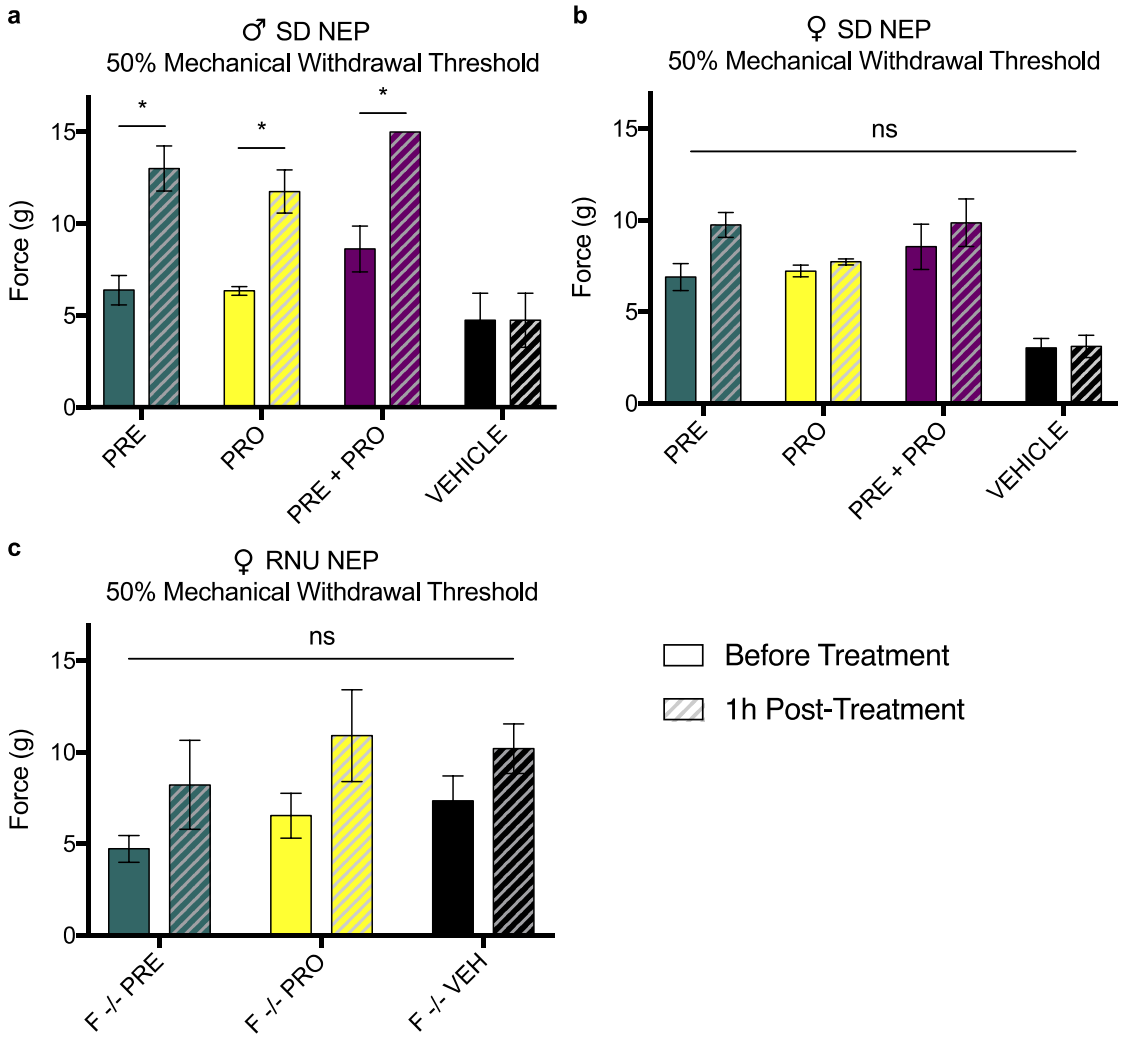

Figure 11.

Male rat models of sciatic-cuff induced neuropathic pain show an increase in ipsilateral paw withdrawal thresholds 1-hour post-treatment with pregabalin, progesterone, or combination at post-surgical week 1. This acute response to treatment is not seen in female immunocompetent or immunocompromised neuropathic pain model animals.

All NEP model animals were measured at week 1 pre- and 1-hour post-treatments. **a.** Male SD rat models of sciatic-cuff induced neuropathic pain show an acute response to treatment with pregabalin, progesterone, and combination as an increase in 50%

mechanical paw withdrawal threshold as measured by testing with von Frey filaments. Withdrawal thresholds of vehicle-treated animals do not change following treatment. No acute responses to treatment are seen in any treatment groups of **b.** female immunocompetent SD rats or **c.** immunocompromised RNU -/- neuropathic pain model animals.

Data represent the mean ± SEM from n = 4 male SD rats / group; female SD rats: PRE n = 6, PRO n = 6, PRE+PRO n = 4, VEH n = 4 rats; and female RNU -/- rats: PRE n = 5, PRO n = 5, VEH n = 4, Naïve n = 3 rats. Comparisons within treatment groups are by multiple t-tests (*$P < 0.05$).

CHAPTER 4: RNA-sequencing of lumbar dorsal root ganglia in a rat model of cancer-induced bone pain

Robert G Ungard, Ayesha Shahid, Jennifer Fazzari, Gurmit Singh. Manuscript prepared for submission to: Molecular Pain.

Preface

In this chapter, an author-generated version of the manuscript titled "RNA-sequencing of lumbar dorsal root ganglia in a rat model of cancer-induced bone pain", prepared for submission to Molecular Pain in 2020, is presented. As this is an unpublished manuscript, no copyright license documentation is required.

For this manuscript, I cultured and isolated cells, performed in vitro testing including RNA-isolation, and performed surgery to induce the in vivo CIBP models, performed all behavioural testing, analyzed data including all RNA-Sequencing data, generated plots and drafted the manuscript. RNA samples were measured and sequenced by the Farncombe Metagenomics Facility at McMaster University. Ayesha Shahid performed H&E histochemistry. Jennifer Fazzari undertook research and training to develop this animal model of CIBP and performed surgeries. Gurmit Singh supervised the overall project, edited the manuscript, and provided funding for the study. All authors have read and approved the final manuscript.

Context and Background Information

The work included in this dissertation has regularly referenced structural and molecular changes that occur in the peripheral and central nervous systems in conditions of ongoing pain. The studies supporting this are robust, and some have produced research and therapeutic innovations in pain medicine (Schwei et al. 1999; Bloom et al. 2011; Zhu et al. 2018). In the search for new mechanisms and therapeutic targets in the nervous system to treat painful conditions, investigators are increasingly using RNA-Sequencing (RNA-Seq) to measure gene expression in dorsal root ganglia (DRGs) and the lumbar dorsal horn of the spinal cord (Perkins et al. 2014; Zhang et al. 2015; Hu et al. 2016; Wu et al. 2016; Lopes et al. 2017; Ray et al. 2018; Stephens et al. 2018; Stephens et al. 2019). The studies included in this chapter are the first to evaluate DRG gene expression by RNA-Seq in an animal model of CIBP. We compared gene expression in ipsilateral DRGs from our validated rat model of MRMT-1 CIBP to contralateral DRGs and to sham negative

controls rats and analysed for enriched biological terms and pathways associated with patterns of differential expression.

RNA-sequencing of lumbar dorsal root ganglia in a rat model of cancer-induced bone pain

Robert G Ungard1,2, Ayesha Shahid1,2, Jennifer Fazzari1,2, Gurmit Singh1,2

1 Michael G. DeGroote Institute for Pain Research and Care, Medicine, McMaster University, 1280 Main St. West, Hamilton, ON L8S 4M1, Canada

2 Department of Pathology and Molecular Medicine, McMaster University, 1280 Main St. West, Hamilton, ON L8N 3Z5, Canada

Corresponding Author: Dr. Gurmit Singh

Department of Pathology & Molecular Medicine, McMaster University, 1280 Main Street West, Hamilton, ON L8N 3Z5, Canada

Tel.: +1 905 525 9140 x28144

E-mail address: singhg@mcmaster.ca

Number of tables: 0

Number of figures: 8

Number of words: 8547

Number of supplementary figures: 1

Number of supplementary tables: 2

ABSTRACT

Background: Cancer-induced bone pain (CIBP) is complex and often severe, involving multiple mechanisms contributing to the induction and maintenance of the pain state, including pathological reorganization in the peripheral nervous system. Current interventions for CIBP control are often inadequate and are limited by side-effects.

Aims: To investigate the pathophysiology of CIBP we used a rat model of MRMT-1 breast cancer bone metastasis to bone to investigate differentially expressed genes (DEGs) at the dorsal root ganglia (DRG), including different ontological and pathway enrichment.

Methods: Three weeks after implantation of cancer cells in the femur of female rats or sham surgery, L3-6 DRGs were collected and gene expression was measured by mRNA selective RNA-Seq. Differential expression was compared between CIBP and sham control groups and between ipsilateral and contralateral DRGs of CIBP rats. Enrichment analysis using DAVID was performed to identify enriched Kyoto Encyclopedia of Genes and Genomes (KEGG) pathways and biological process gene ontologies (GO:BP) corresponding to DEGs.

Results: We identified differential expression of 370 transcripts between CIBP and Sham groups and 178 transcripts between CIBP ipsilateral and contralateral comparisons. These genes corresponded to positive enrichment in terms and pathways associated with neuronal signaling and regulation, and reductions in pathways associated with immunity in CIBP models. Several target genes are consistent with other investigations of gene expression in pain, and others have not previously been identified or investigated in pain studies.

Conclusions: These results are the first RNA-Seq data of DRGs from a model of CIBP. Identifying differential gene expression in the sensory nervous system of animal models of CIBP provides mechanistic insight into changes in the peripheral nervous system in

response to pain, and will provide functional targets for further investigation and translational relevance.

INTRODUCTION

Chronic pain states including cancer pain initiate gene expression changes in central and peripheral sensory circuits that can be adaptive or maladaptive and potentially targetable for treatment or indicative of mechanistic insight. Gene expression in dorsal root ganglia (DRGs) and the lumbar dorsal horn of the spinal cord from animal models of injury, neuropathic, and inflammatory pain have been evaluated by numerous microarray-studies [22] and by an increasing number of RNA-Sequencing (RNA-Seq) projects to establish transcriptomic changes in models or to pursue particular targets [24,31,32,39,40,48,50], including by single-cell sequencing [17].

The use of RNA-Seq to investigate neurobiological outcomes in these models has produced a great deal of data and a number of promising gene and pathway targets, as well as scientific tools for model validation and improvement of translational validity [32]. In addition, whole-tissue and single-cell transcriptome sequencing has been extensively utilized to investigate cancer and its effects on the body, however, the global gene expression profile of DRGs or the sensory neurons innervating a painful tumour environment have not yet been investigated.

We have investigated the mRNA expression profile of whole lumbar DRGs containing the cell bodies of sensory afferent neurons that innervate the limb of a rat model of intrafemoral breast cancer-induced bone pain (CIBP). In addition to multiple subpopulations of specialized sensory neurons, DRG tissue includes other cell types that cross-talk with neurons and are closely associated with sensory signalling, including resident immune cells, and satellite glial cells which envelope the sensory neuron and have been demonstrated to contribute to nociceptive signaling [46]. L3-6 DRGs were isolated from female rat CIBP models and sham-surgery negative controls, and

differentially expressed genes (DEGs) between CIBP and sham models and between ipsilateral and contralateral DRGs were determined by mRNA-selective RNA-Seq.

Tumours in the bone compromise patient functional status, quality of life, and survival, and can produce debilitating and intractable pain, which is frequently reported by late-stage patients [36]. Current therapies for CIBP involve many approaches, described by the WHO cancer pain ladder as progression from non-opioid analgesics to strong opioids as is necessary to treat progressive pain [47]. Including targeting the tumour mass itself, adjuvant interventions intended for pain treatment are employed throughout including radiotherapy, bisphosphonates, biologics, and pharmacotherapies that are regularly employed for pain including anticonvulsants and antidepressants. These therapies induce a wide array of dose-limiting and undesirable side-effects that cause both patients and caregivers to limit treatment resulting in unmanaged cancer pain [29].

We chose to utilize a rat model of breast cancer bone metastasis as bone the most common site of distant breast cancer metastasis, and breast cancers makes up a plurality of cases of metastatic tumours in bone [8]. As such, we utilized only female rats in our investigation, although the MRMT-1 model of breast CIBP has been induced in male rats [12], and sex differences in DRG gene expression have been found in other animal models of painful nerve injury [24,40].

Studies of DRG and spinal cord gene expression in animal models of pain and nerve injury have identified important targets, some of which have shown functional relevance in follow-up study [23,33,50]. Our results show similarities and differences in particular transcripts and wider patterns of expression compared to published DRG gene expression profiles from animal studies. To our knowledge, this is the first investigation to utilize RNA-Seq on DRGs from an animal model of cancer pain. These results can generate new therapeutic and research targets and can be compared to expression profiles of healthy tissue and that of other pain states to more comprehensively distinguish the unique profile of CIBP.

MATERIALS AND METHODS

Cell Culture

The mammary rat metastasis tumour (MRMT-1) rat mammary carcinoma cell line (provided by Dr. Philippe Sarret of the Université de Sherbrooke, Sherbrooke, QC) was used in CIBP rat models. Cells were maintained in a humidified incubator at 37 °C with 5 % CO_2 in RPMI 1640 (Thermo Fisher Scientific, Inc., Waltham, MA) growth medium supplemented with 10% fetal bovine serum (FBS) and antibiotics (100 U ml-1 penicillin sodium and 1% antibiotic/antimycotic (Thermo Fisher Scientific). MRMT-1 cells were tested for mycoplasma contamination prior to experimental use. Cell harvesting for in vivo implantation was performed on sub-confluent cultures; adherent cells were suspended and kept lightly agitated in sterile Hank's Balanced Salt Solution (HBSS) on ice.

Cancer-Induced Bone Pain Model

All procedures were conducted according to the guidelines of the Committee for Research and Ethical Issues of the International Association for the Study of Pain [53] and guidelines established by the Canadian Council on Animal Care with ethical approval from the McMaster University Animal Research Ethics Board. All experimental animals were housed in pairs with access to food and water ad libitum in a temperature-controlled room under a 12-hour light/dark cycle. Female Sprague-Dawley (SD) rats (Charles River Inc. St. Constant, QC) weighing 170-200 g were utilized for all models. Rats were randomly assigned to cancer or sham surgery groups.

The details of cancer cell implantation to the distal femur for this model have been described in detail in previously published methods by the Sarret group [10,42] and ours [45]. Briefly, rats were anaesthetized and skin and muscle incised to expose the medial epicondyle of the right femur. A small cavity was drilled between the medial epicondyle and the adductor tubercle with a 0.8 A stereotaxic drill equipped with a 1.75 mm burr.

$3.0\times10_4$ MRMT-1 cells resuspended in 20 μL HBSS were implanted in the distal femur of each cancer pain model rat. Cells for sham surgical controls were suspended at the same concentration and inactivated by three heat/freeze cycles prior to implantation. Live MRMT-1 or heat/freeze-inactivated MRMT-1 (sham) cell suspension were dispensed into the canal. The cavity was then sealed with dental amalgam, and muscle, fascia, and skin were sutured.

Behavioural Analyses

Rats were exposed to handling and behavioral testing equipment for a 2-week acclimation period and assigned individual identification prior to model induction. All behavioral testing was performed by the same operator who was blinded to group assignment throughout the duration of the study. Behavioral testing was performed prior to model induction to obtain baseline data, and weekly, beginning on day 7 post-induction continuing until day 21. Dynamic Weight Bearing (DWB) was performed only on day 21. All in-vivo data represent the mean ± SEM from n = 6 female SD rats / group. Differences between treatment groups over time are compared by multiple t-tests, differences between groups at a single timepoint are compared by unpaired t-test (*$P < 0.05$).

Limb Use Scale

The open field observational limb use scale is an operator-derived numerical representation of the use of the animal's ipsilateral limb, scored over a 5-minute period of free ambulation. (0: no use, 1: severe limp, 2: moderate limp, 3: slight limp, 4: normal use). This scale has been validated in mouse [27,43] and rat models of CIBP [45].

Von Frey Mechanical Withdrawal

To quantify mechanical sensitivity, brisk foot withdrawal in response to normally innocuous mechanical stimuli was measured. Von Frey filaments (Stoelting Co., Wood

Dale, IL) were applied to the plantar surface of the ipsilateral hind paw to determine mechanical withdrawal thresholds using the up-down method of Dixon [9] as applied to rodents by Chaplan et al [6]. Our methodology has been previously described in detail [45]. A reduction in 50 % mechanical withdrawal threshold by the tumour-bearing limb was indicative of allodynia.

Dynamic Weight Bearing

Weight, area, and time distribution between all points of pressure of freely moving animals were recorded with the Dynamic Weight Bearing test 2.0 (DWB) (BioSeb, Vitrolles, France). Each animal was recorded in the DWB apparatus for 5 minutes/test and recordings were manually validated with DWB software version 2.0.59 (BioSeb). Results were exported as mean weight and time for each point of pressure across the validated experiment time. DWB has been validated as a useful test for rat and mouse models of CIBP [42,44]. Lesser weight borne by the tumor-afflicted limb relative to bodyweight of the animal was accepted as evidence of an inability or aversion to utilize that limb, providing indirect evidence of nociception.

Tissue Collection

Following data collection on day 21, animals were anaesthetized and sacrificed by decapitation. Ipsilateral hindlimbs were dissected and fixed in formalin for 48 hours. X-Ray scans of all dissected limbs were taken with a Faxitron X-ray system MX-20 (Faxitron X-ray Co., Wheeling, IL) on Kodak MIN-R 2000 Mammography Film (Eastman Kodak, Rochester, NY, USA). Samples were then decalcified in an agitated 10 % EDTA, 4 % Formalin buffered solution for 1-2 weeks, and embedded in paraffin blocks for sectioning. Following sacrifice, ipsilateral and contralateral lumbar L3, L4, L5, and L6 DRGs were immediately harvested by a modification of published methods [38], and placed into RNAlater RNA Stabilization Reagent (Ambion, Waltham, MA, USA), and stored at 4 °C overnight, and then -80 °C until use.

RNA Isolation

L3-6 DRGs were pooled for each animal (n = 6 rats /group, ipsilateral and contralateral DRGs pooled independently, therefore n = 24 samples total). DRGs were manually homogenized in lysis buffer with a scalpel on an RNAse-free surface on ice, and total RNA was isolated and DNase-treated using NucleoSpin RNA XS (Macherey-Nagel, Düren, Germany). RNA purity was measured by spectrophotometric analysis.

RNA Sequencing

RNA samples were sequenced at the Farncombe Metagenomics Facility of McMaster University. RNA quality was assessed using the RNA 6000 Nano kit on a 2100 Bioanalyzer (Agilent Technologies, Santa Clara, CA). RNA libraries were prepared using the NEBNext Ultra Directional RNA Library Prep Kit for Illumina and poly-A mRNA was enriched using the NEBNext Poly(A) mRNA Magnetic Isolation Module (New England Biolabs, Ipswich, MA). Depth of sequencing was estimated at 5X by the Lander-Waterman equation (C = LN/G), where L= paired 50 bp, N = 150 million reads / lane, and G = 3042 Mbp. Libraries were sequenced on two lanes of the Illumina HiSeq 1500 platform using the HiSeq Rapid V2 chemistry with onboard cluster generation and 50 bp paired-end reads (Illumina, San Diego, CA). To mitigate lane effects, each biological replicate was split between two lanes.

RNA-Seq Data Analysis

RNA-seq data FASTQ files were accessed at Illumina Basespace (https://basespace.illumina.com) and uploaded to the Galaxy web platform, and the public server at https://usegalaxy.org was used for all analyses [1]. Sequencing quality of the FASTQ files was evaluated using the FastQC tool (Galaxy Version 0.72) [3] and MultiQC (Galaxy Version 1.7) [11] was used to aggregate and visualize quality reports. Overrepresented and low quality read sequences including remaining Illumina adapter sequences were removed with Trimmomatic (Galaxy Version 0.38.0) [5], and re-assessed

for read quality after trimming with FastQC and MultiQC. Trimmed reads were mapped to the *Rattus norvegicus* reference genome version Rnor 6.0, from the NCBI RefSeq database with the HISAT2 alignment tool (Galaxy Version 2.1.0) [21] and assessed for mapping quality with MultiQC. Hits to exons on the Rnor 6.0 genome were counted using htseq-count (Galaxy version 0.9.1) [2].

Differential gene expression and normalized counts were modeled from count tables using DESeq2 (Galaxy version 2.11.40.6), which corrects for multiple comparisons by the Benjamini-Hochberg procedure [25]. All downstream analyses on RNA-seq data were performed on data generated by DESeq2. Plots were made using DESeq2, Volcano Plot (Galaxy version 0.0.3), and Microsoft Excel. The false discovery rate (FDR) adjusted p-value was (padj < 0.05).

Enrichment

Gene ontology analysis and Kyoto Encyclopedia of Genes and Genomes (KEGG) pathway enrichment analysis were performed using the Database for Annotation, Visualization and Integrated Discovery (DAVID) (https://david.ncifcrf.gov/) [18,19]. The list of DEGs (padj < 0.05) for both ipsilateral CIBP v. Sham and ipsilateral CIBP v. contralateral CIBP comparisons were imported into DAVID's "functional annotation" tool and compared against the *rattus norvegicus* genome. Enriched KEGG pathways and Gene Ontology Biological Process (GO:BP) terms were identified with the Expression Analysis Systematic Explorer (EASE) tool (maximum EASE score/p-value = 0.1) to identify significant gene enrichment. Plots were made using Microsoft Excel.

Histochemistry

Hematoxylin and eosin (H&E) staining of hindlimb sections was performed to determine the presence of tumour cells and dysregulated bone morphology in MRMT-1 injected CIBP models. Paraffin-embedded tissue samples were sliced at 4 µm and mounted on glass slides and baked at 70 °C for 20–30 minutes. Slides were deparaffinized and

rehydrated in multiple washes of xylene, ethanol and dH_2O, and then stained in Gill #3 Hematoxylin (Sigma-Aldrich) diluted 1:2 with dH_2O for 3 minutes, followed by two dH2O rinses and ten seconds in alkaline lithium carbonate. Slides were then stained for 45 seconds in 1 % eosin diluted 1:3 in 80 % ethanol. Following staining, slides were dehydrated in several washes each of ethanol and xylene and coverslipped with xylene miscible permount (Fisher Scientific) for imaging.

RESULTS

All rats utilized in gene expression analyses displayed tumour growth in the femur and behavioural evidence of cancer-induced bone pain, and no sham rats showed evidence of bone dysregulation or pain at week 3 endpoint.

Body weight was evaluated to determine if MRMT-1 breast cancer cell induced rat models of cancer-induced bone pain (CIBP) demonstrated significant signs of illness relative to Sham negative controls. Groups did not differ in body weight (Fig 1a) throughout the 3 week course of the model. CIBP model rats showed behavioural evidence of nociception, including a significant decrease in limb use (Fig 1b) at week 3 relative to sham control, and (Fig 1c) a significant reduction in 50 % mechanical withdrawal threshold at weeks 2 and 3 as measured by von Frey fibres, and a (Fig 1d) reduction in weight borne on the tumour-afflicted limb at week 3. Sham animals show an initial decrease in 50 % mechanical withdrawal threshold (Fig 1c) in the week immediately following surgery, but have recovered to baseline withdrawal thresholds by the time of tissue collection following final data collection on day 21.

All CIBP model animals included expression studies also showed evidence of tumour growth in the bone, and sham animals did not. X-ray imaging (Fig 2a) of ipsilateral rat femurs from the MRMT-1-induced CIBP group show a loss of density in bone cortex and trabecula near the distal epiphysis site of cell implantation relative to Sham control, which

all show normal bone morphology at the implantation site. Hematoxylin and Eosin (H&E) staining (Fig 2b) of sections from the ipsilateral distal femur shows no tumour cell invasion and normal appearance of bone and growth plate in Sham control rats, whereas CIBP model animals (Fig 2c) show tumour-cell invasion and degradation of the growth plate and cortical and trabecular bone.

Dorsal root ganglion gene expression analyzed by RNA-seq identified differential expression of 370 transcripts between CIBP and Sham groups and 178 transcripts between CIBP ipsilateral and contralateral comparisons.

Patterns of differential expression and transcript abundance derived from RNA-sequencing of ipsilateral pooled L3-6 dorsal root ganglia (DRGs) collected at week 3 from CIBP model rats and Sham controls are displayed in Figure 3. 370 genes were significantly (padj < 0.05) differentially expressed, with 192 upregulated and 177 downregulated targets in CIBP DRGs, as identified by DESeq2. Relative gene expression (logFC) and -log10(p-value) of each transcript comparison is plotted by volcano plot (Fig 3a), with significantly upregulated genes indicated in red and significantly downregulated genes indicated in blue. The full list of DEGs for this comparison is available in Supplementary Table S1. The heatmap (Fig 3b) indicates overall gene expression count similarities between all samples included in this analysis, as analyzed by principal component analysis on normalized gene expression counts. An MA plot (Fig 3c) showing global gene expression across this comparison, with differential expression plotted along the y-axis and average expression strength along the x-axis. Genes passing the significance threshold (adjusted p-value < 0.05) are coloured in red.

In the ipsilateral CIBP v. contralateral CIBP comparison of differential DRG gene expression, 178 genes were found to be differentially expressed, with 95 upregulated and 82 downregulated targets in ipsilateral CIBP DRGs, as identified by DESeq2. Relative gene expression (logFC) and -log10(p-value) of each transcript comparison is plotted by volcano plot (Fig 4a), with significantly upregulated genes indicated in red and significantly downregulated genes indicated in blue. The full list of DEGs for this

comparison is available in Supplementary Table S2. Overall gene expression count similarities between all samples included in this analysis, is indicated by heatmap (Fig 4b) as analyzed by principal component analysis on normalized gene expression counts. Global gene expression across this comparison is indicated by MA plot (Fig 4c) showing differential expression plotted along the y-axis and average expression strength along the x-axis. Genes passing the significance threshold (adjusted p-value < 0.05) are coloured in red.

A principal component analysis plot also shows variation among normalized gene counts of all samples in Supplementary Figure S1 for ipsilateral CIBP vs. Sham groups (Fig S1a), and ipsilateral vs contralateral CIBP (Fig S1b).

Enriched Gene Ontology Biological Process terms are indicative of increased neuronal signalling and cellular reorganization in ipsilateral CIBP DRGs relative to both sham and contralateral comparators.

Enriched Gene Ontology Biological Process (GO:BP) terms associated with upregulated DEGs (adjusted p-value < 0.05) in ipsilateral DRGs from CIBP model rats vs. ipsilateral DRGs from Sham controls (Fig 5) are displayed with bubble size representing the number of upregulated genes in each GO:BP term, and the top 10 terms and genes detailed. Downregulated GO:BP terms and their component genes are detailed in (Fig 6). Overall, in the ipsilateral CIBP vs. ipsilateral Sham comparison there are 84 upregulated GO:BP terms including GO:0007269 (neurotransmitter secretion), GO:0031175 (neuron projection development), and GO:0007017 (microtubule-based process). 188 downregulated GO:BP terms including GO:0051897 (positive regulation of protein kinase B signaling), GO:0008285 (negative regulation of cell proliferation), and GO:0006955 (immune response). There are 33 upregulated KEGG pathways including rno04915 (Estrogen signaling pathway), rno04721 (Synaptic vesicle cycle), and rno04722 (Neurotrophin signaling pathway). 33 downregulated KEGG pathways including rno04514 (Cell adhesion molecules (CAMs)), and rno04640 (Hematopoietic cell lineage).

In the ipsilateral CIBP vs. contralateral CIBP comparison there are fewer DEGs and fewer different enrichment terms and pathways. Upregulated GO:BP terms and their component genes are detailed in (Fig 7), and downregulated GO:BP terms and their component genes are detailed in (Fig 8). These including 24 upregulated GO:BP terms including GO:0045666 (positive regulation of neuron differentiation), GO:0006886 (intracellular protein transport), and GO:0007411 (axon guidance). 23 downregulated GO:BP terms including GO:0098609 (cell-cell adhesion), and GO:0006886 (intracellular protein transport). There is 1 upregulated KEGG pathway, rno04921 (Oxytocin signaling pathway) and 5 downregulated KEGG pathways including rno04141 (Protein processing in endoplasmic reticulum) and rno01100 (Metabolic pathways).

DISCUSSION

Conditions of persistent pain cause pathological reorganization in the peripheral nervous system both in the innervating sensory neurons at the site of injury or disease, and in the spinal cord [4,37,51]. Cancer pain in particular is a complex state involving features of inflammatory and neuropathic pain including dysregulated sensory neuron growth, and distinct neurochemical and cellular features in the spinal cord and DRG that are not shared with inflammatory or neuropathic pain states [16]. Bones are unevenly innervated with sympathetic and sensory nerve fibres including Aβ-, Aδ- and C-fibres in the periosteum, mineralized bone and bone marrow [20,26]. The densely innervated periosteum is highly sensitive to disruption, however many painful bone lesions have been found without periosteal involvement [36]. As such, the mechanisms responsible for the induction and maintenance of CIBP are heterogeneous and complex, involving the noxious substances released by tumour-associated cells, the inflammatory tumour response, bone tissue damage and remodelling, and direct neuronal damage and sprouting. Current therapies for CIBP are often inadequate and produce undesired side effects, and there is an immediate need for effective, non-opioid based therapies that extends beyond cancer-specific pain.

We used a well-established rat model of MRMT-1 breast cancer cell CIBP in this study that involves implantation and growth of a tumour in one femur over the course of three weeks, and a sham control that uses heat / freeze inactivated cancer cells implanted in the same manner. Using naïve rats as control would have eliminated any gene expression changes induced by surgery, but as the intervention in this model is extensive, we chose to utilize a sham to better control for CIBP-specific changes. Behavioural data indicates no evidence of pain in sham animals at the time of tissue collection for sequencing. Behavioural measurements throughout the course of the model and X-Ray and Histology imaging confirmed the validity of every animal model from which tissues were collected.

To obtain a comprehensive sample of innervation of the femur and tumour-affected area in this model, we collected, pooled and extracted RNA for sequencing from the L3-6 DRGs of each rat. L3-6 were chosen as they all contribute innervation to tissues involved with a tumour of the lower limb, through the sciatic and femoral nerves [41].

As opposed to cell-sorting or single-cell RNA-Seq which dissociates tissues and can identify transcriptomic variance in specific cell populations, we chose to examine transcripts in pooled whole DRG tissue. The DRG includes the cell bodies of sensory neurons that innervate the hindlimb, as well as resident macrophages, T- and B-lymphocytes, fibroblasts, vascular smooth muscle and endothelial cells, as well as satellite glial cells [15]. Satellite glial cells are well-established to engage in microenvironment control and cross-talk with sensory neurons that can contribute to pain signaling [46]. In addition, the DRG does not have a functional blood-brain barrier, with fenestrated capillaries allowing blood-borne cells and molecules to infiltrate the DRG [15], including peripheral immune cells which have been demonstrated to infiltrate DRGs in a sex-dependent manner in a mouse model of nerve injury [24]. Our analysis therefore cannot ascribe differential expression of any target transcript to any particular cell type, however the involvement of multiple cell types in the generation and maintenance of chronic and cancer pain is well-established [49], and possible targets may emerge from any cell type in the DRG.

The inclusion of six biological replicates per group subjected to paired-end 50 bp reads allows this study to be well-powered, and the protocols utilized for data analysis including DESeq2 are well-validated to detect differential expression between groups. We included two pairwise comparisons to determine sensory effects when comparing between CIBP and Sham, and to control for potential systemic changes within CIBP models, a comparison between ipsilateral and contralateral gene expression in CIBP rats was included.

We found a substantial number of DEGs in both comparisons, although there were approximately twice as many in the in the ipsilateral CIBP vs. ipsilateral Sham as in the ipsilateral CIBP vs. contralateral CIBP comparison. Overall, fold changes were relatively limited, but results were robustly significant as analyzed by DESeq2.

Many upregulated DEGs in ipsilateral DRGs of the CIBP model in both comparisons are associated with the processes of neurotransmission and neuronal development. These include GO:BP terms for neurotransmitter secretion, neuron projection development, microtubule-based process, axon guidance, neuron differentiation and others. Upregulated KEGG pathways in both comparisons also reflect this trend with upregulated pathways for synaptic vesicle cycle, and neurotrophin signaling pathway significantly enhanced. Given the evidence of increased sensory signalling along DRG neurons in a models of cancer pain [52], as well as the well documented new sensory neuronal growth in bone in response to metastatic cancer [4], the upregulation of genes associated with these processes is expected.

More unexpected were the multiple downregulated DEGs and the resulting enhanced GO:BP terms and KEGG pathways in ipsilateral DRGs of the CIBP model in both comparisons that are associated with inflammation and the immune system. These include GO:BP terms for immune response and response to oxidative stress, as well as KEGG pathways for hematopoietic cell lineage, antigen processing and presenting, and for multiple infections. Given the evidence of increased immune cell infiltration to the DRGs in cases of chronic pain [24]

Contrary to this however, it is notable that some of the most downregulated pathways and terms in ipsilateral DRGs of the CIBP model over both comparisons are related to cell adhesion - processes that regulate immune cell infiltration to the DRG.

Our investigation did not detect many targets identified by other gene-expression work in DRGs from models of neuropathic [50] and cancer pain [34], including categories of ion channels, opioid receptors, cytokines, chemokines, and the MAPK1/ERK2 pathway [34] which was conversely downregulated in our CIBP model. Some of these reported targets from the literature have limited evidence for replicability, while others including P2X purinergic receptors [23] are well-validated in particular models, yet do not appear in our investigation.

Several targets that are established markers of sensory DRG neurons and also known to be associated with pain signalling were upregulated in ipsilateral CIBP DRGs, including NTRK1 and MRGPRD, both of which have been demonstrated to be well-conserved between humans and mice [32]. In addition, the enriched GO:BP and KEGG terms associated with our DEGs were closely aligned with those from recent studies that utilized similar workflows to analyze gene expression of rat spinal cord and DRG after painful nerve injury [39,40], showing thematic consistency between these pain states.

Several DEGs identified in this study present particularly interesting targets of interest despite their omission from gene expression studies of other pain states. These include upregulated Vgf, a neuropeptide precursor that is inducible by nerve growth factor (NGF) and that has been demonstrated to produce an acute hyperalgesic response when injected in rats, and has been investigated for a potential role in neuropathic pain [7]. Another target of interest is upregulated STXBP1 which is associated with neurotransmitter release and has been extensively investigated in epilepsy and several encephalopathies, where loss of function is associated with negative outcomes [28].

Many DEGs identified in this study have not been reported to be associated with pain or have yet to be investigated in this context. These include top upregulated targets such as Fam150b, previously described only as an anaplastic lymphoma kinase activating ligand

[14]; and downregulated Dpt, a principal component of the extracellular matrix, which has recently been revealed to play a significant role in the central nervous system remodelling that is associated and potentially causative of chronic pain [30].

It is also important to note that a proportion of the DEGs identified in our study are likely to be unrelated to CIBP and are in fact a result of other effects of cancer or are artifacts. Transcriptional changes do not necessarily reflect changes in protein or function [13], and functional testing follow-up including knockout or direct targeting would be required to firmly establish a relationship between any of these DEG targets and CIBP following confirmation of differential expression by qPCR.

The findings of this study are limited by our use of only one sex of model animal. While we used a model of breast cancer, it has been repeatedly demonstrated that sex differences are important to account for in pain research [35], although some RNA-seq studies have shown a limited effect of sex on findings [39].

To our knowledge, this is the first investigation to utilize RNA-Seq on DRGs from an animal model of cancer pain. Our findings showed some overlap with differential expression results from other studies of sensory neuron and DRG gene expression in conditions of pain, and a number of unique and interesting potential targets. These results should be a utilized as a resource for functional investigation of DEGs and pathways identified here, and for target validation from other hypothesis-driven investigations.

ACKNOWLEDGEMENTS

We would like to thank Élora Midavaine and Dr. Philippe Sarret of the Université de Sherbrooke, Sherbrooke, QC for generous training and assistance in developing the animal model used in this study, and Natalie Zacal of McMaster University, Hamilton ON for assistance with animal models. This study was supported by grants to G. Singh from the Canadian Breast Cancer Foundation (Ontario) and the Michael G. DeGroote

Institute for Pain Research and Care, and fellowships from the Canadian Institutes of Health Research and the Michael G. DeGroote Institute for Pain Research and Care to R. Ungard.

DISCLOSURE OF INTEREST

The authors report no conflict of interest.

REFERENCES

[1] Afgan E, Baker D, Batut B, Van Den Beek M, Bouvier D, Ech M, Chilton J, Clements D, Coraor N, Grüning BA, Guerler A, Hillman-Jackson J, Hiltemann S, Jalili V, Rasche H, Soranzo N, Goecks J, Taylor J, Nekrutenko A, Blankenberg D. The Galaxy platform for accessible, reproducible and collaborative biomedical analyses: 2018 update. Nucleic Acids Res. 2018;46:W537–W544.

[2] Anders S, Pyl PT, Huber W. HTSeq--a Python framework to work with high-throughput sequencing data. Bioinformatics 2015;31:166–169.

[3] Andrews S. FastQC A Quality Control tool for High Throughput Sequence Data. n.d. Available: http://www.bioinformatics.babraham.ac.uk/projects/fastqc/.

[4] Bloom AP, Jimenez-Andrade JM, Taylor RN, Castañeda-Corral G, Kaczmarska MJ, Freeman KT, Coughlin KA, Ghilardi JR, Kuskowski MA, Mantyh PW. Breast cancer-induced bone remodeling, skeletal pain, and sprouting of sensory nerve fibers. J. Pain 2011;12:698–711.

[5] Bolger AM, Lohse M, Usadel B. Trimmomatic: a flexible trimmer for Illumina sequence data. Bioinformatics 2014;30:2114–2120.

[6] Chaplan SR, Bach FW, Pogrel JW, Chung JM, Yaksh TL. Quantitative assessment of tactile allodynia in the rat paw. J. Neurosci. Methods 1994;53:55–63.

[7] Chen YC, Pristerá A, Ayub M, Swanwick RS, Karu K, Hamada Y, Rice ASC, Okuse K. Identification of a receptor for neuropeptide VGF and its role in neuropathic pain. J. Biol. Chem. 2013;288:34638–34646.

[8] Coleman RE. Clinical Features of Metastatic Bone Disease and Risk of Skeletal Morbidity. Clin. Cancer Res. 2006;12:6243s-6249s.

[9] Dixon WJ. The Up-and-Down Method for Small Samples. J. Am. Stat. Assoc. 1965;60:967.

[10] Doré-Savard L, Otis V, Belleville K, Lemire M, Archambault M, Tremblay L, Beaudoin J-F, Beaudet N, Lecomte R, Lepage M, Gendron L, Sarret P. Behavioral, medical imaging and histopathological features of a new rat model of bone cancer pain. PLoS One 2010;5:e13774.

[11] Ewels P, Magnusson M, Lundin S, Käller M. MultiQC: summarize analysis results for multiple tools and samples in a single report. Bioinformatics 2016;32:3047–3048.

[12] Falk S, Al-Dihaissy T, Mezzanotte L, Heegaard AM. Effect of sex in the MRMT-1 model of cancer-induced bone pain. F1000Research 2015;4:445.

[13] Feder ME, Walser JC. The biological limitations of transcriptomics in elucidating stress and stress responses. Journal of Evolutionary Biology.2005, Vol. 18. pp. 901–910.

[14] Guan J, Umapathy G, Yamazaki Y, Wolfstetter G, Mendoza P, Pfeifer K, Mohammed A, Hugosson F, Zhang H, Hsu AW, Halenbeck R, Hallberg B, Palmer RH. FAM150A and FAM150B are activating ligands for anaplastic lymphoma kinase. Elife 2015;4.

[15] Haberberger RV, Barry C, Dominguez N, Matusica D. Human dorsal root ganglia. Front. Cell. Neurosci. 2019;13:271.

[16] Honore P, Rogers SD, Schwei MJ, Salak-Johnson JL, Luger NM, Sabino MC, Clohisy DR, Mantyh PW. Murine models of inflammatory, neuropathic and cancer pain each generates a unique set of neurochemical changes in the spinal cord and sensory neurons. Neuroscience 2000;98:585–98.

[17] Hu G, Huang K, Hu Y, Du G, Xue Z, Zhu X, Fan G. Single-cell RNA-seq reveals distinct injury responses in different types of DRG sensory neurons. Sci. Rep. 2016;6:1–11.

[18] Huang DW, Sherman BT, Lempicki RA. Bioinformatics enrichment tools: paths toward the comprehensive functional analysis of large gene lists. Nucleic Acids Res. 2009;37:1–13.

[19] Huang DW, Sherman BT, Lempicki RA. Systematic and integrative analysis of large gene lists using DAVID bioinformatics resources. Nat. Protoc. 2009;4:44–57.

[20] Jimenez-Andrade JM, Mantyh WG, Bloom AP, Xu H, Ferng AS, Dussor G, Vanderah TW, Mantyh PW. A phenotypically restricted set of primary afferent nerve fibers innervate the bone versus skin: therapeutic opportunity for treating skeletal pain. Bone 2010;46:306–13.

[21] Kim D, Langmead B, Salzberg SL. HISAT: A fast spliced aligner with low memory requirements. Nat. Methods 2015;12:357–360.

[22] Lacroix-Fralish ML, Austin JS, Zheng FY, Levitin DJ, Mogil JS. Patterns of pain: Meta-analysis of microarray studies of pain. Pain 2011;152:1888–1898.

[23] Liu M, Yang H, Fang D, Yang JJ, Cai J, Wan Y, Chui DH, Han JS, Xing GG. Upregulation of P2X3 receptors by neuronal calcium sensor protein VILIP-1 in dorsal root ganglions contributes to the bone cancer pain in rats. Pain 2013;154:1551–1568.

[24] Lopes DM, Malek N, Edye M, Jager SB, McMurray S, McMahon SB, Denk F. Sex differences in peripheral not central immune responses to pain-inducing injury. Sci. Rep. 2017;7:16460.

[25] Love MI, Huber W, Anders S. Moderated estimation of fold change and dispersion for RNA-seq data with DESeq2. Genome Biol. 2014;15:550.

[26] Mach DB, Rogers SD, Sabino MC, Luger NM, Schwei MJ, Pomonis JD, Keyser CP, Clohisy DR, Adams DJ, O'Leary P, Mantyh PW. Origins of skeletal pain: sensory and sympathetic innervation of the mouse femur. Neuroscience 2002;113:155–66.

[27] Miladinovic T, Ungard RG, Linher-Melville K, Popovic S, Singh G. Functional effects of TrkA inhibition on system x C − -mediated glutamate release and cancer-induced bone pain. Mol. Pain 2018;14:174480691877646.

[28] O'Brien S, Ng-Cordell E, Astle DE, Scerif G, Baker K. STXBP1-associated neurodevelopmental disorder: A comparative study of behavioural characteristics. J. Neurodev. Disord. 2019;11:17.

[29] Pargeon KL, Hailey BJ. Barriers to effective cancer pain management: a review of the literature. J. Pain Symptom Manage. 1999;18:358–68.

[30] Parisien M, Samoshkin A, Tansley SN, Piltonen MH, Martin LJ, El-Hachem N, Dagostino C, Allegri M, Mogil JS, Khoutorsky A, Diatchenko L. Genetic pathway analysis reveals a major role for extracellular matrix organization in inflammatory and neuropathic pain. Pain 2019;160:932–944.

[31] Perkins JR, Antunes-Martins A, Calvo M, Grist J, Rust W, Schmid R, Hildebrandt T, Kohl M, Orengo C, McMahon SB, Bennett DLH. A comparison of RNA-seq and exon arrays for whole genome transcription profiling of the L5 spinal nerve transection model of neuropathic pain in the rat. Mol. Pain 2014;10:7.

[32] Ray P, Torck A, Quigley L, Wangzhou A, Neiman M, Rao C, Lam T, Kim J-Y, Kim TH, Zhang MQ, Dussor G, Price TJ. Comparative transcriptome profiling of the human and mouse dorsal root ganglia. Pain 2018;159:1325–1345.

[33] Reyes-Gibby CC, Spitz MR, Yennurajalingam S, Swartz M, Gu J, Wu X, Bruera E, Shete S. Role of Inflammation Gene Polymorphisms on Pain Severity in Lung Cancer Patients. Cancer Epidemiol. Biomarkers Prev. 2009;18:2636–2642.

[34] Reyes-Gibby CC, Wang J, Silvas MRT, Yu R, Yeung SCJ, Shete S. MAPK1/ERK2 as novel target genes for pain in head and neck cancer patients. BMC Genet. 2016;17:40.

[35] Rosen S, Ham B, Mogil JS. Sex differences in neuroimmunity and pain. J. Neurosci. Res. 2017;95:500–508.

[36] Sabino MAC, Mantyh PW. Pathophysiology of bone cancer pain. J. Support. Oncol. 2005;3:15–24.

[37] Schwei MJ, Honore P, Rogers SD, Salak-Johnson JL, Finke MP, Ramnaraine ML, Clohisy DR, Mantyh PW. Neurochemical and cellular reorganization of the spinal cord in a murine model of bone cancer pain. J. Neurosci. 1999;19:10886–97.

[38] Sleigh JN, Weir GA, Schiavo G. A simple, step-by-step dissection protocol for the rapid isolation of mouse dorsal root ganglia. BMC Res. Notes 2016;9:82.

[39] Stephens KE, Chen Z, Sivanesan E, Raja SN, Linderoth B, Taverna SD, Guan Y. RNA-seq of spinal cord from nerve-injured rats after spinal cord stimulation. Mol. Pain 2018;14:1744806918817429.

[40] Stephens KE, Zhou W, Ji Z, Chen Z, He S, Ji H, Guan Y, Taverna SD. Sex differences in gene regulation in the dorsal root ganglion after nerve injury. BMC Genomics 2019;20:147.

[41] Takahashi Y, Chiba T, Kurokawa M, Aoki Y. Dermatomes and the central organization of dermatomes and body surface regions in the spinal cord dorsal horn in rats. J. Comp. Neurol. 2003;462:29–41.

[42] Tétreault P, Dansereau M-A, Doré-Savard L, Beaudet N, Sarret P. Weight bearing evaluation in inflammatory, neuropathic and cancer chronic pain in freely moving rats. Physiol. Behav. 2011;104:495–502.

[43] Ungard RG, Linher-Melville K, Nashed M, Sharma M, Wen J, Singh G. xCT knockdown in human breast cancer cells delays onset of cancer-induced bone pain. Mol. Pain 2019;15.

[44] Ungard RG, Seidlitz EP, Singh G. Inhibition of breast cancer-cell glutamate release with sulfasalazine limits cancer-induced bone pain. Pain 2014;155:28–36.

[45] Ungard RG, Zhu YF, Yang S, Nakhla P, Parzei N, Zhu KL, Singh G. Response to Pregabalin and Progesterone Differs in Male and Female Rat Models of Neuropathic and Cancer Pain. Can. J. Pain 2020:24740527.2020.1724776.

[46] Villa G, Fumagalli M, Verderio C, Abbracchio MP, Ceruti S. Expression and contribution of satellite glial cells purinoceptors to pain transmission in sensory ganglia: An update. Neuron Glia Biol. 2010;6:31–42.

[47] WHO | WHO's cancer pain ladder for adults. n.d. Available: https://www.who.int/cancer/palliative/painladder/en/. Accessed 17 Feb 2020.

[48] Wu S, Marie Lutz B, Miao X, Liang L, Mo K, Chang Y-J, Du P, Soteropoulos P, Tian B, Kaufman AG, Bekker A, Hu Y, Tao Y-X. Dorsal root ganglion transcriptome analysis following peripheral nerve injury in mice. Mol. Pain 2016;12.

[49] Yang Y, Li H, Li TT, Luo H, Gu XY, Lü N, Ji RR, Zhang YQ. Delayed activation of spinal microglia contributes to the maintenance of bone cancer pain in female Wistar rats via P2X7 receptor and IL-18. J. Neurosci. 2015;35:7950–7963.

[50] Zhang Y, Laumet G, Chen S-R, Hittelman WN, Pan H-L. Pannexin-1 Up-regulation in the Dorsal Root Ganglion Contributes to Neuropathic Pain Development. J. Biol. Chem. 2015;290:14647–55.

[51] Zhu YF, Kwiecien JM, Dabrowski W, Ungard R, Zhu KL, Huizinga JD, Henry JL, Singh G. Cancer pain and neuropathic pain are associated with A β sensory neuronal plasticity in dorsal root ganglia and abnormal sprouting in lumbar spinal cord. Mol. Pain 2018;14.

[52] Zhu YF, Ungard R, Seidlitz E, Zacal N, Huizinga J, Henry JL, Singh G. Differences in electrophysiological properties of functionally identified nociceptive sensory

neurons in an animal model of cancer-induced bone pain. Mol. Pain 2016;12:174480691662877.

[53] Zimmermann M. Ethical guidelines for investigations of experimental pain in conscious animals. Pain 1983;16:109–10.

FIGURES

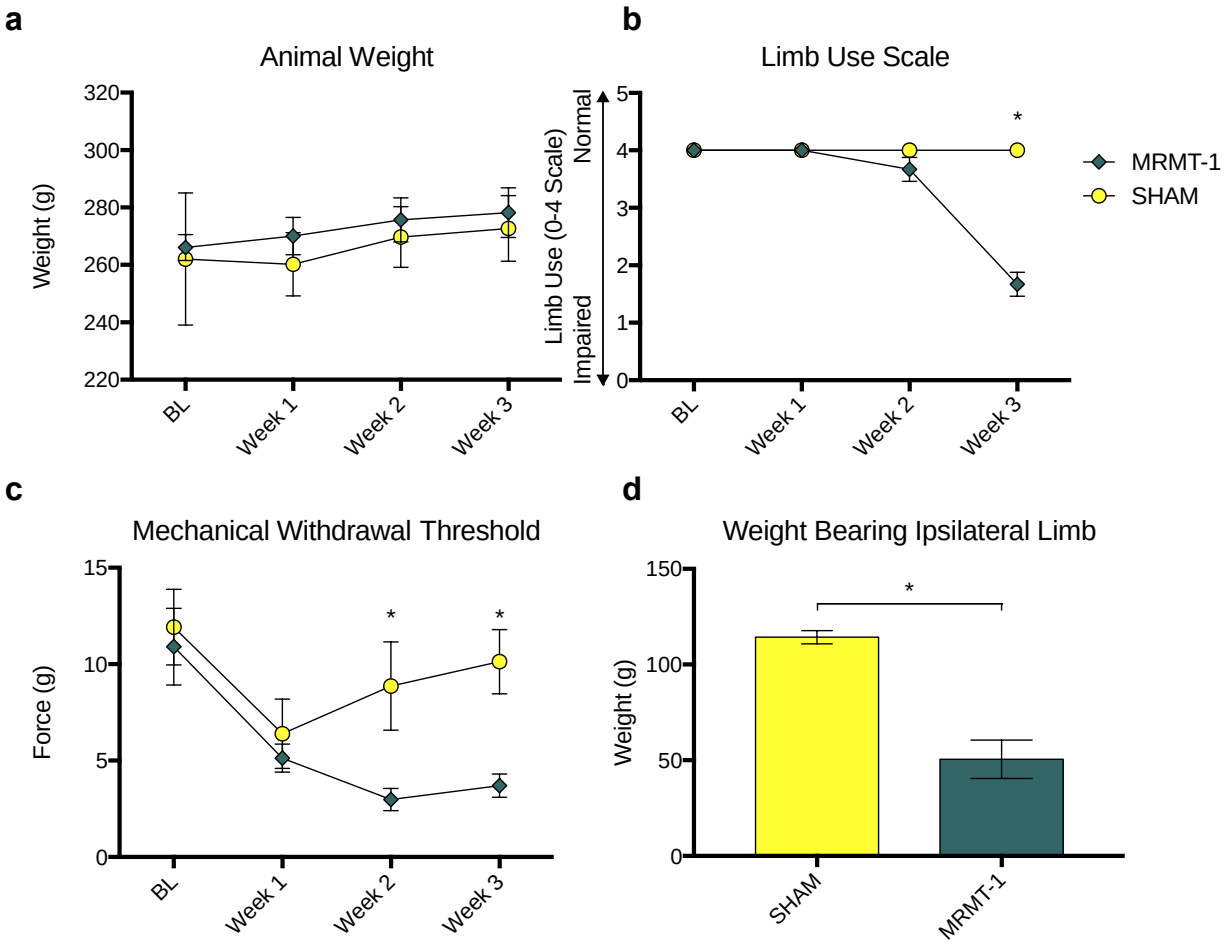

Figure 1.

MRMT-1 cell induced rat models of cancer-induced bone pain (CIBP) do not differ in body weight (a) from Sham control rats through the 3 week course of the model. CIBP model rats show behavioural evidence of nociception including a significant decrease in limb use (b) at week 3 relative to sham control, and (c) a significant reduction in 50% mechanical withdrawal threshold at weeks 2 and 3 as measured by von Frey fibres, and a (d) reduction in weight borne on the tumour-afflicted limb at week 3. Data represent the mean ± SEM from n = 6 female SD rats / group. Differences between treatment groups

over time (a, b, c) are compared by multiple t-tests, differences between groups in DWB (d) are compared by unpaired t-test (*P < 0.05).

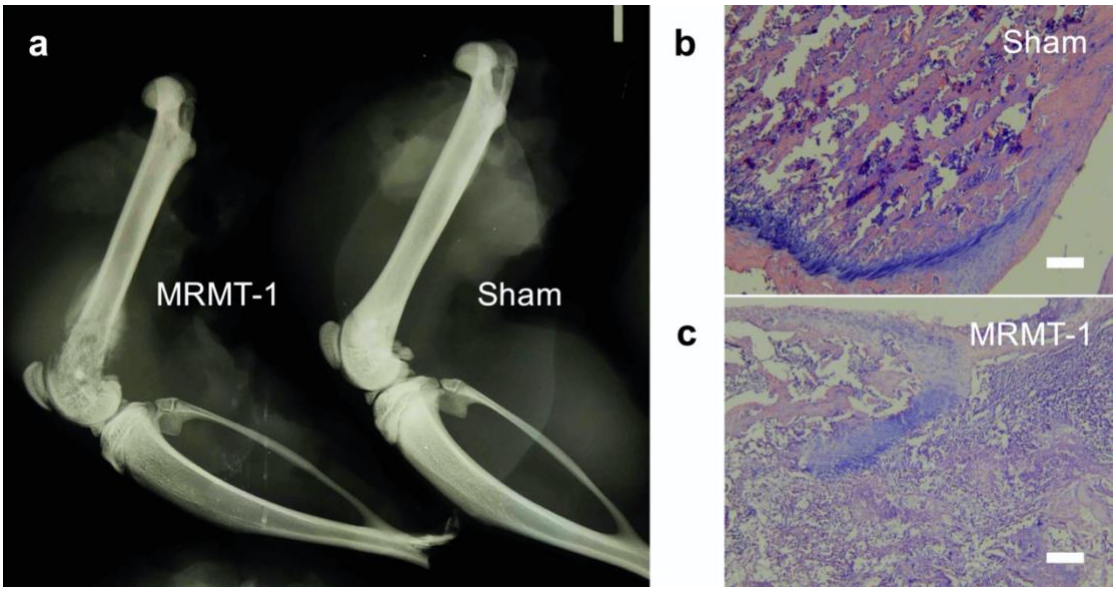

Figure 2.

Representative X-ray images (a) of ipsilateral rat femurs from the MRMT-1-induced cancer-induced bone pain (CIBP) group show a loss of density in bone cortex and trabecula near the distal epiphysis site of cell implantation relative to Sham control, which show normal bone morphology at the implantation site. (b) Hematoxylin and Eosin (H&E) staining of sections from the ipsilateral distal femur shows no tumour cell invasion and normal appearance of bone and growth plate in Sham control rats. (c) MRMT-1 CIBP model animals show tumour-cell invasion and degradation of the growth plate and cortical and trabecular bone. (Scale bars = 200 µM).

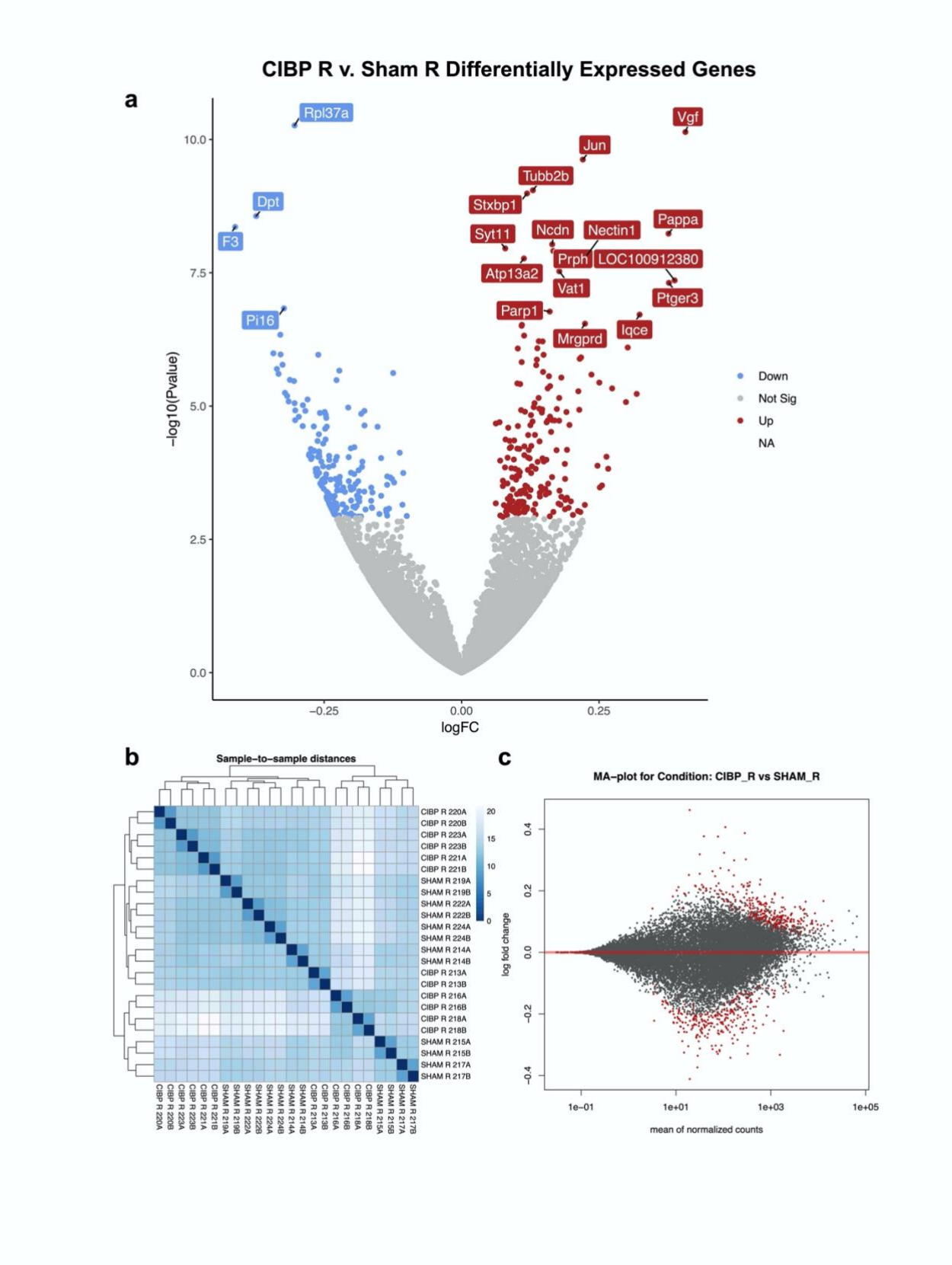
CIBP R v. Sham R Differentially Expressed Genes
a
Rpl37a
Vgf
Jun
Tubb2b
Dpt
Stxbp1
F3
Syt11
Ncdn
Nectin1
Pappa
Prph
LOC100912380
Atp13a2
Vat1
Ptger3
Parp1
Pi16
Iqce
Mrgprd
−log10(Pvalue)
logFC
Down
Not Sig
Up
NA
b
Sample−to−sample distances
c
MA−plot for Condition: CIBP_R vs SHAM_R
log fold change
mean of normalized counts

Figure 3.

A visual summary of patterns of differentially expressed genes (DEGs) derived from RNA-sequencing of ipsilateral pooled L3-6 dorsal root ganglia (DRGs) collected at week 3 from cancer-induced bone pain (CIBP) model rats and Sham controls, (n = 6) rats / group.

A volcano plot (a) shows both up- (indicated in red) and down-regulated (indicated in blue) DEGs in CIBP ipsilateral DRGs relative to sham. The top 20 most significant DEGs (by adjusted p-value) are named. The heatmap (b) indicates overall gene expression count similarities between all samples included in this analysis, as analyzed by principal component analysis on normalized gene expression counts. An MA plot (c) showing global gene expression across this comparison, with differential expression plotted along the y-axis and average expression strength along the x-axis. Genes passing the significance threshold (adjusted p-value < 0.05) are coloured in red.

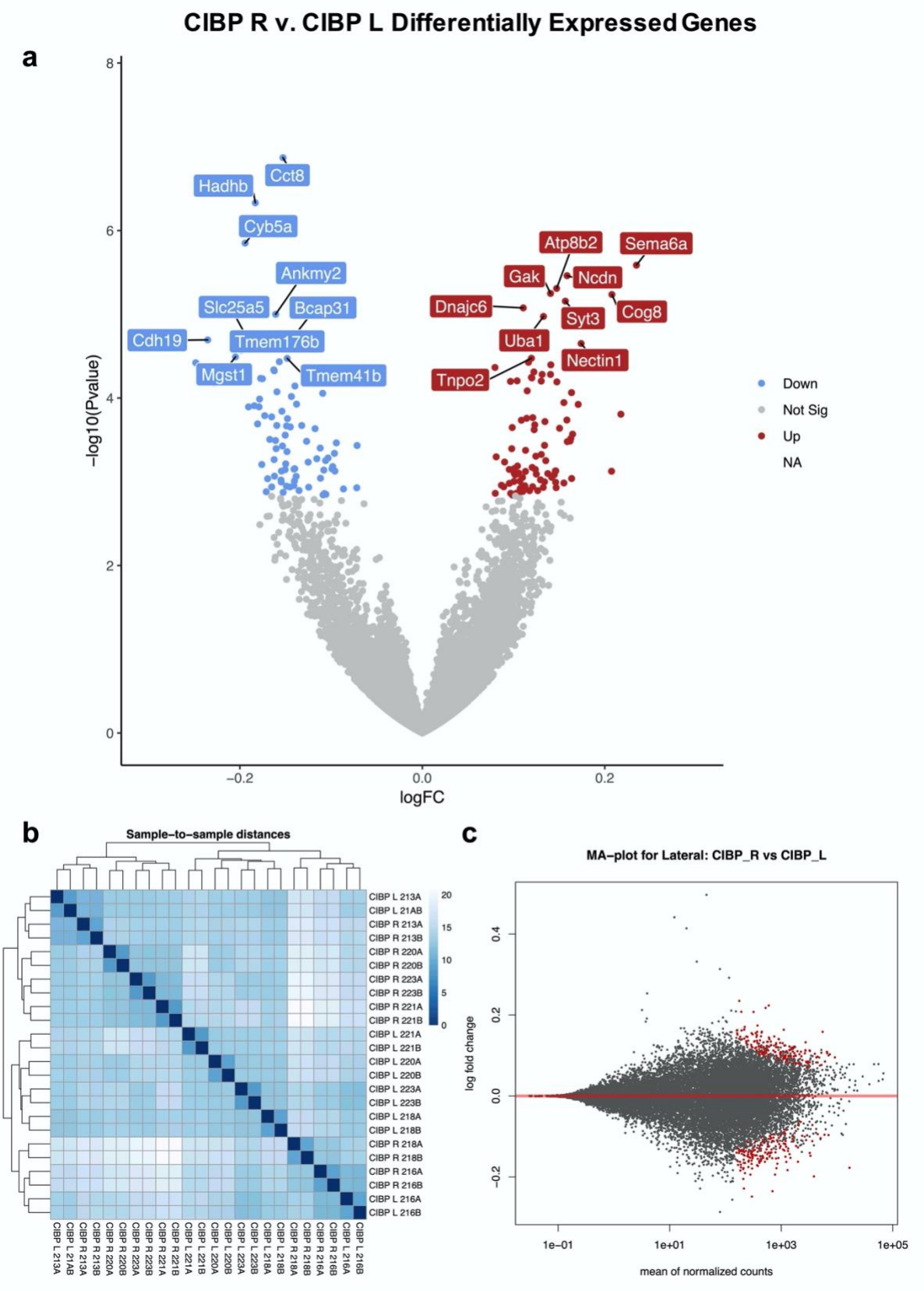
CIBP R v. CIBP L Differentially Expressed Genes
a
−log10(Pvalue)
logFC
Hadhb
Cct8
Cyb5a
Ankmy2
Slc25a5
Bcap31
Cdh19
Tmem176b
Mgst1
Tmem41b
Atp8b2
Sema6a
Gak
Ncdn
Dnajc6
Syt3
Cog8
Uba1
Nectin1
Tnpo2
Down
Not Sig
Up
NA
b
Sample−to−sample distances
c
MA−plot for Lateral: CIBP_R vs CIBP_L
log fold change
mean of normalized counts

Figure 4.

A visual summary of patterns of differentially expressed genes (DEGs) derived from RNA-sequencing of ipsilateral and contralateral pooled L3-6 dorsal root ganglia (DRGs) collected at week 3 from cancer-induced bone pain (CIBP) model rats (n = 6).

A volcano plot (a) shows both up- (indicated in red) and down-regulated (indicated in blue) DEGs in ipsilateral DRGs from CIBP animals. The heatmap (b) indicates overall gene expression count similarities between all samples included in this analysis, as analyzed by principal component analysis on normalized gene expression counts. An MA plot (c) showing global gene expression across this comparison, with differential expression plotted along the y-axis and average expression strength along the x-axis. Genes passing the significance threshold (adjusted p-value < 0.05) are coloured in red.

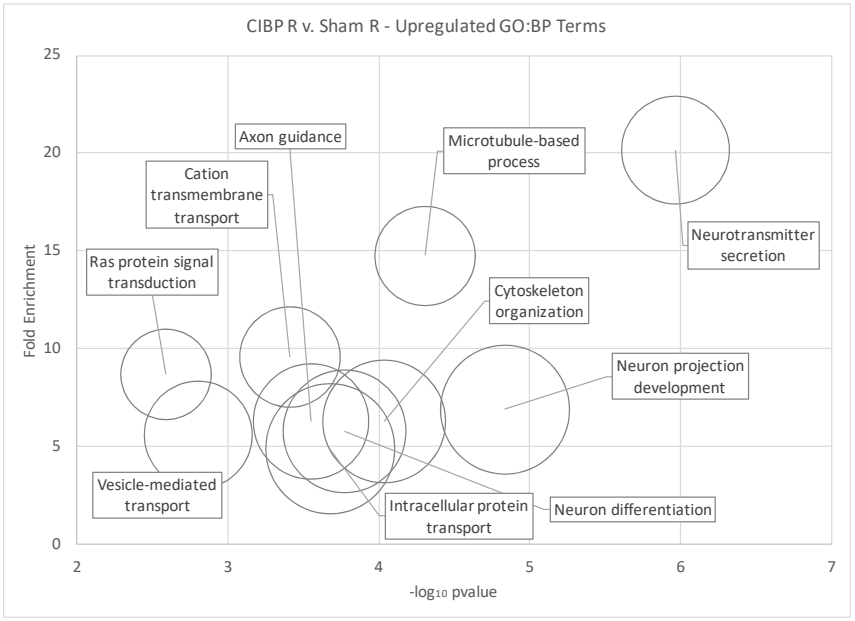

GO:BP Term	Genes
neurotransmitter secretion	SYT1, PPFIA3, NRXN2, SYN1, SYN2, STXBP1, BRSK1
neuron projection development	LINGO1, GNAO1, NPTXR, NCDN, MAPT, GFRA1, CNTNAP1, SHC1, GDPD5, ADCYAP1
microtubule-based process	TUBB2B, MAPT, TUBB5, TUBA1A, TUBB3, DCTN1
axon guidance	SEMA4F, NTRK1, KIF5C, NECTIN1, ROBO2, NGFR, TUBB3, VASP, DRGX
neuron differentiation	RET, MAPT, GFRA1, SHC1, BRSK1, TLX3, VGF, TUBB3, DRGX
intracellular protein transport	STX1A, AP2A2, COPG1, AP1B1, AP2A1, AP3B2, SYTL3, NGFR, RPH3A, APBA1
cytoskeleton organization	MAST1, PACSIN1, TUBB2B, CNTNAP1, TUBA1A, TUBB3, ADD2, THY1
cation transmembrane transport	P2RX3, CHRNA5, CHRNA7, CHRNA6, HTR3B, ATP13A2
vesicle-mediated transport	STX1A, AP2A2, CHMP1A, COPG1, AP1B1, AP2A1, SPIRE2
Ras protein signal transduction	GRB2, NTRK1, JUN, SHC1, DHCR24

Figure 5.

Gene Ontology Biological Process (GO:BP) pathways associated with upregulated Differentially Expressed Genes (DEGs) (adjusted p-value < 0.05), in ipsilateral dorsal root ganglia (DRGs) from cancer-induced bone pain (CIBP) model rats vs. DRGs from Sham controls, (n = 6) rats / group. The 10 most significant GO:BP terms are displayed with bubble size representing the number of upregulated genes / GO:BP term. The top 10 terms and genes are detailed in the table.

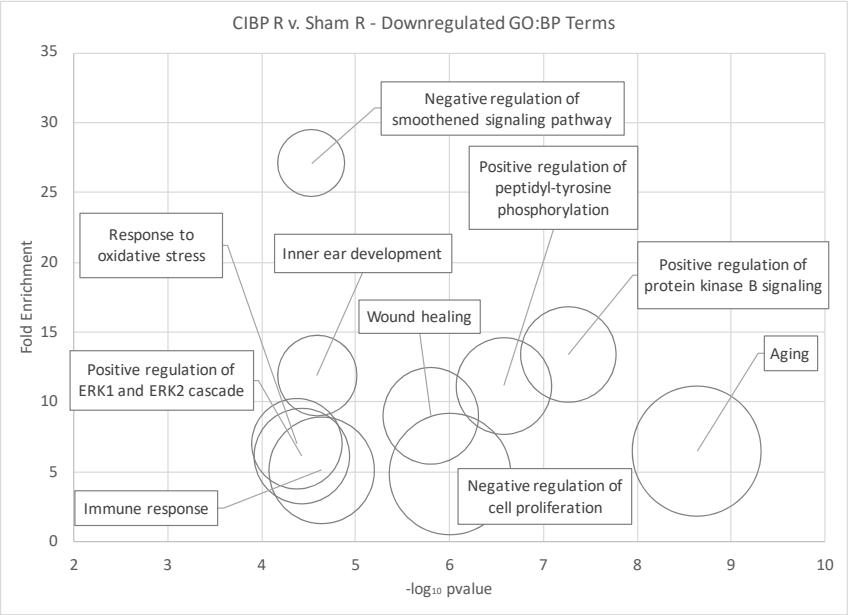

GO:BP Term	Genes
Aging	FADS1, TGFB3, IGF1, SERPING1, DCN, GJB6, MMP2, CDKN1C, GPX1, GSTM2, C1QB, CCR5, SERPINF1, GSN, F3, PDGFRA, AOC3, IGFBP5
Positive regulation of protein kinase B signaling	SEMA5A, VEGFB, EGFR, GPX1, F3, HCLS1, IGF1, ANGPT1, IGF2, IGFBP5
Positive regulation of peptidyl-tyrosine phosphorylation	VEGFB, FGFR3, HCLS1, PDGFRA, IGF1, TNFRSF14, ANGPT1, CD4, IGF2, CD74
Negative regulation of cell proliferation	BMP4, CAV1, FGFR3, TGFB3, IGF1, GJB6, KANK2, CD37, WISP2, LOC102552895, GPC3, SERPINE2, BTG1, SFRP4, CSF1R, DPT
Wound healing	BMP4, EGFR, CAV1, GSN, PECAM1, TGFB3, PDGFRA, IGF2, DCN, SDC2
Immune response	RT1-A2, C1QB, CCR5, RT1-DB1, IRF8, RT1-CE10, TGFBR3, TNFRSF14, TNFSF13, RT1-BA, RT1-DA, CD74
Inner ear development	C1QB, FGFR3, IGFBP7, TGFB3, PDGFRA, IGF1, GJB6
Negative regulation of smoothened signaling pathway	GPC3, FGFR3, SERPINE2, GLIS2, GAS1
Positive regulation of ERK1 and ERK2 cascade	BMP4, VEGFB, EGFR, FGFR3, PYCARD, PDGFRA, ANGPT1, CD74, CSF1R, MT3
Response to oxidative stress	ALDH1A1, EGFR, TXNIP, GPX1, BTG1, MMP2, NDUFA12, SOD3, MT3

Figure 6.

Gene Ontology Biological Process (GO:BP) pathways associated with downregulated Differentially Expressed Genes (DEGs) (adjusted p-value < 0.05), in ipsilateral dorsal root ganglia (DRGs) from cancer-induced bone pain (CIBP) model rats vs. DRGs from Sham controls, (n = 6) rats / group. The 10 most significant GO:BP terms are displayed with bubble size representing the number of upregulated genes / GO:BP term. The top 10 terms and genes are detailed in the table.

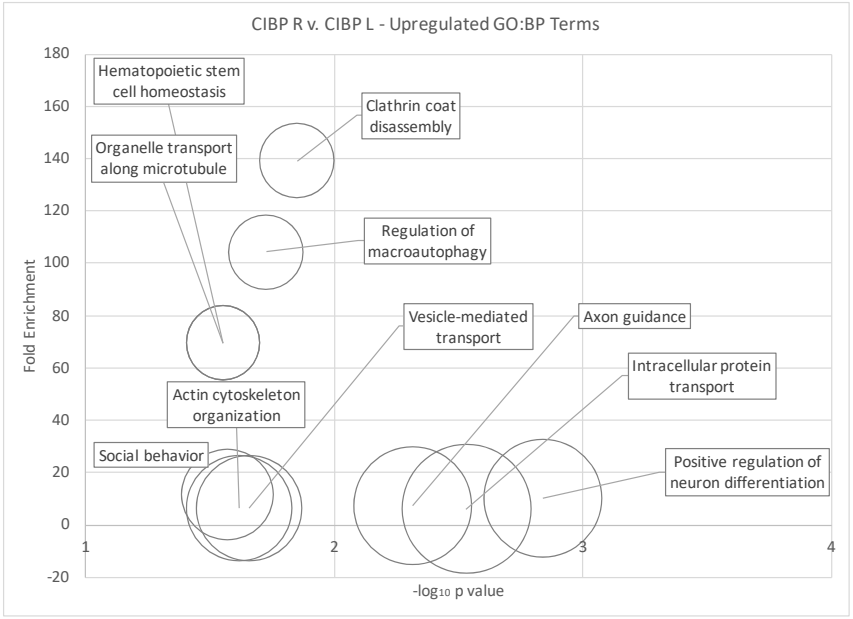

GO:BP Term	Genes
positive regulation of neuron differentiation	EIF4G1, NCOA1, MMD, MAPK8IP3, TIMP2
intracellular protein transport	COPG1, AP1B1, TBC1D9, RPH3A, NSF, TBC1D9B
axon guidance	SEMA6A, NECTIN1, MAPK8IP3, ROBO2, GAP43
clathrin coat disassembly	DNAJC6, GAK
regulation of macroautophagy	ATP6V0A1, PRKAA2
vesicle-mediated transport	COPG1, AP1B1, MAPK8IP3, NSF
actin cytoskeleton organization	CORO2B, MTSS1, FLII, WDR1
social behavior	NRXN2, MAPK8IP2, DLG4
organelle transport along microtubule	COPG1, KIF3C
hematopoietic stem cell homeostasis	ATP8B2, ADAR

Figure 7.

Gene Ontology Biological Process (GO:BP) pathways associated with upregulated Differentially Expressed Genes (DEGs) (adjusted p-value < 0.05), in ipsilateral dorsal root ganglia (DRGs) from cancer-induced bone pain (CIBP) model rats vs. DRGs from contralateral rats of the same group (n = 6). The 10 most significant GO:BP terms are displayed with bubble size representing the number of upregulated genes / GO:BP term. The top 10 terms and genes are detailed in the table.

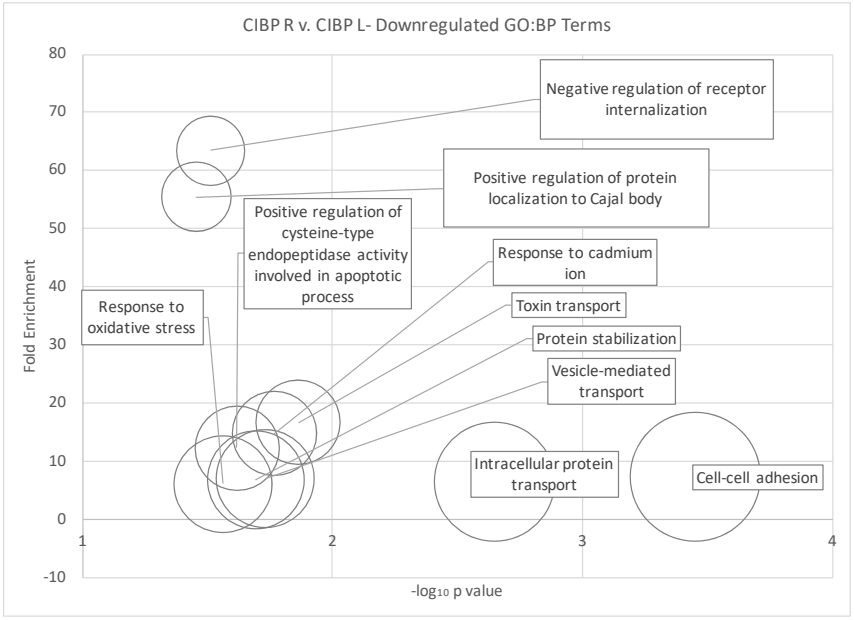

GO:BP Term	Genes
cell-cell adhesion	BZW1, DDX3X, SNX5, RPL15, CCT8, SDCBP, ANXA2
intracellular protein transport	COPB2, COPG2, SNX5, VAMP1, SAR1A, BCAP31
toxin transport	COPB2, CCT4, CCT8
response to cadmium ion	DTYMK, CYB5A, PRNP
vesicle-mediated transport	COPB2, COPG2, VAMP1, SAR1A
protein stabilization	SUMO1, CCT4, CCT8, MT3
positive regulation of cysteine-type endopeptidase activity involved in apoptotic process	DDX3X, MTCH2, BCAP31
response to oxidative stress	APOE, PRNP, OXR1, MT3
negative regulation of receptor internalization	SDCBP, ANXA2
positive regulation of protein localization to Cajal body	CCT4, CCT8

Figure 8.

Gene Ontology Biological Process (GO:BP) pathways associated with downregulated Differentially Expressed Genes (DEGs) (adjusted p-value < 0.05), in ipsilateral dorsal root ganglia (DRGs) from cancer-induced bone pain (CIBP) model rats vs. DRGs from contralateral rats of the same group (n = 6). The 10 most significant GO:BP terms are displayed with bubble size representing the number of upregulated genes / GO:BP term. The top 10 terms and genes are detailed in the table.

Supplemental Figures and Tables

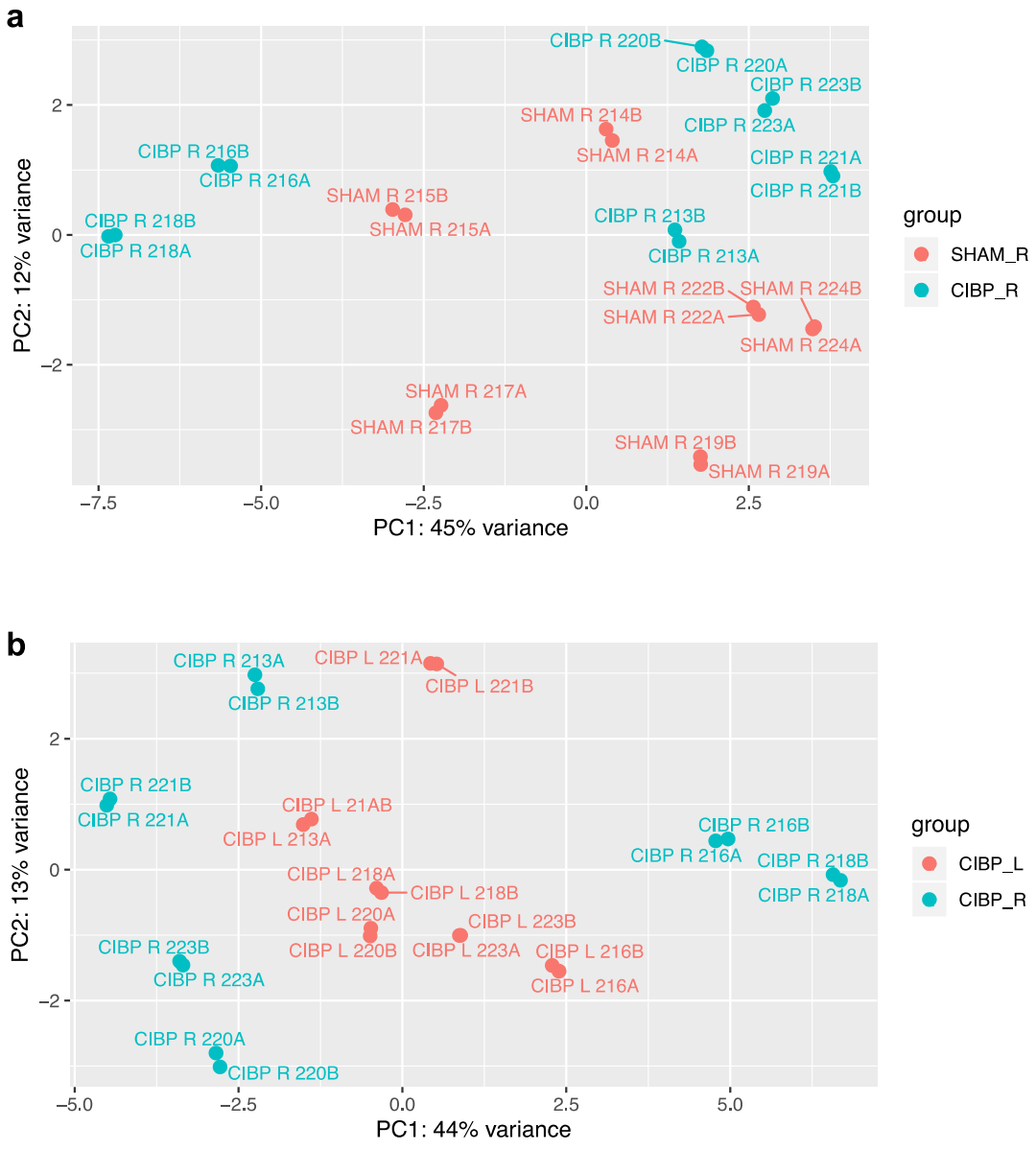

Figure S1.

Principal component analysis plot showing variation among normalized gene counts of all samples in (a) ipsilateral CIBP vs. Sham groups, and (b) Ipsilateral vs contralateral CIBP. Neither analysis shows batch effects.

Table S1.

All Differentially Expressed Genes CIBP v Sham ipsilateral groups (adjusted p-value < 0.05).

	baseMean	log2FC	lfcSE	stat	pvalue	padj
Fam150b	19.45	0.46	0.06	7.23	5.01E-13	7.62E-09
Rpl37a	328.19	-0.30	0.05	-6.56	5.45E-11	3.67E-07
Vgf	110.02	0.41	0.06	6.52	7.24E-11	3.67E-07
Jun	589.04	0.22	0.03	6.33	2.38E-10	9.03E-07
Stxbp1	5914.86	0.12	0.02	6.11	1.03E-09	2.60E-06
Tubb2b	1554.94	0.13	0.02	6.13	8.95E-10	2.60E-06
Dpt	28.40	-0.37	0.06	-5.95	2.73E-09	5.94E-06
F3	19.53	-0.41	0.07	-5.87	4.35E-09	8.28E-06
Pappa	77.23	0.38	0.06	5.82	5.83E-09	9.85E-06
Ncdn	5433.80	0.16	0.03	5.74	9.26E-09	1.41E-05
Syt11	7970.47	0.08	0.01	5.71	1.10E-08	1.52E-05
Prph	12929.36	0.17	0.03	5.70	1.23E-08	1.56E-05
Nectin1	363.00	0.23	0.04	5.66	1.47E-08	1.72E-05
Atp13a2	1588.93	0.11	0.02	5.64	1.70E-08	1.85E-05
Vat1	1772.07	0.18	0.03	5.54	2.96E-08	3.01E-05
LOC100912380	283.45	0.39	0.07	5.47	4.39E-08	4.17E-05
Ptger3	38.84	0.38	0.07	5.46	4.88E-08	4.37E-05
Pi16	72.18	-0.32	0.06	-5.26	1.47E-07	0.000123987
Parp1	788.92	0.16	0.03	5.23	1.69E-07	0.000135057
Iqce	103.82	0.32	0.06	5.21	1.92E-07	0.000146301
Mrgprd	322.96	0.22	0.04	5.13	2.84E-07	0.000205932
Pirt	4327.12	0.11	0.02	5.12	2.99E-07	0.0002061
Scg3	2231.72	0.11	0.02	5.12	3.12E-07	0.0002061
Brsk1	1492.38	0.11	0.02	5.04	4.77E-07	0.000290014
RT1-A2	76.43	-0.33	0.07	-5.04	4.59E-07	0.000290014
Dctn1	5104.66	0.14	0.03	4.99	6.06E-07	0.000344228
P2rx3	3229.17	0.15	0.03	4.99	6.11E-07	0.000344228
Ankrd52	884.31	0.14	0.03	4.93	8.23E-07	0.000421469
LOC100910768	298.35	0.30	0.06	4.94	7.96E-07	0.000421469
Mapt	3734.59	0.10	0.02	4.93	8.31E-07	0.000421469
Ddr2	140.57	-0.34	0.07	-4.89	1.02E-06	0.000488559
Igfbp5	325.99	-0.33	0.07	-4.88	1.08E-06	0.000488559

Sdc2	252.07	-0.26	0.05	-4.87	1.09E-06	0.000488559
Shc2	772.66	0.15	0.03	4.87	1.09E-06	0.000488559
Nt5dc3	355.99	0.22	0.04	4.85	1.22E-06	0.000530833
Tes	325.22	0.21	0.04	4.84	1.30E-06	0.000548772
Ret	4831.34	0.14	0.03	4.83	1.34E-06	0.000551851
Eif3a	1237.55	0.11	0.02	4.81	1.50E-06	0.000598723
RGD1564963	14.85	-0.33	0.07	-4.79	1.67E-06	0.000649707
Usp20	1231.15	0.14	0.03	4.79	1.71E-06	0.000649707
Esam	28.84	-0.34	0.07	-4.75	2.01E-06	0.0007456
Eya1	3.48	-0.22	0.05	-4.74	2.16E-06	0.000783344
Tuba1b	4096.75	0.15	0.03	4.73	2.28E-06	0.000808179
Itm2b	2094.13	-0.12	0.03	-4.72	2.39E-06	0.000827689
Gsn	1557.10	-0.33	0.07	-4.71	2.49E-06	0.000841058
Gna14	611.99	0.24	0.05	4.70	2.57E-06	0.00084915
Prdm12	760.01	0.16	0.03	4.69	2.75E-06	0.000891276
Dpysl4	747.46	0.18	0.04	4.68	2.92E-06	0.000924936
Gpx1	277.37	-0.23	0.05	-4.65	3.26E-06	0.000991375
RT1-Db1	31.95	-0.31	0.07	-4.66	3.22E-06	0.000991375
Zic1	18.20	-0.30	0.07	-4.65	3.39E-06	0.001010688
Tgfb1i1	167.47	0.25	0.05	4.63	3.63E-06	0.001060688
Spock2	8999.96	0.10	0.02	4.62	3.76E-06	0.0010784
Actr1a	3037.86	0.11	0.02	4.62	3.86E-06	0.001087225
Lingo1	615.42	0.16	0.03	4.60	4.22E-06	0.001166501
Plaur	86.72	0.27	0.06	4.58	4.66E-06	0.001243343
Rtfdc1	576.12	0.16	0.03	4.58	4.65E-06	0.001243343
Dmtf1	265.93	0.21	0.05	4.55	5.27E-06	0.001382865
Prelp	83.77	-0.32	0.07	-4.54	5.64E-06	0.001455109
Celf3	31.73	0.32	0.07	4.53	5.91E-06	0.001497111
Scara5	82.78	-0.32	0.07	-4.51	6.46E-06	0.001611079
Esyt1	1998.44	0.14	0.03	4.49	7.03E-06	0.001698174
Stac	521.06	0.18	0.04	4.49	7.03E-06	0.001698174
Rps28	154.19	-0.28	0.06	-4.48	7.52E-06	0.001786206
LOC100912041	59.18	-0.31	0.07	-4.46	8.18E-06	0.001914514
Chrna6	168.78	0.30	0.07	4.45	8.41E-06	0.001938059
Glis2	57.14	-0.30	0.07	-4.44	8.82E-06	0.001973446
Slc45a4	762.37	0.13	0.03	4.44	8.81E-06	0.001973446
Clec4a3	13.66	-0.29	0.07	-4.43	9.64E-06	0.002124103
Ap1b1	929.39	0.13	0.03	4.41	1.05E-05	0.002274972

Jam2	299.39	-0.21	0.05	-4.40	1.06E-05	0.002278571
Kcna6	788.90	0.14	0.03	4.39	1.12E-05	0.002360157
Tbcd	1070.27	0.17	0.04	4.39	1.13E-05	0.002360848
Emp1	91.00	-0.30	0.07	-4.38	1.20E-05	0.002369166
Gnao1	2732.15	0.11	0.02	4.38	1.19E-05	0.002369166
Mmd	157.63	0.21	0.05	4.38	1.17E-05	0.002369166
Ntrk1	1688.31	0.15	0.03	4.39	1.15E-05	0.002369166
Rpl12	199.17	-0.28	0.06	-4.37	1.23E-05	0.002369166
Rps16	872.23	-0.18	0.04	-4.37	1.23E-05	0.002369166
Gdpd5	307.95	0.19	0.04	4.36	1.29E-05	0.002399952
Lum	259.18	-0.25	0.06	-4.36	1.29E-05	0.002399952
Syt1	1359.72	0.12	0.03	4.36	1.28E-05	0.002399952
Rgs3	1861.13	0.15	0.03	4.36	1.32E-05	0.002422418
Iah1	89.43	-0.26	0.06	-4.35	1.35E-05	0.002436919
Rfng	298.34	-0.18	0.04	-4.34	1.39E-05	0.002493023
Fxyd1	268.65	-0.25	0.06	-4.34	1.45E-05	0.002573321
Eepd1	704.75	0.13	0.03	4.33	1.47E-05	0.002575383
Nploc4	788.51	0.16	0.04	4.32	1.58E-05	0.002709603
Vsig10l	159.56	-0.30	0.07	-4.32	1.59E-05	0.002709603
Ptgds	491.79	-0.25	0.06	-4.31	1.66E-05	0.002813317
Cd4	68.71	-0.30	0.07	-4.28	1.84E-05	0.003003258
Ppfia3	618.74	0.16	0.04	4.28	1.86E-05	0.003003258
RGD1562618	400.03	0.17	0.04	4.28	1.86E-05	0.003003258
Sema4f	518.36	0.18	0.04	4.28	1.88E-05	0.003003258
Spire2	540.52	0.17	0.04	4.28	1.84E-05	0.003003258
Nptxr	1194.41	0.13	0.03	4.27	1.94E-05	0.003081575
Dagla	699.41	0.15	0.04	4.26	2.02E-05	0.003128453
Mapk3	3613.35	0.07	0.02	4.26	2.01E-05	0.003128453
Rab6b	7888.78	0.06	0.01	4.25	2.12E-05	0.003256719
Ggt7	1194.75	0.13	0.03	4.24	2.28E-05	0.003435782
Thop1	201.70	0.20	0.05	4.24	2.26E-05	0.003435782
Rpl35	480.69	-0.18	0.04	-4.23	2.31E-05	0.003442659
Cdipt	1325.95	0.10	0.02	4.23	2.37E-05	0.003468152
Lsp1	30.23	-0.29	0.07	-4.23	2.37E-05	0.003468152
Abi3bp	170.69	-0.27	0.06	-4.22	2.41E-05	0.003473422
Cav1	303.48	-0.25	0.06	-4.22	2.42E-05	0.003473422
Tmem255a	377.84	-0.15	0.04	-4.22	2.44E-05	0.003473422
Add2	3117.19	0.08	0.02	4.21	2.54E-05	0.003582582

Id3	228.80	-0.25	0.06	-4.20	2.66E-05	0.003716273
Oxct1	1040.22	0.16	0.04	4.17	3.05E-05	0.004216185
Tlr8	11.42	-0.26	0.06	-4.15	3.38E-05	0.004628455
Impdh1	1738.07	0.13	0.03	4.14	3.47E-05	0.00469769
Rph3a	2662.49	0.12	0.03	4.14	3.49E-05	0.00469769
Atp5i	230.67	-0.25	0.06	-4.10	4.22E-05	0.005596873
Fam189b	3494.32	0.08	0.02	4.09	4.23E-05	0.005596873
MAST1	1865.17	0.10	0.02	4.08	4.42E-05	0.00578979
Klc2	3048.00	0.09	0.02	4.08	4.50E-05	0.005821451
Txnip	449.32	-0.26	0.06	-4.08	4.52E-05	0.005821451
Ngfr	4297.48	0.14	0.03	4.08	4.59E-05	0.005864699
Igf2	50.28	-0.25	0.06	-4.05	5.05E-05	0.006402129
Ccdc92	2771.65	0.13	0.03	4.03	5.59E-05	0.007026645
Syn2	1282.09	0.11	0.03	4.03	5.69E-05	0.007094652
Copg1	2182.50	0.09	0.02	4.02	5.85E-05	0.007229451
Rpl27	323.16	-0.20	0.05	-4.02	5.91E-05	0.007243941
Hsp90ab1	11443.53	0.09	0.02	4.01	6.12E-05	0.007445239
RT1-Ba	21.15	-0.20	0.05	-4.00	6.20E-05	0.007487536
Anxa5	4911.24	0.10	0.03	4.00	6.26E-05	0.007497009
Fcer1g	26.94	-0.27	0.07	-4.00	6.38E-05	0.007523944
Kif21a	4495.88	0.10	0.03	4.00	6.34E-05	0.007523944
Adam19	1217.79	0.19	0.05	3.99	6.61E-05	0.007735963
Chrna7	499.10	0.17	0.04	3.99	6.71E-05	0.007736176
Rbfox3	616.20	0.12	0.03	3.99	6.66E-05	0.007736176
Sfrp4	28.85	-0.27	0.07	-3.98	6.83E-05	0.007815434
LOC108350833	27.69	-0.27	0.07	-3.98	6.97E-05	0.00791496
Serpinf1	137.49	-0.26	0.07	-3.97	7.06E-05	0.007957738
Rnf14	2042.28	-0.11	0.03	-3.96	7.48E-05	0.008368442
LOC100360573	98.52	-0.26	0.07	-3.95	7.81E-05	0.008674993
Angpt1	26.93	-0.28	0.07	-3.94	7.98E-05	0.008796293
Syn1	1686.10	0.11	0.03	3.94	8.32E-05	0.009101581
Rbp4	46.19	-0.28	0.07	-3.93	8.43E-05	0.009162543
Igfbp4	423.48	-0.24	0.06	-3.93	8.57E-05	0.009246731
C1qb	35.17	-0.26	0.07	-3.92	9.00E-05	0.009399321
Clec3b	40.89	-0.27	0.07	-3.92	9.03E-05	0.009399321
Clec7a	14.97	-0.26	0.07	-3.92	8.84E-05	0.009399321
Mt3	812.04	-0.21	0.05	-3.91	9.08E-05	0.009399321
Ptger4	59.16	0.26	0.07	3.92	8.92E-05	0.009399321

Siglec5	8.85	-0.23	0.06	-3.92	8.96E-05	0.009399321
Atp9a	3181.68	0.08	0.02	3.91	9.29E-05	0.009485561
Nub1	1030.17	0.12	0.03	3.91	9.24E-05	0.009485561
Fam20c	307.36	-0.15	0.04	-3.90	9.45E-05	0.009572381
Htr3b	942.68	0.15	0.04	3.90	9.56E-05	0.009572381
Uba1	2699.44	0.12	0.03	3.90	9.57E-05	0.009572381
Gas1	31.97	-0.27	0.07	-3.89	9.85E-05	0.009797264
Pcdha4	1846.31	0.10	0.02	3.89	0.000100464	0.009923141
Sh3gl2	632.80	0.15	0.04	3.89	0.000101667	0.009977128
Hcls1	12.33	-0.24	0.06	-3.89	0.000102323	0.009977156
Fmo3	10.56	-0.23	0.06	-3.88	0.000103647	0.01004183
Timp2	2942.23	0.07	0.02	3.88	0.000105386	0.010145722
Chmp1a	759.95	0.15	0.04	3.87	0.000109559	0.010419349
Dcn	1855.98	-0.25	0.07	-3.87	0.000109924	0.010419349
Pacsin1	640.96	0.14	0.04	3.87	0.000110968	0.010419349
Reep3	231.99	-0.18	0.05	-3.87	0.000110391	0.010419349
Ncoa5	158.16	0.19	0.05	3.84	0.000121416	0.011330379
PCOLCE2	98.44	-0.23	0.06	-3.83	0.000129951	0.012052947
Chrna5	67.30	0.25	0.06	3.82	0.000131312	0.012105356
Adap1	959.27	0.13	0.03	3.82	0.000135221	0.012316473
Igf1	124.28	-0.25	0.07	-3.82	0.000134785	0.012316473
Fgfr3	5.92	-0.18	0.05	-3.81	0.000137973	0.012487957
Gpr34	12.69	-0.24	0.06	-3.81	0.000138746	0.012487957
Cacnb3	1924.72	0.08	0.02	3.81	0.000141292	0.012642348
Ctsb	9712.71	0.09	0.02	3.80	0.000146187	0.013003818
Dbnl	738.39	0.13	0.04	3.79	0.000149991	0.013081651
Gpc3	81.01	-0.27	0.07	-3.79	0.000151362	0.013081651
Hus1	129.94	0.27	0.07	3.79	0.000149627	0.013081651
Itgbl1	77.19	-0.26	0.07	-3.79	0.000150687	0.013081651
Tubb5	7343.34	0.10	0.03	3.79	0.000149527	0.013081651
Dync1i1	1821.31	0.12	0.03	3.78	0.000157395	0.013526179
Msi2	252.05	-0.19	0.05	-3.78	0.000159696	0.013627739
Tuba1a	7445.58	0.10	0.03	3.77	0.000160368	0.013627739
Ap3b2	1904.64	0.11	0.03	3.76	0.000172653	0.014590162
LOC498555	47.38	-0.26	0.07	-3.75	0.000174162	0.014636381
Btg1	167.72	-0.20	0.05	-3.75	0.000177679	0.014814773
Dazap2	660.06	-0.11	0.03	-3.75	0.000179926	0.014814773
Phf24	8550.95	0.13	0.03	3.75	0.000180181	0.014814773

Sgsh	16.84	-0.26	0.07	-3.75	0.000179233	0.014814773
Gpm6a	164.36	-0.20	0.05	-3.73	0.000188468	0.015412854
Pdgfra	117.43	-0.25	0.07	-3.73	0.000189484	0.015413019
Ehd3	2631.19	0.10	0.03	3.71	0.000203845	0.016347446
Mrvi1	35.64	-0.26	0.07	-3.71	0.000203315	0.016347446
Rusc1	1336.70	0.10	0.03	3.71	0.000204195	0.016347446
Sepp1	1194.71	-0.14	0.04	-3.71	0.000208449	0.016600588
Cox17	107.30	-0.22	0.06	-3.70	0.000211684	0.016770451
Wfs1	572.41	0.16	0.04	3.70	0.00021457	0.016911005
Epb41l3	7512.10	0.09	0.02	3.70	0.00021666	0.01696115
Gjb6	4.13	-0.13	0.04	-3.70	0.000217692	0.01696115
Mefv	14.48	-0.25	0.07	-3.70	0.000218551	0.01696115
Csrp1	807.87	-0.13	0.03	-3.68	0.000232155	0.017686342
Eif3c	1217.68	0.19	0.05	3.68	0.000232069	0.017686342
LOC102551963	9.03	-0.23	0.06	-3.68	0.000231393	0.017686342
Ptprc	32.75	-0.25	0.07	-3.68	0.000232547	0.017686342
Anpep	22.12	-0.24	0.06	-3.67	0.000238455	0.018045461
Rap1gds1	2682.87	0.10	0.03	3.67	0.000239879	0.018063329
Aif1l	96.66	-0.23	0.06	-3.67	0.000245697	0.018320072
Thbd	92.37	-0.25	0.07	-3.67	0.000245175	0.018320072
Thy1	9723.96	0.08	0.02	3.66	0.000250969	0.018621895
Ccr5	12.34	-0.22	0.06	-3.66	0.000252658	0.018656235
RT1-Da	88.58	-0.21	0.06	-3.66	0.000255579	0.018741362
Slc6a20	11.77	-0.19	0.05	-3.66	0.000256275	0.018741362
LOC102552895	35.69	-0.25	0.07	-3.65	0.000263952	0.019210368
Tns3	1062.46	-0.12	0.03	-3.64	0.000270935	0.019624722
Igfbp7	457.98	-0.22	0.06	-3.64	0.000276191	0.019910612
LOC108350698	33.91	-0.26	0.07	-3.63	0.000282537	0.020179186
Pcbp4	1639.42	0.08	0.02	3.63	0.00028257	0.020179186
Cpne4	814.18	0.16	0.04	3.63	0.000285637	0.020302919
Lhfp	150.45	-0.19	0.05	-3.62	0.000289712	0.020496812
Tnfrsf14	3.38	-0.14	0.04	-3.62	0.00029917	0.021067964
Kank2	158.16	-0.23	0.06	-3.61	0.000308462	0.021482727
Kcnh2	1164.78	0.12	0.03	3.61	0.000309297	0.021482727
Snurf	31.70	0.26	0.07	3.61	0.000307476	0.021482727
Aldh1a1	77.78	-0.25	0.07	-3.61	0.000310963	0.021500258
Cbx6	2025.98	0.08	0.02	3.60	0.000316119	0.021757872
Gfra1	1380.66	0.12	0.03	3.59	0.000326232	0.02219384

Hip1	520.43	0.14	0.04	3.59	0.000326344	0.02219384
Tubb2a	418.93	-0.20	0.06	-3.59	0.000326831	0.02219384
Il7	18.78	0.25	0.07	3.59	0.000335588	0.022586822
Wisp2	11.16	-0.22	0.06	-3.59	0.000335379	0.022586822
Micb	6.27	-0.16	0.05	-3.58	0.000337466	0.022613228
Maz	321.48	0.15	0.04	3.57	0.000354448	0.023458604
Sod3	321.66	-0.20	0.06	-3.57	0.000353158	0.023458604
Tnfsf13	21.26	-0.25	0.07	-3.57	0.000354709	0.023458604
Kif5c	4274.06	0.09	0.03	3.56	0.0003642	0.023982014
Bin2	8.94	-0.20	0.06	-3.56	0.000371793	0.02427612
Cd74	335.76	-0.22	0.06	-3.56	0.000376646	0.02427612
Dhcr24	1698.34	0.11	0.03	3.56	0.000374338	0.02427612
Eef1a2	5146.55	0.13	0.04	3.56	0.000373952	0.02427612
Zfand2a	359.31	0.15	0.04	3.56	0.000376551	0.02427612
Fam198b	87.62	-0.23	0.06	-3.55	0.000384433	0.024610964
Slc18a2	274.34	0.18	0.05	3.55	0.000385077	0.024610964
Dok4	1702.65	0.11	0.03	3.55	0.000387462	0.024659739
Ctnnal1	261.52	-0.19	0.05	-3.54	0.000395028	0.025012572
Parm1	1064.36	0.11	0.03	3.54	0.000396294	0.025012572
Hnrnpdl	433.89	-0.18	0.05	-3.54	0.000401094	0.025210891
Pecam1	34.94	-0.25	0.07	-3.54	0.000404365	0.025311899
Procr	9.52	-0.21	0.06	-3.54	0.00040694	0.025368715
Efemp1	222.75	-0.16	0.05	-3.53	0.000417368	0.0259126
Galnt18	417.09	0.16	0.05	3.53	0.0004219	0.026087456
Tex261	371.85	0.14	0.04	3.52	0.000424317	0.026130693
Aoc3	64.26	-0.24	0.07	-3.52	0.000431534	0.026467969
Jph4	831.56	0.12	0.03	3.52	0.000434144	0.026521151
Ap2a1	1653.37	0.11	0.03	3.52	0.000437732	0.026633339
Btbd2	873.69	0.10	0.03	3.51	0.000447706	0.027131703
Galnt14	372.29	0.15	0.04	3.51	0.000455238	0.027478668
Plscr4	122.45	-0.19	0.05	-3.49	0.00047656	0.028651982
Fads1	1127.51	-0.15	0.04	-3.49	0.000481853	0.028856175
Pkd2	91.75	-0.23	0.07	-3.49	0.00048414	0.028879443
Irf8	23.64	-0.24	0.07	-3.49	0.000487684	0.028963776
Rap1gap2	1251.65	0.09	0.03	3.49	0.000489362	0.028963776
C1s	116.38	-0.25	0.07	-3.48	0.000500974	0.029096289
Grb2	418.63	0.14	0.04	3.48	0.000497353	0.029096289
LOC108350419	8.61	0.18	0.05	3.48	0.000501165	0.029096289

Mrc2	54.97	-0.24	0.07	-3.48	0.000499151	0.029096289
Rnf20	476.83	0.12	0.04	3.48	0.000499186	0.029096289
Prdm6	11.55	-0.19	0.05	-3.47	0.000515774	0.02983059
LOC100911951	14.98	0.19	0.06	3.47	0.000522664	0.030114548
Itga4	22.43	-0.25	0.07	-3.46	0.000531056	0.030421252
Sh3bp5	74.68	-0.23	0.07	-3.46	0.000531987	0.030421252
Tpm2	40.74	-0.24	0.07	-3.46	0.000537161	0.030602093
Pip5k1c	1769.08	0.08	0.02	3.46	0.000546231	0.031002693
Tll1	118.83	-0.19	0.05	-3.45	0.000553761	0.031313224
Ctsk	40.63	-0.24	0.07	-3.45	0.000569846	0.032103441
LOC102553010	15.71	0.19	0.05	3.44	0.000578107	0.032448663
Lix1l	109.29	-0.20	0.06	-3.44	0.000590337	0.033013281
Bmp4	6.60	-0.16	0.05	-3.43	0.000596634	0.033243223
Tusc5	3773.07	0.09	0.03	3.43	0.000603912	0.033525944
Aebp1	151.42	-0.24	0.07	-3.43	0.00060619	0.03353003
Plk3	90.75	0.20	0.06	3.43	0.000611798	0.033717611
Arap3	173.20	-0.19	0.05	-3.42	0.000615587	0.03380397
Cntnap1	2337.69	0.11	0.03	3.42	0.000618169	0.033823622
Dync1li1	728.74	0.10	0.03	3.42	0.000624885	0.033826076
Entpd4	1521.23	0.11	0.03	3.42	0.000622918	0.033826076
Ndn	1334.53	0.09	0.03	3.42	0.000623759	0.033826076
Apba2	598.22	0.11	0.03	3.42	0.000630446	0.034006064
Mdk	58.52	-0.23	0.07	-3.41	0.000649342	0.034901544
Csf1r	111.93	-0.24	0.07	-3.40	0.000668721	0.035591326
Endod1	3760.70	0.06	0.02	3.40	0.000666978	0.035591326
Npm3	13.89	-0.23	0.07	-3.40	0.000669195	0.035591326
Adcyap1	354.47	0.18	0.05	3.40	0.000674485	0.035747713
Abcg1	626.83	0.13	0.04	3.40	0.000685162	0.036155839
Kcnab2	5760.23	0.09	0.03	3.39	0.00068694	0.036155839
Serping1	187.43	-0.24	0.07	-3.39	0.000693934	0.036272932
Sspn	74.64	-0.22	0.06	-3.39	0.000692966	0.036272932
LOC102549756	11.70	-0.22	0.06	-3.39	0.000696366	0.036275438
Ap2a2	2217.18	0.10	0.03	3.38	0.000714056	0.036475023
Col8a1	44.26	-0.24	0.07	-3.39	0.000708554	0.036475023
Golim4	580.36	-0.11	0.03	-3.39	0.000708068	0.036475023
Msr1	15.99	-0.23	0.07	-3.38	0.000716983	0.036475023
Ppef1	787.10	0.11	0.03	3.38	0.000715367	0.036475023
Rps10l1	79.40	0.22	0.07	3.38	0.000714251	0.036475023

Stx1a	169.28	0.18	0.05	3.39	0.000709378	0.036475023
Hspa12a	5167.49	0.08	0.02	3.38	0.00071967	0.036489681
LOC102546824	30.39	-0.24	0.07	-3.38	0.00073479	0.037132502
Il13ra2	8.68	-0.19	0.06	-3.37	0.000743638	0.037408465
Ndufa12	40.12	-0.24	0.07	-3.37	0.000747439	0.037408465
RT1-CE10	17.97	-0.24	0.07	-3.37	0.000747628	0.037408465
Fbn1	258.50	-0.23	0.07	-3.37	0.000762609	0.037908664
Vcp	3986.22	0.10	0.03	3.37	0.000760973	0.037908664
Cd37	13.72	-0.23	0.07	-3.36	0.000771147	0.037921772
Nrxn2	1601.13	0.10	0.03	3.36	0.000772845	0.037921772
Tgfbr3	284.16	-0.20	0.06	-3.36	0.000768281	0.037921772
Wars	1122.19	0.09	0.03	3.36	0.000768472	0.037921772
Kif3c	1583.47	0.10	0.03	3.36	0.000779465	0.0381236
Btbd3	714.18	0.10	0.03	3.36	0.000785483	0.038294807
Serpine2	368.97	-0.16	0.05	-3.36	0.000792353	0.038506312
Apba1	2044.17	0.12	0.04	3.35	0.000799126	0.03871179
Rnf125	115.34	0.19	0.06	3.35	0.000805932	0.038726985
Slc47a1	15.15	-0.19	0.06	-3.35	0.000806258	0.038726985
Soga3	1994.33	0.08	0.02	3.35	0.000807077	0.038726985
Ghdc	49.39	-0.21	0.06	-3.35	0.000812547	0.038854147
Tgfb3	161.56	-0.16	0.05	-3.35	0.000814836	0.038854147
Mmp2	128.66	-0.24	0.07	-3.35	0.000819962	0.038854962
Tm4sf1	50.07	-0.23	0.07	-3.35	0.000818572	0.038854962
Ndufab1	399.27	-0.13	0.04	-3.34	0.000835319	0.039459725
Cybb	31.18	-0.23	0.07	-3.34	0.00084936	0.039998804
Adam11	1787.04	0.12	0.04	3.33	0.000856418	0.040011372
Cyth4	26.60	-0.24	0.07	-3.33	0.000854038	0.040011372
Lyz2	687.31	-0.23	0.07	-3.33	0.000858949	0.040011372
Sytl3	100.62	0.19	0.06	3.33	0.000860148	0.040011372
Gm2a	206.52	-0.17	0.05	-3.33	0.000869243	0.04031116
Rpl15	408.77	-0.14	0.04	-3.33	0.000874646	0.040438426
Capn2	2128.08	0.09	0.03	3.33	0.000882778	0.04069073
Atf6b	401.81	0.11	0.03	3.32	0.000887319	0.04069211
Tmem164	418.73	0.13	0.04	3.32	0.000888159	0.04069211
Nacad	2090.19	0.10	0.03	3.32	0.000896163	0.04093552
Ebf2	38.66	-0.23	0.07	-3.32	0.000899613	0.04097011
C1qc	54.64	-0.23	0.07	-3.32	0.000912529	0.041338225
Caskin1	1520.99	0.09	0.03	3.32	0.000913132	0.041338225

LOC103693777	11.32	0.21	0.06	3.31	0.000926782	0.041831691
Dock10	323.50	-0.14	0.04	-3.30	0.000970244	0.042964195
Frmpd3	269.69	0.22	0.07	3.30	0.000969964	0.042964195
Gstm2	123.87	-0.21	0.06	-3.30	0.000963119	0.042964195
Shc1	651.21	0.11	0.03	3.30	0.000966656	0.042964195
Syngr3	1255.60	0.08	0.02	3.30	0.00095476	0.042964195
Uck2	227.20	0.17	0.05	3.30	0.000964586	0.042964195
Vasp	493.40	0.11	0.03	3.30	0.000971644	0.042964195
Robo2	1588.07	0.10	0.03	3.30	0.000977771	0.043109785
Tspan33	24.49	-0.23	0.07	-3.29	0.000986974	0.043389775
Drgx	566.22	0.10	0.03	3.29	0.001000957	0.043877688
Tubb3	19445.29	0.10	0.03	3.28	0.001023168	0.044722426
Cdkn1c	13.43	-0.20	0.06	-3.28	0.001028577	0.044830056
Sema5a	571.20	-0.15	0.05	-3.28	0.001056021	0.045894675
Egfr	47.50	-0.23	0.07	-3.27	0.001064706	0.046009218
Vash1	857.54	0.10	0.03	3.27	0.001061955	0.046009218
Slc15a2	68.46	-0.21	0.06	-3.27	0.001071871	0.046187628
Kcnc4	631.12	0.13	0.04	3.27	0.001081522	0.046471848
Prss23	30.65	-0.23	0.07	-3.27	0.001092028	0.046791085
Tlx3	310.92	0.20	0.06	3.26	0.001098396	0.046931742
Dnajc6	1233.34	0.08	0.03	3.26	0.001105699	0.047111456
Fermt3	19.72	-0.22	0.07	-3.26	0.001122654	0.047700241
Eef2	6659.86	0.07	0.02	3.26	0.001126204	0.04771778
Snx5	251.95	-0.14	0.04	-3.26	0.00113327	0.04784038
Vegfb	115.24	-0.20	0.06	-3.25	0.001135387	0.04784038
Foxp1	74.54	-0.19	0.06	-3.25	0.00115723	0.048358864
Gpm6b	2046.17	-0.10	0.03	-3.25	0.001152822	0.048358864
Pycard	7.37	-0.19	0.06	-3.25	0.001154686	0.048358864
Baiap2l1	284.59	0.16	0.05	3.25	0.001169296	0.048575089
Elk4	151.15	-0.19	0.06	-3.25	0.001171985	0.048575089
LOC108349640	76.04	-0.21	0.06	-3.25	0.001167315	0.048575089
Lilra5	8.74	-0.18	0.06	-3.24	0.001178076	0.048694866
Usp32	1386.40	0.08	0.02	3.24	0.001195532	0.049282497

Table S2.

All Differentially Expressed Genes CIBP ipsilateral v CIBP contralateral groups (adjusted p-value < 0.05).

	baseMean	log2FC	lfcSE	stat	pvalue	padj
Jun	598.75	0.22	0.04	6.09	1.16E-09	7.07E-06
Cct8	1463.93	-0.15	0.03	-5.27	1.35E-07	0.00041192
Hadhb	1299.22	-0.18	0.04	-5.04	4.67E-07	0.000948477
Cyb5a	280.47	-0.19	0.04	-4.82	1.41E-06	0.002155522
Sema6a	177.26	0.23	0.05	4.70	2.60E-06	0.003162963
Ncdn	5539.99	0.16	0.03	4.64	3.46E-06	0.003517996
Atp8b2	753.54	0.15	0.03	4.57	4.92E-06	0.00393556
Cog8	192.71	0.21	0.05	4.53	5.81E-06	0.00393556
Gak	614.06	0.14	0.03	4.54	5.64E-06	0.00393556
Syt3	446.15	0.16	0.03	4.49	6.97E-06	0.004250254
Dnajc6	1245.80	0.11	0.02	4.45	8.40E-06	0.004653279
Ankmy2	402.80	-0.16	0.04	-4.42	1.00E-05	0.00497701
Uba1	2744.22	0.13	0.03	4.40	1.06E-05	0.00497701
Bcap31	789.52	-0.14	0.03	-4.30	1.73E-05	0.007030491
Slc25a5	775.31	-0.19	0.05	-4.30	1.73E-05	0.007030491
Cdh19	699.14	-0.24	0.06	-4.26	2.02E-05	0.007708981
Nectin1	375.81	0.17	0.04	4.24	2.23E-05	0.008010638
Tmem176b	3867.91	-0.20	0.05	-4.20	2.70E-05	0.009143708
Acadm	442.68	-0.16	0.04	-4.13	3.69E-05	0.009629119
Clk1	298.78	-0.25	0.06	-4.12	3.79E-05	0.009629119
Mgst1	209.23	-0.20	0.05	-4.16	3.23E-05	0.009629119
Nrxn2	1623.09	0.12	0.03	4.12	3.75E-05	0.009629119
Tmem41b	465.10	-0.15	0.04	-4.15	3.37E-05	0.009629119
Tnpo2	1679.02	0.12	0.03	4.15	3.35E-05	0.009629119
Ankrd52	899.08	0.14	0.03	4.11	4.02E-05	0.009790213
Ap1b1	957.50	0.10	0.03	4.00	6.23E-05	0.01002875
Apoe	16794.39	-0.18	0.04	-4.02	5.83E-05	0.01002875
Btbd2	885.67	0.12	0.03	4.02	5.76E-05	0.01002875
Cbln2	433.96	0.15	0.04	4.00	6.42E-05	0.01002875
Copg1	2234.50	0.08	0.02	4.09	4.32E-05	0.01002875
Flii	908.35	0.14	0.03	4.05	5.23E-05	0.01002875
Galnt5	258.43	-0.18	0.04	-4.02	5.89E-05	0.01002875

Gfra1	1406.42	0.12	0.03	4.06	4.88E-05	0.01002875
Kcna1	1062.22	0.13	0.03	4.00	6.28E-05	0.01002875
Kif3c	1600.81	0.12	0.03	4.03	5.68E-05	0.01002875
Pabpc1	1151.61	0.10	0.02	4.00	6.33E-05	0.01002875
Sepp1	1235.94	-0.16	0.04	-4.07	4.61E-05	0.01002875
Stt3a	511.19	-0.16	0.04	-4.07	4.73E-05	0.01002875
Tbc1d9	957.39	0.13	0.03	4.05	5.23E-05	0.01002875
Itm2a	214.59	-0.23	0.06	-3.99	6.64E-05	0.010110271
Usp15	643.51	-0.14	0.04	-3.97	7.19E-05	0.010687727
Abhd2	1113.59	0.16	0.04	3.93	8.62E-05	0.011911635
Acer3	294.05	-0.16	0.04	-3.93	8.44E-05	0.011911635
Clip2	1508.04	0.11	0.03	3.94	8.21E-05	0.011911635
Copg2	854.09	-0.11	0.03	-3.92	8.80E-05	0.011911635
Elp2	564.99	-0.14	0.04	-3.90	9.60E-05	0.01271256
Oat	823.92	-0.18	0.05	-3.88	0.00010295	0.01334841
Kcnh1	294.66	0.16	0.04	3.86	0.000113409	0.01439817
Anapc4	377.71	-0.14	0.04	-3.85	0.00011841	0.014534585
Clpb	222.33	0.17	0.04	3.85	0.000119253	0.014534585
Dtymk	185.26	-0.18	0.05	-3.84	0.00012372	0.014677139
Pdp1	224.27	-0.19	0.05	-3.83	0.000127648	0.014677139
Tspan31	301.25	-0.18	0.05	-3.83	0.000127452	0.014677139
Copb2	305.41	-0.15	0.04	-3.80	0.000143815	0.016229792
LOC108348122	524.23	0.22	0.06	3.78	0.000156088	0.01729451
Kcnip1	382.36	-0.17	0.05	-3.77	0.000162419	0.017674622
Dync1i2	3358.77	-0.15	0.04	-3.75	0.000176403	0.017916657
Gap43	1424.52	0.11	0.03	3.75	0.00017469	0.017916657
Gba	808.50	0.12	0.03	3.76	0.00017153	0.017916657
Prpsap2	223.90	-0.17	0.04	-3.76	0.000168051	0.017916657
Pgm1	369.97	0.16	0.04	3.74	0.000183296	0.018111007
Rtn4rl1	786.99	0.11	0.03	3.74	0.00018426	0.018111007
Slc4a2	650.28	0.13	0.04	3.73	0.000191235	0.018498199
Exosc9	208.39	-0.18	0.05	-3.71	0.000203851	0.01933893
Fam65a	551.84	0.12	0.03	3.71	0.000209252	0.01933893
Mtch2	671.94	-0.13	0.04	-3.70	0.000213004	0.01933893
Rpl15	419.49	-0.15	0.04	-3.70	0.000215794	0.01933893
Rpl32	262.01	-0.16	0.04	-3.70	0.000212862	0.01933893
Enpp4	311.07	-0.14	0.04	-3.69	0.000221614	0.019572724
Gtf2i	1347.39	0.10	0.03	3.69	0.00022521	0.019606168

Cct4	1108.56	-0.12	0.03	-3.68	0.000232189	0.019652199
Pnmal2	367.11	0.15	0.04	3.68	0.000229698	0.019652199
LOC100294508	579.14	0.12	0.03	3.67	0.000239145	0.019963657
Antxr2	218.13	0.16	0.05	3.64	0.000270231	0.022253904
Ggta1	306.82	-0.15	0.04	-3.64	0.000277647	0.022559784
Mmd	163.50	0.16	0.05	3.61	0.000304849	0.024444069
Dynlrb1	854.14	-0.17	0.05	-3.60	0.000312297	0.02471608
Adgrb2	194.52	0.16	0.05	3.59	0.000326573	0.02496051
Pcmt1	1996.08	-0.13	0.04	-3.59	0.000329061	0.02496051
Rps4x	427.71	-0.16	0.04	-3.60	0.000321802	0.02496051
Vars	450.63	0.16	0.04	3.59	0.000331769	0.02496051
Prnp	4521.50	-0.09	0.03	-3.58	0.000343374	0.025518542
Ncoa1	559.83	0.13	0.04	3.56	0.000367512	0.026775581
Rufy3	3619.97	-0.07	0.02	-3.56	0.000369076	0.026775581
Ppef1	891.24	-0.15	0.04	-3.56	0.000373842	0.026802249
Bclaf1	735.82	-0.11	0.03	-3.54	0.000395773	0.027895035
Fam162a	411.37	-0.16	0.05	-3.54	0.000402176	0.027895035
Ube2o	2304.03	0.10	0.03	3.54	0.000402816	0.027895035
Wdr7	1404.16	0.11	0.03	3.53	0.000421353	0.028850879
Hace1	247.65	-0.15	0.04	-3.52	0.000436471	0.02955392
Vamp1	7065.98	-0.10	0.03	-3.50	0.000458202	0.03068446
Nploc4	812.17	0.13	0.04	3.50	0.000472246	0.031281168
Gpc1	1140.69	0.12	0.04	3.48	0.000495336	0.032457844
Timp2	2986.50	0.08	0.02	3.48	0.000504272	0.032691876
Grik1	906.29	-0.10	0.03	-3.47	0.000520558	0.033392431
Gnai3	500.25	-0.12	0.03	-3.46	0.000530957	0.033704693
RGD1565002	182.13	-0.16	0.05	-3.46	0.00054359	0.034150926
Inpp5j	333.84	0.14	0.04	3.45	0.000559888	0.034464187
Sar1a	630.08	-0.11	0.03	-3.45	0.0005585	0.034464187
Wdr1	1241.22	0.09	0.03	3.44	0.000581173	0.03514557
Zcchc18	1225.27	-0.13	0.04	-3.44	0.000582491	0.03514557
Rpl19	1196.31	-0.15	0.04	-3.43	0.000611093	0.036509802
Asmtl	189.67	-0.18	0.05	-3.42	0.000622315	0.036819279
Rtn1	4006.13	0.10	0.03	3.41	0.000648601	0.038005546
Anxa2	5996.61	-0.10	0.03	-3.37	0.00074515	0.038204787
Impact	589.47	-0.14	0.04	-3.39	0.000698063	0.038204787
LOC100912380	319.56	0.21	0.06	3.37	0.000748788	0.038204787
LOC361990	525.17	-0.11	0.03	-3.38	0.000726544	0.038204787

Man2a2	551.58	0.12	0.04	3.38	0.000712942	0.038204787
Mapk8ip3	4270.16	0.10	0.03	3.38	0.000712654	0.038204787
Mdh1	3257.29	-0.14	0.04	-3.39	0.000705942	0.038204787
Mt3	809.73	-0.15	0.05	-3.37	0.000746622	0.038204787
Ogfod1	184.93	0.15	0.04	3.37	0.000741749	0.038204787
Oxr1	2381.37	-0.10	0.03	-3.41	0.000658334	0.038204787
Rab11fip5	1206.56	0.10	0.03	3.39	0.000695025	0.038204787
Rap1gds1	2719.60	0.11	0.03	3.37	0.00075231	0.038204787
Rpl3	1592.63	-0.10	0.03	-3.39	0.000701919	0.038204787
Skiv2l	359.79	0.15	0.04	3.37	0.000741863	0.038204787
Smc6	261.42	-0.15	0.04	-3.38	0.000716497	0.038204787
Tmem184b	836.14	0.12	0.04	3.40	0.000674252	0.038204787
Dlg4	978.20	0.10	0.03	3.35	0.000803284	0.039477497
Eef2	6698.72	0.11	0.03	3.36	0.000788685	0.039477497
Gars	975.70	0.10	0.03	3.36	0.000791882	0.039477497
Prep	416.23	0.14	0.04	3.35	0.000798686	0.039477497
Pcsk2	652.29	0.12	0.04	3.35	0.000810903	0.039533139
Chd3	709.64	0.10	0.03	3.34	0.000826996	0.039682793
Eif4g1	603.05	0.14	0.04	3.34	0.000824397	0.039682793
Snx5	257.69	-0.14	0.04	-3.33	0.000862683	0.040753392
Ufsp2	259.88	-0.16	0.05	-3.33	0.000857507	0.040753392
Large1	1616.45	0.11	0.03	3.32	0.000886396	0.041234325
Mtss1	218.38	0.14	0.04	3.32	0.000885248	0.041234325
Fam160b1	216.08	0.16	0.05	3.32	0.000914568	0.041809591
Pcmtd2	188.82	-0.17	0.05	-3.31	0.000919344	0.041809591
Sdcbp	3613.18	-0.11	0.03	-3.32	0.000907525	0.041809591
Ctps2	378.91	-0.15	0.05	-3.30	0.000955001	0.042792475
Prkaa2	399.95	0.13	0.04	3.31	0.000949469	0.042792475
Dctn1	5260.16	0.11	0.03	3.30	0.000981981	0.043363695
Ube2e1	290.61	-0.14	0.04	-3.30	0.00097835	0.043363695
Atp6v0a1	1803.46	0.10	0.03	3.29	0.000992996	0.04353464
Ogdh	573.81	0.13	0.04	3.29	0.001001656	0.043544711
Polr2b	440.94	-0.15	0.05	-3.29	0.001008302	0.043544711
Trim44	249.10	0.15	0.04	3.29	0.001014662	0.043544711
Prkg1	162.35	0.16	0.05	3.28	0.001034484	0.04408494
Arhgef11	1115.67	0.10	0.03	3.28	0.00104469	0.0442107
Actb	6600.84	0.11	0.03	3.25	0.001144738	0.044731856
Atp13a1	237.23	0.15	0.05	3.24	0.001175893	0.044731856

Cic	1250.48	0.09	0.03	3.26	0.001100929	0.044731856
Coro2b	1300.66	0.09	0.03	3.25	0.001148686	0.044731856
Dagla	723.18	0.11	0.03	3.25	0.001136191	0.044731856
Eif3i	289.87	-0.14	0.04	-3.26	0.001110418	0.044731856
Eny2	300.79	-0.15	0.04	-3.25	0.001153939	0.044731856
Mapk8ip2	2259.16	0.11	0.03	3.25	0.001171815	0.044731856
Nsf	3222.00	0.11	0.03	3.26	0.00111656	0.044731856
RGD1305455	446.33	0.11	0.03	3.24	0.00118179	0.044731856
Rph3a	2720.38	0.11	0.03	3.25	0.001172337	0.044731856
Rpl7l1	300.55	-0.15	0.05	-3.26	0.001130887	0.044731856
Serinc3	2003.54	-0.07	0.02	-3.24	0.001179647	0.044731856
Sidt2	479.54	0.13	0.04	3.25	0.001168329	0.044731856
Steap3	429.80	0.12	0.04	3.25	0.001145118	0.044731856
Suclg1	798.11	-0.12	0.04	-3.25	0.001161184	0.044731856
Tbce	406.42	-0.17	0.05	-3.25	0.0011524	0.044731856
Atxn2	469.50	0.11	0.03	3.24	0.001205322	0.045340938
Cyp51	1835.45	-0.09	0.03	-3.23	0.001219223	0.045582497
Adar	532.54	0.12	0.04	3.22	0.00127751	0.046898462
Clcn7	289.65	0.13	0.04	3.22	0.001277159	0.046898462
Derl1	284.84	-0.14	0.04	-3.22	0.001272796	0.046898462
Cmip	966.73	0.11	0.03	3.21	0.001312326	0.047459376
Parm1	1082.69	0.11	0.03	3.22	0.001304393	0.047459376
Sumo1	369.35	-0.17	0.05	-3.21	0.001316153	0.047459376
Plcd4	476.72	-0.15	0.05	-3.21	0.001340239	0.048043614
Bzw1	1097.77	-0.11	0.03	-3.20	0.001382667	0.048425122
Nacad	2129.22	0.10	0.03	3.20	0.00136964	0.048425122
Robo2	1630.02	0.08	0.02	3.20	0.001374809	0.048425122
Slc24a2	4501.36	0.10	0.03	3.20	0.001375269	0.048425122
Nrn1	1589.97	-0.11	0.03	-3.19	0.001412686	0.04919378
Ddx3x	2794.94	-0.11	0.03	-3.19	0.001434334	0.04959624
Tbc1d9b	1501.78	0.10	0.03	3.19	0.001440521	0.04959624

CHAPTER 5: Summary and Future Directions

Summary

The work presented in this dissertation addresses important approaches to pain research and has made important contributions that allow a better understanding of cancer pain and more effective future therapies. The literature cited below contributed to the fundamental hypothesis that was investigated in this dissertation:

Sharma MK, Seidlitz EP, Singh G. Cancer cells release glutamate via the cystine/glutamate antiporter. Biochem. Biophys. Res. Commun. 2010;391:91–5.

Ungard RG, Seidlitz EP, Singh G. Inhibition of breast cancer-cell glutamate release with sulfasalazine limits cancer-induced bone pain. Pain 2014;155:28–36.

Dableh LJ, Henry JL. Progesterone prevents development of neuropathic pain in a rat model: Timing and duration of treatment are critical. J. Pain Res. 2011;4:91–101.

Sorge RE, Mapplebeck JCS, Rosen S, Beggs S, Taves S, Alexander JK, Martin LJ, Austin J-S, Sotocinal SG, Chen D, Yang M, Shi XQ, Huang H, Pillon NJ, Bilan PJ, Tu Y, Klip A, Ji R-R, Zhang J, Salter MW, Mogil JS. Different immune cells mediate mechanical pain hypersensitivity in male and female mice. Nat. Neurosci. 2015;18:1081–3.

Mantyh WG, Jimenez-Andrade JM, Stake JI, Bloom AP, Kaczmarska MJ, Taylor RN, Freeman KT, Ghilardi JR, Kuskowski MA, Mantyh PW. Blockade of nerve sprouting and neuroma formation markedly attenuates the development of late stage cancer pain. Neuroscience 2010;171:588–598.

Nashed MG, Linher-Melville K, Frey BN, Singh G. RNA-sequencing profiles hippocampal gene expression in a validated model of cancer-induced depression. Genes, Brain Behav. 2016;15:711–721.

Therefore, I hypothesized:

> *Cancer-induced bone pain is a unique pain state that shares features with but is distinct from neuropathic and inflammatory pain states, and that is generated and maintained by the direct effects of cancer cells on their metastatic microenvironment, including unique signalling properties and gene expression changes in sensory neurons and associated cells.*

This hypothesis was investigated through three distinct objectives, which will be discussed in the context of the papers presented in the previous chapters.

Objective 1: *Establish and investigate the impact of genetic knock-down of xCT in human cancer cells on cancer-induced bone pain.*

This work builds on the findings from our lab and others that pharmacological inhibition of system xC- in mouse models induces a reduction and delay to onset of cancer pain-related behaviour (Ungard et al. 2014; Slosky et al. 2016; Fazzari et al. 2017). Targeting features of the cancer cell may spare the broad side effects of centrally-acting analgesics and have the added benefit of potentially compromising cancer cell growth and survival itself. In particular, we are targeting cancer cell-derived glutamate, which has been demonstrated to directly activate and sensitize primary afferent nociceptors in musculoskeletal tissues (Cairns et al. 2002). Glutamate is recognized as a critical intercellular signalling molecule in bone and is used extensively by osteoblasts, osteoclasts, and osteocyte cells for their normal functions (Takarada and Yoneda 2008; Seidlitz et al. 2010; Skerry). Disruption of glutamatergic signalling in bone cells has been shown to influence cell differentiation (Peet et al. 1999; Merle et al. 2003) and functions (Itzstein et al. 2000; Taylor 2002; Seidlitz et al. 2010), although a definitive model of these interactions has yet to be produced. Disrupted bone cell metabolism and signalling is a feature of bone metastases, often resulting in the development of pathological and painful alterations of bone resorption and apposition (Orr et al. 2000).

Creating and testing a model of xCT knockdown cancer cells allows this potentially therapeutic target to be evaluated in the context of CIBP with more precision than pharmacological approaches. To do so we developed two shRNA-mediated xCT (SLC7A11) knockdown cell lines in the human breast adenocarcinoma cell line MDA-MB-231; a stable clone and an IPTG-inducible clone, and respective negative controls. The stable clone was validated in vitro and successfully implanted in our established intrafemoral mouse model of CIBP and evaluated for pain-related behaviour as described in the published study included in **Chapter 2**. Our findings demonstrated the validity of our cell line and that despite no discerned changes in tumour growth, the time to onset of pain-related behaviour was extended in mice implanted with the xCT knockdown cell line as opposed to vector-control mice.

Our IPTG-inducible clone in MDA-MB-231 was similarly validated in vitro and subcutaneously in vivo, and then tested in the same intrafemoral mouse model of CIBP for pain-related behaviour relative to an uninduced control group, however insufficient numbers of mice successfully grew and retained tumours to draw conclusions from our data. The methodology and results of this investigation are presented in **Appendix 3**.

Objective 2: *Investigate the impact of the neuroprotective treatments progesterone and pregabalin on neuropathic pain and cancer-induced bone pain.*

It has been established that chronic pain states can become a pathology of the nervous system, even if their initiating insults are removed. Metastatic cancers can sensitize, invade, and destroy peripheral neuronal tissues, and neuropathic pain signaling develops in addition to the nociceptive pain of a tumour in bone. Thus, treatments that prevent pathological neuronal signaling and subsequent changes in nociceptive circuits may prevent the progression of cancer pain to an intractable state.

Both progesterone and pregabalin have demonstrated neuroprotective properties and utility in some models neurological disease states, through mechanisms associated with inhibition of voltage gated calcium channels (Luoma et al. 2011 Mar; Verma et al. 2014). Treatment with progesterone has been shown to reduce excitotoxic cell death, de-myelination, and reduction of neuronal inflammation and edema, all which feature in the generation of ectopic signaling characteristic of neuropathic pain (Finnerup and Jensen 2007; Verma et al. 2014). Pregabalin is used as a first-line clinical therapy for neuropathic pain, however its evidence of effectiveness is inconsistent (Gong et al. 2001; Ha et al. 2008). The reported effects of PRO and PRE on cancer cell growth are also inconsistent.

We investigated the utility of the experimental neuroprotective compounds progesterone and pregabalin to reduce or prevent the development of neuropathic pain and CIBP in animal models as described in the published study included in **Chapter 3**. As these treatments had not been tested in models of cancer pain or in female rats, we included groups of both sexes in models of each disease. We chose to utilize a rat model of MRMT-1 breast cancer-induced CIBP and a rat model of sciatic-cuff induced neuropathic pain in order to accommodate the use in intracellular in vivo electrophysiology to record the membrane properties of DRG neurons. Our results showed striking sex and model effects in the behavioural and electrophysiological responses to treatment in both pain states. Pregabalin and progesterone induced robust recoveries in male models of neuropathic pain, while females showed a lesser response and models of CIBP largely did not demonstrate behavioural responses to treatment, despite clear electrophysiological changes in pregabilin-treated male models of CIBP. Applying a T-cell deficient rat model of neuropathic pain did not indicate any clear reliance on microglia or T-cells that would explain the sex differences observed here.

Objective 3: *Investigate gene expression by mRNA selective RNA-Sequencing of dorsal root ganglia isolated from a model of cancer-induced bone pain.*

Chronic pain states including cancer pain initiate pathological changes in the peripheral nervous system that can contribute to the genesis and maintenance of those pain states. DRGs from animal models of neuropathic and inflammatory pain have been evaluated by RNA-Seq to evaluate changes in gene expression (Perkins et al. 2014; Zhang et al. 2015; Wu et al. 2016; Stephens et al. 2018; Stephens et al. 2019), however the global gene expression profile of DRGs innervating a painful tumour environment had not yet been investigated prior to our study.

As described in the study included in **Chapter 4**, we have investigated the mRNA expression profile of DRGs containing satellite glial cells, immune cells and sensory afferent neurons that innervate the limb of a rat model of intrafemoral cancer-induced bone pain in by RNA-seq. Ipsilateral and contralateral L3-6 DRGs were isolated from rat CIBP models and Sham-surgery negative controls, and differentially-expressed genes were determined by mRNA-specific RNA-Seq. Our analysis revealed differentially expressed genes (DEGs) between two comparisons: ipsilateral CIBP vs. Sham groups, and ipsilateral vs contralateral CIBP. Some but not all DEGs from both comparisons had also been observed to be differentially expressed in gene expression studies of other painful conditions, suggesting that there may be gene targets in our sample that are unique to CIBP. However, some targets in this sample are certain to be unrelated to pain, and possibly a result of other effects of cancer. Functional testing is required to ascertain the role of any particular transcript in CIBP signalling.

These results will be archived online and comparable to other gene expression profiles to elucidate distinctions between mRNA expression profiles of different pain states, and as a resource for target validation from other hypothesis-driven investigations.

Future Directions

The role of the system xC- cystine/glutamate transporter in cancer pain has been clarified through the model developed and applied to CIBP in **Chapter 2**. This transporter is now clearly a therapeutic target of value in the search for novel, mechanism-based, non-opioid therapeutics in the treatment of cancer pain. In addition, system xC- and xCT are targets of interest in oncology, particularly in glioma (Robert et al. 2015), drug addiction (Kau et al. 2008), epilepsy and neurodegenerative disease (Massie et al. 2008). To date, the only two clinical studies that have evaluated targeting system xC- (ISRCTN45828668 and NCT01577966) which evaluated seizure relief in glioma patients, used sulfasalazine which the authors argue contributed to limited findings, side-effects, and early termination of the first study (Robe et al. 2009; Robert et al. 2015). As such, new methods of silencing xCT or inhibiting the function of system xC- cystine/glutamate transport are critical to furthering the development of this therapeutic target. Our lab has undertaken several efforts in this area, including a promising study targeting upstream glutaminase activity in cancer cells, thereby limiting glutamate release by system xC- (Fazzari and Singh 2019). In addition, we undertook efforts to identify new pharmacological inhibitors of glutamate release from breast cancer cells by high-throughput screen of a library of 30,000 compounds (Fazzari et al. 2015). This led to the follow-up investigation on a candidate compound capsazepine, previously described as an inhibitor of TRPV1, which we established to also be an inhibitor of system xC- cystine/glutamate transport, and to show efficacy in reducing CIBP in a mouse model (Fazzari et al. 2017).

Other groups have also undertaken efforts to identify or develop new inhibitors of system xC- (Shukla et al. 2011; Newell et al.) although it is not apparent that any candidates from these studies have been tested further in pre-clinical functional investigations. It is important that the investigation and development of novel inhibitors of system xC- continues. The therapeutic potential is clear, and further investigation is primarily limited by a lack of drug candidates.

Our study presented in **Chapter 3** revealed evidence of a mechanistically unclear divergence of the electrophysiological and behavioural response to treatment with pregabalin and progesterone between rat models of CIBP and neuropathic pain. In addition, there was also a marked and unexplained sexual dimorphism in the responses of both models to treatment. The divergence between models of pain is further evidence of the uniqueness of CIBP as a pain state, and demonstrative of a need to evaluate potential pain therapies in specific and accurate pre-clinical models.

Current research around sex differences in pain has largely focussed on differential actions of the female and male neuroimmune systems where microglia have been shown to perpetuate chronic neuropathic and inflammatory pain states in male rats and mice, but not in females. In female animals peripheral T-cells that have infiltrated the spinal cord have demonstrated a role in maintaining chronic pain (Sorge et al. 2015). Utilizing T-cell deficient animal models of pain has allowed some investigators to readily observe the important role that these immune cells play in chronic pain in females, however we did not observe that in our RNU -/- model. Other mechanisms of sex differences are rapidly accumulating, although there is by no means a cohesive model of these effects.

Future work from this project should focus on elucidating the mechanisms of model and sex differences observed here. The most productive avenue is to establish the mechanism of efficacy in male rat models of neuropathic pain, particularly whether the progesterone and pregabalin are acting as hypothesized, as an antagonist of P/Q, N, and L-type voltage gated calcium channels on sensory neurons to confer a neuroprotective action (Ha et al. 2008; Luoma et al. 2011 Mar). To do so, both drugs should be tested for excitotoxicity in vitro in dissociated cultures of sensory DRG neurons exposed to a depolarizing environment. Including positive drug controls for voltage-gated calcium channel inhibition would allow determination if there is an effect on neuronal cell death in these neuron populations. In addition, dissociated neuron cultures incubated with fluorescent Ca^{2+} indicators and recorded under microscopy would indicate intracellular Ca^{2+} flux by, further elucidating the link between any neuroprotective effects of progesterone and pregabalin and Ca^{2+} channels in peripheral sensory neurons.

The differential gene expression in rat models of CIBP presented in **Chapter 4** is already an important resource for reference and hypothesis generation. However the targets identified here require follow-up with functional interventional experimentation to determine their validity as true markers of CIBP and if they hold therapeutic potential. These investigations would begin with confirming by qPCR the differential expression seen here in DRG tissues from other CIBP models and measuring whether these transcript-level changes correspond with changes in protein level. Following those conformational steps, experimentation directly targeting a gene or protein can be undertaken. We have identified several promising targets from this data for further study including Fam150b, Vgf, and STXBP1.

In addition, further hypothesis-generating investigation of gene expression by RNA-Seq is warranted in other animal models of cancer pain and CIBP. This should be undertaken in peripheral nervous tissues as was done here, and in the central nervous system and other tissues of interest including the immediate tumour microenvironment. Utilizing a greater sequencing depth than 50 bp as was done in our investigation would allow investigators to identify isoforms and gene-splicing events. In addition, more precise identification of cell-type could be advantageous to future sequencing projects. Depending on the intended application of data, these approaches would include single cell RNA-Seq on micro-dissected samples from tissue, and bulk sequencing on cell or tissue samples dissociated and sorted by flow-cytometry to identify specific cell-types based on markers.

Finally, performing RNA-Seq in male rat models of CIBP is essential to the determination of whether the DEGs identified here represent sex-specific features, or if they are generalizable between sexes. These experiments can and should be undertaken with the same Sprague-Dawley rat model of MRMT-1 breast CIBP as was utilized here.

Conclusion

The studies detailed in this dissertation utilize distinct and essential approaches to researching the pathology of cancer pain. This work supports the conceptualization of cancer-induced bone pain as a unique pain state with a multitude of contributing mechanisms including the direct effects of cancer cells on their host tissue, unique patterns of sensory neuronal signalling, and gene expression changes in sensory neurons and associated cells. The findings presented here make important contributions to better understanding and treating cancer pain.

Reference List

Bloom AP, Jimenez-Andrade JM, Taylor RN, Castañeda-Corral G, Kaczmarska MJ, Freeman KT, Coughlin KA, Ghilardi JR, Kuskowski MA, Mantyh PW. 2011. Breast cancer-induced bone remodeling, skeletal pain, and sprouting of sensory nerve fibers. J Pain. 12(6):698–711. doi:10.1016/j.jpain.2010.12.016.

Buckingham SC, Campbell SL, Haas BR, Montana V, Robel S, Ogunrinu T, Sontheimer H. 2011. Glutamate release by primary brain tumors induces epileptic activity. Nat Med. 17(10):1269–74. doi:10.1038/nm.2453.

Cain DM, Wacnik PW, Turner M, Wendelschafer-Crabb G, Kennedy WR, Wilcox GL, Simone DA. 2001. Functional interactions between tumor and peripheral nerve: changes in excitability and morphology of primary afferent fibers in a murine model of cancer pain. J Neurosci. 21(23):9367–76.

Cairns BE, Gambarota G, Svensson P, Arendt-Nielsen L, Berde CB. 2002. Glutamate-induced sensitization of rat masseter muscle fibers. Neuroscience. 109(2):389–99.

Chen J, Chopp M, Li Y. 1999. Neuroprotective effects of progesterone after transient middle cerebral artery occlusion in rat. J Neurol Sci. 171(1):24–30.

Chung WJ, Lyons SA, Nelson GM, Hamza H, Gladson CL, Gillespie GY, Sontheimer H. 2005. Inhibition of cystine uptake disrupts the growth of primary brain tumors. J Neurosci. 25(31):7101–10. doi:10.1523/JNEUROSCI.5258-04.2005.

Donovan-Rodriguez T, Dickenson AH, Urch CE. 2004. Superficial dorsal horn neuronal responses and the emergence of behavioural hyperalgesia in a rat model of cancer-induced bone pain. Neurosci Lett. 360(1–2):29–32. doi:10.1016/j.neulet.2004.01.048.

Fazzari J, Balenko M, Zacal N, Singh G. 2017. Identification of capsazepine as a novel inhibitor of system xc− and cancer-induced bone pain. J Pain Res. Volume 10:915–925. doi:10.2147/JPR.S125045.

Fazzari J, Lin H, Murphy C, Ungard R, Singh G. 2015. Inhibitors of glutamate release from breast cancer cells; New targets for cancer-induced bone-pain. Sci Rep. 5. doi:10.1038/srep08380.

Fazzari J, Singh G. 2019. Effect of glutaminase inhibition on cancer-induced bone pain. Breast Cancer Targets Ther. 11:273–282. doi:10.2147/BCTT.S215655.

Finnerup NB, Jensen TS. 2007. Clinical use of pregabalin in the management of central neuropathic pain. Neuropsychiatr Dis Treat. 3(6):885–91.

Gibson CL, Murphy SP. 2004. Progesterone Enhances Functional Recovery After Middle Cerebral Artery Occlusion in Male Mice. J Cereb Blood Flow Metab. 24(7):805–813. doi:10.1097/01.WCB.0000125365.83980.00.

Gong HC, Hang J, Kohler W, Li L, Su TZ. 2001. Tissue-specific expression and gabapentin-binding properties of calcium channel alpha2delta subunit subtypes. J Membr Biol. 184(1):35–43.

Ha K-Y, Kim Y-H, Rhyu K-W, Kwon S-E. 2008. Pregabalin as a neuroprotector after spinal cord injury in rats. Eur Spine J. 17(6):864–72. doi:10.1007/s00586-008-0653-6.

Hu G, Huang K, Hu Y, Du G, Xue Z, Zhu X, Fan G. 2016. Single-cell RNA-seq reveals distinct injury responses in different types of DRG sensory neurons. Sci Rep. 6(1):1–11. doi:10.1038/srep31851.

Itzstein C, Espinosa L, Delmas PD, Chenu C. 2000. Specific Antagonists of NMDA Receptors Prevent Osteoclast Sealing Zone Formation Required for Bone Resorption. Biochem Biophys Res Commun. 268(1):201–209. doi:10.1006/bbrc.2000.2097.

Kau KS, Madayag A, Mantsch JR, Grier MD, Abdulhameed O, Baker DA. 2008. Blunted cystine-glutamate antiporter function in the nucleus accumbens promotes cocaine-induced drug seeking. Neuroscience. 155(2):530–537. doi:10.1016/j.neuroscience.2008.06.010.

Khasabov SG, Hamamoto DT, Harding-Rose C, Simone DA. 2007. Tumor-evoked hyperalgesia and sensitization of nociceptive dorsal horn neurons in a murine model of cancer pain. Brain Res. 1180:7–19. doi:10.1016/j.brainres.2007.08.075.

Lopes DM, Malek N, Edye M, Jager SB, McMurray S, McMahon SB, Denk F. 2017. Sex differences in peripheral not central immune responses to pain-inducing injury. Sci Rep. 7(1):16460. doi:10.1038/s41598-017-16664-z.

Luoma JI, Kelley BG, Mermelstein PG. 2011 Mar. Progesterone inhibition of voltage-gated calcium channels is a potential neuroprotective mechanism against excitotoxicity. Steroids. doi:10.1016/j.steroids.2011.02.013.

Massie A, Schallier A, Mertens B, Vermoesen K, Bannai S, Sato H, Smolders I, Michotte Y. 2008. Time-dependent changes in striatal xCT protein expression in hemi-Parkinson rats. Neuroreport. 19(16):1589–92. doi:10.1097/WNR.0b013e328312181c.

Merle B, Itzstein C, Delmas PD, Chenu C. 2003. NMDA glutamate receptors are expressed by osteoclast precursors and involved in the regulation of osteoclastogenesis. J Cell Biochem. 90(2):424–36. doi:10.1002/jcb.10625.

Newell JL, Keyari CM, McDaniel SW, Diaz PJ, Natale NR, Patel SA, Bridges RJ. Novel di-aryl-substituted isoxazoles act as noncompetitive inhibitors of the system xc-cystine/glutamate exchanger. Neuroch Int. 73:132–138.

Orr FW, Lee J, Duivenvoorden WC, Singh G. 2000. Pathophysiologic interactions in skeletal metastasis. Cancer. 88(12 Suppl):2912–8.

Ozacmak VH, Sayan H. 2009. The effects of 17beta estradiol, 17alpha estradiol and progesterone on oxidative stress biomarkers in ovariectomized female rat brain subjected to global cerebral ischemia. Physiol Res. 58(6):909–12.

Peet NM, Grabowski PS, Laketic-Ljubojevic I, Skerry TM. 1999. The glutamate receptor antagonist MK801 modulates bone resorption in vitro by a mechanism predominantly involving osteoclast differentiation. FASEB J. 13(15):2179–85.

Perkins JR, Antunes-Martins A, Calvo M, Grist J, Rust W, Schmid R, Hildebrandt T, Kohl M, Orengo C, McMahon SB, et al. 2014. A comparison of RNA-seq and exon arrays for whole genome transcription profiling of the L5 spinal nerve transection model of neuropathic pain in the rat. Mol Pain. 10:7. doi:10.1186/1744-8069-10-7.

Peters CM, Ghilardi JR, Keyser CP, Kubota K, Lindsay TH, Luger NM, Mach DB, Schwei MJ, Sevcik MA, Mantyh PW. 2005. Tumor-induced injury of primary afferent sensory nerve fibers in bone cancer pain. Exp Neurol. 193(1):85–100. doi:10.1016/j.expneurol.2004.11.028.

Ray P, Torck A, Quigley L, Wangzhou A, Neiman M, Rao C, Lam T, Kim J-Y, Kim TH, Zhang MQ, et al. 2018. Comparative transcriptome profiling of the human and mouse dorsal root ganglia. Pain. 159(7):1325–1345. doi:10.1097/j.pain.0000000000001217.

Robe PA, Martin DH, Nguyen-Khac MT, Artesi M, Deprez M, Albert A, Vanbelle S, Califice S, Bredel M, Bours V. 2009. Early termination of ISRCTN45828668, a phase 1/2 prospective, randomized study of sulfasalazine for the treatment of progressing malignant gliomas in adults. BMC Cancer. 9:372. doi:10.1186/1471-2407-9-372.

Robert SM, Buckingham SC, Campbell SL, Robel S, Holt KT, Ogunrinu-Babarinde T, Warren PP, White DM, Reid MA, Eschbacher JM, et al. 2015. SLC7A11 expression is associated with seizures and predicts poor survival in patients with malignant glioma. Sci Transl Med. 7(289):289ra86. doi:10.1126/scitranslmed.aaa8103.

Schwei MJ, Honore P, Rogers SD, Salak-Johnson JL, Finke MP, Ramnaraine ML, Clohisy DR, Mantyh PW. 1999. Neurochemical and cellular reorganization of the spinal cord in a murine model of bone cancer pain. J Neurosci. 19(24):10886–97.

Seidlitz EP, Sharma MK, Singh G. 2010. Extracellular glutamate alters mature osteoclast and osteoblast functions. Can J Physiol Pharmacol. 88(9):929–36. doi:10.1139/y10-070.

Shukla K, Thomas AG, Ferraris D V., Hin N, Sattler R, Alt J, Rojas C, Slusher BS, Tsukamoto T. 2011. Inhibition of x c - Transporter-mediated cystine uptake by

sulfasalazine analogs. Bioorganic Med Chem Lett. 21(20):6184–6187. doi:10.1016/j.bmcl.2011.07.081.

Skerry TM. The role of glutamate in the regulation of bone mass and architecture. J Musculoskelet Neuronal Interact. 8(2):166–73.

Slosky LM, BassiriRad NM, Symons AM, Thompson M, Doyle T, Forte BL, Staatz WD, Bui L, Neumann WL, Mantyh PW, et al. 2016. The cystine/glutamate antiporter system xc− drives breast tumor cell glutamate release and cancer-induced bone pain. Pain. 157(11):2605–2616. doi:10.1097/j.pain.0000000000000681.

Sorge RE, Mapplebeck JCS, Rosen S, Beggs S, Taves S, Alexander JK, Martin LJ, Austin J-S, Sotocinal SG, Chen D, et al. 2015. Different immune cells mediate mechanical pain hypersensitivity in male and female mice. Nat Neurosci. 18(8):1081–3. doi:10.1038/nn.4053.

Stephens KE, Chen Z, Sivanesan E, Raja SN, Linderoth B, Taverna SD, Guan Y. 2018. RNA-seq of spinal cord from nerve-injured rats after spinal cord stimulation. Mol Pain. 14:1744806918817429. doi:10.1177/1744806918817429.

Stephens KE, Zhou W, Ji Z, Chen Z, He S, Ji H, Guan Y, Taverna SD. 2019. Sex differences in gene regulation in the dorsal root ganglion after nerve injury. BMC Genomics. 20(1):147. doi:10.1186/s12864-019-5512-9.

Takarada T, Yoneda Y. 2008. Pharmacological topics of bone metabolism: glutamate as a signal mediator in bone. J Pharmacol Sci. 106(4):536–41.

Taylor AF. 2002. Osteoblastic glutamate receptor function regulates bone formation and resorption. J Musculoskelet Neuronal Interact. 2(3):285–90.

Ungard RG, Seidlitz EP, Singh G. 2014. Inhibition of breast cancer-cell glutamate release with sulfasalazine limits cancer-induced bone pain. Pain. 155(1). doi:10.1016/j.pain.2013.08.030.

Urch CE, Donovan-Rodriguez T, Dickenson AH. 2003. Alterations in dorsal horn neurones in a rat model of cancer-induced bone pain. Pain. 106(3):347–56.

Verma V, Singh N, Singh Jaggi A. 2014. Pregabalin in neuropathic pain: evidences and possible mechanisms. Curr Neuropharmacol. 12(1):44–56. doi:10.2174/1570159X1201140117162802.

Wang J, Jiang C, Liu C, Li X, Chen N, Hao Y. 2010. Neuroprotective effects of progesterone following stroke in aged rats. Behav Brain Res. 209(1):119–122. doi:10.1016/j.bbr.2010.01.026.

Wright DW, Kellermann AL, Hertzberg VS, Clark PL, Frankel M, Goldstein FC, Salomone JP, Dent LL, Harris OA, Ander DS, et al. 2007. ProTECT: A Randomized Clinical Trial of Progesterone for Acute Traumatic Brain Injury. Ann Emerg Med. 49(4):391-402.e2. doi:10.1016/j.annemergmed.2006.07.932.

Wu S, Marie Lutz B, Miao X, Liang L, Mo K, Chang Y-J, Du P, Soteropoulos P, Tian B, Kaufman AG, et al. 2016. Dorsal root ganglion transcriptome analysis following peripheral nerve injury in mice. Mol Pain. 12. doi:10.1177/1744806916629048.

Xiao G, Wei J, Wu Z, Wang W, Jiang Q, Cheng J, Lu F, Wu J, Xu H, Fang R. 2007. [Clinical study on the therapeutic effects and mechanism of progesterone in the treatment for acute severe head injury]. Zhonghua Wai Ke Za Zhi. 45(2):106–8.

Xiao G, Wei J, Yan W, Wang W, Lu Z. 2008. Improved outcomes from the administration of progesterone for patients with acute severe traumatic brain injury: a randomized controlled trial. Crit Care. 12(2):R61. doi:10.1186/cc6887.

Zhang Y, Laumet G, Chen S-R, Hittelman WN, Pan H-L. 2015. Pannexin-1 Up-regulation in the Dorsal Root Ganglion Contributes to Neuropathic Pain Development. J Biol Chem. 290(23):14647–55. doi:10.1074/jbc.M115.650218.

Zhao J, Pan H-L, Li T-T, Zhang Y-Q, Wei J-Y, Zhao Z-Q. 2010. The sensitization of peripheral C-fibers to lysophosphatidic acid in bone cancer pain. Life Sci. 87(3–4):120–5. doi:10.1016/j.lfs.2010.05.015.

Zheng Q, Fang D, Cai J, Wan Y, Han J-S, Xing G-G. 2012. Enhanced excitability of small dorsal root ganglion neurons in rats with bone cancer pain. Mol Pain. 8:24. doi:10.1186/1744-8069-8-24.

Zhu YF, Kwiecien JM, Dabrowski W, Ungard R, Zhu KL, Huizinga JD, Henry JL, Singh G. 2018. Cancer pain and neuropathic pain are associated with A β sensory neuronal plasticity in dorsal root ganglia and abnormal sprouting in lumbar spinal cord. Mol Pain. 14. doi:10.1177/1744806918810099.

APPENDIX 1

Springer Copyright License

SPRINGER NATURE LICENSE TERMS AND CONDITIONS

Feb 12, 2020

This Agreement between McMaster University ("You") and Springer Nature ("Springer Nature") consists of your license details and the terms and conditions provided by Springer Nature and Copyright Clearance Center.

License Number: 4766580686566

License date: Feb 12, 2020

Licensed Content Publisher: Springer Nature

Licensed Content Publication: Springer eBook

Licensed Content Title: Cancer-Induced Pain

Licensed Content Author: Robert G. Ungard, Norman Buckley, Gurmit Singh

Licensed Content Date: Jan 1, 2016

Type of Use: Thesis/Dissertation

Requestor type: academic/university or research institute

Format: print and electronic

Portion: full article/chapter

Will you be translating? No

Circulation/distribution: 500 - 999

Author of this Springer Nature content: yes

Title: STUDIES ON THE PATHOPHYSIOLOGY OF NEUROPATHIC CANCER PAIN

Institution name: McMaster University

Expected presentation date: Mar 2020

Requestor Location: McMaster University 1280 Main St West MDCL 2102 Hamilton, ON L8S4K1 Canada Attn: McMaster University

Total: 0.00 CAD

Terms and Conditions

Springer Nature Customer Service Centre GmbH Terms and Conditions

This agreement sets out the terms and conditions of the licence (the Licence) between you and Springer Nature Customer Service Centre GmbH (the Licensor). By clicking 'accept' and completing the transaction for the material (Licensed Material), you also confirm your acceptance of these terms and conditions.

1. Grant of License

1. 1. The Licensor grants you a personal, non-exclusive, non-transferable, world-wide licence to reproduce the Licensed Material for the purpose specified in your order only. Licences are granted for the specific use requested in the order and for no other use, subject to the conditions below.

1. 2. The Licensor warrants that it has, to the best of its knowledge, the rights to license reuse of the Licensed Material. However, you should ensure that the material you are requesting is original to the Licensor and does not carry the copyright of another entity (as credited in the published version).

1. 3. If the credit line on any part of the material you have requested indicates that it was reprinted or adapted with permission from another source, then you should also seek permission from that source to reuse the material.

2. Scope of Licence

2. 1. You may only use the Licensed Content in the manner and to the extent permitted by these Ts&Cs and any applicable laws.

2. 2. A separate licence may be required for any additional use of the Licensed Material, e.g. where a licence has been purchased for print only use, separate permission must be obtained for electronic re-use. Similarly, a licence is only valid in the language selected and does not apply for editions in other languages unless additional translation rights have been granted separately in the licence. Any content owned by third parties are expressly excluded from the licence.

2. 3. Similarly, rights for additional components such as custom editions and derivatives require additional permission and may be subject to an additional fee. Please apply to Journalpermissions@springernature.com/bookpermissions@springernature.com for these rights.

2. 4. Where permission has been granted free of charge for material in print, permission may also be granted for any electronic version of that work, provided that the material is incidental to your work as a whole and that the electronic version is essentially equivalent to, or substitutes for, the print version.

2. 5. An alternative scope of licence may apply to signatories of the STM Permissions Guidelines, as amended from time to time.

3. Duration of Licence

3. 1. A licence for is valid from the date of purchase ('Licence Date') at the end of the

relevant period in the below table:

4. Acknowledgement

4. 1. The Licensor's permission must be acknowledged next to the Licenced Material in print. In electronic form, this acknowledgement must be visible at the same time as the figures/tables/illustrations or abstract, and must be hyperlinked to the journal/book's homepage. Our required acknowledgement format is in the Appendix below.

5. Restrictions on use

5. 1. Use of the Licensed Material may be permitted for incidental promotional use and minor editing privileges e.g. minor adaptations of single figures, changes of format, colour and/or style where the adaptation is credited as set out in Appendix 1 below. Any other changes including but not limited to, cropping, adapting, omitting material that affect the meaning, intention or moral rights of the author are strictly prohibited.

Scope of Licence	Duration of Licence
Post on a website	12 months
Presentations	12 months
Books and journals	Lifetime of the edition in the language purchased

5. 2. You must not use any Licensed Material as part of any design or trademark.

5. 3. Licensed Material may be used in Open Access Publications (OAP) before publication by Springer Nature, but any Licensed Material must be removed from OAP sites prior to final publication.

6. Ownership of Rights

6. 1. Licensed Material remains the property of either Licensor or the relevant third party and any rights not explicitly granted herein are expressly reserved.

7. Warranty

IN NO EVENT SHALL LICENSOR BE LIABLE TO YOU OR ANY OTHER PARTY OR ANY OTHER PERSON OR FOR ANY SPECIAL, CONSEQUENTIAL, INCIDENTAL OR INDIRECT DAMAGES, HOWEVER CAUSED, ARISING OUT OF

OR IN CONNECTION WITH THE DOWNLOADING, VIEWING OR USE OF THE MATERIALS REGARDLESS OF THE FORM OF ACTION, WHETHER FOR BREACH OF CONTRACT, BREACH OF WARRANTY, TORT, NEGLIGENCE, INFRINGEMENT OR OTHERWISE (INCLUDING, WITHOUT LIMITATION, DAMAGES BASED ON LOSS OF PROFITS, DATA, FILES, USE, BUSINESS OPPORTUNITY OR CLAIMS OF THIRD PARTIES), AND

WHETHER OR NOT THE PARTY HAS BEEN ADVISED OF THE POSSIBILITY OF SUCH DAMAGES. THIS LIMITATION SHALL APPLY NOTWITHSTANDING ANY FAILURE OF ESSENTIAL PURPOSE OF ANY LIMITED REMEDY PROVIDED HEREIN.

8. Limitations

8. 1. BOOKS ONLY:Where 'reuse in a dissertation/thesis' has been selected the following terms apply: Print rights of the final author's accepted manuscript (for clarity, NOT the published version) for up to 100 copies, electronic rights for use only on a personal website or institutional repository as defined by the Sherpa guideline (www.sherpa.ac.uk/romeo/).

9. Termination and Cancellation
9. 1. Licences will expire after the period shown in Clause 3 (above).

9. 2. Licensee reserves the right to terminate the Licence in the event that payment is not received in full or if there has been a breach of this agreement by you.

Appendix 1 — Acknowledgements:

For Journal Content:
Reprinted by permission from [the Licensor]: [Journal Publisher (e.g. Nature/Springer/Palgrave)] [JOURNAL NAME] [REFERENCE CITATION (Article name, Author(s) Name), [COPYRIGHT] (year of publication)

For Advance Online Publication papers:
Reprinted by permission from [the Licensor]: [Journal Publisher (e.g. Nature/Springer/Palgrave)] [JOURNAL NAME] [REFERENCE CITATION (Article name, Author(s) Name), [COPYRIGHT] (year of publication), advance online publication, day month year (doi: 10.1038/sj.[JOURNAL ACRONYM].)

For Adaptations/Translations:
Adapted/Translated by permission from [the Licensor]: [Journal Publisher (e.g. Nature/Springer/Palgrave)] [JOURNAL NAME] [REFERENCE CITATION (Article name, Author(s) Name), [COPYRIGHT] (year of publication)

Note: For any republication from the British Journal of Cancer, the following credit line style applies:

Reprinted/adapted/translated by permission from [the Licensor]: on behalf of Cancer Research UK: : [Journal Publisher (e.g. Nature/Springer/Palgrave)] [JOURNAL NAME] [REFERENCE CITATION (Article name, Author(s) Name), [COPYRIGHT] (year of publication)

For Advance Online Publication papers:
Reprinted by permission from The [the Licensor]: on behalf of Cancer Research UK: [Journal Publisher (e.g. Nature/Springer/Palgrave)] [JOURNAL NAME] [REFERENCE CITATION (Article name, Author(s) Name), [COPYRIGHT] (year of publication), advance online publication, day month year (doi: 10.1038/sj. [JOURNAL ACRONYM])

For Book content:
Reprinted/adapted by permission from [the Licensor]: [Book Publisher (e.g. Palgrave Macmillan, Springer etc) [Book Title] by [Book author(s)] [COPYRIGHT] (year of publication)

Other Conditions: Version 1.2

APPENDIX 2

SAGE Publishing Copyright License

APPENDIX 3

Inducible xCT Knockdown Project

Preface

The experiments included in this Appendix chapter describe the methodology and results to develop and validate an inducible xCT knockdown cell line, and subsequent testing of that cell line in a mouse model of cancer-induced bone pain (CIBP).

This work has not been published.

For these experiments, I performed in vivo work and data analysis and assisted with in vitro work. Adam Merlo assisted with in vivo work and performed in vitro work with Hanxin Lin, Natalie Zacal, and Katja Linher-Melville. Dr. Singh provided conceptual input.

The IPTG-inducible xCT (SLC7A11) knockdown cell lines in the human breast adenocarcinoma cell line MDA-MB-231 was validated at the transcript, protein and functional levels in vitro and subcutaneously in vivo, and then tested in our validated immunocompromised intrafemoral mouse model of CIBP for pain-related behaviour relative to an uninduced control group. Insufficient numbers of mice successfully grew and retained tumours to draw conclusions from our data.

Development and testing of an IPTG-inducible xCT knockdown cancer cell line in cancer-induced bone pain

Methods

Cell Culture

Human breast adenocarcinoma MDA-MB-231, was used in all in vitro and in vivo work. Testing for mycoplasma contamination was performed regularly with the LookOut Mycoplasma PCR Detection Kit (Sigma), and contaminated cells were treated with Plasmocin (InvivoGen) for two weeks. All cells were maintained at sub-confluent densities in a humidified incubator with 5% CO2 in room air at 37°C using DMEM supplemented with 10% fetal bovine serum (FBS) and 1% antibiotic/antimycotic. Following transfection and transduction, 1µg/mL Puromycin was added to media.

Inducible xCT Knockdown Cell Generation

MDA-MB-231 cells were infected with lentiviral particles containing different shRNA constructs. Three different solute carrier family 7 member 11 shRNA lentiviral transduction particles were used: SHCLNV—NM_012331 TRCN0000043123 (sh43123), SHCLNV—NM_012331 TRCN0000043125 (sh43125), SHCLNV—NM_012331 TRCN0000043126 (sh43126) shRNA, and sh332 non-target shRNA as a control. The multiplicity of infection used was 5 titer units (TU)/cell. The viral titer used was calculated according to the titer units of lentivirus available for each shRNA construct. Following centrifugation and incubation with the virus, 1µg/mL puromycin-substituted DMEM (10% FBS, 1% A/A) was added to select successfully transduced cells. Cells were plated to form colonies, passaged regularly in puromycin-substituted DMEM. Five colonies for each strain were selected with Scienceware cloning discs and expanded prior to screening.

Puromycin & IPTG Dose Selection

Puromycin and IPTG Kill curves were completed for uninfected MDA-MB-231 cells to determine the dose of puromycin required to select clones, and to determine if IPTG would have any effects on cell viability. Cell number was measured by crystal violet following 48h incubation. All doses were tested in triplicate.

RNA Isolation

Following 72h treatment, cell pellets were harvested and RNA isolated with the Qiagen RNEasy kit. Total RNA purity and quantity were measured by spectrophotometry. For tumour tissue RNA extraction, TRIzol (Invitrogen) was used to protect samples during homogenization, and chloroform (Sigma) was used to separate samples upon centrifugation. The top aqueous layer was combined with ethanol and RNA was extracted with the RNEasy kit.

qPCR

cDNA was isolated from treated cells with the cDNA synthesis kit, and quantitative real-time PCR was carried out using primers: SLC7A11-FOR (5′-CCTCTATTCGGACCCATTTAGT-3′) and SLCA11-REV (5′-CTGGGTTTCTTGTCCCATATAA-3′) to amplify the human xCT gene. Actin or RNA Polymerase II were used as housekeepers for all samples tested in these experiments. The $2(-\Delta\Delta Ct)$ method was used to calculate fold changes in mRNA compared to un-induced controls. To verify the product produced by the primers used in qPCR, samples were run on a 3 % agarose gel.

Sample Lysates and Western Blots

Cells were lysed in buffer with protease inhibitor cocktail tablets (Complete Mini) and sonicated on ice. Lysates were centrifuged and a Bradford Protein Assay (Bio-Rad) was performed to determine protein concentration in each sample. Tissue samples were passed

through a 20-guage needle for mechanical homogenization. 50 µg of protein from each lysate was added to a 10-lane 10 % Poly-Acrylamide gel (with stacking and separating gels). Gels were transferred onto an Immobilon PVDF membrane (Millipore), blocked in 5 % skim milk/TBS-T overnight, and blotted with primary xCT anti-rabbit antibody (Novus) (1:1000), and secondary HRP IgG-Linked antibody (Cell Signaling Technology) (1:5000). Calnexin anti-rabbit primary antibody (Santa Cruz Biotechnology) was used as a loading control (1:2000). Three 10-minute washes in TBS-T were completed between antibody treatments. Blots were then treated with Amersham ECL Western Blotting Detection Reagents (Cedarlane), and exposed to Amersham Hyperfilm ECL High performance chemiluminescence film (GE Healthcare) for 5 seconds to 5 minutes. Blots were stripped and re-probed as necessary if membranes were over-exposed. Films were scanned and analyzed for densitometry analysis using the ImageJ software.

Animal Models

4-6 week-old female Balb/c nu/nu immunocompromised mice were used for all experiments. Mice were exposed to handling and the behavioural testing equipment daily for a ~1 week acclimation period, and assigned individual identification. Three days prior to cell implantation, Balb/c nu/nu mice were anaesthetized by isoflurane inhalation and 21 day-release pellets containing 0.25 mg of 17β-estradiol, were implanted in each animal subcutaneously. Although MDA-MB-231 are estrogen receptor negative, estrogen receptors are found throughout bone and play a role in the regulation of bone remodelling. In experiments done previously in this lab, it was found that 17β-estradiol pellets implanted prior to cancer cell inoculation improved the consistency of tumour growth in bone and subcutaneously.

Cell harvesting was performed on sub-confluent cultures and adherent cells were suspended and kept lightly agitated in sterile PBS. Mice for subcutaneous tumour models (n = 5 / group) were injected at the rear right flank without anaesthesia. Subcutaneous tumor growth was monitored by measuring tumor dimensions with digital calipers and calculated according to the hemiellipsoid equation length×width×height×(π/6).

Mice for intra-femoral implantation (These groups were initiated at n = 9 each, however a total of 11/18 mice did not develop an observable lesion in bone, or display behavioural evidence of nociception, resulting in final group sizes of (IPTG: n = 2; and Vehicle n = 5)). were anaesthetized by isoflurane inhalation and injected subcutaneously with 0.05 mL 1:10 buprenorphine analgesic. Cancer cells were percutaneously injected into the right distal epiphysis of the femur. The contralateral hind limb of each animal served as a negative control specific to each animal. Animals were randomly selected for sham injections of 25 μL sterile PBS containing heat/freeze killed cells to mimic the disruption of the surgery but not the disruption of the tumour. To minimize necessary tissue damage and resulting pain from surgery, mice were laid supine while the ipsilateral knee is held bent at ~90°, allowing clearance of the patella. A 26 ga. needle is then placed between the medial and lateral condyles of the distal epiphysis parallel to the length of the femur and rotated manually to penetrate the cortical bone and enter the epiphysis. The cell solution is then slowly injected into the bone and the needle is gently removed. No plug is utilized as tumour invasion into the periosteum and beyond the confines of the bone more closely mimics a metastasis. This method of intrafemoral injection results in a small hole and little damage to the surrounding tissues.

All animals were sacrificed at ethical endpoints. Tumours were collected from the mice and either snap frozen in tubes on dry ice, or were divided for freezing and fixation, based on tumour size. Brain, spinal cord, and dorsal root ganglia were isolated within 30 minutes, and stored for genetic analysis in RNAlater solution.

Radiographic scans of all mice in the prone position were taken. The ipsilateral and contralateral tibia, fibula, femur, and some surrounding tissue were then dissected and fixed in 10 % buffered formalin solution for 48 hours. Following fixation, bone samples were immersed in an agitated 10 % EDTA, 4 % Formalin buffered solution for decalcification. This process was completed over several weeks with weekly changes of the decalcification solution. All fixed and decalcified tissues were embedded in paraffin blocks to be sectioned for histological staining.

Behavioural Analysis

Behavioural testing was performed a minimum of 3 times prior to model induction to obtain baseline data, and 2-3 days a week beginning on day 1 following model induction and continuing until endpoint. The tests performed include three tests for spontaneous pain behaviours: the Dynamic Weight Bearing system (DWB), Limb Use Scale, and Guarding Time, and one test for elicited pain behaviour, the Dynamic Plantar Aesthesiometer (DPA).

Open field observational testing includes limb use over a 2-minute observation period. Limb use is an operator-derived numerical representation of the use of the animals ipsilateral limb (0: No use, 1: severe limp, 2: moderate limp, 3: slight limp, 4: Normal use).

Radiograph Lesion Scoring

The extent of osteolytic lesions in the ipsilateral femurs as imaged as a loss of bone density by post-mortem radiograph was scored using a custom four point (0-3) scale of bone destruction. The scale designations are as follows: (0) Normal bone, no visible lesion; (1) minor loss of bone density, minimal lesion; (2) Moderate to substantial loss of bone density, lesion limited to bone trabecula and cortex; (3) substantial loss of bone density, lesion includes clear periosteal involvement or fracture.

Cell Growth

Cell numbers in all experiments were quantified using the crystal violet assay. The extent of staining was read with a microplate spectrophotometer at λ=570 nm.

Glutamate Release

Glutamate levels in culture media were quantified using the AMPLEX Red glutamic acid assay kit and analyzed on a CytoFluor Series 4000 Fluorescence Multi-Well Plate Reader.

The AMPLEX Red glutamic acid assay kit quantifies l-glutamate in a sample through the indirect measurement of a fluorescent product, resorufin, linked 1:1 with glutamate in the test sample.

Cystine Uptake

Cells were seeded in 6-well plates at 150,000 cells/well and allowed to adhere overnight. IPTG treatment of 1mM was performed for 72 hours, changed daily. Media was collected for glutamate analysis (described above), and cells were rinsed with HBSS. Cells were incubated in 14C-L-Cystine (Sigma) for 20 minutes, and then washed three times with cold HBSS. Cells were lysed in cystine uptake lysis buffer for thirty minutes, and 100µL of lysate was placed into Scintillation tubes with 1mL of Ecoscint-H (National Diagnostics), where the samples were read on the scintillation counter for Carbon-14. Cells were normalized to amount of protein, determined from a Bradford assay (Bio-Rad).

Statistical Analysis

All behavioural data is confirmed for normal distribution and analyzed across treatment groups with one-way repeated-measures ANOVA followed by Bonferonni post hoc test. All in vitro work was analyzed with one-way ANOVA followed by Bonferonni post hoc test where indicated. The significance level was set at $P < 0.05$.

All data are presented as mean ± the standard error of the mean (SEM).

A power analysis was performed based on DPA results as primary measurement with a type II error ($\beta = 20$ %), and a type I error ($\alpha = 5$ %).

Results

IPTG-inducible xCT knockdown in MDA-MB-231 is viable in-vitro.

(i) xCT is reduced at the mRNA level

Induced cells were treated with 1mM IPTG for 72 hours, changed daily, while uninduced cells were exposed to media without IPTG. The scramble shRNA vector (termed sh332) served as a negative control in all experiments. A knockdown of approximately 50% ($p<0.05$) was found in xCT mRNA as measured by qPCR in colonies selected from cells infected with the sh43126 construct compared to the scramble control and uninfected MDA-MB-231 cells, (Fig 3A). Clones infected with other constructs (sh43123 and sh43125) did not reveal a change in xCT expression compared to controls.

To ensure that the primers used for the target and housekeeper genes produced the anticipated product, samples were separated on a 3% agarose gel to verify product size. Primer products were seen at 300bp for xCT and above 500bp for actin (Fig 3B).

(ii) xCT is reduced at the protein level

Western blots of in vitro samples showed changes in xCT expression in clones with the sh43126 construct. Different colonies were tested to determine changes in expression. In Fig 4A, colony #4 and colony #3 were plated with and without IPTG for 72 hours, media changed daily, and samples were lysed and separated on a 10% poly-acrylamide gel. A band to represent endogenous xCT existed around 37kDa, and the calnexin housekeeper at ~90kDa. A knockdown of xCT when the inducible system was activated with IPTG was seen in both samples, but a significant fold change in the densitometry for colony #4 only was seen ($p<0.05$) (Fig 4B). Each blot was probed with calnexin as a loading control, and all densitometry results for xCT were normalized to the amount of calnexin using ImageJ.

(iii) Inducible knockdown affects xCT functional activity

To test for functional changes in system xC- activity, the cystine uptake assay was used Cells were plated and treated with IPTG (1mM) for 72 hours, changed daily, or no treatment. Cell lysates were used to determine the amount of radioactivity present in each sample based on the amount of intracellular 14C-L-Cystine, and all samples were normalized to protein. Three experimental repeats revealed approximately a 45% decrease ($p<0.01$) in cystine uptake in induced cells for colony #4, but not for colony #3 (Fig 5A).

Amplex Red glutamate assay was used to measure the amount of glutamate present in the extracellular environment. Media samples were taken from each cystine uptake experiment. Corresponding absorbance values were converted to glutamate concentrations from a standard curve, and all samples were normalized to protein. Fold changes were represented (Fig 5B), and a 50% increase in glutamate output ($p<0.05$) was seen in cell colonies containing the scrambled shRNA, and a statistically insignificant decrease in glutamate output was found in sh43126 #4 cell colony.

Inducible Knockdown does not affect tumour growth in vivo

Colony #4 of sh43126 was utilized to investigate subcutaneous tumour growth. Fifteen animals were arranged into three groups of n=5 ea. Groups were treated with either IPTG (10mM) in drinking water (changed daily), intraperitoneal IPTG (10mg/kg), or no treatment.

Tumour measurements were performed three times per week beginning seven days post-injection, when tumours of a measurable size were present. At day 19, animals were rearranged to provide all groups with the same average tumour size on day 1 of IPTG treatment. No statistically significant difference in tumour progression was found between groups (Fig 6A). A preference or aversion to IPTG drinking water was also examined, where animal fluid intake was monitored daily for each cage. No statistically significant difference was seen in fluid intake between the three cages (Fig 6B).

Inducible Knockdown affects xCT mRNA in vivo

Tumours were isolated following sacrifice and RNA was isolated for cDNA synthesis. Primers were for human xCT as the target and RNA Polymerase II as the housekeeper. The results indicated a 50% knockdown of xCT mRNA ($p<0.05$) in animals that received a 10mg/kg daily IP injection of IPTG. Though a decrease in xCT mRNA was noted in animals that received IPTG in the drinking water, the results were not statistically significant (Fig 7).

Despite changes in xCT mRNA, no notable differences in xCT protein levels as measured by western blotting were seen between groups (Fig 8).

Figures

A

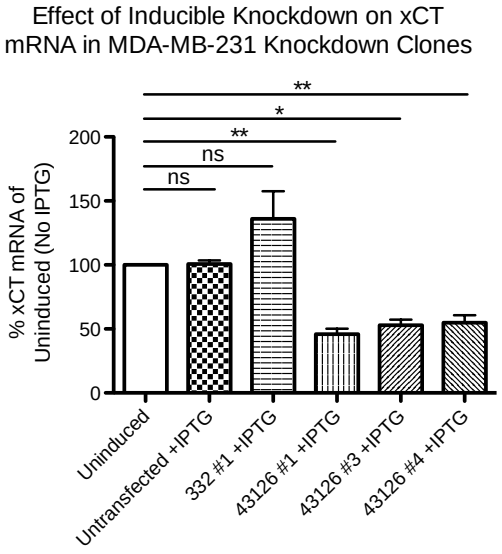

B

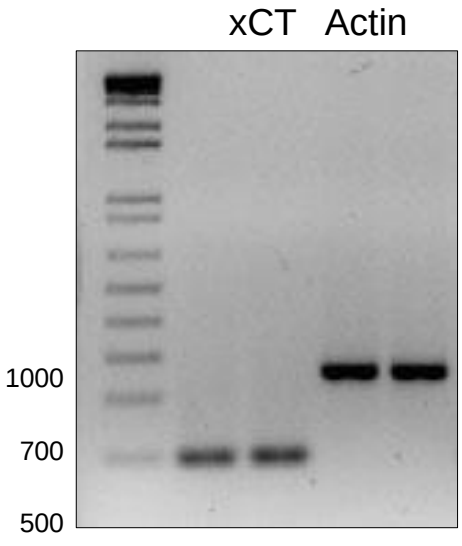

Fig 1.

Inducible Knockdown of xCT mRNA present in sh43126 colonies. A. Cells were plated at 7.5×104 cells/mL in 60mm plates. IPTG was added to one plate, changed daily for 72 hours. cDNA was synthesized, and qPCR reactions were performed in duplicate. CT values were obtained from the Real-Time machine and % xCT RNA was determined via the 2(-ΔΔCt) method.37 **p<0.01, *p<0.05. B. qPCR products were separated on 3% agarose gel to verify product sizes with a 1kb DNA ladder. Lanes 1 and 2 are for xCT primers, and lanes 3 and 4 for actin (housekeeper).

A B

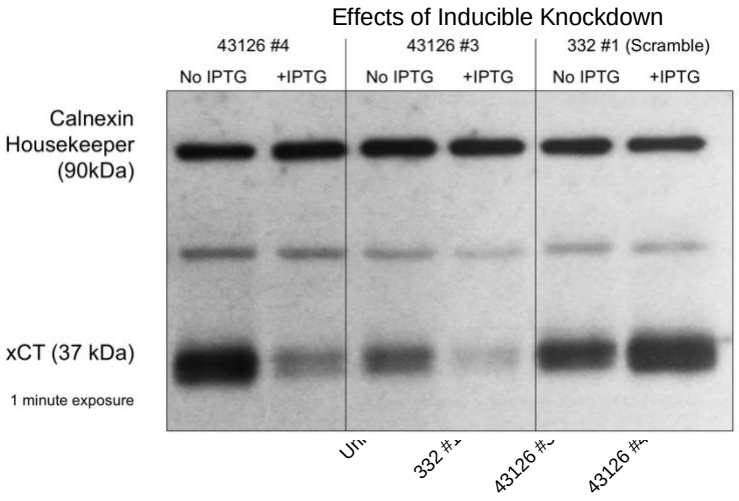

Fig 2.

Inducible Knockdown of xCT Protein Present in 43126 colonies. A. Cells were plated at 7.5×104 cells/mL in 10cm plates. IPTG was added to one plate for each sample, changed daily for 72 hours. Cells were lysed and separated on 10% poly-acrylamide gel. Blot was cut and the top portion incubated with calnexin primary (1:2000) and the bottom with xCT primary (1:1000). HRP IgG-linked secondary antibody used (1:5000), and blots exposed for 1 minute to Hyperfilm. B. Densitometry analysis of all western blots using ImageJ to quantify protein expression. **p<0.01.

A B

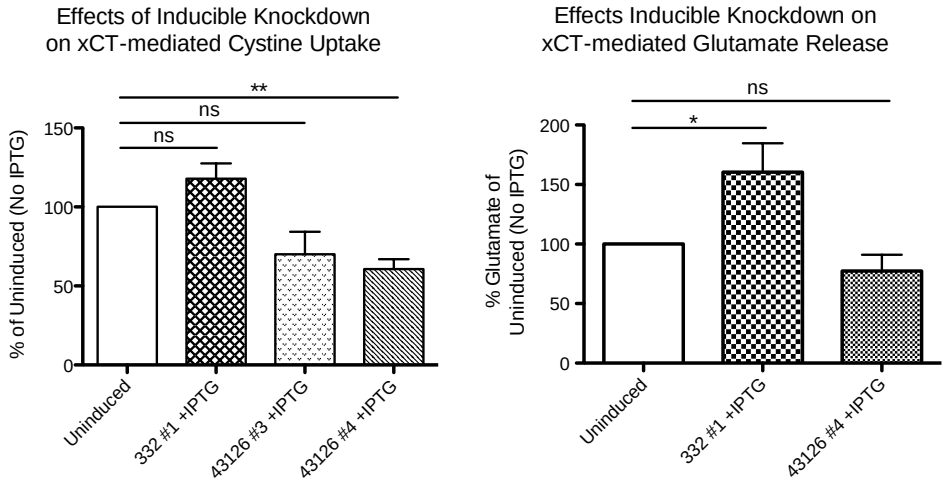

Fig 3.

Inducible Knockdown of xCT affects functionality of system Xc-. A. Cells were plated at 7.5×104 cells/mL in 6-well plates. IPTG was added to 3 of the wells, changed daily for 72 hours. Cells were incubated in radioactive cystine, washed and lysed. Lysates were used to normalize results to protein (Bradford Assay) and radioactivity was measured in each sample. B. Media was obtained from the plates used for cystine uptake assay, and tested in triplicate to obtain the [glutamate] in each sample. Fold changes on graphs relative to un-induced cells (no IPTG). **$p<0.01$, *$p<0.05$.

A

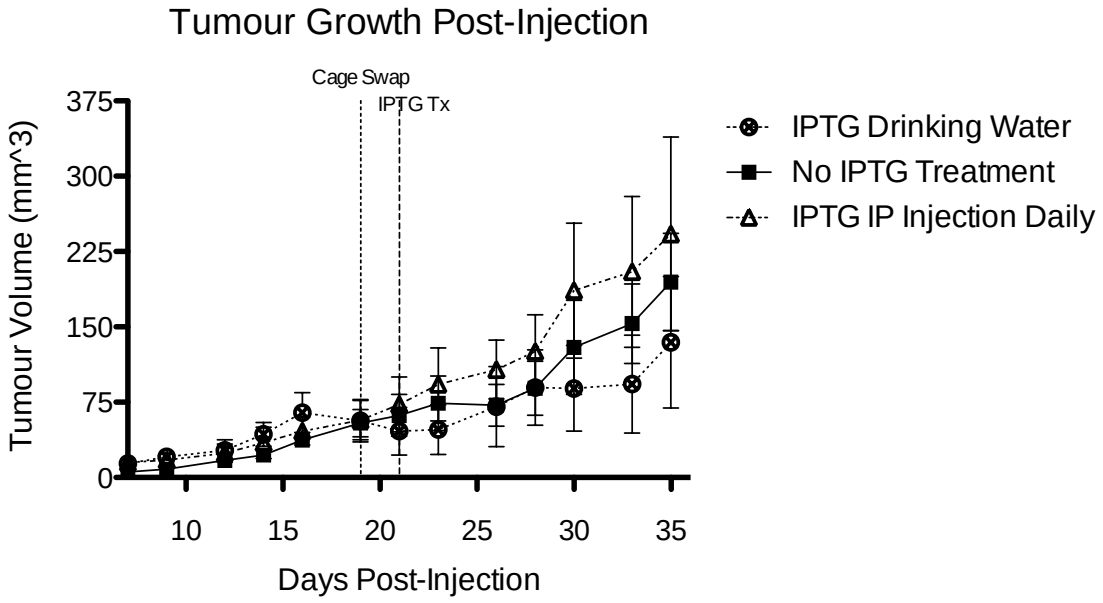
Tumour Growth Post-Injection
Cage Swap
IPTG Tx
Tumour Volume (mm^3)
375
300
225
150
75
0
10
15
20
25
30
35
Days Post-Injection
IPTG Drinking Water
No IPTG Treatment
IPTG IP Injection Daily

B

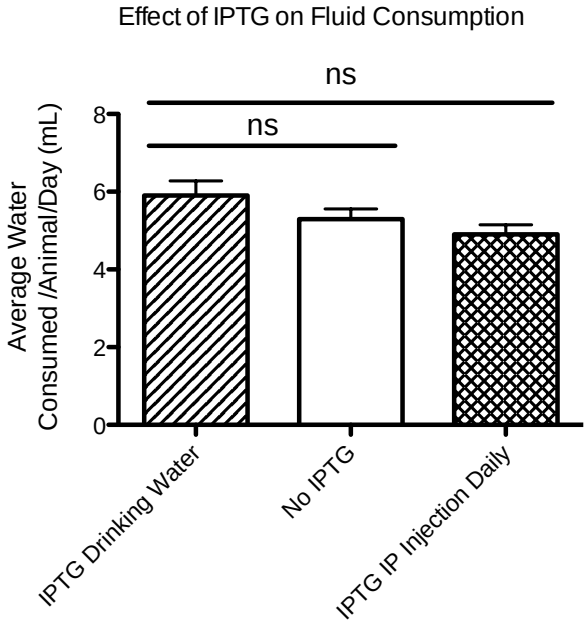
Effect of IPTG on Fluid Consumption
ns
ns
Average Water Consumed /Animal/Day (mL)
8
6
4
2
0
IPTG Drinking Water
No IPTG
IPTG IP Injection Daily

Fig 4.

Inducible Knockdown does not affect tumour development, and IPTG drinking water does not affect fluid intake. A. Animal tumours were measured three times per week beginning 7 days post-injection. The height, length, and width of each tumour was measured to determine tumour volume (mm3), and average values and standard errors calculated in Microsoft Excel and reported in Prism. B. Animal fluid intake was calculated per mouse by weighting the drinking bottles in each cage daily and calculating the fluid consumed per mouse each day. Data presented as a daily average over the course of the study.

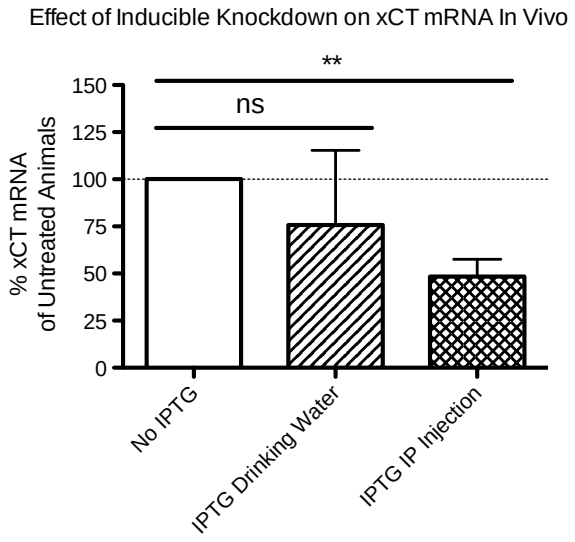

Fig 5.

Inducible Knockdown of xCT mRNA functional in nude mice. Animals were sacrificed upon humane endpoint, and RNA extracted from each tumour sample according to a TRIzol™ method with RNEasy purification. cDNA was synthesized, and qPCR reactions were performed in duplicate. CT values were obtained from the Real-Time machine and % xCT RNA was determined via the 2(-ΔΔCt) method, with RNA polymerase II as the housekeeping gene, optimized for xCT. **$p<0.01$.

A

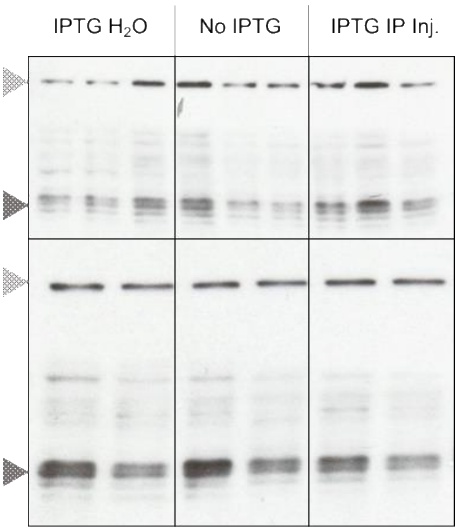

B

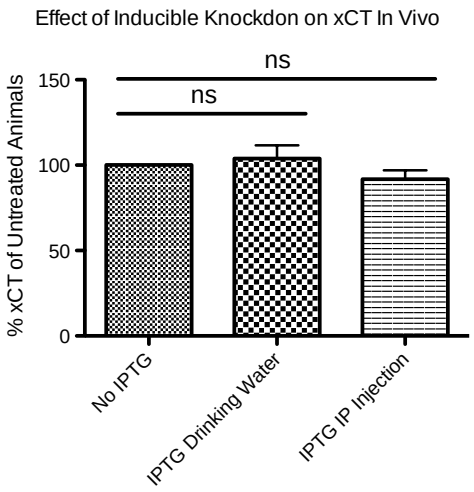

Fig 6.

Inducible Knockdown of xCT Protein undetermined in nude mice. A. Animals were sacrificed upon humane endpoint, and a portion of each tumour sample was lysed and separated on 10% poly-acrylamide gel. Membrane was cut and the top portion incubated with calnexin primary (1:2000) and the bottom with xCT primary (1:1000). HRP IgG-linked secondary antibody used (1:5000), and blots exposed for 1 minute to Hyperfilm. Light grey arrow indicated calnexin housekeeper (95kDa), and dark grey arrow represents xCT (~40kDa). B. Densitometry analysis of all bands shown as a fold change to the mean of untreated animals. ImageJ was used to quantify protein expression.

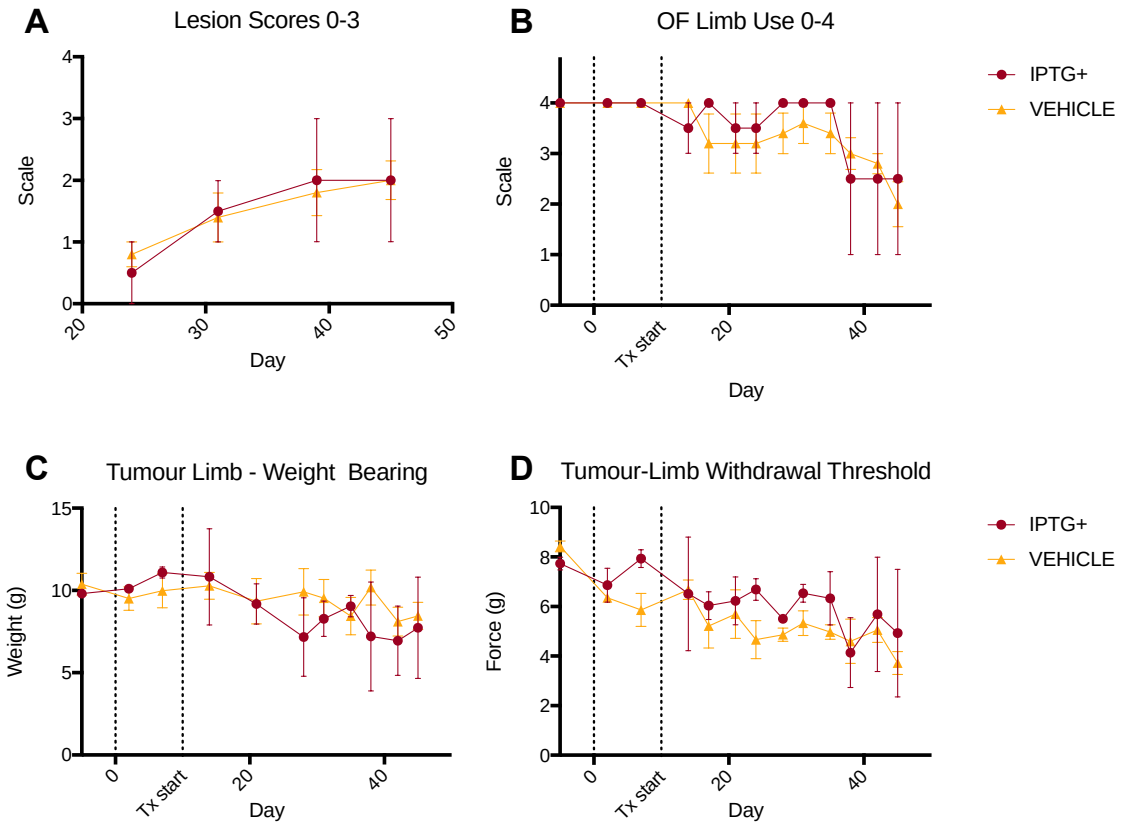

Fig 7.

These in vivo results are compiled from group sizes: (IPTG n = 2) (Vehicle n = 5) and are therefore inconclusive and require repetition. In these figures, no differences are observed between groups of mice implanted intrafemorally with IPTG-inducible xCT knock-down MDA-MB-231 cells when treated with IPTG to induce genetic silencing of xCT or with vehicle as negative control.